L'interleukine-1 alpha comme cible thérapeutique suite à une lésion de la moelle épinière : Détermination des effets sur l'inflammation, le stress oxydatif et les oligodendrocytes

Thèse

Floriane Bretheau

Doctorat en médecine moléculaire
Philosophiæ doctor (Ph. D.)

Québec, Canada

L'interleukine-1 alpha comme cible thérapeutique suite à une lésion de la moelle épinière : Détermination des effets sur l'inflammation, le stress oxydatif et les oligodendrocytes.

Thèse

Floriane Bretheau

Sous la direction de :

Dr. Steve Lacroix

Résumé

Les lésions de la moelle épinière (LME) sont provoquées lorsque la moelle épinière est endommagée à la suite d'un impact ou d'une compression mécanique prolongée sur la colonne vertébrale, pouvant causer une paraplégie voire même une tétraplégie. Chaque année, entre 250 000 et 500 000 personnes dans le monde souffrent de LME selon l'organisation mondiale de la santé, dont 86 000 cas recensés au Canada. Les dommages causés aux neurones et aux cellules gliales à la suite d'une LME engendrent des dommages tissulaires irréversibles ainsi que l'activation de mécanismes inflammatoires principalement médiés par des cytokines. Initialement, la LME entraine la nécrose des microglies et la libération de leur contenu cellulaire qui inclut l'interleukine-1 alpha (IL-1α). Ce signal de danger hautement actif (alarmine) déclenche la neuroinflammation se traduisant à court terme par le recrutement des neutrophiles et des monocytes inflammatoires au site lésionnel et, à moyen terme, par la mort des oligodendrocytes (Ols) par apoptose. Des travaux de recherche récemment publiés par notre équipe ont montré que l'infiltration des cellules immunitaires du sang est significativement diminuée lorsque le gène Il1a ou Il1b est invalidé chez les souris. Cependant, seules les souris *Il1a*$^{-/-}$ ont montré des améliorations rapides et permanentes de la locomotion ainsi qu'un volume lésionnel réduit dès le premier jour suivant la lésion. L'objectif de cette thèse était d'investiguer le mécanisme d'action l'IL-1α au niveau du système nerveux central (SNC) afin de mieux comprendre comment cette cytokine médie ses effets néfastes et ainsi permettre de les inhiber dans un contexte de LME. Nous avons ainsi mis en évidence que l'IL-1α entraîne principalement l'infiltration massive de neutrophiles ainsi que la diminution rapide des Ols. L'utilisation de différentes lignées murines transgéniques nous a permis d'induire une délétion ou une restauration spécifique du récepteur de l'IL-1, IL-1R1, dans les différents types cellulaires du SNC, afin de mieux comprendre le mécanisme d'action de l'IL-1α. Nous avons ainsi pu observer que l'infiltration des cellules immunitaires requiert la présence de l'IL-1R1 endothélial. Nous avons également montré que l'effet délétère de l'IL-1α sur les Ols est principalement médié par les astrocytes. De plus, nous avons montré que les astrocytes sont capables d'induire la mort des Ols via la production de dérivés oxygénés réactifs (*Reactive Oxygen Species*, ROS) dont l'effet peut être inhibé grâce à l'administration de l'antioxydant N-acétylcystéine. Ainsi, la meilleure compréhension du mécanisme d'action de l'IL-1α et de ses effets subséquents permet

d’ouvrir la possibilité à de nouvelles cibles thérapeutiques dont les effets pourraient aider à réduire les dommages suite aux LME et, ainsi, favoriser la récupération des patients.

Abstract

Over 4 million people suffer from SCI worldwide, and about 250 000 to 500 000 new injuries occur annually. At the site of trauma, SCI causes direct damage to cell bodies of neurons and glial cells. This is followed by a second wave of tissue degeneration characterized by damage to myelin and the death of oligodendrocytes (Ols) and neurons that survive the initial trauma, thus resulting in an amplification of the motor and sensory deficits. We recently demonstrated that dead and dying microglia at sites of SCI rapidly release the danger signal interleukin (IL)-1α, which in return triggers neuroinflammation. Accordingly, mice lacking the *Il1a* gene have an impaired inflammatory response and recover faster and to a greater extent than control mice after SCI. The main goal of this thesis was to investigate the mechanism of action and effects of IL-1α in the central nervous system (CNS) in order to prevent its detrimental consequences in the context of SCI. We uncovered that intra-cisterna magna (i.c.m.) delivery of recombinant IL-1α in mice leads to massive infiltration of neutrophils, the rapid death (within 24 hours) of mature Ols along the rostro-caudal spinal cord axis, damage to myelin sheaths, and strong activation of neurons. Using novel transgenic mouse lines in which we induced cell-specific deletion of the gene coding for the interleukin-1 receptor type I (IL-1R1), we found that Ol cell death was indirect and involved other types of CNS-resident cells such as astrocytes and endothelial cells (ECs), as well as blood-derived myeloid cells. Altogether, our data suggest that IL-1α released by damaged/dead microglia after SCI regulates Ol cell death and myelin damage through a mechanism that involves astrocytes, ECs and myeloid cells. Understanding the mechanism underlying Ol cell death and disruption of myelin integrity after SCI could allow the development of novel therapeutic strategies to protect and/or rescue this cell population and improve recovery after CNS injury and demyelinating diseases.

Table des matières

Liste des figures

Liste des tableaux

Liste des abréviations, sigles, acronymes

ADN	Acide désoxyribonucléique
ADNc	Acide désoxyribonucléique complémentaire
ARN	Acide ribonucléique
ARNm	Acide ribonucléique messager
ATP	Adénosine 5'-triphosphate
AVC	Accident vasculaire cérébral
BHE	Barrière hémato-encéphalique (*Blood-brain barrier*, BBB)
BHS	Barrière hémato-spinale
BMPs	Bone morphogenic proteins
BMS	Basso Mouse Scale
BrdU	Bromodéoxyuridine
CAMs	Complexe d'attaque membranaire
CCR2	*C-C chemokine receptor type 2*
CD40L	*Cluster of differention 40 ligand*
CLR	Récépteurs de lectines de type-C (*C-type lectin receptors*)
CMH	Complexe majeur d'histocompatibilité
CNTF	*Ciliary neurotrophic factor*
CPA	Cellule présentatrice d'antigènes
CSF	Liquide cérébrospinal (*Cerebrospinal fluid*)
CSF-1	*Colony stimulating factor 1*
CSF-1R	*Colony stimulating factor 1 receptor*
CSPG	Protéoglycanes de type chondroïtine sulfate (*Chondroitin sulfate proteoglycans*)
Cx3Cr1	Récepteur de la fractalkine
CXCL1	*C-X-C motif ligand 1*
CXCL10	*C-X-C motif ligand 10*
CXCL-12	*CXC-motif chemokine ligand 12*
CXCL2	*C-X-C motif ligand 2*
CXCR4	*CXC-receptor 4*
DAMP	Molécules associées aux dommages (*Damage-associated molecular patterns*)
EAE	Encéphalomyélite autoimmunitaire expérimentale (*Experimental autoimmune encephalomyelitis*)
ER	Récepteur aux oestrogènes
ERG	*ETS-related gene*
FADD	*FAS-associated death domain*
FGF	Facteur de croissance des fibroblastes
FGF-2	Facteur de croissance des fibroblastes 2
G-CSF	Facteur de croissance granulocytaire
GDFs	Facteurs de croissance et de différentiation
GFAP	Protéine acide fibrillaire gliale (*Glial fibrillary acid protein*)
GFP	Protéine fluorescente verte (*Green fluorescent protein*)

Hes5	*Hes family bHLH transcription factor 5*
HGF	Facteur de croissance des hépatocytes (*Hepatocyte growth factor*)
HMGB1	High-mobility group box protein B1
HSCs	Cellules souches hématopoïétiques (*Hemtaopoietic stem cells*)
HSPs	Protéines de choc thermique (*Heat shock proteins*)
ICAM-1	Molécule d'adhésion intercellulaire 1
Id2	*DNA-binding protein inhibitor 2*
Id4	*DNA-binding protein inhibitor 4*
IFN-β	Interféron bêta
IFN-ϒ	Interféron gamma
IL	Interleukine
IL-1R1	Récepteur de l'IL-1 de type I
IL-1R2	Récepteur de l'IL-1 de type II
IL-1RAcP	Protéine accessoire du récepteur de l'IL-1
IL-1α	Interleukine-1 alpha
IL-1β	Interleukine-1 beta
IL-6	Interleukine-6
IRAKs	Kinases associées au récepteur de l'IL-1 (*Interleukin-1 receptor-associated kinase 1*)
Irf8	Facteur 8 de régulation l'interféron
Iκβ	*Nuclear factor of kappa light polypeptide gene enhancer in B-cells*
JNK	Kinase c-jun N-terminale
LME	Lésion de la moelle épinière
LNP	Lésion du nerf périphérique
LPS	Lipopolysaccharide
MAG	Glycoprotéine associée à la myéline
MAPKs	*Mitogen-activated protein kinase*
MDMs	Macrophages dérivés des monocytes
MHCII	Complexe majeur d'histocompatibilité de classe II (*Major histocompatibility complex class II*)
MyD88	Gène de réponse primaire de différenciation de cellules myéloïdes 88 (*Myeloid differentiation factor* 88)
Myrf	*Myelin regulatory factor*
NAC	N-acétylcystéine
NET	Pièges extracellulaires des neutrophiles (*Neutrophil extracellular traps*)
NF- Kβ	Facteur nucléaire kappa B (*Nuclear factor-kappa B*)
NG2	*Neural/glial antigen 2*
Nkx2,2	*NK2 homeobox 2*
NLR	Récepteurs de type NOD (*NOD-like receptors*)
NOD	Récepteur à domaine d'oligomérisation de nucléotides
NSCs	Cellules souches neuronales (*Neural stem cells*)
OHT	*4-hydroxytamoxifen*
Olig1	Facteur de transcription d'oligodendrocyte 1
Olig2	Facteur de transcription d'oligodendrocyte 2

Ols	Oligodendrocytes
OMgp	Glycoprotéine d'oligodendrocytes
OPCs	Cellules progénitrices des oligodendrocytes (*Oligodendrocyte progenitor cells*)
P53	*p53 tumor suppressor*
PAMP	Motif moléculaire associé aux pathogènes (*Pathogen-associated molecular patterns*)
PDGF	Facteur de croissance dérivé des plaquettes (*Platelet-derived growth factor*)
PDGF-A	Facteur de croissance dérivé des plaquettes alpha (*Platelet-derived growth factor alpha*)
PDGFRα	Récepteur du facteur de croissance dérivé des plaquettes (*Platelet-derived growth factor receptor alpha*)
PI3K	Phosphoinositide 3-kinase
PMN	Neutrophiles polymorphonucléaires (*Polymorphonuclear neutrophils*)
PRRs	Récepteurs de reconnaissance des motifs moléculaires (*Pattern recognition receptors*)
Rel-A	Sous-unité du facteur nucléaire NF-kappa-B p65 (*Nuclear factor NF-kappa-B p65 subunit*)
RLR	*Retinoic acid-inducible (RIG)-I-like receptors*
ROS	Dérivés réactifs de l'oxygène (*Reactive oxygen species*)
SEP	Sclérose en plaques
Shh	Sonic hedgehog
SNC	Système nerveux central
SNP	Système nerveux périphérique
Sox10	*SRY-box transcription factor 10*
STAT3	*Signal transducer and activator of transcription 3*
TACE	Enzyme de conversion du TNF (*TNF-converting enzyme*)
TGF-β	Facteur de croissance tumoral bêta (*Tumor growth factor beta*)
TGF-βRI	Récepteur de type I du TGF-β
TGF-βRII	Récepteur de type II du TGF-β
TK	Thymidine kinase
TLR	Récepteur de type Toll (*Toll-like receptor*)
TNF	Facteur de nécrose tumorale (*Tumor necrosis factor*)
TNFR2	Récepteur de type II du TNF
TNRC9	*Trinucleotide repeat containing 9*
TOX3	*Tox high mobility group box family member 3*
TRADD	Protéine de domaine de mort associée au récepteur du TNF (*TNFR-associated death domain*)
TRAF6	Facteur associé au récepteur du TNF (*Receptor-associated factor 6*)
VEGF	Facteur de croissance de l'endothélium vasculaire (*Vascular endothelial growth factor*)
WD	Dégénéréscence Wallérienne (*Wallerian degeneration*)
WNT	*Wingless-type mouse mammary tumor virus integration site*

< « Je suis de ceux qui pensent que la science est d'une grande beauté. Un scientifique dans son laboratoire est non seulement un technicien : il est aussi un enfant placé devant des phénomènes naturels qui l'impressionnent comme des contes de fées. »
- Marie Curie>

Remerciements

Alors que je n'avais que 12 ans, l'idée de faire une thèse a commencé à germer dans mon esprit. D'années en années, cette volonté s'est trouvée renforcée au fil de mes études et j'étais bien décidée à poursuivre dans cette direction. Et, finalement, il y a un peu plus de 5 ans, j'ai eu la chance d'être acceptée en doctorat à l'Université Laval. Aujourd'hui, alors que cette thèse s'achève, je tiens à remercier plusieurs personnes sans qui cette aventure, à la fois scientifique et humaine, n'aurait pas été possible.

Avant tout, je tiens à remercier mon directeur de recherche, le Dr. Steve Lacroix, qui m'a donné cette chance unique de pouvoir faire ma thèse dans son laboratoire. Vous avez donné à cette jeune étudiante de 22 ans que j'étais, timide et peu confiante, la chance de montrer ce qu'elle valait, et ça je ne vous en remercierai jamais assez. Steve, vous avez été un directeur de thèse formidable, patient et compréhensif, et surtout vous m'avez fait confiance en permettant de tester mes propres idées et ainsi de gagner en autonomie et en indépendance. Je tiens également à souligner l'exemple que vous êtes d'un point de vue rigueur et intégrité scientifiques.

Et qu'aurait été mon doctorat sans l'aide et le soutien inestimables de toute l'équipe. Un grand merci à Nadia Fortin, notre incroyable chirurgienne, pour toutes ces heures passées à faire des chirurgies, des injections, des perfusions (maintenant nous sommes bien rôdés !). Merci également à Martine Lessard pour tout le temps que tu as consacré à la mise au point et aux expériences pour mon projet. Ta précision et ta rigueur technique sont d'une qualité remarquable. Merci également à Nicolas Vallières pour tous tes conseils et ta patience, tu as toujours été là pour répondre à la moindre de mes questions, même les plus absurdes (« C'est étrange que le Fluorojade ne se dissout pas… »).

Et enfin, merci à tous mes collègues Victor, Alexandre, Jorge, Sébastien que j'ai connus tout au long de mon doctorat. En particulier, un énorme merci à Benoît, pour TOUT. Nous avons commencé notre doctorat en même temps et, sans toi, je ne sais même pas si j'aurai pu descendre un jour à l'animalerie. Et merci à Roxanne. Merci pour votre patience, nos discussions interminables, nos lab meetings en salle de lunch et tous ces moments que nous avons partagés en dehors du laboratoire… Bien plus que des collègues, Ben et Rox, vous êtes devenus de véritables amis, et ça c'est formidable et je sais que cette amitié durera encore longtemps.

Je tiens également à remercier tout particulièrement le Dr. Julia Hernandez-Rapp. Bien plus que la gestionnaire de l'Axe, tu es devenue une amie et surtout, une incroyable mentor. Merci pour tous tes conseils et toutes ces discussions inestimables qui m'ont beaucoup aidé à « y voir plus clair ». Tu es pour moi un véritable exemple.

Une thèse, c'est une aventure scientifique, mais aussi une aventure humaine, qui plus est si on est étranger. Vos amis deviennent alors votre deuxième famille et vous savez que vous pouvez compter sur eux, que ce soit dans les bons moments ou les moments difficiles. Alors un ENORME merci à tous mes amis de Québec avec qui j'ai eu la chance de partager des moments inoubliables. Qu'auraient été ces cinq dernières années sans les soirées brainstorming avec vous, Clothilde et Marianne, sans les soirées quiz avec mes petits Quizz de Poulet, Aurore, Anna, Ophélie, Romain, Léo, sans les soirées jeux de société avec vous, Maxime, Jonathan, Guillaume, Stéphanie, sans nos parties de badminton, Morgan, Ben, Maxime, Rémi, sans les parties de soccer avec les Cervolants, sans les évènements organisés grâce à tous les membres, anciens et nouveaux, du CéNS, Marie, Héléna, Shireen,…. Sans oublier tous ces amis rencontrés dans cette dernière année et avec qui j'espère partager de beaux moments dans les années à venir, Estelle, Marion, Eva, Cha, Quentin, Coco … Et un gros merci à toutes ces personnes qui ont été particulièrement présentes dans cette dernière année, Quentin, Max, Rox, Aurore, Morgan…

Enfin, je n'aurai jamais pu réaliser ce doctorat sans l'aide et le soutien de ma famille, et, en particulier, de mes parents. Merci à vous d'avoir cru en moi durant toutes ces années. Je me souviens encore du jour où je vous annonçais que je partais à Québec, vous avez cru que c'était une « joke », c'est vrai que je ne m'étais jamais dit que je partirais dans un pays « froid ». Je sais que cela n'a pas été facile pour vous de me voir partir aussi loin, mais vous avez toujours été là. Je ne vous remercierai jamais assez pour tout ce que vous avez fait pour moi.

Avant-propos

Durant mes cinq années passées au Centre de recherche du CHU de Québec–Université Laval, j'ai eu la chance de travailler sur différentes thématiques. Le principal de mes recherches, et plus précisément mon projet principal, s'est porté sur les lésions de la moelle épinière. Toutefois, j'ai également eu l'occasion de m'intéresser aux autres thématiques développées au sein du laboratoire, en particulier le modèle murin de la sclérose en plaques ou encore les lésions du nerf sciatique.

Cette thèse est divisée en cinq chapitres portant sur le thème principal de mes études doctorales. Le premier chapitre fait office d'introduction et présente les différents thèmes et concepts étudiés au cours de mon doctorat.

Le deuxième chapitre est une revue de littérature nommée « ANTI-ALARMINS THERAPIES: NEW INSIGHTS IN CNS PROTECTION MECHANISMS ». Cette revue de littérature s'intéresse aux différentes thérapies ciblant les signaux de danger, nommés alarmines, jouant un rôle critique au cours des atteintes au SNC.

Le troisième chapitre traite de l'article intitulé « MICROGLIA ARE AN ESSENTIAL COMPONENT OF THE NEUROPROTECTIVE SCAR THAT FORMS AFTER SPINAL CORD INJURY » paru dans le journal *Nature Communication* en 2019. Cette étude multicentrique dirigée par Dr. Steve Lacroix a été effectuée en collaboration avec Dre. Molly Schoichet de l'Université de Toronto. Dr. Victor Bellver-Landete est le premier auteur. Pour ma part, je suis deuxième auteure sur l'article. J'ai participé activement à l'article en réalisant la partie *in vitro* ainsi que la majeure partie des expériences *in vivo,* des quantifications et des analyses nécessaires pour les révisions de l'article. J'ai également pris part à la rédaction et la relecture de l'article.

Le quatrième chapitre contient quant à lui mon article principal de doctorat, intitulé « RELEASE OF THE ALARMIN INTERLEUKIN-1 ALPHA BY SPINAL CORD INJURED MICROGLIA TRIGGERS SECONDARY DEGENERATION THROUGH REACTIVE ASTROCYTES AND ENDOTHELIAL CELLS». Cette étude a été pilotée par Dr. Steve Lacroix. En tant que première auteure, j'ai participé à la conception et la réalisation

de la majeure partie des expérimentations ainsi qu'à la rédaction du manuscrit. J'ai également pu compter sur l'aide du Dr. Lacroix pour le design et l'écriture de l'article.

Enfin, le cinquième et dernier chapitre constitue une discussion autour des chapitres précédents et un retour sur les conclusions de chaque article.

Au cours de mon doctorat, outre la thématique des lésions de la moelle épinière, j'ai eu la chance de contribuer à la production de deux autres articles scientifiques :

Neuronal interleukin-1 receptors mediate pain in chronic inflammatory diseases. Benoit Mailhot, Marine Christin, Nicolas Tessandier, Chaudy Sotoudeh, Floriane Bretheau, Roxanne Turmel, Ève Pellerin, Feng Wang, Cyril Bories, Charles Joly-Beauparlant, Yves De Koninck, Arnaud Droit, Francesca Cicchetti, Grégory Scherrer, Eric Boilard, Reza Sharif-Naeini, Steve Lacroix. ***J Exp Med***. 2020 Sep 7;217(9):e20191430.

CNS endothelial cells induce an ASC-independent cleavage of monocyte-derived IL-1β during actively-induced EAE. Benoit Mailhot, Sébastien A. Lévesque, Floriane Bretheau, Jean-Philippe Gagné, Martine Lessard, Marie-Ève Janelle, Alexandre Paré, Jean-François Richard, Luc Vallières, Juan Pablo de Rivero Vaccari, Robert W. Keane, Guy G. Poirier and Steve Lacroix. Article en préparation.

Introduction

En 1948, Peter Medawar, un biologiste britannique principalement connu pour ses travaux sur le système immun et codétenteur du prix Nobel de physiologie en 1960, introduisit la notion de privilège immun, également connue sous le terme d'immuno-privilège (Medawar, 1948). Ce terme sera dès lors utilisé pour désigner certaines parties de l'organisme, telles que le système nerveux central (SNC), capables de tolérer la présence d'antigènes sans provoquer de réponse immunitaire inflammatoire. Pourtant, malgré ce statut d'immuno-privilégié, il existe une communication extrêmement importante entre le SNC et le système immunitaire, à la fois dans un contexte sain que dans un contexte physiologique. Les cellules immunitaires et les molécules neuro-immunitaires sont au cœur de la modulation des fonctions du SNC. La neuro-inflammation et la neuro-immunologie jouent donc un rôle fondamental dans un large éventail de désordres neurologiques, depuis les accidents vasculaires cérébraux (AVC) jusqu'aux maladies neurodégénératives, en passant bien sûr par les lésions de la moelle épinière (LME), principal sujet de cette thèse.

1.1 Système nerveux

1.1.1 Système nerveux central

Le SNC, comprenant l'encéphale et la moelle épinière, se divise en sept parties principales : les hémisphères cérébraux, le diencéphale, le mésencéphale, le cervelet, le pont, le bulbe et la moelle épinière. La moelle épinière étant le sujet principal de cette thèse, nous nous attarderons plus longuement à la description de cette dernière dans la section 0.1.1.2.

1.1.1.1. Cerveau

Le mésencéphale, le pont et le bulbe rachidien constituent ce que l'on appelle le tronc cérébral, localisé entre le diencéphale et la moelle épinière. Les bosses et les renflements formés par la substance grise et par la substance blanche permettent d'identifier ces différentes subdivisions du tronc cérébral. Le tronc cérébral joue un rôle essentiel dans le bon fonctionnement des activités sensorielles et motrices de la tête et du cou, tout en régulant les niveaux de conscience. Il constitue également un point de croisement important entre les

faisceaux sensitifs ascendants et les faisceaux moteurs descendants. Le cervelet se situe quant à lui au-dessus du pont, juste en-dessous du lobe occipital des hémisphères cérébraux.

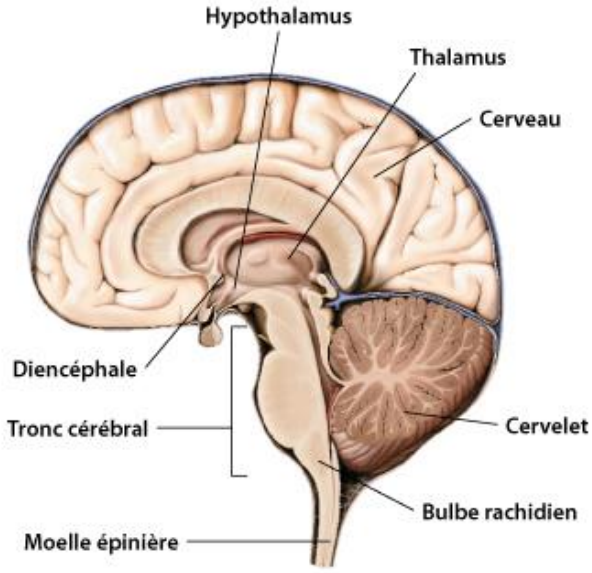

Figure 1.1. Vue sagittale médiane de l'encéphale humain. *Tirée de* : De Boeck, Neurosciences 4° édition.

1.1.1.2 Moelle épinière

La moelle épinière, protégée par la colonne vertébrale, assure la transmission du signal nerveux entre le cerveau et le reste de l'organisme. La moelle épinière et la colonne vertébrale sont toutes deux divisées en 5 régions : cervicale, thoracique, lombaire, sacrée et coccygienne.

Trente-et-une (31) paires de nerfs segmentaires émergent de la moelle épinière et sont à l'origine des nerfs périphériques innervant la plus grande partie du corps. La région cervicale se compose de 8 paires de nerfs cervicaux (C1-C8). La région thoracique comprend quant à elle 12 paires de nerfs thoraciques (T1-T12), la région lombaire comprend 5 paires de nerfs lombaires (L1-L5), la région sacrée comprend 5 paires de nerfs sacrés (S1-S5) et la région coccygienne comprend une paire de nerfs coccygiens (C1).

Le diamètre de la moelle épinière varie en fonction de la localisation. En particulier, les régions associées au traitement de l'information des membres inférieurs et postérieurs présentent un renflement correspondant à un surcroît de cellules et de connexions. Le renflement cervical comprend les segments spinaux C5-T1 et correspond à la région des

membres supérieurs. L'information des membres inférieurs est quant à elle traitée au niveau du renflement lombaire, comprenant les segments L2-S3.

La colonne vertébrale étant plus longue que la moelle épinière, il est possible d'observer un amas de fibres nerveuses au niveau des vertèbres lombaires et sacrés, correspondant aux nerfs lombaires et sacrés. C'est au niveau de cet amas, appelé queue de cheval, que sont effectuées les ponctions lombaires. En effet, le risque d'endommager la moelle étant minimisé à cet endroit, il est possible d'y insérer une aiguille afin de prélever du liquide cérébrospinal ou encore d'y injecter des anesthésiques locaux.

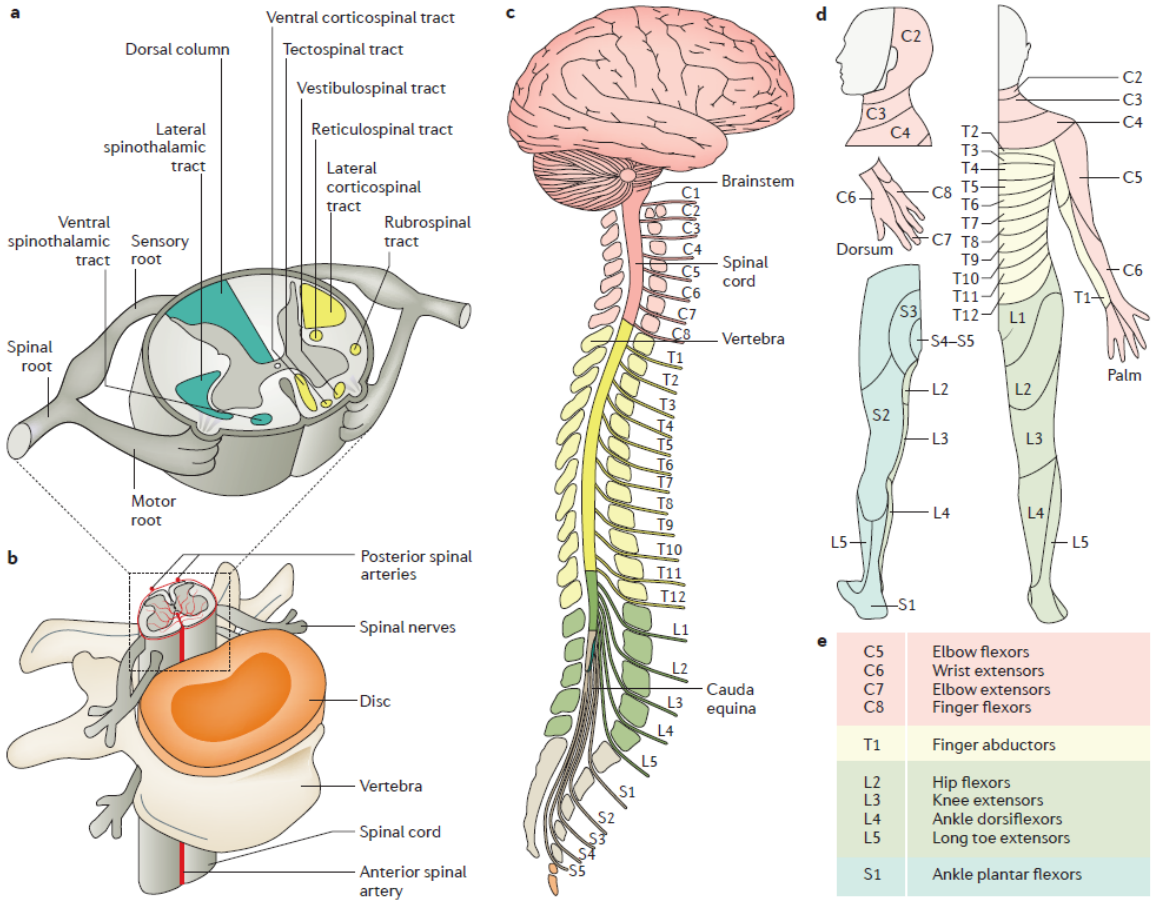

Figure 1.2 Anatomie de la moelle épinière. *Tirée de* : Ahuja et *al.* (2017)

La moelle épinière se compose de deux régions principales : la matière grise, située au centre, et la matière blanche. Au centre se trouve également le canal central, qui est contact direct avec le liquide cérébrospinal.

La matière grise est essentiellement constituée des corps cellulaires des neurones, des cellules gliales et des axones non-myélinisés. Elle se divise en plusieurs régions : les cornes dorsales (ou postérieures), latérales et ventrales (ou antérieures). Au niveau des cornes dorsales, les neurones reçoivent les informations sensorielles entrant dans la moelle épinière via les racines dorsales des nerfs spinaux. Au niveau des cornes latérales, qui sont situées essentiellement dans la région thoracique, on retrouve des motoneurones viscéraux préganglionnaires projetant sur les ganglions sympathiques. Enfin, au niveau des cornes ventrales, on retrouve les corps cellulaires des neurones moteurs qui sortent par les racines ventrales et se terminent sur les muscles striés. La matière blanche est pour sa part constituée des axones myélinisés et de cellules gliales. La myéline, produite dans le SNC par les cellules appelées oligodendrocytes, favorise la propagation des potentiels d'action des axones ascendants et descendants. La myéline humaine est constituée à 70% de cholestérol et à 30% de protéines (Brady and Siegel, 2012; Quarles, 1998), ce qui confère la couleur blanche à cette région de la moelle épinière.

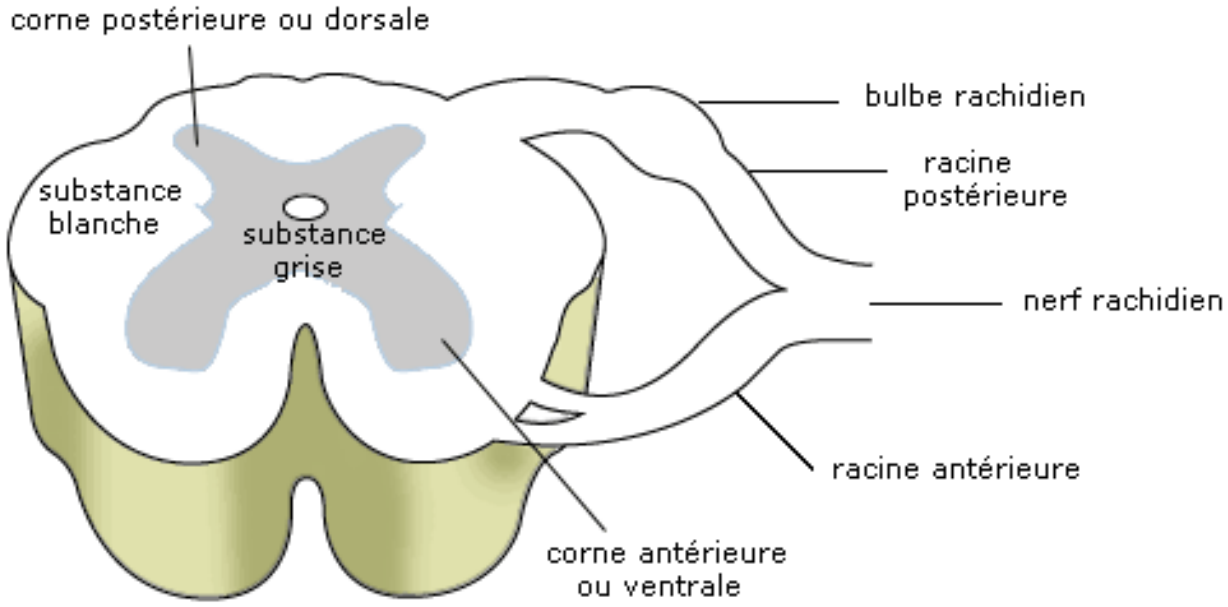

Figure 1.3 Représentation schématique d'une coupe de moelle épinière. *Tirée de* : Ahuja et *al.* (2017)

1.1.2 Système nerveux périphérique

Le système nerveux périphérique (SNP) est constitué des neurones sensitifs qui connectent les récepteurs sensoriels du corps au SNC. Deux composantes constituent la fraction moteur du SNP : le contingent moteur somatique et le contingent moteur végétatif (ou autonome). La composante somatique comprend les axones moteurs reliant l'encéphale et la moelle épinière aux muscles. Le contingent moteur végétatif est quant à lui constitué des neurones et des axones innervant les muscles lisses, le muscle cardiaque et les glandes. Le rôle de myélinisation des neurones est assuré par les cellules de Schwann.

1.1.3 Cellules du SN

L'avènement de la microscopie a permis d'initier l'idée que le SNC est un assemblage de nombreuses unités indépendantes semblables à celles constituants les autres parties de l'organisme. C'est en effet au début du XX^{ème} que Santiago Ramón y Cajal (prix Nobel en 1906) a observé que les cellules nerveuses sont des unités distinctes, communicant entre elles via des contacts spécialisés. Ces contacts, plus tard décrits et nommées synapses par Sir Charles Scott Sherrington (prix Nobel en 1932), se sont révélés être médiés par communication électrique. Le doute planant sur l'indépendance morphologique des neurones a totalement été aboli dans les années 1950 grâce aux preuves apportées par microscopie électronique. Les observations histologiques réalisées par Cajal et d'autres scientifiques ont amené à distinguer deux grandes classes de cellules constituant le SNC : d'une part, les neurones, spécialisés dans la communication intercellulaire, et d'autre part, les cellules de soutient, nommées névroglies (Somjen, 1988).

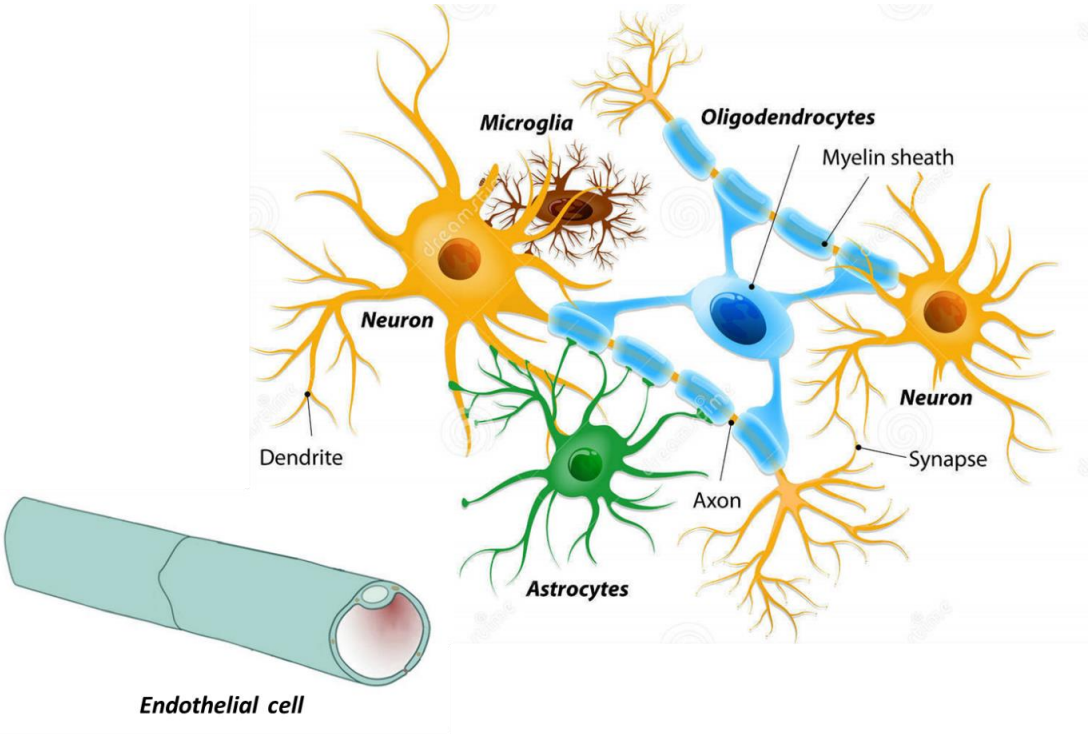

Figure 1.4 Illustration des principaux types cellulaires présents au niveau du système nerveux central. ***Adaptée de*** **: https://toxtutor.nlm.nih.gov/14-004.html.**

1.1.3.1 Neurones

Les neurones sont les cellules du SNC spécialisées dans la transmission de signaux électriques, appelés influx nerveux. Les neurones peuvent présenter une ou plusieurs ramifications issues de leur corps cellulaire, que l'on nomme dendrites. Les dendrites constituent la cible principale des signaux synaptiques provenant des autres neurones.

La grande variété de neurones se traduit par une diversité morphologique de ces cellules, allant de neurones dépourvus de dendrites jusqu'à des neurones extrêmement arborisés. Le nombre de ramifications dendritiques influe directement sur le nombre de terminaisons afférentes. Il existe trois grandes catégories de neurones : les neurones afférents, transportant l'information vers le SNC, les neurones efférents qui transmettent l'information provenant du SNC et les interneurones, qui transmettent l'information de manière locale. Les neurones sont organisés en circuits neuronaux. Parmi ceux-ci, nous distinguons les systèmes sensoriels, captant et traitant les informations de l'environnement (e.g système visuel, système auditif, …), et les systèmes moteurs permettant à l'organisme de répondre aux informations captées par les systèmes sensoriels.

1.1.3.2 Cellules gliales

1.1.3.2.1 Généralités

Les cellules gliales, également appelées névroglie ou glie, sont très différentes des cellules nerveuses et sont approximativement trois fois plus nombreuses. La névroglie regroupe plusieurs types de cellules qui ne participent pas directement à la production et à la communication du signal électrique mais qui servent de soutien aux neurones et sont donc essentielles au bon fonctionnement du SNC. En conditions normales, ces cellules ont pour fonctions de maintenir l'homéostasie, de protéger le tissu nerveux, de maintenir et de réguler les connexions synaptiques entre les neurones et d'apporter des facteurs nécessaires à la croissance et la survie neuronale. Parmi ces cellules, nous retrouvons les microglies, les oligodendrocytes et les astrocytes.

1.1.3.2.2 Microglies

Pio del Rio-Hortega a été le premier, en 1919, à observer l'existence des cellules microgliales. Il a décrit les microglies comme un groupe cellulaire d'origine mésodermale, distinct des neurones et des autres types de cellules gliales. Rio-Hortega suggéra que les microglies colonisent le cerveau à travers les vaisseaux sanguins tôt lors du développement. Les microglies sont les seules cellules immunitaires résidents de manière permanente dans le parenchyme nerveux (Prinz and Mildner, 2011; Ransohoff and Cardona, 2010). Cependant, nous avons désormais la preuve que les microglies, contrairement aux autres cellules de l'immunité innée (e.g monocytes, macrophages), ne seraient pas issues de l'infiltration via les vaisseaux sanguins. Les microglies proviennent de progéniteurs érythro-myéloïdes issus du sac vitellin embryonnaire et colonisent le SNC au stade embryonnaire 8.5 chez la souris (Ginhoux et al., 2010; Perdiguero et al., 2015). De plus, contrairement aux cellules de la moelle osseuse qui ne vivraient que quelques semaines, la durée de vie des microglies serait tangiblement plus importante (Ginhoux et al., 2010; Perdiguero et al., 2015).

Au cours du processus de colonisation du SNC, les microglies expriment certains facteurs spécifiques aux cellules myéloïdes (e.g PU.1 et Irf8), cytokines (e.g CSF), protéines adaptatrices (e.g Dap12) et récepteurs (e.g CSFR, Cx3cr1) permettant d'assurer leur développement et leur migration vers le SNC (Elmore et al., 2014; Erblich et al., 2011;

Ginhoux et al., 2010; Kierdorf et al., 2013; Squarzoni et al., 2014). Chez l'adulte, en conditions physiologiques, les microglies sont des cellules ramifiées (del Rio-Hortega, 1919), distribuées de manière précise, définissant une zone bien définie. Avec un faible taux de renouvellement, le nombre de microglies reste relativement stable, dépendamment la zone du SNC (Ajami et al., 2007; del Rio-Hortega, 1919; Lawson et al., 1992, 1990). Comme précédemment évoqué, les microglies constituent les macrophages résidents du SNC. De ce fait, chaque cellule microgliale est responsable d'un territoire spécifique qu'elle va surveiller (Nimmerjahn et al., 2005; Parkhurst et al., 2013; Sierra et al., 2010; Tremblay et al., 2010). Comme toute cellule immunitaire, les microglies sont sensibles au contrôle de l'homéostasie, leur rôle étant de maintenir le bon fonctionnement du SNC. En conditions pathologiques, les microglies sont activées et vont alors subir des transformations rapides, de l'ordre de la seconde à la minute (Ajami et al., 2007; Lawson et al., 1992, 1990). Les microglies réactives se transforment en macrophages. Cette activation entraîne l'activation de différentes voies cellulaires et se caractérise principalement par des modifications morphologiques (Haynes et al., 2006). En effet, une fois activées, les microglies perdent leurs ramifications et acquièrent une forme amiboïde caractéristique. Elles libèrent alors des facteurs pro-inflammatoires telles que des cytokines (e.g IL-1α) (Bastien et al., 2015; Luheshi et al., 2011b). Le phénotype des microglies activées est très similaire à celui des macrophages dérivés des monocytes (MDMs) qui infiltrent le SNC après une LME. Le devenir des cellules microgliales à la suite d'une LME sera décrit plus précisément dans la section 0.3.2.

1.1.3.2.3 Oligodendrocytes

La matière blanche contient des axones myélinisés assurant la communication entre des régions distantes du cerveau. Les feuillets de myéline entourant ces axones sont essentiels afin d'assurer une communication efficace. En effet, la myéline assure une propagation rapide et efficace des potentiels d'action tout en servant de support trophique et de protection aux neurones (Fünfschilling et al., 2012; Saab et al., 2016).

Au niveau du SNC, ce sont les oligodendrocytes qui assurent la production de la myéline. Les oligodendrocytes, qui ont fait l'objet de nombreuses études depuis leur identification par Pio del Rio-Hortega, en 1921 (Bergles and Richardson, 2016; Pérez-Cerdá et al., 2015), sont des cellulles issues de la différentiation de précurseurs d'oligodendrocytes (*oligodendrocyte*

precursor cells, OPCs). Les OPCs, dérivés de cellules souches nerveuses (*neural stem cells*, NSC), se différencient alors en oligodendrocytes immatures pré-myélinisants (premyelinating oligodendrocytes, pre-Ols) puis finalement en oligodendrocytes matures qui débutent la production de myéline au contact des axones neuronaux (Emery, 2010). Les OPCs proviennent essentiellement des zones neuro-épithéliales environnant les ventricules (Schoenwolf and Alvarez, 1989). En effet, à la suite de la gastrulation et de la spécification ectodermique, les cellules neuroépithéliales se forment et croissent le long de l'axe neural, formant ce qui deviendra les ventricules (Schoenwolf and Alvarez, 1989). Au niveau de ces zones, les NSC se différencient et donnent successivement les neurones, les cellules gliales radiales, les astrocytes et les progéniteurs à bi-potentiel astrocytes-oligodendrocytes qui coloniseront ultérieurement le SNC (Huttner and Brand, 1997; Jan and Jan, 2001). Ces derniers s'engagent dans la lignée des oligodendrocytes sous l'influence de facteurs de transcription tels que Olig1, Olig2, Nkx2.2 et Sox10 (Emery, 2010). Une autre origine possible des OPCs au cours du développement serait les cellules gliales radiales (Casper and McCarthy, 2006; Merkle et al., 2004).

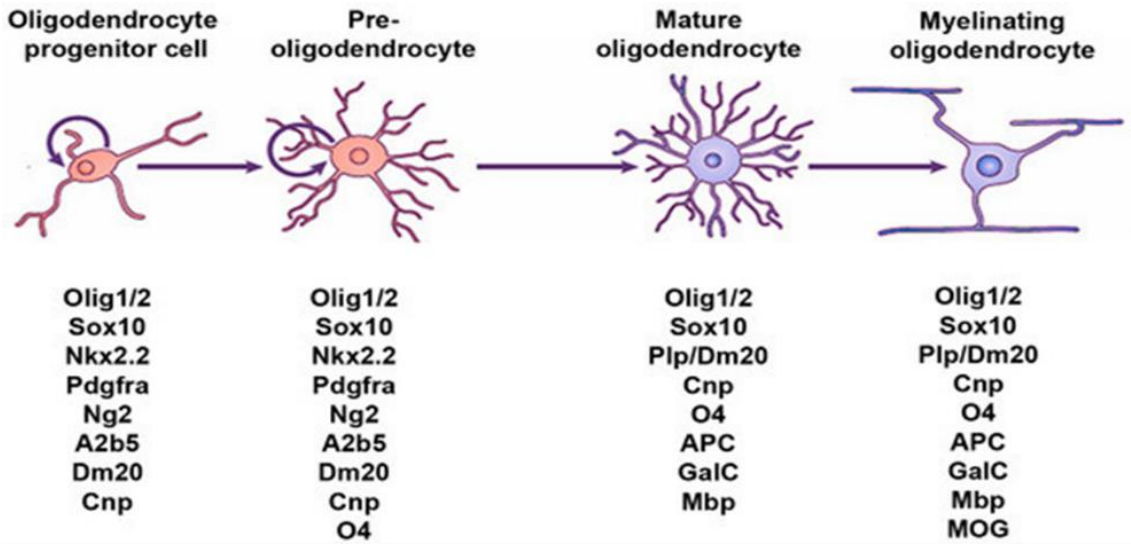

Figure 1.5. Stade de différentiation des cellules de la lignée oligodendrogliale. *Tirée de :* Traiffort et *al.* (2016).

Au niveau de la moelle épinière, les OPCs peuplent la moelle en développement au cours de trois vagues successives. Les premiers OPCs apparaissent à E12.5 chez la souris et sont issus du domaine neuronal prémoteur ventral (pMN) (Orentas et al., 1999; Ravanelli and Appel, 2015; Richardson et al., 2000). Cette première vague se déroule sous le contrôle de l'expression ventrale de Sonic hedgehog (SHH), qui contrôle *Nkx6.1* et *Nkx6.2* et régule la transcription d'*Olig1* et *Olig2* (Orentas et al., 1999; Vallstedt et al., 2005). Il est intéressent de noter que la signalisation de SHH est suffisante pour induire l'expression d'*Olig1* et d'*Olig2* et, de ce fait, générer des OPCs (Lu et al., 2000). A E15.5, une deuxième vague d'OPCs est générée à partir des domaines précurseurs dorsaux de la moelle épinière, indépendamment de l'expression de SHH (Cai et al., 2005; Fogarty et al., 2005; Vallstedt et al., 2005). La génération de ces cellules est sous le contrôle de *Dbx1* et *Ascl1* et requiert également une induction de la signalisation du *fibroblast growth factor* (FGF) et une diminution de la signalisation de la *bone morphogenetic protein* (BMP) (Fogarty et al., 2005; Sugimori et al., 2008). Les OPCs de la moelle épinière issus de la première et de la deuxième vague se répartissent le long de la moelle épinière. Toutefois, compte tenu de leur retard de génération, les OPCs dérivés de la vague dorsale ne représentent que 10 à 20% des OPCs de la moelle épinière, le reste étant issu de la vague ventrale (Erblich et al., 2011; Fogarty et al., 2005; Vallstedt et al., 2005). Finalement une troisième vague de production des OPCs se déroule lors de la naissance, provenant à la fois de la prolifération des progéniteurs résidents issus des première et deuxième vagues et de l'arrivée de nouveaux progéniteurs issus du canal central (Rowitch and Kriegstein, 2010).

Au niveau du cerveau antérieur, la génération des OPCs suit un processus similaire à ce qui se passe au niveau de la moelle épinière (Rowitch and Kriegstein, 2010; Woodruff et al., 2001). Tout comme dans la moelle épinière, l'expression de SHH induit la production initiale des progéniteurs gliaux à la suite de la période de neurogénèse (Kessaris et al., 2006; Nery et al., 2001; Orentas et al., 1999). Ces OPCs migrent ensuite de manière tangentielle et dorsale afin de coloniser la totalité du cerveau antérieur (Kessaris et al., 2006; Klämbt, 2009). Quelques jours plus tard, une deuxième vague d'OPCs émerge du cerveau antérieur médian sous le contrôle transcriptionnel de *Gsh2* et migre de manière dorsale jusqu'au cortex (Kessaris et al., 2006; Klämbt, 2009). Enfin, une troisième vague de production d'OPCs survient juste avant la naissance, tirant son origine de la zone dorsale sous-ventriculaire

(SVZ) vers le corps calleux (Kessaris et al., 2006). Les origines des OPCs des structures profondes du cerveau n'ont pas été étudiées de manière exhaustive. Il est probable que ces OPCs dérivent également des régions neuro-épithéliales entourant les ventricules, depuis lesquelles ils migrent vers les régions profondes avant de proliférer (van Tilborg et al., 2018).

De nombreuses molécules sont impliquées dans le processus de migration des OPCs. Parmi celles-ci, notons par exemple les gradients tissulaires de BMPs, SHH et de *Wingless-type mouse mammary tumor virus integration site* (Wnt) qui déterminent la direction de migration des OPCs (van Tilborg et al., 2018). Certains facteurs de croissance influencent également la migration des OPCs, tels que *platelet-derived growth factor* (PDGF), *vascular endothelial growth factor* (VEGF), *fibroblast growth factor* (FGF) ou encore *hepatocyte growth factor* (HGF) (Bribián et al., 2006; Hayakawa et al., 2011).

Au cours du développement, les OPCs répondent à des signaux stimulant la prolifération mais également inhibant la différentiation. Parmi les signaux inhibant la différenciation des OPCs, notons par exemple PDGF, Notch ou encore Wnt. Ces molécules de signalisation extracellulaires entraînent l'expression de facteurs de transcription inhibant la différentiation, tels que *DNA-binding protein inhibitor 2* (Id)2, Id4 et Hes5 (Genoud et al., 2002; Givogri et al., 2002; Hammond et al., 2015; Kremer et al., 2011; Wang et al., 1998). Lorsque que la prolifération des OPCs permet d'atteindre l'équilibre souhaité, l'inhibition de la différentiation est levée. Les OPCs peuvent alors se différencier en pré-Ols puis finalement en Ols matures myélinisants sous l'influence de facteurs de transcription capables de promouvoir la différentiation tels que *myelin regulatory factor* (Myrf) (Bujalka et al., 2013). Lorsque cet équilibre est modifié à la suite de mort cellulaire ou de migration, la prolifération des OPCs dans les zones déficitaires est stimulée afin de rééquilibrer le nombre d'OPCs (Hughes et al., 2013).

1.1.3.2.4 Cellules dendritiques/Astrocytes

Les astrocytes sont les cellules les plus abondantes du SNC. Ils ont pour rôle de fournir un support trophique aux neurones, de promouvoir la formation et la fonction des synapses et d'éliminer les synapses par phagocytose (Chung et al., 2013; Clarke and Barres, 2013; Konishi et al., 2020; Liddelow and Barres, 2015; Sofroniew and Vinters, 2010). De plus, de par leur rôle essentiel dans la régulation du glutamate ou encore dans la régulation des ions

d'hydrogène et de potassium (Chen and Swanson, 2003), les astrocytes participent activement au maintien de l'homéostasie et à la survie des neurones et des autres cellules gliales. Les astrocytes jouent aussi un rôle essentiel dans le maintien de l'étanchéité de la barrière hémato-encéphalique (Abbott et al., 2006; Bush et al., 1999). Ils interagissent de manière étroite avec les cellules endothéliales et péricytes.

Lorsque des dommages sont causés au SNC, ou dans le cas de certaines maladies, les astrocytes peuvent se transformer en un type cellulaire réactif. Cette transformation, appelée astrocytose réactive, se caractérise par la surexpression de certains gènes (Anderson et al., 2016; Zamanian et al., 2012). Les astrocytes activés vont alors produire et libérer différentes cytokines et chimiokines (John et al., 2005). En effet, les astrocytes présentent à leur surface des récepteurs spécialisés dans la reconnaissance d'agents pathogènes ou de signaux de danger, appelés *pattern recognition receptors* (PPRs) (Jack et al., 2005), faisant donc d'eux des acteurs importants du processus de neuro-inflammation. En particulier, les astrocytes expriment fortement TLR3 ainsi que de faibles niveaux de TLR1, 4, 5 et 9 (Jack et al., 2005). La signalisation via le TLR3 entraîne la production d'IL-6, de CXCL10 et d'IFN-β par les astrocytes, ce qui contribue à stimuler l'inflammation (Jack et al., 2005).

Liddelow et ses collaborateurs, (Liddelow et al., 2017b) ont caractérisé par séquençage de l'ARN les profils d'expression des astrocytes de type 1 (A1), dits « réactifs », et des astrocytes de type 2 (A2), présents en conditions normales. Il a été démontré que les astrocytes A1 sont pro-inflammatoires et capables de produire des molécules causant la mort des neurones et des oligodendrocytes. La production combinée d'IL-1α, de TNF et de C1q par les microglies activées est capable d'induire le phénotype A1. Le phénotype A2 serait quant à lui neuroprotecteur.

L'existence des astrocytes A1 et A2 est toutefois remise en question aujourd'hui. De même, la question à savoir si les astrocytes ont un rôle bénéfique ou néfaste dans le cas d'une atteinte aiguë au SNC, par exemple lors d'une LME, reste encore sujet à débat. Cette question sera discutée dans la section 1.3.2.

1.1.3.3 Péricytes

Les péricytes sont localisés au niveau de la base de la membrane des capillaires sanguins. Ils sont un composant essentiel de l'unité vasculaire cérébral, constituée également des cellules

endothéliales, des cellules gliales et des neurones (Winkler et al., 2011). Les péricytes représentent une population cellulaire très hétérogène, aussi bien en termes de morphologie que de fonctions. C'est pourquoi l'identification précise de ce qu'est un péricyte est encore sujette à débats (Attwell et al., 2016; De Souza et al., 2016).

Parmi les nombreuses fonctions assurées par les péricytes, on retrouve en particulier la participation à la formation de la barrière hémato-encéphalique (BHE), la cicatrisation non-gliale ou encore la régulation du débit sanguin cérébral (Rustenhoven et al., 2017). Des études récentes ont permis de mettre en évidence que les péricytes joueraient également un rôle important dans la régulation du processus neuro-inflammatoire au niveau de l'unité vasculaire (Jansson et al., 2014; Kovac et al., 2011; Voisin et al., 2010). En effet, les péricytes remplieraient certains rôles normalement attribués aux cellules immunitaires tels que de produire des molécules inflammatoires et de répondre à celles-ci (Kovac et al., 2011), présenter des antigènes (Gasque et al., 1998) et même de phagocyter (Bell et al., 2011; Winkler et al., 2011).

1.1.3.4 Cellules endothéliales

La BHE est un élément essentiel du SNC. En effet, cette unité vasculaire, principalement constituée de cellules endothéliales, assure la croissance et la survie des cellules résidentes du SNC en leur apportant les éléments indispensables tels que le glucose, tout en jouant un rôle de barrière imperméable assurant la sécurité et l'intégrité du SNC. Cette imperméabilité des vaisseaux est assurée par la formation de jonctions serrées et adhérentes entre les cellules endothéliales, formant des liens empêchant les éléments étrangers de pénétrer dans le SNC.

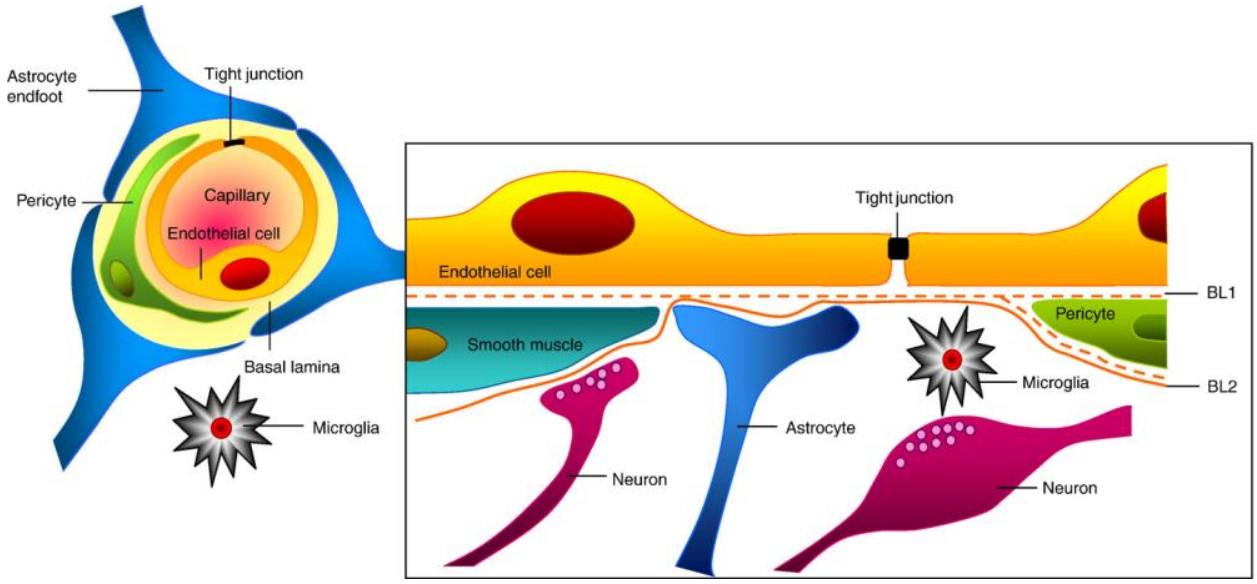

Figure 1.6 Structure et fonction de la barrière hématoencéphalique. *Tirée de* : Abott et *al.* (2006).

La perte de l'imperméabilité de la BHE est un élément crucial dans la pathogénèse de différentes affections du SNC. C'est en effet une caractéristique commune à un large éventail de neuropathologies, telles que les maladies neurodégénératives comme la sclérose en plaques (Graesser et al., 2002; Heye et al., 2014; Lévesque et al., 2016) et la maladie d'Huntington (Di Pardo et al., 2017; Sweeney et al., 2018), ou de lésions du SNC, comme c'est le cas lors des LME (Paul M Carvey, Bill Hendey, 2009; Sweeney et al., 2018). La perte d'intégrité de cette membrane constitue une porte d'entrée au SNC, d'une part pour les différents pathogènes qui pourraient se retrouver dans la circulation sanguine, mais également pour les cellules immunitaires de la périphérie. À ce sujet, une inflammation massive et non contrôlée dans le SNC pourrait s'avérer néfaste. Il est donc indispensable de mieux comprendre les mécanismes de contrôle de l'étanchéité de la BHE et d'essayer de trouver des moyens efficaces de réguler celle-ci afin de mieux contrôler le processus inflammatoire tout en permettant à l'organisme de se défendre en présence de pathogènes.

Différents éléments peuvent être à l'origine de cette perte d'étanchéité de la BHE, dépendamment du type de pathologie et de la sévérité mis en cause. Concernant les LME, le choc violent est en lui seul suffisant pour rompre la barrière (Tator, 1995; Tator and Koyanagi, 1997). Les événements qui s'en suivent et qui seront décrits dans les paragraphes à venir ont pour effet d'accroitre cette perméabilité par la libération de facteurs qui activent les cellules endothéliales et les rendent perméables aux cellules immunitaires (Schnell,

1999). Dans d'autres types de pathologies, telles que la sclérose en plaques (SEP), l'ouverture de la BHE n'est pas due à un choc, mais simplement à la libération de certains facteurs agissant directement sur les cellules endothéliales. Dans une étude menée au sein de notre laboratoire (Lévesque et al., 2016), nous avons montré que l'interleukine-1 beta (IL-1β) libérée par les cellules inflammatoires est capable d'activer les cellules endothéliales du SNC. Cette activation conduit à l'expression par ces cellules de molécules d'adhésion des cellules immunitaires et de la diminution des jonctions serrées.

1.2 Inflammation, immunité et SNC

1.2.1 Généralités

La première description du processus inflammatoire a été dressée par le romain Aulus Cornelius Celsus, il y a de cela 2000 ans. Dans « le traité de Celsus sur l'inflammation », Celsus rapporte les caractéristiques suivantes : *rubor* (rougeur), *calor* (chaleur), *tumor* (gonflement), *dolor* (douleur). En 1858, Rudolf Virchow ajoute à cette description la caractéristique de *functio laesa* (impotence fonctionnelle), s'inspirant de recherches précédemment menées à Wutzbourg.

De manière générale, l'inflammation désigne de nos jours la réaction que le système immunitaire met en place afin de faire face à une agression externe (par exemple : bactérie, virus) ou interne (par exemple : cellules cancéreuses). Elle regroupe l'ensemble des réponses impliquant les cellules immunitaires et leurs médiateurs. Dans le cas d'une inflammation médiée par un pathogène, l'inflammation sera dite non-stérile, en opposition à une inflammation stérile qui n'implique aucun microbe. Le système immunitaire regroupe un grand nombre de cellules distinctes aux fonctions elles aussi bien différentes. Ces médiateurs cellulaires de l'inflammation peuvent être regroupés en deux grandes catégories : les cellules de l'immunité innée, également appelées myéloïdes, et les cellules de l'immunité adaptative, dites lymphoïdes. Dans les deux cas, le contrôle de l'agression repose sur la coordination efficace des réponses immunitaires innée et adaptative.

L'immunité innée est la première ligne de défense de l'organisme contre les pathogènes. Outre les barrières naturelles physiques et mécaniques, telles que la barrière

épithéliale ou le pH gastrique, les cellules immunitaires innées sont des éléments essentiels de cette réponse innée. Cette réponse repose également sur la présence de certaines protéines, comme les protéines du système du complément, ou de divers médiateurs, tels que les cytokines, jouant un rôle crucial dans la régulation et coordination de l'inflammation.

1.2.2 Réponse immunitaire innée

L'immunité innée constitue la première ligne de défense contre les agents infectieux et pathogènes qui nous entourent. La réponse immunitaire primaire est induite par un signal de danger qui est émis à la suite de l'interaction spécifique entre des récepteurs du soi, les *pattern recognition receptors* (PRR), et des motifs moléculaires spécifiques, associés soit au non soi, soit à un signal de danger interne à l'organisme (Takeuchi and Akira, 2010). Le signal de danger induit permet alors le recrutement des cellules de l'immunité innée qui sont les premiers répondants au foyer inflammatoire et assurent la mise en place de l'immunité adaptative.

1.2.2.1 PRR

Les PRR sont au cœur de l'initiation de la réponse immunitaire primaire. Ces récepteurs sont en effet capables de reconnaître des patrons moléculaires associés au danger (*danger-associated molecular patterns*, DAMP) ou aux pathogènes (*pathogen-associated molecular patterns*, PAMP) (Takeuchi and Akira, 2010), envoyant ainsi au corps le signal de déclencher une réponse adéquate. Les PPR sont des protéines principalement exprimées par les cellules du système immunitaire inné, telles que les cellules dendritiques, les macrophages, les monocytes, les neutrophiles et les cellules épithéliales (Lewis et al., 2002; Schroder and Tschopp, 2010). Afin de détecter la plus grande variété de DAMP et PAMP possibles, les PRR sont exprimés dans différents compartiments cellulaires tels que la membrane cytoplasmique, les endosomes et le cytoplasme. Parmi les plus grandes classes de PRR, nous retrouvons les *Toll-like receptors* (TLR), les *Retinoic acid-inducible (RIG)-I-like receptors* (RLR) les *NOD-like receptors* (NLR) et les *C-type lectin receptors* (CLR). Les TLR et NLR sont capables de lier des ligands aussi bien endogènes qu'exogènes. Les RLR et les CLR reconnaissant quant à eux des patrons moléculaires essentiellement d'origine bactérienne, virale ou fongique (Chen and Nuñez, 2010; Netea et al., 2011; Takeuchi and Akira, 2010).

La reconnaissance par le PRR d'un signal de danger entraîne une augmentation de l'état inflammatoire de la cellule qui l'exprime, déclenchant en particulier la production de cytokines, chimiokines et médiateurs lipidiques permettant le recrutement de différents types de cellules immunitaires (Takeuchi and Akira, 2010).

Le recrutement des cellules immunitaires au foyer inflammatoire se déroule en plusieurs étapes bien distinctes.

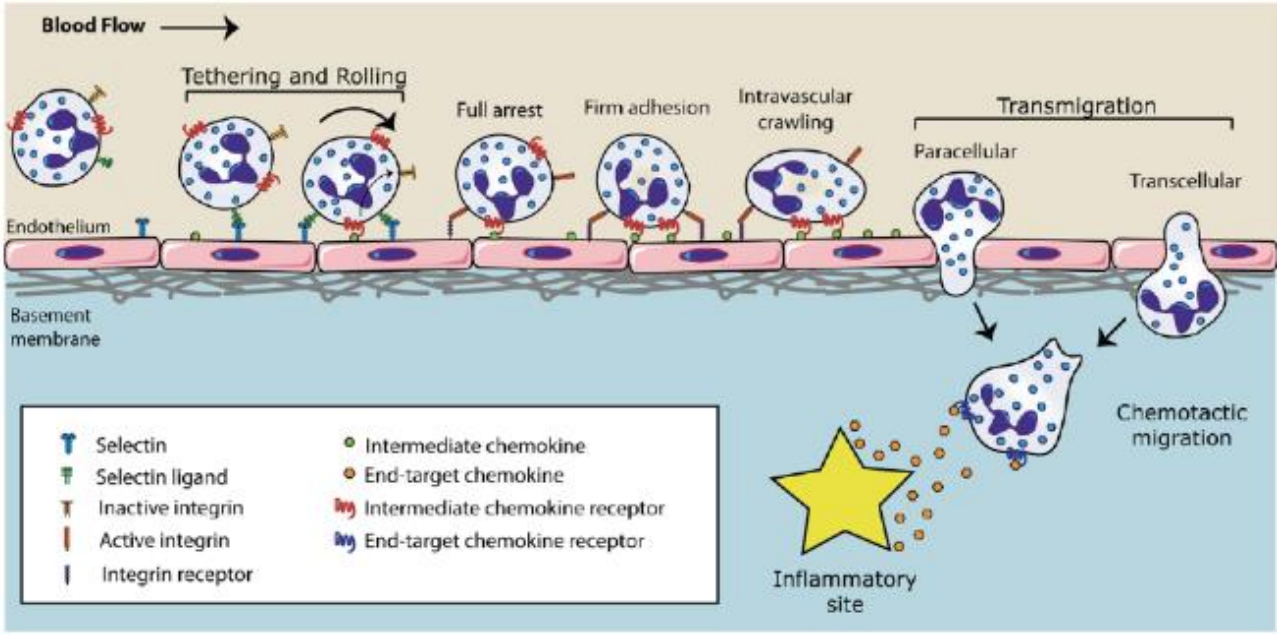

Figure 1.7 Etapes impliquées dans la migration des leucocytes vers le foyer inflammatoire. *Tirée de* : Deniset et Kubes (2016).

Dans un premier temps, l'attachement des cellules immunitaires en circulation aux vaisseaux est faible, et ces dernières subissent un phénomène de roulement (*rolling*) médié par des sélectines. Ensuite, les différentes cytokines exprimées au niveau la zone d'inflammation activent des intégrines qui assurent l'arrêt des leucocytes sur l'endothélium. Les leucocytes vont ensuite ramper à la surface des cellules endothéliales (*crawling*) jusqu'à un site favorable à leur transmigration. Une fois dans le tissu, un gradient de cytokines guide les leucocytes vers le foyer inflammatoire (Kubes and Deniset, 2016; Ley et al., 2007).

1.2.2.2 Cellules de l'immunité innée

Le principal groupe cellulaire de l'immunité innée est le groupe des phagocytes. Les phagocytes appartiennent à deux lignées majeures : les monocytes/macrophages et les granulocytes polymorphonucléaires. Les granulocytes polymorphonucléaires regroupent les neutrophiles, les éosinophiles et les basophiles.

❖ Neutrophiles

Les neutrophiles, également appelés neutrophiles polymorphonucléaires (PMN), sont issus des cellules souches hématopoïétiques dont la production est stimulée par le facteur de croissance granulocytaire (G-CSF) dans la moelle osseuse. Il est d'ailleurs intéressant de noter que le G-CSF est le traitement le plus couramment utilisé pour traiter les patients atteints de neutropénie ou sujets à des infections opportunistes à la suite de chimiothérapies (Jansen et al., 2005). Les neutrophiles représentent 95% des granulocytes circulant et constituent 60 à 70% des leucocytes totaux circulants chez l'humain. Avec une demi-vie de 5,4 jours dans le sang, les neutrophiles sont des cellules immunitaires de durée de vie courte. Ils mesurent de 10 à 20 µm et possèdent un noyau plurilobé.

Acteurs de l'immunité innée et originellement décrits comme cellules bactéricides, les neutrophiles sont les premiers à être recrutés au site infectieux ou lésionnel. Ils détectent des stimuli chimiotactiques tels que des fragments protéiques provenant de l'activation du complément (C5a), des produits des autres cellules immunitaires, ou encore des éléments d'origine bactérienne. Les neutrophiles forment des réseaux de fibres extracellulaires appelés *neutrophil extracellular traps* (NET) capables de tuer les bactéries. Ces réseaux sont principalement composés d'ADN provenant des neutrophiles et d'enzyme protéolytiques (Brinkmann et al., 2004). Ils répondent en particulier à deux chimiokines : *C-X-C motif ligand 1* (CXCL1) et *C-X-C motif ligand 2* (CXCL2) via la liaison à leur récepteur CXCR2 (Borregaard, 2010; Mayadas et al., 2014).

Dans le contexte d'une LME, les neutrophiles sont les premières cellules à être recrutées au site de la lésion (Fleming et al., 2006; Popovich et al., 1997; Stirling and Yong, 2008a), dès 6 heures suivant la lésion. Le nombre de neutrophiles au site lésionnel atteint un pic aux alentours de 24 heures post-lésion dans le modèle murin et leur présence devient quasiment inexistante 4 jours suivant la LME (Fleming et al., 2006; Popovich et al., 1997;

Stirling and Yong, 2008a). Toutefois, certaines études suggèrent qu'une seconde vague d'infiltration de neutrophiles se déroulerait entre 14 et 35 jours après la lésion, mais principalement localisée au niveau des méninges et du CSF (Popovich et al., 1997; Stirling and Yong, 2008b).

De façon similaire aux astrocytes et à la cicatrice gliale, le rôle des neutrophiles dans le contexte des LME reste extrêmement controversé. Leur implication dans le contexte des LME sera développé dans la partie 1.3.3.2 Rôles des cellules immunitaires.

❖ Monocytes/Macrophages

Parmi les autres phagocytes de l'immunité innée, on retrouve les monocytes, au niveau du sang, et les macrophages, localisés au niveau des tissus. Les monocytes dérivent des cellules souches hématopoïétiques (*hematopoietic stem cells*, HSCs) résident dans la moelle osseuse et la rate (Geissmann et al., 2010). Le système hématopoïétique assure un auto-renouvellement constant de la réserve de monocytes sanguins. Les deux principales classes de monocytes retrouvées chez la souris sont les monocytes pro-inflammatoires dits M1 et les monocytes anti-inflammatoires dits M2. Les M1, caractérisés par le profil d'expression $Ly6C^{hi}CCR2^{hi}Cx3Cr1^{lo}$, produisent des cytokines pro-inflammatoires (IL-1β, IL-6, IL-12, TNF) et peuvent avoir des effets neurotoxiques. Les M2, $Ly6C^{lo}Cx3Cr1^{hi}$ jouent quant à eux un rôle dans la résolution de l'inflammation via la libération de cytokines anti-inflammatoires (IL-10, IL-13) (Brown et al., 2014; Wynn et al., 2013; Zhou et al., 2014). Les macrophages M2 facilitent également la croissance axonale et la remyélinisation via la production de facteurs de croissances et de facteurs neurotrophiques (Barrette et al., 2008; Hashimoto et al., 2005; Kigerl et al., 2009; Miron et al., 2013; Richardson and Lu, 1994). Il est intéressant de noter que les macrophages-dérivés des monocytes (MDMs) ont un profil d'expression similaire aux microglies, caractérisés avec des marqueurs tels Iba-1, F4/80, CD68 (ED-1) et Cx3Cr1.

1.2.3 Réponse immunitaire adaptative

Les cellules présentatrices d'antigènes sont essentielles à l'activation des lymphocytes et constituent donc l'interface entre l'immunité innée et l'immunité adaptative. Les cellules

présentatrices d'antigènes (CPA) peuvent être des macrophages, des cellules dendritiques ou des lymphocytes B. Les CPA présentent les peptides antigéniques via les protéines du complexe majeur d'histocomptabilité (CMH) présents à leur surface. Les CMH sont spécifiques à chaque individu et ne peuvent donc qu'activer les lymphocytes de l'individu de qui ils proviennent, sinon ils sont détectés comme des étrangers et déclenchent une réponse innée. Un grand nombre de lymphocytes est produit chaque jour au niveau des organes lymphoïdes primaires comme le thymus et la moelle osseuse. Les lymphocytes migrent ensuite vers les organes lymphoïdes secondaires (rate, ganglions lymphatiques et tissus lymphoïdes associés aux muqueuses).

Les lymphocytes sont divisés en deux grandes classes : les lymphocytes T et les lymphocytes B. Il existe différents types de lymphocytes T, caractérisés par l'expression du marqueur CD3, exclusive à cette lignée cellulaire. Les lymphocytes T α/β se divisent en lymphocytes T CD4 helper, exerçant des fonctions auxiliaires ou stimulantes, et les lymphocytes T CD8 cytotoxiques. Il est intéressant de noter qu'une petite partie des lymphocytes T α/β n'expriment pas les marqueurs de différentiation CD4 et CD8. Ces lymphocytes T correspondraient à des cellules régulatrices. Les lymphocytes B représentent 5 à 15% des lymphocytes circulants. Au cours d'une réponse immunitaire, les lymphocytes B activés prolifèrent et se différencient en plasmocytes, cellules spécialisées dans la production d'anticorps dirigés contre les antigènes pathogéniques.

1.2.4 Facteurs pro-inflammatoires impliqués dans un contexte lésionnel

Dans le courant des années 1940, l'intérêt de Menkin et Beeson (Beeson, 1948) s'est porté sur l'étude de la pathogénèse du phénomène de fièvre. Leurs recherches ont permis de montrer que des cellules isolées à partir du péritoine de lapins pouvaient relâcher des facteurs capables d'induire de la fièvre. Trente ans plus tard, Waksman et ses collaborateurs (Dinarello, 2015; Gery and Waksman, 1972) ont décrit l'existence d'un facteur soluble, libéré par les cellules d'origine myéloïde et capable d'activer les lymphocytes, qu'ils nommèrent facteur d'activation lymphocytaire. Par la suite, ce facteur fut renommé interleukine à l'occasion du « Second International Lymphokine Workshop » qui pris place en 1979 à Ermatingen, en Suisse ("Revised nomenclature for antigen-nonspecific T cell proliferation and helper factors.," 1979).

1.2.4.1 Famille de l'interleukine 1

C'est en 1974 que Dinarello, Goldin et Wolff (Dinarello et al., 1974) ont pour la première fois montré l'existence de deux médiateurs pyrogéniques, capables d'induire un certain nombre de processus biologiques liés à l'inflammation. Ils en ont caractérisé les propriétés chimiques et biologiques et ont déterminé qu'un de ces facteurs se trouvait être produit par les leucocytes humains dérivés du sang, tandis que l'autre était d'origine neutrophilique. Les séquences d'ADNc de ces deux cytokines, localisées sur le chromosome 2 chez l'humain, furent clonées et séquencées en 1984 (Auron et al., 1984). On leur donna les noms d'interleukine-1 alpha (IL-1α) et d'interleukine-1 beta (IL-1β). Lomedico et ses collaborateurs. (Lomedico et al., n.d.) clonèrent et séquencèrent également les séquences d'origine murine en 1984. Suite à la découverte des deux premiers membres de la famille de l'IL-1, d'autres cytokines partageant des structures similaires ont été découvertes (Dinarello, 1994). Ces cytokines, dont les gènes sont tous localisés sur le chromosome 2 chez l'humain (Dinarello, 1994), présentent des propriétés aussi bien inflammatoires que dans la résolution de l'inflammation. La famille de l'IL-1 regroupe aujourd'hui 11 membres. Cette thèse portant sur l'l'IL-1α, nous nous attarderons tout particulièrement sur l'IL-1α et l'IL-1β.

1.2.4.1.1 IL-1α et IL-1β

Bien qu'elles ne partagent que de 25 à 30% d'homologie de séquence en acides aminés, l'IL-1α et l'IL-1β présentent une structure tridimensionnelle et des propriétés biologiques similaires (Dinarello, 1991; Graves et al., 1990a). Parmi les nombreux effets médiés par ces cytokines, nous retrouvons en particulier le recrutement de différents types de cellules immunitaires, l'activation des cellules endothéliales et l'extravasation des leucocytes circulants (I. Cohen et al., 2010; Rider et al., 2011, 2013a).

L'IL-1α et l'IL-1β sont toutes deux synthétisées sous forme de précurseurs (pro-formes) de poids moléculaires approximant les 31 kDa. Leurs formes matures, d'approximativement 17 kDa, interagissent avec les protéines de la famille des récepteurs de l'IL-1 (IL-1R) et déclenchent des réponses biologiques similaires. Toutefois, ces deux cytokines possèdent des caractéristiques distinctes. Alors que l'IL-1β n'est produite qu'en cas d'activation par des cellules d'origine hématopoïétique, l'IL-1α est produite dans un contexte normal par une grande variété de cellules. La pro-forme de l'IL-1β n'est pas

biologiquement active, alors qu'au contraire la pro-IL-1α l'est. Il est intéressant de noter que la forme mature de 17 kDa de l'IL-1α possède une activité inflammatoire plus importante que sa pro-forme (Afonina et al., 2011; Zheng et al., 2013). L'IL-1α est fonctionnelle tant sous forme sécrétée que liée à la membrane, alors que l'IL-1β agit seulement comme protéine secrétée. Le clivage de la pro-IL-1β requiert l'inflammasome alors que le clivage de la pro-IL-1α est indépendant de l'inflammasome.

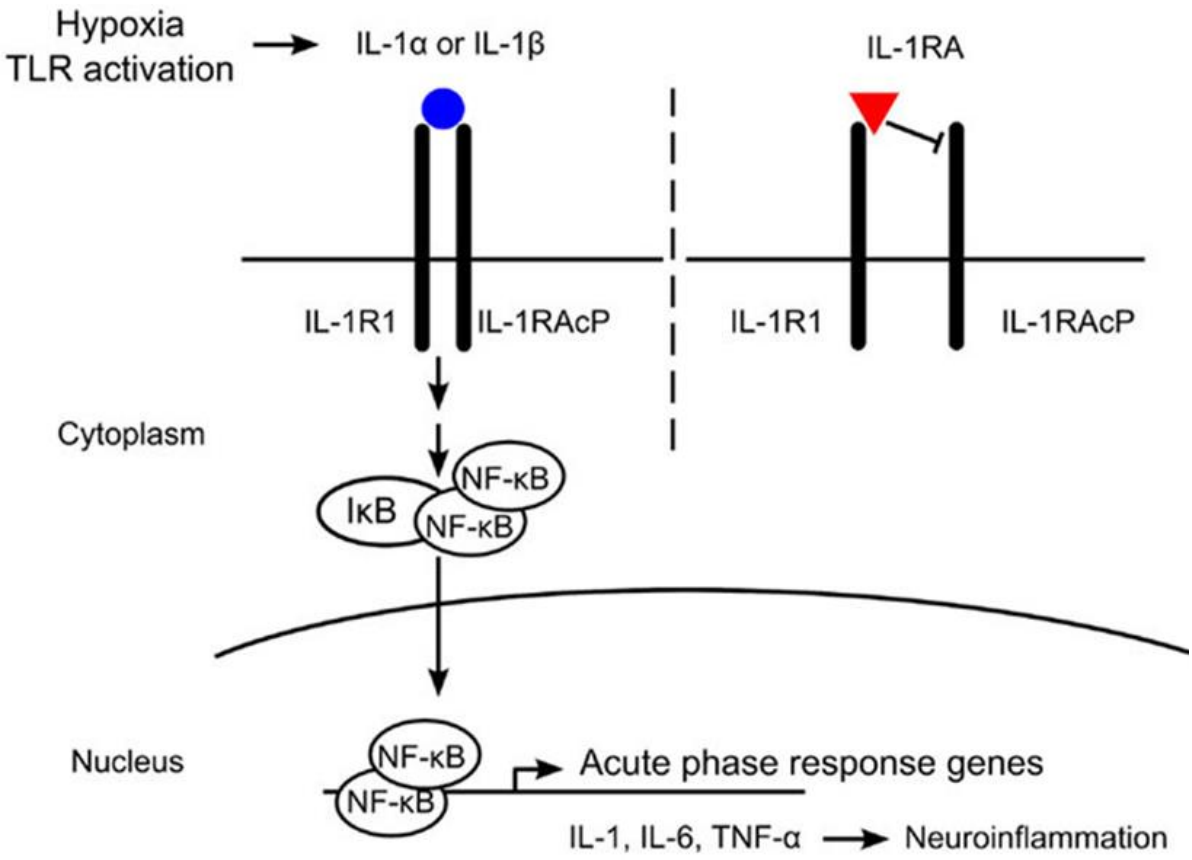

Figure 1.8 Mécanisme de signalisation de l'interleukine-1 α et β. *Tirée de* : Rosenzweig et *al.* (2014).

❖ <u>IL-1α</u>

De par sa fonction de cytokine pro-inflammatoire, l'IL-1α est un puissant médiateur de l'inflammation, lui valant son rôle d'alarmine, ou DAMP (C. J. Chen et al., 2007). L'IL-1α est exprimée de manière constitutive dans de nombreux types cellulaires dans un large

éventail de tissus sains et possède des effets nucléaires et extracellulaires bien distincts (Bersudsky et al., 2014; Garlanda et al., 2013; Rider et al., 2012). Les régions régulatrices TATA et CAAT box sont absentes dans le promoteur du gène *Il1a* et remplacées par un site de fixation pour Sp1 (McDowell et al., 2005), un facteur de transcription connu pour réguler l'expression des gènes domestiques (de l'appellation anglaise *housekeeping genes*) en conditions homéostatiques (Wierstra, 2008). Son expression peut toutefois être augmentée en réponse à des stimuli physiologiques, tels que les stress oxydatifs (McCarthy et al., 2013a, 2013b; Rider et al., 2012), la surcharge lipidique (Freigang et al., 2013; Tynan et al., 2014), une stimulation hormonale (Itoh et al., 2007), l'exposition à différentes cytokines, incluant l'IL-1α et l'IL-1β elles-mêmes (Bandman et al., 2002; Kimura et al., 1998; Weber et al., 2010), ou encore des médiateurs inflammatoires d'origine microbienne (Weber et al., 2010).

La forme précurseur de l'IL-1α présente un peptide de signalisation nucléaire fonctionnel (NLS) LKKRRL (Luheshi et al., 2009; Rider et al., 2013b; Wessendorf et al., 1993), conservé lors du clivage de la pro-IL-1α par des protéases telles que la calpaïne. Cette séquence de localisation permet la translocation de l'IL-1α cytosolique au noyau où elle régule la transcription de gènes pro-inflammatoires (Buryskova et al., 2004; Werman et al., 2004). Bien que la pro-forme et la forme clivée de l'IL-1α soient toutes deux actives, le clivage de la pro-IL-1α accroît sa capacité de signalisation (Afonina et al., 2011).

Dans les cellules apoptotiques, l'IL-1α demeure associée à la chromatine et est retenue dans les corps apoptotiques, prévenant le déclenchement du processus inflammatoire. Cependant, lorsque les cellules sont en nécrose, l'IL-1α médie alors ses effets de manière extracellulaire. En effet, l'IL-1α liée à la chromatine est relâchée par les cellules nécrotiques dans le milieu extracellulaire où elle se lie alors à l'IL-1R1 des cellules voisines, induisant un processus inflammatoire important (I. Cohen et al., 2010; Luheshi et al., 2009), qui sera décrit plus en précision dans la section 1.2.4.1.2. C'est d'ailleurs dans ce cas que l'IL-1α tient une place importante dans le processus d'inflammation stérile, qui occurrent dans certaines formes de maladies et de cancers (Afsar et al., 2018; Dinarello, 2014; Lewis et al., 2006). L'IL-1α joue en particulier un rôle dans le recrutement des cellules immunitaires primaires, neutrophiles et monocytes. En effet, plusieurs études ont montré que, dans le cas de dommages au SNC, la stimulation de la voie de la signalisation de l'IL-1R1 par l'IL-1α entraîne la production des molécules d'adhésion ICAM-1 et VCAM-1 par les cellules

endothéliales, ainsi que la libération des chimiokines CXCL1 et CXCL2, jouant ainsi indirectement un rôle de chimio-attractant pour les neutrophiles (Eigenbrod et al., 2008; Luheshi et al., 2011b; Thornton et al., 2010a). En induisant l'entrée des cellules immunitaires périphériques dans le SNC, l'activation de l'endothélium cérébral par l'IL-1α constitue une étape critique de la neuro-inflammation.

- IL-1β

Comme précédemment décrit, l'IL-1β est synthétisé sous forme de pro-forme. Toutefois, le clivage de la pro-IL-1β par la caspase-1 en une forme bioactive de 17 kDa est nécessaire pour la liaison à l'IL-1R1 (Afonina et al., 2011; Kim et al., 2013; Man and Kanneganti, 2015; Martinon et al., 2002; Mosley et al., 1987). Contrairement à l'IL-1α, l'IL-1β n'est pas produite de manière constitutive. L'expression de cette cytokine peut être induite dans différents contextes, comme c'est le cas lors d'une infection (bactérienne, fongique ou virale), d'une lésion tissulaire, d'une condition d'hypoxie ou de produits biologiques (ex. : acide urique, LPS, ATP, *etc.*). De par son rôle clé dans le processus inflammatoire et la voie des inflammasomes, l'IL-1β est impliquée dans un vaste éventail de pathologies, telles que la goutte, l'asthme, le psoriasis, l'arthrite, *etc*. En particulier, au niveau du SNC, il est connu que l'IL-1β peut affecter les cellules gliales, les cellules endothéliales et même les neurones, exprimant toutes l'IL1R1 (Allan et al., 2005; Lévesque et al., 2016; Mailhot et al., 2020). Plusieurs études menées au sein de notre laboratoire ont montré que l'IL-1β joue un rôle clé dans le développement et la progression de l'encéphalomyélite autoimmune expérimentale (EAE), un modèle murin de la SEP (Lévesque et al., 2016). En effet, des souris invalidées (*knockout*, KO) pour les gènes *Il1b* ou *Il1r1* ne présentent aucun signe de la maladie, ce qui n'est pas le cas de souris IL-1α-KO qui développent la maladie de manière similaire aux souris *sauvages* (*wild-type*, WT). En ce qui concerne les LME, bien que l'absence d'IL-1α permet une meilleure récupération des fonctions locomotrices et ce dès le premier jour suivant la lésion chez les souris *Il1a*$^{-/-}$(Bastien et al., 2015), ce n'est pas les cas chez les *Il1b*$^{-/-}$.

1.2.4.1.2 Récepteurs de l'IL-1

L'IL-1α et l'IL-1β médient leurs actions sur une grande variété de types cellulaires (Chizzonite et al., 1989). La diversité des actions de l'IL-1 est médiée par différents récepteurs.

Le récepteur le plus étudié de ces cytokines est l'IL-1R1. L'IL-1R1 possède un domaine extracellulaire combiné à un domaine cytosolique Toll-like/IL-R. Conséquemment, ce récepteur appartient à la famille des IL-1R/*Toll-like récepteur* (TLR) (O'Neill and Dinarello, 2000). L'activation de l'IL-1R1 par les cytokines de la famille de l'IL-1 conduit au recrutement du récepteur accessoire de l'IL-1 (IL-1RAcP). C'est une fois cette sous-unité assemblée au complexe IL-1/IL-1R1 que la protéine adaptatrice *myeloid differentiation factor 88* (MyD88) est à son tour recrutée. MyD88 recrute ensuite les kinases associées au récepteur de l'IL-1 (IRAKs) et le *tumor necrosis factor* (TNF) *receptor-associated factor 6* (TRAF6). Le recrutement de ces récepteurs conduit à l'activation de différents facteurs de transcription, en particulier le *nuclear factor-Kappa B* (NF-KB), ainsi qu'à l'activation de *mitogen-activated protein kinases* (MAPKs) telles que *c-Jun-N-terminal kinase* (JNK) (Dowling et al., 2008). Plus particulièrement, la cascade de signalisation IL-1R1/MyD88 stimule l'expression des chimiokines CXCL1 et CXCL2 par les astrocytes, jouant ainsi un rôle fondamental dans le recrutement des neutrophiles et des monocytes M1 pro-inflammatoires à la suite d'une LME (Pineau et al., 2010).

Il est intéressant de noter qu'il existe une isoforme de l'IL-1RAcP, l'IL-1RAcPb, possédant un domaine TIR différent et dont l'expression est limitée aux neurones du SNC (Smith et al., 2009) (Nguyen et al., 2011). Dans un contexte d'EAE, les souris déficientes pour le gène *Acpb* ont montré une neuro-inflammation plus importante, ainsi qu'une dégénérescence neuronale accrue en comparaison à des souris *WT*. L'IL-1RAcPb jouerait un rôle dans la modulation des réponses du SNC en faisant le lien entre l'inflammation et la survie neuronale.

D'autre part, différents promoteurs ont été identifiés pour le gène de l'IL-1R1. Dans une étude publiée en 2008, Chen et ses collaborateurs (Q. Chen et al., 2009) ont identifié trois sites potentiels d'initiation de la transcription en mettant à profit les techniques d'amplification de l'ADNc. Ils ont ensuite évalué le potentiel d'activation de la voie NF-κB des différents types d'IL-1R1 issus de ces séquences. Ils ont ainsi pu valider que ces trois

séquences agissent bel et bien comme des promoteurs de la transcription du gène *Il1r1*, ce qui leur a valu leur appellation de P1, P2 et P3. Notamment, au niveau du cerveau, c'est l'ARNm issu du promoteur P3 qui est préférentiellement exprimé au niveau du gyrus denté, suggérant l'existence d'une variabilité dans les fonctions assurées par l'IL-1R1 et ce dépendamment de son promoteur et de sa localisation. Le promoteur P3, adjacent à l'exon 3 du gène de l'*Il1r1*, induirait l'expression de l'IL-1R3, une forme tronquée de l'IL-1R1 (Qian et al., 2012). En effet, ces protéines sont codées par le même gène, mais possèdent des tailles significativement différentes, les 200 premiers acides aminés N terminaux de l'IL-1R1 étant absents chez l'IL-1R3. L'existence de l'IL-1R3 étant encore remise en question, il reste courant de trouver dans la nomenclature la notion d'IL-1R3 en référence à l'IL-1RAcP. Toutefois, nous utiliserons dans la présente thèse la notion d'IL-1R3 pour désigner le récepteur et nous nous restreindrons au terme IL-1RAcP pour parler de la protéine accessoire. Alors que la partie extracellulaire de l'IL-1R1 possède deux sites de liaison pour l'IL-1 (site A et site B), l'IL-1R3 possède uniquement le site de liaison B. Il s'avère également que l'IL-1R3 est capable de lier l'IL-1 seulement si la protéine accessoire IL-1RAcPb est présente. La forme IL-1RAcP ne permet pas, quant à elle, la liaison de l'IL-1 au récepteur IL-1R3. La cascade de signalisation canonique de l'IL-1 conduit à l'activation du facteur de transcription NF-KB. Toutefois, l'IL-1R3 ne stimule pas la voie de signalisation classique de l'IL-1. L'IL-1R3 interagit avec l'IL-1RAcPb pour stimuler une voie alternative de signalisation induisant l'augmentation de potassium (Qian et al., 2012).

Il existe également un autre récepteur de l'IL-1, le récepteur de type 2 de l'IL-1, IL-1R2. Ce dernier est capable de lier l'IL-1α et l'IL-1 β, mais il ne possède aucune propriété de signalisation. Il est intéressant de noter que l'IL-1α est dix fois plus affin pour l'IL-1R1 et cent fois moins affin pour l'IL-1R2 que l'IL-1β (McMahan et al., 1991; Bersudsky et al.,2014). Il est important de noter que l'IL-1R2 ne possède pas de capacité de transduction du signal, mais agit comme un inhibiteur endogène de la voie de l'IL-1 en réduisant sa biodisponibilité (Peters et al., 2013).

1.2.4.1.3 IL-1Ra

Plusieurs thérapies dans des pathologies impliquant des processus inflammatoires reposent sur l'administration de l'antagoniste de l'IL-1, IL-1Ra, afin de bloquer la signalisation de

l'IL-1R1. La forme recombinante de l'IL-1Ra disponible commercialement, anakinra, est utilisée dans de nombreux traitements cliniques contre des maladies inflammatoires telles que la fièvre familiale Européenne, l'arthrite rhumatoïde, la goutte et le diabète de type 2 (M Bersudsky et al., 2014; Dinarello, 2013; Rider et al., 2011). Dans le cas de pathologies touchant au SNC, l'administration d'IL-1Ra après un MCAO transitoire a permis de réduire la rupture de la BHE, l'infiltration de neutrophiles, l'activation de microglies et les niveaux d'IL-6 dans le cerveau (Pradillo et al., 2012). Dans les cas d'atteintes à la moelle épinière, différentes études ont montré des effets bénéfiques de l'administration de l'IL-1Ra. En effet, l'administration intrathécale chronique de l'IL-1RA réduit significativement l'apoptose et l'activation de la caspase-3 (Nesic et al., 2001). D'autre part, l'application d'une substance gélatineuse contenant de l'IL-1Ra sur la moelle épinière de rats ayant subi une contusion a permis d'améliorer de manière notable leurs fonctions motrices jusqu'à 4 semaines suivant la contusion (Zong et al., 2012). Enfin, dans un modèle murin de LME, l'administration intrathécale d'IL-1Ra réduit l'inflammation et améliore significativement la locomotion et la récupération dans le temps des souris lésées (Bastien et al., 2015).

1.2.4.1.4 Autres membres

Outre l'IL-1α, l'IL-1β et l'IL-1Ra, la famille de l'IL-1 comprend 9 autres membres dont l'IL-18, l'IL-33, l'IL-36, l'IL-37 et l'IL-38. Les fonctions de ces différentes cytokines sont résumées dans le tableau ci-dessous.

Tableau 1.1. Les membres de la famille de l'IL-1 et leurs récepteurs. *Tiré de* : Afonina et *al.* (2015).

Cytokine	Alternative Name	Receptor	Co-receptor	Inhibitory Ligands and Receptors	Main Function
IL-1α	IL-1F1	IL-1R1	IL-1RAcP	IL-1RA, IL-1R2	pro-inflammatory
IL-1β	IL-1F2	IL-1R1	IL-1RAcP	IL-1RA, IL-1R2	pro-inflammatory
IL-18	IL-1F4	IL-18Rα	IL-18Rβ	IL-18BP	pro-inflammatory
IL-33	IL-1F11	ST2 (IL-1RL1)	IL-1RAcP	sST2	pro-inflammatory
IL-36α IL-36β IL-36γ	IL-1F6 IL-1F8 IL-1F9	IL-36R (IL-1Rrp2)	IL-1RAcP	IL-36RA	pro-inflammatory
IL-37	IL-1F7	IL-18Rα	SIGIRR (TIR8, IL-1R8)	unknown	anti-inflammatory
IL-38	IL-1F10	IL-36R (IL-1Rrp2)	–	unknown	anti-inflammatory
IL-1RA	IL-1F3	IL-1R1	–	NA	IL-1R antagonist
IL-36RA	IL-1F5	IL-36R	–	NA	IL-36R antagonist

1.2.4.2 TNF

Tout comme l'IL-1, le *tumor necrosis factor* (TNF) joue un rôle essentiel dans l'initiation du processus inflammatoire. Le TNF possède deux formes actives : une forme transmembranaire et une forme soluble qui peut agir comme un régulateur autocrine ou paracrine de l'inflammation (Sriram and O'Callaghan, 2007). Le TNF est synthétisé sous la forme d'un précurseur associé à la membrane de 26 kDa qui peut ensuite être clivé en une forme mature de 17 kDa par l'enzyme *TNF-converting enzyme* (TACE ou ADAM17). Le TNF peut agir via deux récepteurs différents : le récepteur de type I du TNF (TNFR1) ou TNFR2. Ces deux récepteurs appartiennent à la super famille des TNFR et, de manière similaire à l'IL1-R1, entraînent la signalisation de facteurs de transcription tels que NF-kB, JNK, ERK-1/2, p38 et MAPK (Cabal-Hierro and Lazo, 2012). La forme soluble du TNF possède une affinité plus importante pour le TNFR1, qui possède un domaine de mort capable d'activer deux voies de signalisation opposées. La première voie implique le *TNFR-associated death domain* (TRADD), prévenant la mort cellulaire grâce à la production de protéines anti-apoptotiques. La seconde voie est quant à elle liée au TNFR2 et implique à la fois TRADD et *FAS-associated death domain* (FADD), entraînant la mort cellulaire par nécroptose et initiant l'inflammation (Micheau and Tschopp, 2003). La forme mature du TNF, mTNF, possède quant à elle une affinité plus importante pour le TNFR2.

1.2.4.3 NF-κB

La signalisation de l'IL-1 et du TNF entraîne l'activation de la voie NF-κB (Perkins and Gilmore, 2006; Schmid and Birbach, 2008; Schütze et al., 1995; Stylianou et al., 1992), une famille de facteurs de transcription jouant un rôle essentiel dans l'inflammation et l'immunité innée (Ben-Neriah and Karin, 2011; Lawrence, 2009). NF-κB représente en effet un facteur central dans l'inflammation, la réponse au stress, la prolifération et la différentiation cellulaire, de même que la mort cellulaire. Il existe deux mécanismes distincts d'activation de la voie NF-κB. La voie d'activation classique, dite canonique, est activée par des composés d'origine microbienne ou des cytokines pro-inflammatoires, comme c'est le cas de l'IL-1 et du TNF. Cette voie, passant par l'activation de complexes contenant Rel-A et IκB (revisé par (Karin and Ben-Neriah, 2000; Schmid and Birbach, 2008)), est décrite plus en détails dans le schéma ci-dessous. La voie d'activation alternative, dite non-canonique,

peut-être être activée par la grande majorité des cytokines de la famille du TNF et de la lymphotoxine β (Dejardin et al., 2002; Senftleben et al., 2001), à l'exception du TNF lui-même ainsi que CD40L et le facteur d'activation des lymphocytes B (Senftleben et al., 2001).

La voie de signalisation NF-κB peut également être influencée par d'autres facteurs de transcription (e.g. STAT3, P53, ERG), kinases (e.g. p38 ou PI3K), ROS ou mêmes des miRNAs qui modulent l'activité transcriptionnelle de NF-κB ou sa signalisation.

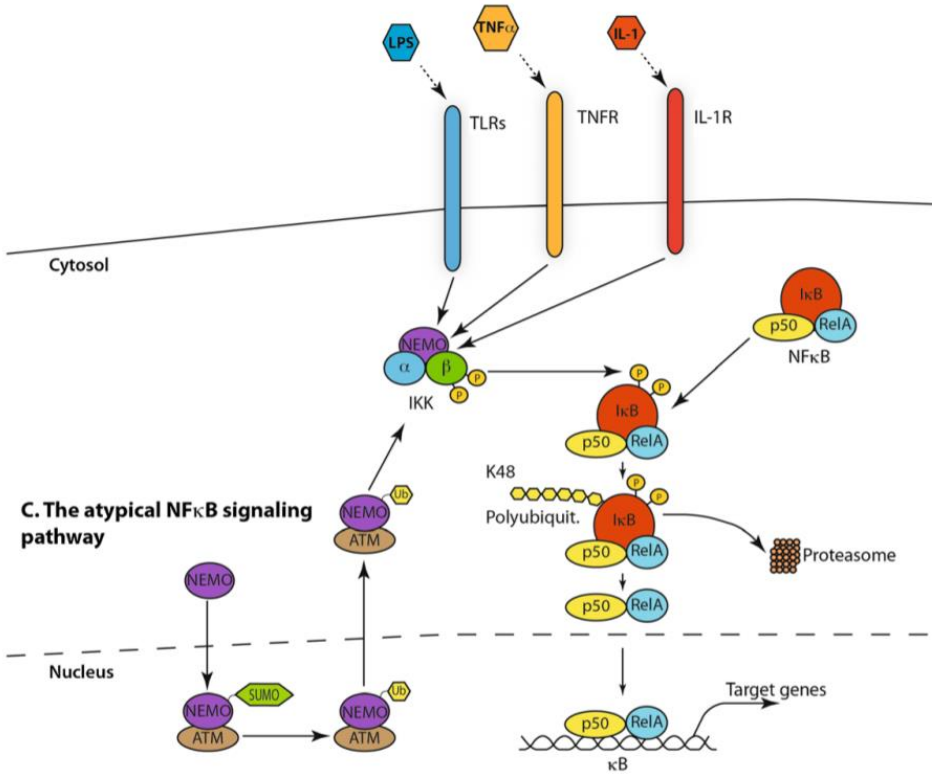

Figure 1.9 Activation canonique de la voie NF-κB. *Tirée de* : Hoesel et Schmid (2013).

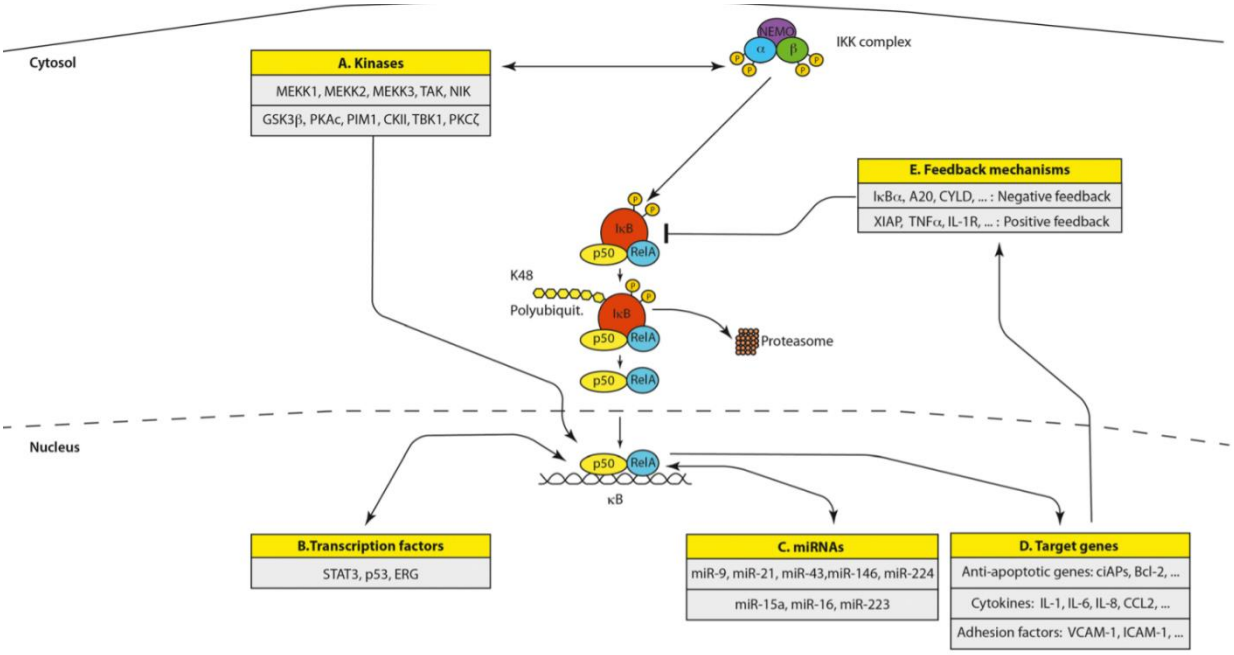

Figure 1.10 Voies de signalisation induite par l'activation de la voie NF-κB. *Tirée de* : Hoesel et Schmid (2013).

1.2.5 Facteurs anti-inflammatoires impliqués dans un contexte lésionnel

1.2.5.1 TGF-β

La superfamille du facteur de croissance transformant bêta (*transforming growth factor-beta*, TGF-β) regroupe une trentaine de ligands différents dont les TGF-βs (TGF-β1, TGF-β2 et TGF-β3), les activines, les *bone morphogenetic factors* (BMPs) ainsi que les *growth and differentiation factors* (GDFs) (Schmierer and Hill, 2007). Ces différents ligands régulent un large éventail de réponses biologiques telles que la croissance et la différentiation cellulaire, la production de protéines de la matrice extracellulaire, de même que la survie cellulaire. Les TGF-βs sont les membres les plus étudiés de cette famille, en particulier en raison de leur rôle important dans la régulation de la réponse immunitaire (Li and Flavell, 2008).

L'action des trois protéines TGF-βs est régulée via un complexe-récepteur sérine/thréonine, constitué des récepteurs de type I (TGF-βRI) et de type II (TGF-βRII). TGF-β fixe initialement TGF-βRII qui recrute ensuite TGF-βRI qui active la phosphorylation (Miyazono et al., 2000). S'ensuit la phosphorylation des protéines SMAD et la propagation

du signal (Massagué, 2000). Les TGF-βs régulent l'expression de gènes codant pour la régulation du cycle cellulaire, des facteurs de régulation, les CAMs et des médiateurs de l'inflammation (Massagué, 2000), ce qui leur confère un rôle important lors du développement et dans différentes neuropathologies (Massagué, 2000; Wyss-Coray and Mucke, 2002). En particulier, elles diminuent les niveaux d'expression de l'ARNm codant pour le facteur de transcription T-bet (Tbx21) grâce à l'interaction des protéines SMAD avec le promoteur du gène *Tbx21* (Lin et al., 2005). Conséquemment, TGF-β1 supprime l'expression de l'IFN-γ par l'intermédiaire des protéines SMAD2, SMAD3 et SMAD4 qui se lient au domaine proximal de T-bet, situé dans le locus de l'IFN-γ (Yu et al., 2006).

Bien que les propriétés anti-inflammatoires des TGF-βs ont été mises en évidence dans de nombreuses études, leur rôle dans le contexte des LME reste sujet à interrogation. Dans le contexte des LME, TGF-β1 et TGF-β2 sont toutes deux surexprimées chez l'homme et la souris. L'expression de TGF-β2 a été principalement détectée dans les astrocytes réactifs formant la cicatrice gliale ainsi que dans les cellules immunitaires infiltrantes $CD68^+$ (Buss et al., 2008; Lagord et al., 2002; McTigue et al., 2000). TGF-β1 fut quant à lui détecté dans les neurones et les cellules immunitaires (Buss et al., 2008; Lagord et al., 2002; McTigue et al., 2000). Au premier regard, il semblerait donc que TGF-β1 jouerait un rôle dans la régulation des réponses neuronales et immunitaires, alors que TGF-β2 serait impliqué dans la formation de la cicatrice gliale, en modulant la production des protéines de la matrice extracellulaire comme le collagène, la fibronectine et les CSGPG. Toutefois, la présence de la cytokine anti-inflammatoire TGF-β1 a également été détectée dans les microglies situées au niveau de la matière blanche qui dégénère (Pineau and Lacroix, 2007), ce qui pourrait laisser présager d'un rôle dans l'inhibition de la phagocytose des débris de myéline par les microglies dans un contexte de LME. En accord avec cette supposition, des cellules TGF-$\beta1^+$ ont été observées au niveau de la corne dorsale de la moelle épinière, à la jonction de la zone d'entrée des racines dorsales dans la moelle épinière, une région considérée comme étant hautement réfractaire à la repousse d'axones lésés. D'autre part, il a été démontré dans des études *in vitro* que le TGF-β1 inhibe la capacité à phagocyter la myéline des microglies (Mosley and Cuzner, 1996). L'administration intrathécale d'un anticorps neutralisant du TGF-β1 chez des rats ayant subi une LME a résulté en l'augmentation de l'expression de Iba1 dans les microglies, suggérant un niveau de réactivité plus élevé de ces cellules (Kohta

et al., 2009). Ce traitement permettant de bloquer le TGF-β1 a même permis d'améliorer la récupération motrice chez les rats lésés. Enfin, la délétion du gène *Tgfr2* spécifiquement dans les microglies a eu pour conséquence d'induire leur transition rapide vers un phénotype macrophagique, caractérisé par l'augmentation de l'expression des marqueurs CD45, F4/80, MHCII, CD11c et CD169/Siglec-1 (Buttgereit et al., 2016). Ainsi, en raison de son potentiel anti-inflammatoire, le TGF-β1 pourrait limiter l'activation microgliale et la phagocytose après une LME, favorisant du même coup la régénérescence d'axones lésés.

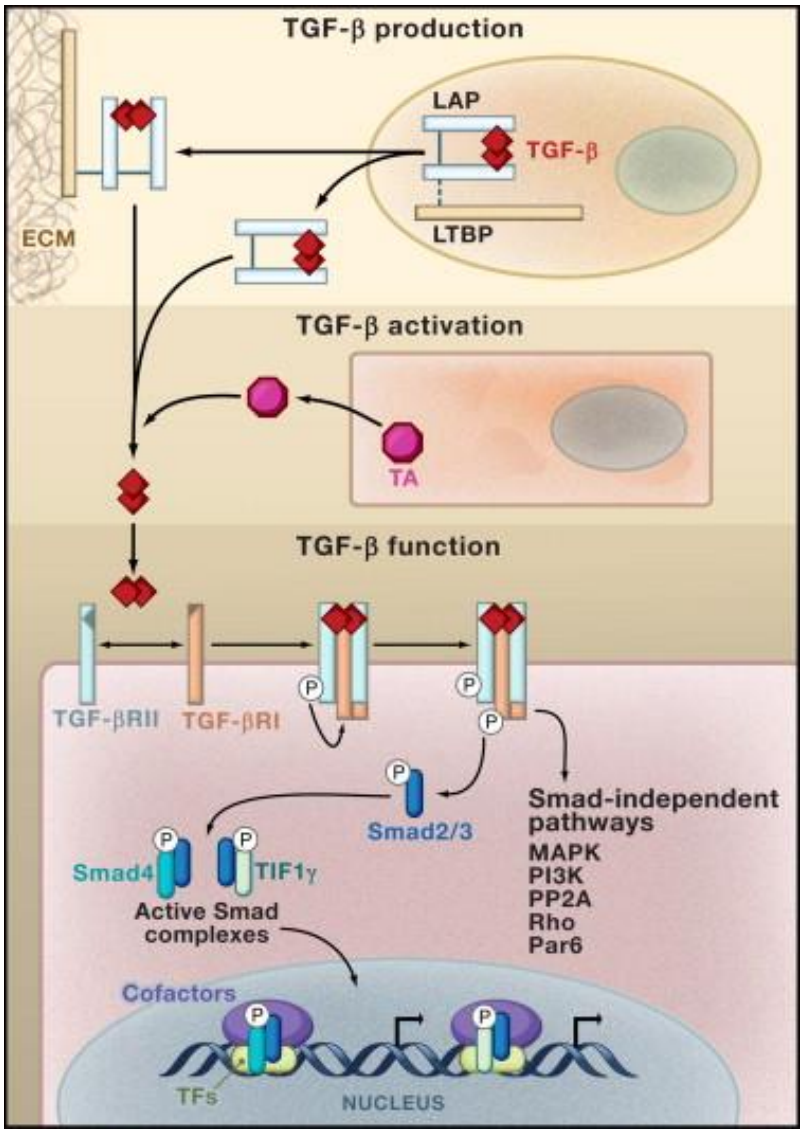

Figure 1.11 Mécanisme de régulation cellulaire par le TGFβ. *Tirée de* : Li et Flavell (2008).

1.3 Lésions de la moelle épinière

1.3.1 Généralités

Les LME sont provoquées lorsque la moelle épinière est endommagée à la suite d'un impact ou d'une compression mécanique prolongée sur la colonne vertébrale, pouvant causer une paraplégie voire même une tétraplégie. Chaque année, entre 250 000 et 500 000 personnes dans le monde souffrent de LME selon l'organisation mondiale de la santé ("http://www.who.int/mediacentre/factsheets/fs384/fr/," 2013, n.d.), dont 86 000 cas recensés au Canada (Krueger et al., 2013; Noonan et al., 2012). On estime à 3 millions de dollars par personne le coût rattaché aux LME (Krueger et al., 2013; Noonan et al., 2012). Les accidents de la route, les chutes et les accidents liés au sport comptent parmi les causes majeures de LME. Les hommes entre 16 et 34 ans sont les plus touchés par les LME de type traumatique, alors que les femmes âgées de 40 ans et plus sont plus sujettes aux LME non traumatiques résultantes de complications faisant suite à des tumeurs ou des infections. Il n'existe à l'heure actuelle pas de traitement pour les LME. Parmi les études cliniques en cours sur LME, ce sont les thérapies géniques et cellulaires qui prédominent, bien qu'on trouve également quelques essais basés sur l'utilisation de molécules, telles que la minocycline ("https://clinicaltrials.gov/ct2/home," n.d.).

Les conséquences des LME dépendent de la sévérité et du niveau de la lésion. Une lésion complète affectera l'ensemble des divisions de la moelle épinière, entraînant le plus souvent une perte complète des fonctions motrices et sensorielles. Une lésion incomplète affectera quant à elle des régions spécifiques de la moelle épinière et la perte des fonctions dépendra des régions touchées.

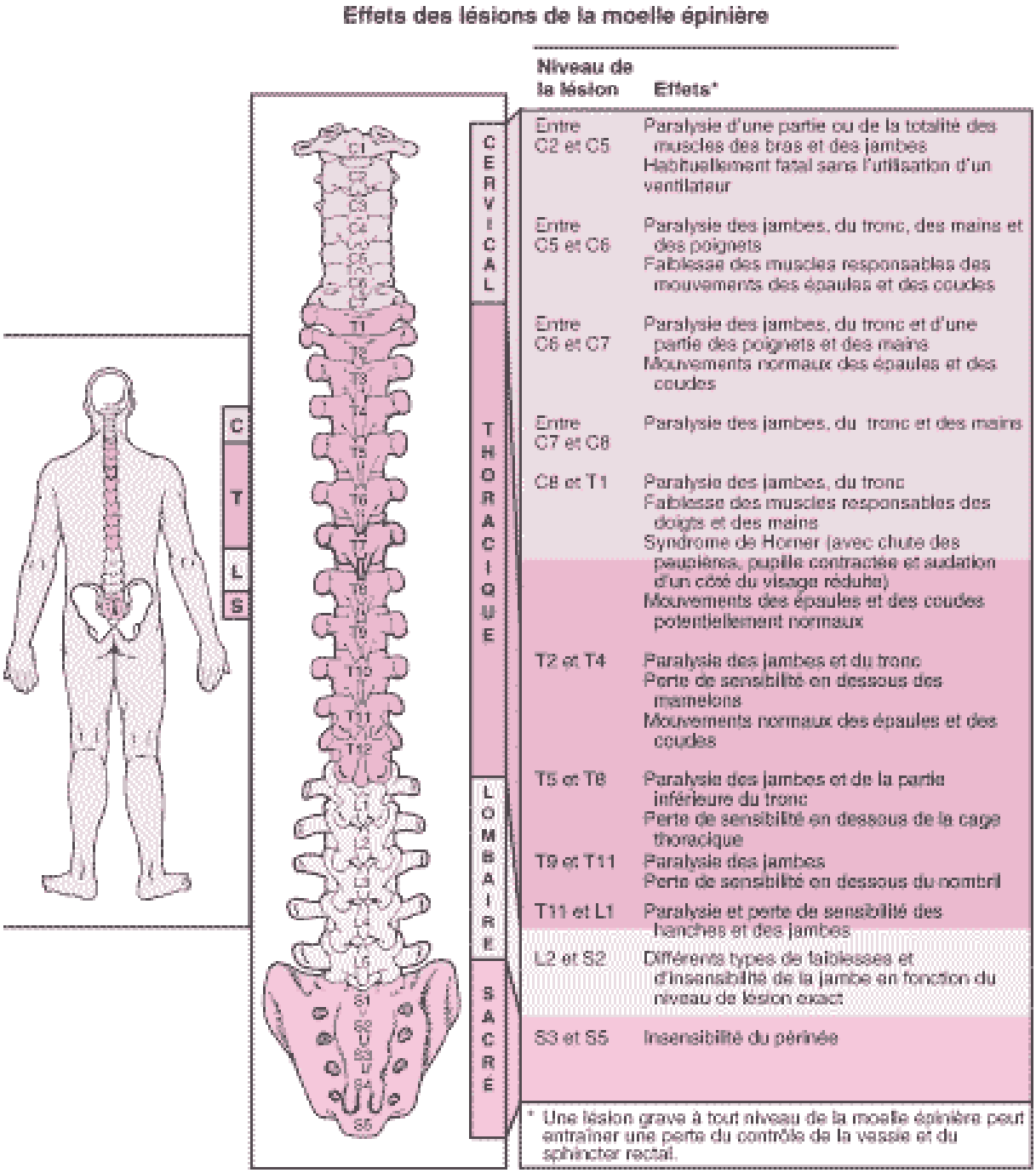

Figure 1.12 Conséquences des lésions de la moelle épinière en fonction de la zone affectée.

Tiré de https://www.merckmanuals.com/fr-ca/professional/troubles-neurologiques/troubles-de-la-moelle-%C3%A9pini%C3%A8re/revue-g%C3%A9n%C3%A9rale-des-affections-de-la-moelle-%C3%A9pini%C3%A8re

1.3.2 Les différentes phases d'une LME

La pathophysiologie d'une LME peut se diviser chronologiquement en trois grandes phases distinctes, dépendamment des mécanismes cellulaires et moléculaires enclenchés : la lésion primaire, la lésion secondaire et la lésion chronique. La lésion primaire, principalement caractérisée comme une phase de mort cellulaire par nécrose, se déroule depuis les quelques secondes suivant la lésion à quelques jours post-LME. La lésion secondaire, aussi appelée phase de dégénérescence secondaire, correspond à l'expansion de la lésion primaire aux tissus adjacents (par le biais de l'apoptose ou d'autres mécanismes encore non-identifiés) et peut durer de quelques heures à plusieurs semaines après la lésion. Enfin, la lésion chronique se déroule de quelques semaines à plusieurs mois après la lésion et se caractérise principalement par la formation de la cicatrice gliale. La chronologie exacte des phases d'une LME dépend du type et de la sévérité de la lésion.

1.3.2.1 Lésion primaire

La lésion primaire résulte de la force physique appliquée sur la moelle lors de l'évènement traumatique initial. La sévérité de la lésion dépend donc directement du type et de la puissance de cette atteinte, qui peut être une compression, un cisaillement, une lacération ou encore un étirement de la moelle (Ackery et al., 2004). La lésion primaire se caractérise par la mort des cellules résidentes de la moelle épinière, incluant les neurones, les cellules gliales et les cellules de la vasculature, résultant en la formation d'une zone nécrotique (Anthes et al., 1995; Tator, 1995). La rupture de l'étanchéité de la barrière hémato-spinale (BHS) entraîne également une hémorragie importante dans le tissu nécrosé ainsi que l'infiltration de plaquettes, de leucocytes et d'érythrocytes qui s'accumulent dans le parenchyme de la moelle épinière (Losey and Anthony, 2014; Profyris et al., 2004). Cette phase se caractérise aussi par la libération de messages de danger, appelés DAMPs. En particulier, dans un article publié en 2015 par notre laboratoire, nous avons démontré que 4 heures après la lésion, un niveau élevé de la cytokine pro-inflammatoire IL-1α est relâché par les microglies réactives (Bastien et al., 2015). D'autres signaux de danger sont également détectés en quantités importantes dans les premières heures suivant la LME, comme par exemple l'IL-33 (Gadani et al., 2015; Korhonen et al., 2015; Pomeshchik et al., 2015a) ou encore *High-mobility group*

box protein B1(HMGB1) (Kigerl et al., 2017). La libération de ces signaux de danger, qui se fait dans les premières heures après la lésion, est en grande partie responsable de l'aggravation des dommages. Ainsi, agir dans les 4 premières heures suivant la lésion afin d'empêcher l'accumulation de ces DAMPs pourrait permettre de réduire les dommages secondaires et, par conséquent, réduire la sévérité de la lésion et des déficits observés (Badhiwala et al., 2019; Fehlings et al., 2017; Kwon et al., 2011).

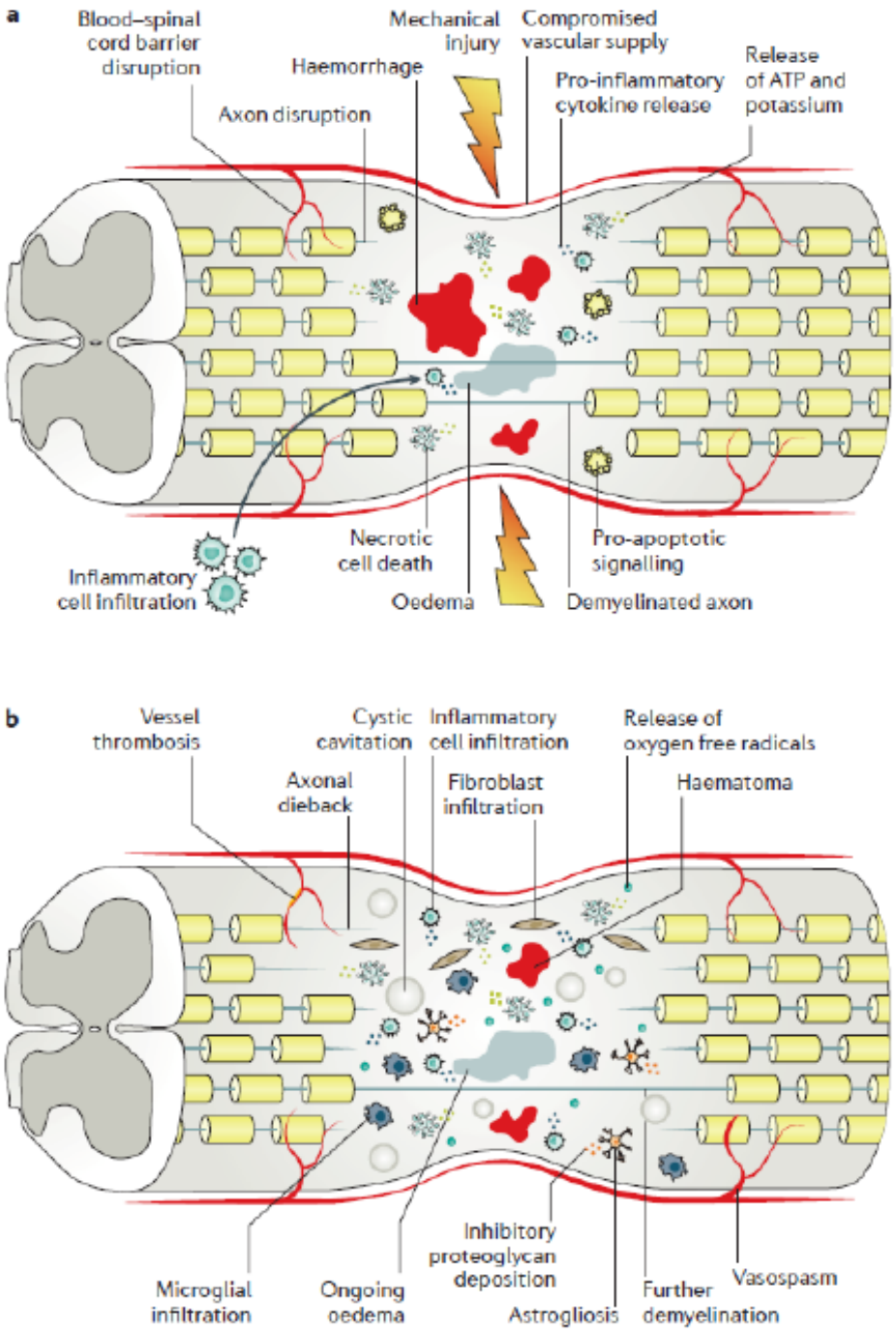

Figure 1.13 Représentation schématique des évènements se déroulant durant la phase primaire d'une lésion de la moelle épinière. a) dommages liés à la lésion initiale, de 0 à 48 heures post-lésion. b) phase de dégénérescence secondaire, se déroulant de 2 à 4 jours post-lésion. *Tirée de* : Ahuja, C. S. et *al.* (2017).

1.3.2.2 Dégénérescence secondaire

Suite à la lésion primaire survient une dégénérescence secondaire qui se caractérise par une excitotoxicité, une production de radicaux libres ainsi qu'une infiltration de cellules immunitaires (Almad et al., 2011). Cette dégénérescence secondaire est principalement provoquée par la libération du contenu intracellulaire des cellules nécrotiques, en particulier la libération de DAMPs, des molécules associées au danger. Parmi les DAMPs les plus étudiés dans le cas des LME, nous retrouvons les dérivés nucléotidiques (e.g. ATP), les *heat shock proteins* (HSPs) et l'IL-1α, respectivement reconnus par les récepteurs purinergiques, les TLRs et l'IL-1R1 (Rider et al., 2012) (Thundyil and Lim, 2015). La libération de DAMPS au site lésionnel déclenche la libération de médiateurs de l'inflammation, tels que des cytokines pro-inflammatoires, en particulier l'IL-1β et le TNF, par les cellules survivantes. Ce contexte inflammatoire active les cellules endothéliales et augmente la perméabilité de la BHS, entrainant le recrutement rapide de leucocytes au site lésionnel (Lee et al., 2011; Pineau et al., 2010; Stirling and Yong, 2008b; Thawer et al., 2013).

Les leucocytes (e.g. granulocytes, monocytes, lymphocytes), sont recrutés à l'épicentre de la lésion. Ils participent non seulement dans les évènements inflammatoires déclenchés par la LME, mais sont également impliqués dans la limitation et la réparation des dommages.

Initialement, l'infiltration des cellules immunitaires au niveau du parenchyme de la moelle épinière lésée dans les quelques heures suivant une LME accroît l'inflammation. Chez la souris, une très forte augmentation du nombre de neutrophiles en circulation est observée dès 12h post-lésion, tandis que le nombre de monocytes circulants augmente à partir de 24h post-lésion et que les lymphocytes diminuent significativement (Stirling and Yong, 2008a). Au niveau du tissus lésé, le nombre de leucocytes dérivés du sang augmente de manière constante entre 12h et 96h post-lésion. Plus précisément, les neutrophiles sont les premiers à arriver au site lésionnel, atteignant un pic à 24h post-lésion. Les monocytes sont quant à eux recrutés au niveau du parenchyme du système nerveux central et se différencient en macrophages dérivés des monocytes (MDMs). Alors qu'il ne reste quasiment plus de neutrophiles 4 jours après la lésion, les MDMs restent jusqu'à plusieurs semaines après la lésion. En tirant profit du modèle murin *Lys*-EGFP-*Ki*, Thawer et ses collaborateurs (Thawer et al., 2013) ont pu distinguer les monocytes périphériques des microglies résidentes. Ils ont

observé que de 1 à 3 jours post-lésion, des macrophages hématopoïétiques dits « classiques » (M1) infiltrent la moelle épinière. Toutefois, de 7 jours à 14 jours post-lésion, ce sont des macrophages hématopoïétiques de type « non-classique » qui sont présents dans le tissu lésé, alors que 6 semaines suivant la lésion, ce sont de nouveaux les macrophages de type classique qui sont retrouvés dans le tissu.

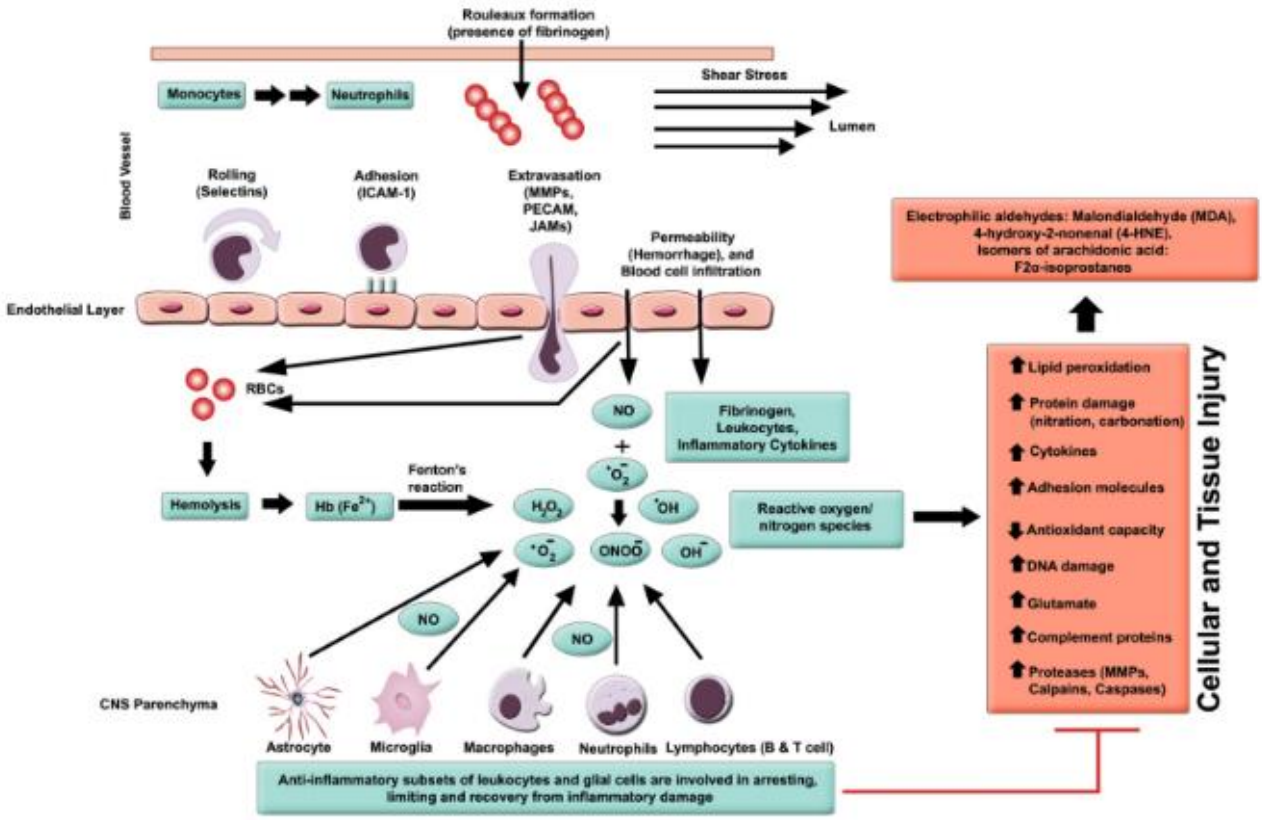

Figure 1.14 Milieu inflammatoire produit par la dégénérescence secondaire. *Tirée de* : Anwar, Al Shehabi et Eid (2016).

Une augmentation dans la perméabilité vasculaire est initiée par le processus d'hémorragie. S'ensuit l'extravasation de leucocytes activés qui relâchent des ligands inflammatoires comme les MMPs afin de dégrader la matrice extracellulaire et les protéines intracellulaires.

Les cellules gliales résidentes de la moelle épinière réagissent rapidement à ce contexte inflammatoire. Comme précédemment décrit, l'inflammation est rapidement

déclenchée par la libération de DAMPs au site lésionnel. Ce sont les microglies qui sont en majeure partie responsables de la libération de DAMPs au site lésionnel. Elles produisent et libèrent de nombreuses cytokines pro-inflammatoires, en particulier l'IL-1α, l'IL-1β et le TNF.

D'autre part, les astrocytes sont eux aussi activés et participent en majeur partie à la formation de la cicatrice gliale (Sofroniew, 2009). La cicatrice gliale a fait l'objet de nombreuses études et a été rapportée comme ayant à la fois des effets bénéfiques et néfastes. Suite à une LME, la formation de la cicatrice gliale permettrait de restreindre les dommages tissulaires et limiterait l'infiltration des cellules immunitaires sanguines (Eddleston and Mucke, 1993;Faulkner, 2004). Leurs effets sur la croissance et la régénération axonale demeurent toutefois sujet à discussion. En effet, alors que plusieurs études ont montré que les astrocytes sécrètent des molécules de la matrice extracellulaire, telles que les *chondroïtines sulfates protéoglycanes* (CSPGs), la tenascine, l'éphrine B2 et les protéines slit, qui inhibent la croissance et la régénération axonale (Bradbury et al., 2002; J Silver and Miller, 2004; Tang et al., 2003), une étude récente menée par le laboratoire du Dr. Sofroniew a montré qu'inhiber la formation de la cicatrice gliale réduit de manière significative la repousse d'axones lésés (Anderson et al., 2016).

La phase aigüe d'une LME se caractérise principalement par des dommages au niveau de la vasculature, une accumulation de neurotransmetteurs (excitotoxicité), une formation de radicaux libres, une peroxidation de lipides, une forte inflammation, ainsi que la mort de cellules par nécrose (Medsker et al., 2016a; Oyinbo, 2011; Von Leden et al., 2017). Cet ensemble génère un environnement particulièrement toxique pour les Ols (Almad et al., 2011). Chez la souris, le nombre d'Ols diminue rapidement durant les 24 premières heures post-lésion et atteint son pic à 7 jours (Lytle and Wrathall, 2007). L'apoptose des Ols a été observée jusqu'à 2 à 3 semaines suivant la lésion (Casha et al., 2001; Li et al., 1999). Cette perte prolongée des Ols, associée à la dégénérescence des segments distaux des axones séparés physiquement de leurs corps cellulaires suite à la lésion, un phénomène communément appelé dégénérescence Wallérienne, serait une conséquence de la fragmentation des axones qui fournissent un support trophique aux OLs (Li et al., 1999; Warden et al., 2001).

Les précurseurs d'oligodendrocytes (OPCs) appartiennent à une population hétérogène de cellules progénitrices exprimant les protéines *neural/glial antigen 2* (NG2) et *platelet-derived growth factor receptor alpha* (PDGFRα) et capables de se différencier en différents types cellulaires (Nishiyama et al., 2009; Trotter et al., 2010). Les OPCs, localisés à l'âge adulte aussi bien dans la matière grise que dans la matière blanche, réagissent à la démyélinisation en modulant leur morphologie et en accélérant leur cycle cellulaire suite aux différents signaux (ou encore l'absence de signaux) qu'ils reçoivent (Lytle et al., 2009; Tripathi and McTigue, 2007). La prolifération des OPCs est rapidement augmentée suite à une lésion nerveuse et ce pendant plusieurs semaines (Hughes et al., 2013;Chen et al., 2002). Les cellules NG2 sont capables de proliférer pendant au moins 4 semaines post-LME (McTigue et al., 2001). Dans les jours qui suivent une LME, les OPCs en prolifération sont situés à proximité du site lésionnel, au niveau de la pénombre alors qu'à des temps plus tardifs, ces cellules se retrouvent dans la matière blanche non lésée (Hesp et al., 2015). Les OPCs migrent ensuite aux zones démyélinisées (Almad et al., 2011; Blakemore and Keirstead, 1999; Carroll et al., 1998; Watanabe et al., 2002; Wolswijk and Noble, 1989). Ces cellules se différencient en Ols matures pendant et après leur migration.

L'ensemble des facteurs agissant sur les OPCs, comprenant entre autres les facteurs de croissance, les cytokines et chimiokines, les neurotrophines et les facteurs de transcription, jouent un rôle fondamental dans le processus de remyélinisation qui survient après la LME (Li et al., 2015). Des facteurs de croissance tels que *platelet-derived growth factor alpha* (PDGF-A) et *fibroblast growth factor 2* (FGF-2) agissent directement sur le développement de la lignée des Ols (Y. Chen et al., 2007), en plus d'être essentiels à la prolifération et la différentiation des OPCs dans un contexte de LME (Furusho et al., 2015). Les niveaux élevés de *ciliary neurotrophic factor* (CNTF) post-lésion indiquent aussi un rôle important de ce facteur de croissance pour la remyélination (Tripathi and McTigue, 2008). Suite à une LME, l'expression de nombreuses cytokines et chimiokines est également modifiée. Toutefois seulement certaines d'entre elles, dont plus particulièrement le *CXC-motif chemokine ligand 12* (CXCL-12) et son récepteur *CXC-receptor 4* (CXCR4), modulent la prolifération des OPCs et, conséquemment, affectent la formation de la gaine de myéline (Kadi et al., 2006).

Il est important de noter que les OPCs ne seraient potentiellement pas l'unique source d'Ols matures. En effet, certaines études ont montré que les cellules épendymaires possèdent

également un fort potentiel de cellules neurales progénitrices (Lacroix et al., 2014; Llorens-Bobadilla et al., 2020; Meletis et al., 2008) et seraient capables de se différencier en OLs, en particulier en cas de dommage à la moelle épinière.

1.3.2.3 Lésion chronique

La phase de lésion chronique survient suite à la phase de dégénérescence secondaire et se caractérise par l'apparition de la cicatrice gliale. Chez la souris, cette phase débute généralement à partir de 2 à 4 semaines suivant la lésion. Le centre de la lésion se compose principalement de cellules non neuronales telles que des fibroblastes, des cellules endothéliales et des cellules immunitaires issues de la périphérie. Ces cellules relâchent des protéines de la matrice extracellulaire, telles que le collagène-1 capable d'interagir avec les N-cadhérines présentent à la surface des astrocytes formant la cicatrice gliale. Ces astrocytes « réactifs » bordent la lésion et inhiberaient la régénération axonale (Hara et al., 2017).

La formation de cette cicatrice, qui sépare le tissu fibrotique non-neuronal des cellules réactives de la moelle épinière, constitue une étape critique pour la régénération du tissu nerveux et la récupération après une lésion de la moelle épinière. L'aspect bénéfique ou néfaste de la cicatrice gliale demeure une question très discutée encore aujourd'hui. En effet, alors que certaines études tendent à prouver que la cicatrice constituerait une cause majeure de l'échec de la régénérescence axonale, d'autres études montrent que la cicatrice permettrait de prévenir des dommages additionnels à la moelle lésée. Par exemple, en 2004, Faulkner *et al*. ont adressé la question de l'importance des astrocytes dans un contexte de LME en utilisant des souris transgéniques *Gfap-TK* exprimant spécifiquement le gène suicide *thymidine kinase* (TK) sous le contrôle du promoteur *Gfap* (Faulkner, 2004). Ils ont ainsi pu montrer que l'inhibition de la prolifération astrocytaire perturbe la formation de la cicatrice gliale, augmente la perméabilité de la BHE ainsi que la neuroinflammation, augmente la mort des neurones et des Ols et réduit la récupération des fonctions locomotrices après une LME. En 2006, Okada et ses collaborateurs ont également montré qu'une diminution de la réactivité des astrocytes, induite par l'inhibition de la voie de signalisation STAT3 dans les cellules exprimant la Nestine, affecte négativement la formation de la cicatrice gliale (Okada et al., 2006). D'autre part, la délétion spécifique du gène *Socs3* dans les astrocytes, entraînant une augmentation de l'expression de STAT3, a permis de favoriser la formation de la cicatrice

gliale et d'améliorer la récupération motrice après une LME (Okada et al., 2006). Ces différentes études montrent toute l'importance de la réponse astrocytaire et le rôle bénéfique de la cicatrice gliale à la suite d'une LME.

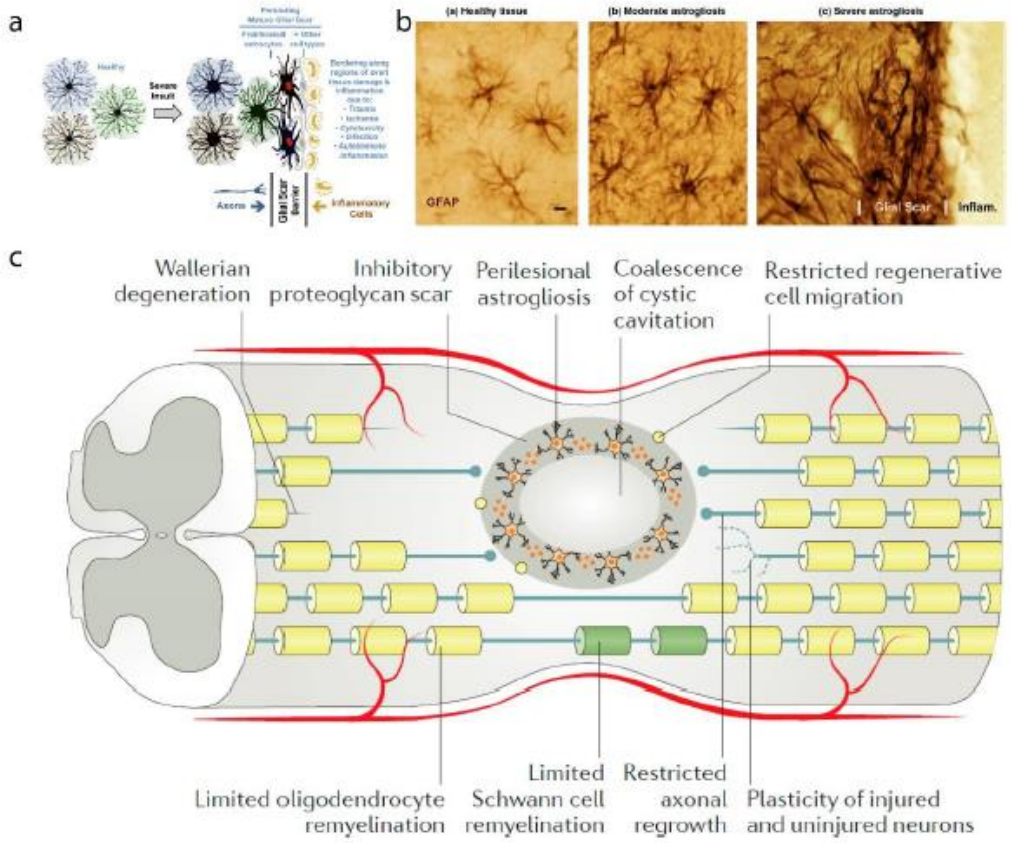

Figure 1.15 Formation de la cicatrice gliale - phase chronique. A) et **B)** montrent la prolifération et l'activation des astrocytes durant la formation de la cicatrice gliale, *Tirée de* : Sofroniew (2009). **C)** est une représentation schématique des principaux événements de la phase chronique, se déroulant de 7 jours à plusieurs mois après le LME, *Tirée de* : Ahuja et *al.* (2017).

Outre les astrocytes, il est important de noter que d'autres cellules participent activement à la formation de la cicatrice gliale (Göritz et al., 2011; Vanlandewijck et al., 2018). En effet, le site lésionnel est également envahi par des OPCs, des fibroblastes et d'autres cellules immunitaires pro-inflammatoires comme des MDMs (Cregg et al., 2014). Les cellules fibrotiques associées aux vaisseaux sanguins prolifèrent et s'accumulent au centre de la

lésion (Bellver-Landete et al., 2019). La régénération axonale est d'ailleurs particulièrement limitée par la présence d'une grande quantité de CSPGs, des protéines de la matrice extracellulaire incluant NG2, neurocane, aggrécane, brévicane, versicane et phosphocane, toutes reconnues comme étant de puissants inhibiteurs de la repousse axonale (J Silver and Miller, 2004). D'autres protéines contenues dans la myéline produite par les Ols contribuent également à l'inhibition de la régénération axonale, comme c'est le cas de la glycoprotéine associée à la myéline (MAG), la glycoprotéine d'oligodendrocytes (OMgp), Nogo (David and Lacroix, 2003), l'éphrine (Benson et al., 2005) et la sémaphorine (Moreau-Fauvarque et al., 2003).

1.3.3 Protection et régénération du SNC

1.3.3.1 Importance des DAMPs lors de la phase primaire

Comme précédemment décrit, la relâche de signaux de danger (DAMPs) lors de la phase primaire de la lésion est un élément critique de la dégénérescence faisant suite à une LME. La compréhension des mécanismes sous-jacents à la leur libération, de même qu'à leurs actions, pourraient aider à réduire leurs effets et potentiellement contribuer à l'élaboration de thérapies neuroprotectrices contre les LME.

Plusieurs études suggèrent que les microglies activées à la suite d'une lésion au SNC pourraient constituer la principale source de DAMPs. En effet, nous avons précédemment démontré que les microglies produisent de l'IL-1α dès 4 heures post-LME (Bastien et al., 2015). Fait intéressant, nous avons montré dans cette même étude que les souris n'exprimant pas l'IL-1α (*Il1a*$^{-/-}$) présentent une lésion moins sévère ainsi qu'un volume lésionnel plus faible, concomitant à une meilleure récupération des fonctions locomotrices. D'autre part, dans une étude publiée en 2017, Dr. Ben Barres et son équipe ont identifié plusieurs molécules produites par les microglies réactives (e.g. IL-1α, TNF, C1q) qui seraient capables de moduler le phénotype des astrocytes, les transformant en astrocytes aux propriétés toxiques, dits A1, pouvant engendrer la mort des neurones et des Ols (Liddelow et al., 2017b). Développer des thérapies afin d'inhiber l'activation des astrocytes A1 ou identifier les facteurs toxiques relâchés par ces derniers constituerait une avancée pour l'élaboration de thérapies neuroprotectrices, aussi bien dans un contexte de LME que dans d'autres contextes neuroinflammatoires.

1.3.3.2 Rôles des cellules immunitaires

En périphérie, les cellules immunitaires jouent un rôle critique dans la stérilisation des blessures et la cicatrisation. Toutefois, au niveau du SNC leur rôle reste controversé. L'inflammation est une composante fondamentale dans la pathophysiologie des LME. Il est difficile d'affirmer avec certitude si l'inflammation est néfaste ou au contraire bénéfique. Plusieurs études ont investigué le rôle des cellules immunitaires dans un contexte de LME. Lee et ses collaborateurs ont rapporté que la déplétion des neutrophiles, à l'aide de l'anticorps anti-Ly6G, ou la déplétion des monocytes, à l'aide de liposomes dans lesquels furent encapsulé du clodronate, n'est pas suffisante à elle seule pour voir des effets bénéfiques dans un modèle murin de LME (Lee et al., 2011). Toutefois, une amélioration des fonctions sensori-motrices, déterminée sur la base de différents tests de performance (score BMS, rotarod et *grid-walking test*), fut observée lorsque les neutrophiles et les monocytes sont déplétés de manière concomitante. Fait intéressant, cette récupération motrice accrue s'accompagne d'une diminution du stress oxydatif et de la peroxydation des lipides ainsi qu'une augmentation de l'étanchéité de la BHE. Cette étude soulève donc un aspect délétère des cellules immunitaires dans le cadre des LME, une affirmation également soutenue par de nombreuses autres études (Bao et al., 2008; Gris et al., 2004; Mabon et al., 2000; Popovich et al., 2002, 1999; Stirling et al., 2004).

Cependant, le rôle des cellules immunitaires ne se limiterait pas à un rôle néfaste. En effet, certaines études ont mis en évidence l'existence d'une classe de macrophages « activés de manière non-classiques », qui, lorsque pré-incubés *ex-vivo* avec des segments de nerfs périphériques, joueraient un rôle bénéfique dans la réparation du SNC (Rapalino et al., 1998). D'autres études ont également montré que les macrophages sont capables de sécréter des facteurs neurotrophiques (Barrette et al., 2008; Hashimoto et al., 2005; Richardson and Lu, 1994) favorisant la repousse axonale (Bouhy et al., 2006; Kotter et al., 2001). Les macrophages participent également à l'élimination des débris cellulaires et de myéline (Barrette et al., 2008; Shechter et al., 2009; Simard et al., 2006). Enfin, comme précédemment décrit (0.2.2.2), les macrophages M2 jouent un rôle dans résolution de l'inflammation via la production de molécules anti-inflammatoires (IL-10, IL-13) (Brown et al., 2014; Shechter et al., 2009; Wynn et al., 2013; Zhou et al., 2014).

Il s'agit donc d'une question de balance adéquate permettant d'assurer un équilibre entre l'inflammation et la résorption de celle-ci. On ne peut nier que les cellules immunitaires, en particulier les neutrophiles, ont un rôle délétère dans un contexte de LME en constituant une source non-négligeable de molécules toxiques (e.g. ROS, NOS) entrainant la mort des neurones et des cellules gliales. Cependant, il ne faut pas négliger l'importance essentielle des cellules immunitaires dans l'élimination des débris faisant suite à une LME.

1.3.3.3 ROS

Les *reactive oxygen species* (ROS) sont un groupe de composés chimiques hautement réactifs contenant de l'oxygène. Les ROS sont généralement divisés en deux catégories : les radicaux libres, comprenant un ou plusieurs électrons appariés, et les ROS non-radicaux, qui ne présentent pas d'électron non-pairé (Liou and Storz, 2010). Les ROS les plus étudiés sont principalement les anions superoxydes (O2 •−), le peroxyde d'hydrogène (H2O2) et le radical hydroxyle (OH•) (Freinbichler et al., 2011).

De par leur rôle dans la respiration cellulaire, les ROS constituent un élément indispensable à différents processus biologiques, tels que la survie cellulaire, la prolifération et la différentiation, de même que la réponse immunitaire (Dröge, 2002). Cependant, de nombreuses études suggèrent que la production de ROS pourrait être impliquée dans un large éventail de maladies se manifestant par de l'inflammation chronique, les maladies liées au vieillissement ou encore les cancers. Produit par les cellules immunitaires dans un contexte inflammatoire, ces dérivés oxygénés sont capables de détruire l'ADN et les protéines. En particulier, les ROS joueraient un rôle important dans l'induction de l'apoptose. Cet effet apoptotique, qui peut être bloqué dans les éosinophiles par l'utilisation de *N*-acétylcystéine (NAC) et de glutathionne, serait régulé par une phosphorylation de la tyrosine (Wedi et al., 1999). L'efficacité du NAC, un dérivé de la cystéine permettant de stimuler l'activité mitochondriale, a également été observée dans le contexte d'atteintes au SNC (Arakawa and Ito, 2007; Berk et al., 2011).

Dans un contexte de LME, il est connu que la production de ROS, en particulier celle du peroxyde d'hydrogène et du radical hydroxyle, augmente en réponse à la lésion (Liu et al., 2004, 2003, 2000, 1998). De plus, les mêmes études ont rapporté que la production de

O2 •− est détectable immédiatement après la lésion et dure jusqu'à 10h post-LME. OH est quant à lui produit entre 5 min post-LME et est détectable jusqu'à 3h suivant la lésion.

Connaissant les dommages associés aux ROS dans un contexte inflammatoire, ces composés oxygénés pourraient constituer une cible intéressante dans le but de diminuer les dommages après une LME et la mort subséquente de nombreuses cellules. Plusieurs études se sont justement intéressées au potentiel antioxydant du NAC dans un contexte de LME (Guo et al., 2015; Karalija et al., 2012), sans toutefois qu'un consensus ne puisse en ressortir. En effet, Guo et al. (Guo et al., 2015) ont montré qu'un pré-traitement au NAC permet de réduire les dommages neuronaux et améliore la récupération motrice après une LME. Cependant, il est loin d'y avoir un consensus sur la question de l'efficacité d'un traitement au NAC comme thérapie pour les LME. Le NAC présente un potentiel intéressant, mais d'autres études doivent être menées, en particulier en prenant en considération qu'un tel traitement ne peut réellement être envisageable que s'il est administré seulement après que la lésion ne se soit produite. Cela n'est pas le cas des études actuelles montrant l'efficacité du NAC, dans lesquelles ce dernier fut administré avant que la lésion soit infligée.

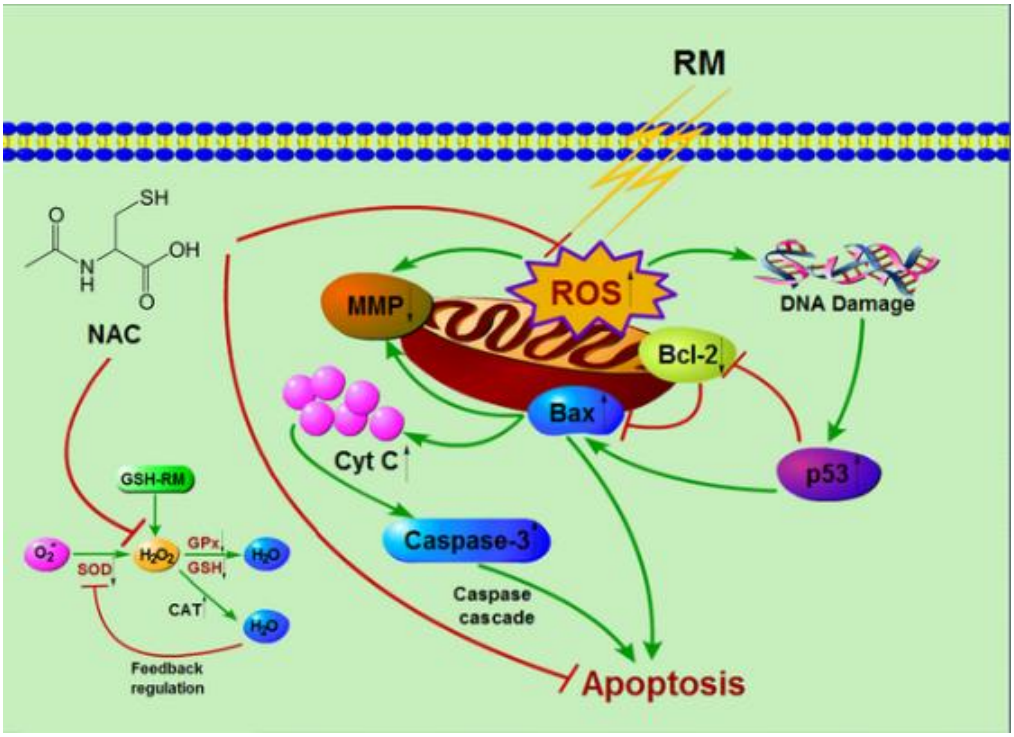

Figure 1.16 Mécanisme de production des ROS et d'induction de l'apoptose. *Tirée de* : Jiao et *al.* (2016).

1.4 Modèles murins transgéniques

Afin de disséquer le mécanisme d'action précis de la cytokine IL-1α, jouant un rôle critique lors des LME, nous avons opté pour une approche impliquant des souris transgéniques inductibles exprimant la recombinase Cre. En effet, comme nous savons que l'IL-1α signalise principalement via le récepteur IL-1R1, nous avons opté pour une stratégie nous permettant de restaurer ou d'invalider le gène codant pour ce récepteur dans un type cellulaire précis du SNC.

1.4.1 Système Cre-loxP

Le système de recombinaison Cre-loxP est une approche couramment utilisée afin de générer une restauration ou invalidation d'un gène spécifique dans une population cellulaire d'intérêt. La Cre recombinase (Cre) est une protéine de 343 acides aminés, constituée de 4 sous-unités. Celle-ci est capable de reconnaître et d'exciser spécifiquement les séquences loxP, qui sont des séquences d'ADN de 34 paires de bases (pb) (Sauer, 1987; Sternberg and Hamilton, 1981; Yarmolinsky and Hoess, 2015). Ce type de recombinaison génétique fut identifié chez le bactériophage P1. En effet, c'est en 1987 que le système Cre-lox fut découvert pour la toute première fois puis transposé chez la levure (Sauer, 1987), pour ensuite être adapté aux cellules de mammifères en culture (Sauer and Henderson, 1988). Grâce au développement d'outils de pointe en génie génétique, il fut ensuite possible d'introduire ces séquences d'ADN de manière stable et héréditaire dans le génome murin afin de créer différents modèles transgéniques murins. A l'heure actuelle, les souris transgéniques basées sur le système Cre-lox constituent un outil couramment utilisé pour l'étude de différents mécanismes biologiques. Le système Cre-loxP a même été optimisé afin de rendre le modèle inductible, comme c'est le cas chez les souris exprimant la séquence Cre^{ERT2}. Chez ces souris, la Cre est produite sous la forme d'une protéine de fusion, la Cre-ERT2, la rendant inactive. L'administration de tamoxifène, par injection intrapéritonéale ou par gavage oral, dépendamment de l'âge de la souris, induit la translocation au noyau de la protéine de fusion Cre-ERT2, ce qui permet alors de rétablir l'activité de la Cre recombinase entraînant du même coup la restauration ou la délétion du gène ciblé.

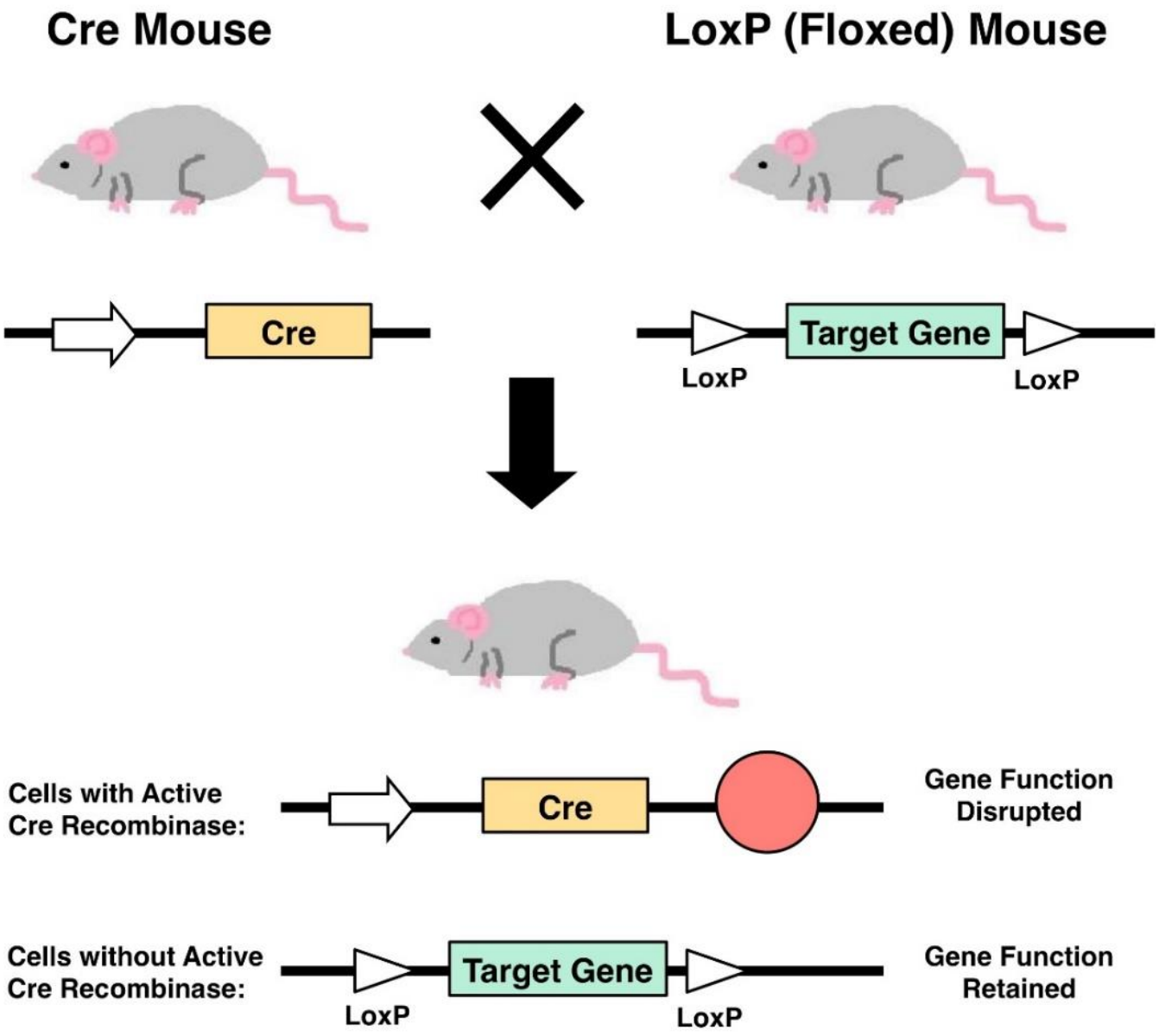

Figure 1.17 Représentation schématique du fonctionnement des souris Cre transgéniques. *Tirée de :* **http://studentblogs.med.ed.ac.uk/reproductive-systems-group-4/androgen-insufficiency/**

1.4.2 Système de restauration ou d'invalidation cellule-spécifique de l'IL-1R1

1.4.2.1 Souris *Il1r1*$^{r/r}$

Afin de restaurer spécifiquement le récepteur IL-1R1 dans différentes populations cellulaires du SNC, nous avons utilisé la souris *Il1r1*$^{r/r}$. Chez cette souris, développée par l'équipe du Dr. Ning Quan à Ohio State University (Liu et al., 2015), l'insertion d'un codon stop flanqué de séquences loxP dans un intron du gène de l'*Il1r1* permet d'invalider l'expression de ce gène. Lorsque cette souris est croisée avec une souris Cre, l'expression de la Cre permet d'exciser le codon stop au niveau des séquences loxP et donc de rétablir l'expression de l'IL-1R1.

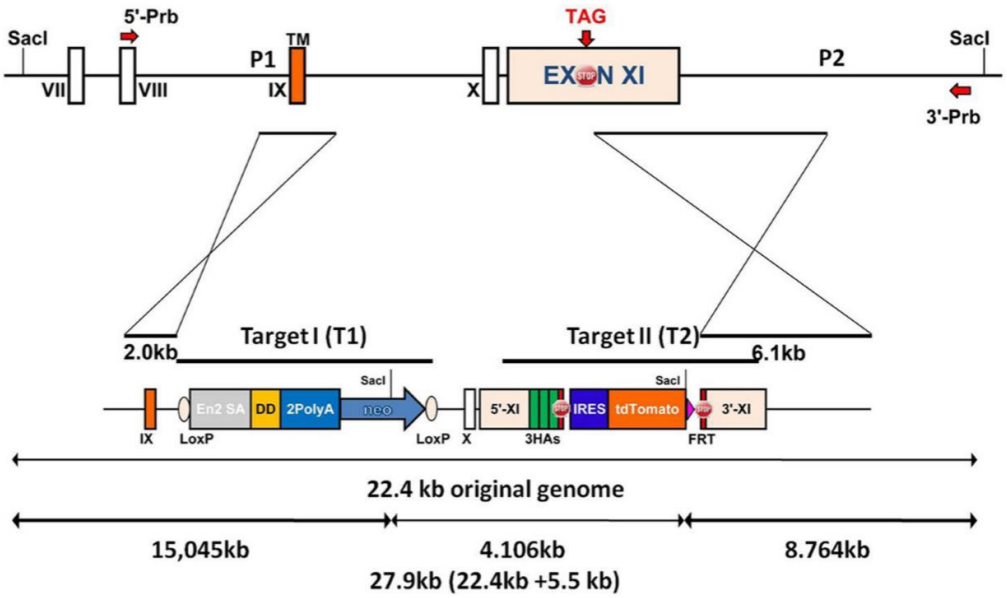

Figure 1.18 Représentation schématique de la construction du modèle murin transgénique *Il1r1*$^{re/re}$. *Tirée de* : Liu et *al.* (2015).

1.4.2.2 Souris *Il1r1*$^{flox/flox}$

Dans le but inverse d'invalider spécifiquement l'expression de l'*Il1r1* dans un type cellulaire spécifique, nous avons utilisé la souris *Il1r1*$^{flox/flox}$. Cette souris présente des séquences loxP insérées respectivement dans les exons 3-4 du gène *Il1r1*. Une fois croisée avec des souris exprimant la recombinase Cre, l'expression du gène *Il1r1* est éliminée grâce à l'excision des exons 3-4 flanqués par les séquences loxP reconnues par l'enzyme.

1.4.2.3 Lignées murines Cre et Cre^{ERT2}

Compte tenu de la grande diversité des souris transgéniques disponibles commercialement, nous avons dû sélectionner spécifiquement les différentes lignées ciblant nos populations d'intérêt en fonction de leurs avantages et inconvénients. Il existe deux grandes classes de lignées de souris Cre : les lignées Cre non-inductibles et les lignées Cre^{ER} inductibles. Chez les lignées non-inductibles, la recombinase Cre est produite sous sa forme active dans les cellules dans lesquelles le promoteur sélectionné est induit, entraînant ainsi le phénomène de recombinaison. Au contraire, dans les cellules des modèles inductibles, la recombinase Cre est produite dans une forme fusionnée au récepteur œstrogène humain muté (*oestrogen receptor*, ER), la rendant active. Il est donc nécessaire d'administrer chez ces lignées un composé, soit le *4-hydroxytamoxifen* (OHT) ou le tamoxifène, pour transformer l'enzyme dans sa forme active (Feil et al., 1997, 2009). Le tamoxifène, par exemple, est un antagoniste du récepteur oestrogénique humain qui une fois lié au ER permettra l'activation de la recombinase Cre. Celle-ci pourra alors effectuer son action de recombinaison. Dans nos études, nous avons utilisé la version la plus récente et la plus efficace de la Cre^{ER}, soit la Cre^{ERT2}.

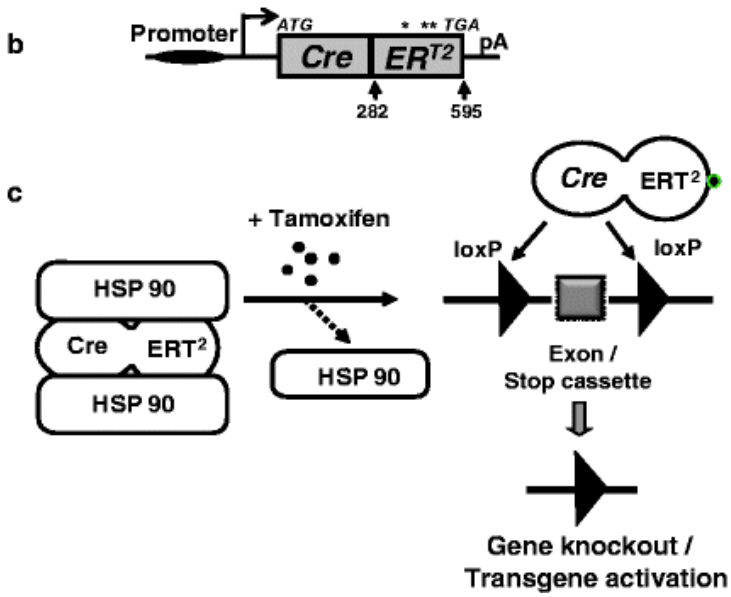

Figure 1.19 Fonctionnement de la stratégie de recombinaison génétique inductible par le système de la Cre ERT2. *Tirée de* : Kühn, Vogt-Weisenhorn et Wurst (2011).

1.4.2.4 Souris *Pdgfra*^{CreERT2}

Il existe de nombreuses lignées de souris transgéniques ciblant les cellules de la lignée des Ols. Une des difficultés majeures pour le choix de la souris Cre ciblant ces cellules repose cependant sur la nécessité d'induire le phénomène de recombinaison à un stade de différenciation bien précis de la lignée, que ce soit au niveau des OPCs ou des Ols dits matures. Dans le cadre de nos travaux, nous avons opté pour la souris *Pdgfra*^{CreERT2} puisqu'elle permet de cibler un maximum de cellules de la lignée des Ols. Bien que le promoteur *Pdgfra* soit spécifiquement induit dans les OPCs, le fait que cette souris soit inductible permet de cibler les OPCs et tous les stades de différenciation subséquents de la lignée des Ols. En effet, bien qu'une première vague de différentiation des OPCs en Ols puisse être observée dans la moelle épinière au stade E15 chez la souris (Pringle and Richardson, 1993), la majeure partie de cette différenciation survient après la naissance, atteignant un pic aux environs de 2 à 4 semaines postnatales et continuant jusqu'à 8 mois après la naissance (Bergles and Richardson, 2016; Rivers et al., 2008). Ainsi, en injectant les souris à un jeune âge (2 injections de tamoxifène à P2 et P4), une forte proportion des OPCs et ainsi des Ols matures peut être ciblée de cette façon.

1.4.2.5 Souris *Cx3cr1*^{CreERT2}

Afin de cibler les microglies, nous nous sommes basés sur des études précédemment réalisées au sein du laboratoire afin de sélectionner la lignée *Cx3cr1*^{CreERT2} (Bellver-Landete et al., 2019). La protéine Cx3cr1, également connue sous le nom de récepteur à la fractalkine, est fortement exprimée par les microglies et les monocytes circulants. Ainsi, grâce à cette lignée de souris transgéniques, il est possible de restreindre le phénomène de recombinaison aux cellules de la lignée myéloïde. En effet, le gavage des souris au tamoxifène aux jours P28 et P30 permet d'induire une recombinaison spécifiquement dans les microglies et les monocytes circulants. Toutefois, un mois suivant le traitement au tamoxifène, seules les microglies demeurent génétiquement modifiées. En effet, les monocytes ayant une demi-vie beaucoup moins longue que celle des microglies (2-5 jours pour les monocytes versus plusieurs mois pour les microglies), ils sont entièrement renouvelés après quelques semaines, contrairement aux microglies (Bellver-Landete et al., 2019; Goldmann et al., 2013; Gu et al., 2016; Parkhurst et al., 2013; Yona et al., 2013).

1.4.2.6 Souris *Cdh5*^{CreERT2}

Tout comme pour les Ols, il existe de nombreux modèles de souris transgéniques permettant de cibler les cellules endothéliales. En se basant sur les différentes études réalisées avec ces modèles (Assmann et al., 2016; M. J. Chen et al., 2009; Kogata et al., 2006; Monvoisin et al., 2006; Y. Wang et al., 2010), nous avons sélectionné la souris *Cdh5*^{CreERT2}. Cette souris permet d'obtenir un taux de recombinaison très élevé en plus de présenter l'avantage d'être spécifique à la vasculature du SNC.

1.4.2.7 Souris *mGfap*^{Cre}

Le modèle transgénique murin le plus couramment utilisé et le mieux caractérisé lorsque vient le temps de cibler les astrocytes est sans aucun doute la souris *mGfap*^{Cre}. Il existe toutefois différentes versions de ce modèle, dépendamment de la construction génétique. La lignée 77.6 du modèle *mGfap*^{Cre}, développée par le groupe de Michael Sofroniew (Gregorian et al., 2009), est non seulement la plus récente et la mieux caractérisé mais aussi la plus spécifique. En effet, la lignée 77.6 permet de cibler spécifiquement les astrocytes du cerveau et de la moelle épinière grâce au promoteur mGFAP. Cependant, contrairement aux souris de la lignée 73.12Mvs, les souris *mGfap*^{Cre} 77.6 ne sont pas associées à de la recombinaison dans les cellules souches neurales (Gregorian et al., 2009). Cette lignée n'est toutefois pas inductible, ce qui veut dire que la recombinaison a lieu dans toutes les cellules exprimant la GFAP sans qu'un traitement au tamoxifène ne soit nécessaire pour rendre la recombinase Cre dans une forme active.

1.5 Hypothèse et objectifs généraux

Les LME se caractérisent par une succession d'évènements distincts, tels que l'inflammation, le recrutement de cellules immunitaires, la formation de la cicatrice gliale ou encore la plasticité et réparation du tissu nerveux. Les cytokines inflammatoires jouent un rôle central dans une grand majorité de ces évènements. Plus particulièrement, des travaux récemment publiés par notre équipe et d'autres groupes de recherche ont montré que la cytokine proinflammatoire IL-1 joue un rôle critique dans l'infiltration des cellules

immunitaires. En effet, l'infiltration de ces cellules est significativement diminuée lorsque le gène *Il1a* ou *Il1b* est invalidé dans un modèle murin de LME (C.-J. Chen et al., 2007;Bastien et al., 2015). Cependant, seules les souris *Il1a*$^{-/-}$ ont montré des améliorations rapides et permanentes de la locomotion ainsi qu'un volume lésionnel réduit dès le premier jour suivant la lésion. De manière intéressante, l'amélioration rapide et permanente de la locomotion chez les souris *Il1a*$^{-/-}$ était également accompagnée d'une diminution de l'infiltration de neutrophiles et de monocytes inflammatoires au site lésionnel ainsi que d'une meilleure survie des oligodendrocytes. En effet, le nombre d'oligodendrocytes matures à l'épicentre était significativement plus important chez les souris *Il1a*$^{-/-}$ à 1 jour post-lésion, et cet effet était encore accru à 14 jours post-lésion.

Ainsi, l'objectif général de mes travaux de thèse était d'élucider le mécanisme d'action de l'IL-1α au niveau du SNC et d'identifier de nouvelles cibles thérapeutiques dans le but de réduire les dommages causés par les LME. Les résultats discutés antérieurement m'ont permis de proposer l'**hypothèse** que l'absence d'IL-1α améliorerait la survie des Ols suite à une LME, permettant ainsi de réduire la sévérité de la lésion chez les souris *Il1a*$^{-/-}$.

1.5.1 Nouvelles thérapies visant à bloquer les DAMPS

Les alarmines, ou DAMPs, sont des acteurs bien connus des lésions affectant le SNC. En particulier, leur rôle de signal de danger confère aux DAMPs de fortes propriétés dans la modulation de l'inflammation. Le chapitre 1 est une revue de littérature faisant le point sur les alarmines, leurs fonctions spécifiques ainsi qu'aux récentes thérapies anti-alarmines développées dans le cadre de lésions du SNC.

1.5.2 Rôle des microglies lors des LME

À la suite d'une LME, l'IL-1α est libérée sous forme de pro-IL-1α par les microglies nécrotiques. Compte tenu des effets bénéfiques de la délétion du gène *Il1a* lors des LME et du rôle controversé des microglies dans ce contexte, il était pertinent de caractériser précisément le rôle de ces cellules. Une des difficultés liées à l'élucidation du rôle des microglies résidait dans l'absence d'outil efficace permettant de distinguer les microglies des MDMs. Nous avons pu surmonter cette problématique grâce à la génération de souris *Cx3cr1*^{creER}. D'autre part, l'utilisation d'inhibiteurs du CSF1R nous a permis de dépléter

efficacement les microglies et, ainsi, de mieux comprendre leur rôle dans le contexte des LME.

Hypothèse : Les microglies protègent la moelle épinière à la suite d'une lésion en régulant la formation de la cicatrice gliale et limitant l'entrée de cellules immunitaires sanguines aux propriétés toxiques.

Objectifs expérimentaux :

- Localiser et évaluer la dynamique des microglies à la suite d'une LME.

- Caractériser la réponse microgliale et les interactions possibles entres les microglies et les astrocytes durant la formation de la cicatrice gliale.

- Investiguer les effets de la déplétion des microglies sur la formation de la cicatrice gliale et la récupération motrice post-LME. Évaluer l'effet de l'administration de MCSF sur la réponse des microglies et la récupération fonctionnelle à la suite d'une LME.

1.5.3 Caractérisation des effets et des mécanismes d'action de l'IL-1α à la suite d'une lésion de la moelle épinière

Au chapitre 3, nous avons caractérisé les effets de l'IL-1α dans la moelle épinière lésée afin de comprendre pourquoi l'absence de l'IL-1α est associée à une meilleure récupération des fonctions motrices. Dans ce but, nous avons développé un modèle *in vivo* simplifié consistant à injecter la cytokine recombinante dans la citerne cérébellomédullaire (*cisterna magna*) chez la souris. Cela nous a permis d'accéder directement au liquide cérébrospinal et de limiter les effets de l'injection en périphérie. D'autre part, afin de disséquer les mécanismes d'action de notre cytokine d'intérêt *in vivo*, nous avons opté pour l'utilisation de souris transgéniques exprimant la recombinase Cre dans des populations cellulaires spécifiques. En effet, comme nous savons que l'IL-1α signalise principalement via le récepteur IL-1R1, nous avons priorisé une stratégie permettant de restaurer ou d'invalider spécifiquement ce récepteur dans un type précis de cellules du SNC.

Hypothèse : L'IL-1α déclenche une forte réponse inflammatoire accompagnée d'une réactivité des cellules gliales au niveau de la moelle épinière, entraînant la mort des Ols.

Objectifs expérimentaux:

- Caractériser les effets de l'IL-1α au niveau de la moelle épinière en termes d'inflammation, d'activation cellulaire et d'effet sur les Ols.
- Identifier les cellules répondant à l'IL-1α.
- Élucider les mécanismes par lesquels les astrocytes activés à l'IL-1α stimulent la mort des Ols et identifier un moyen efficace de bloquer cet effet.

Chapitre 2 ANTI-ALARMINS THERAPIES: NEW INSIGHT IN CNS PROTECTION MECHANISMS

Floriane Bretheau[1], Roxanne Turmel[1] and Steve Lacroix[1]*

[1]Axe Neurosciences du Centre de recherche du Centre hospitalier universitaire (CHU) de Québec–Université Laval et Département de médecine moléculaire de l'Université Laval, Québec, QC, G1V 4G2, Canada.

2.1 Résumé

L'interleukine (IL) -1α, l'IL-33, l'ATP, HMGB1 ou encore les protéines S100 sont quelques exemples d'alarmines ayant un rôle important dans la modulation l'inflammation. Au niveau du SNC, ces alarmines sont libérées à la suite d'une blessure par les neurones et les cellules gliales endommagées ou mourantes. Une fois libérées dans le milieu extracellulaire, les cellules environnantes ressentent ces signaux de danger via leurs récepteurs spécifiques, ce qui déclenche une cascade d'événements conduisant à la libération de cytokines et chimiokines inflammatoires. En fonction de la nature, de la durée et de la gravité de la réponse inflammatoire, le résultat entraînera soit une réparation des tissus, soit des dommages. Ces DAMPs représentent donc des cibles potentielles pour le développement de nouvelles thérapies dans le contexte des lésions du SNC. Cette revue de littérature s'intéresse aux alarmines, à leurs fonctions spécifiques ainsi qu'aux thérapies anti-alarmines récentes développées dans le cadre de lésions du SNC.

2.2 Abstract

Interleukin (IL)-1α, IL-33, ATP, high-mobility group box protein 1 (HMGB1) and S100 proteins are a few examples of alarmins that modulate inflammation in the central nervous system (CNS). In healthy cells, these proteins exert diverse functions such as regulation of gene expression. In the CNS, alarmins are released by stressed or dying neurons and glial cells following injury. Once in the extracellular milieu, the surrounding cells sense these danger signals through their specific receptors and initiate a cascade of events leading to the release of inflammatory cytokines and chemokines. Depending on the nature, duration and severity of the inflammatory response, the outcome will either result in tissue repair or damage. Targeting these DAMPs could be a potential therapy in the context of CNS injuries. In this review, we summarize the most recent literature on alarmins, their specific functions and recent anti-alarmins therapies following CNS injuries

2.3 Introduction

2.3.1 Alarmins, the cellular S.O.S. message

Alarmins are endogenous mediators released after an insult to warn the immune system that a jeopardizing situation is occurring. When trauma or damage occurs in the CNS, alarmins or damage-associated molecular pattern (DAMPs), such as Il1α, S100 proteins, high mobility group box protein 1 (HMGB1), heat shock proteins (HSP), nucleotides, are potentially released as "S.O.S. messages" by damaged or dying cells. These alarmins bind to different pattern recognition receptors leading to the activation of subcellular pathways, upregulating expression of multiples genes that trigger the recruitment of leukocytes at the site of injury and enhance inflammation. The levels of these pro-inflammatory mediators increase at the site of damage with the presence of recruited leukocytes. Phagocytosis and debris clearance promote the resolution of inflammation that, eventually, could nurture tissue reconstruction. However, in some cases, the resolution of inflammation is unsuccessful and then the formation of a glial scar, concomitant with the release of pro- and anti-inflammatory mediators, lead to chronic inflammation, avoiding CNS regeneration and priming permanent disability.

2.3.2 CNS injuries

Spinal cord injury (SCI), stroke and traumatic brain injury (TBI) are the most common injuries affecting the CNS. Once damage occurs, a necrotic area is rapidly formed at the center (core) of the affected area. Within minutes, the injury triggers an inflammatory response, which is believed to promote further tissue damage to surrounding healthy tissue located in an area called the penumbra where cells remain vulnerable but still salvageable. The rapid release of DAMPs at the lesion core by necrotic cells triggers the production of proinflammatory cytokines such as Il-1β and TNF by the surviving cells (Pineau and Lacroix, 2007). Endothelial cells are activated by this inflammatory environment, increasing the blood-brain barrier (BBB) permeability and leading to leukocytes recruitment at the site of injury (Lee et al., 2011; Pineau et al., 2010; Stirling and Yong, 2008a; Thawer et al., 2013) The compromised BBB allows undesirable debris and cells infiltration and with the rise in water transmigration across the BBB due to leaking it finally result in edema (Khan et al.,

2009). Immune cell infiltration in the CNS parenchyma increases the inflammatory process by releasing proinflammatory factors as cytokines and reactive oxygen species (ROS) (Stirling and Yong, 2008a). Additionally, the viability of neurons and oligodendrocytes is severely affected by the acute phase of CNS injuries and these cells undergo apoptotic cell death (Ding et al., 1988). Nonetheless, a beneficial consequence of this proinflammatory milieu is the clearing of axonal and myelin debris by mononuclear phagocytosis. This is a critical step for tissue regeneration and repair (Barrette et al., 2008). However, and for unknown reasons, immune cells are unable to resolve inflammation once the cleaning is completed and they instead remain for weeks in the injured tissue and release additional waves of proinflammatory cytokines.

2.4 IL-1α

2.4.1 IL-1α protein

Interleukin 1 (IL-1) was the first cytokine reported to be released by leukocytes and capable to induce fever. In 1985, two distinct human IL-1 complementary DNAs were cloned and sequenced from a macrophage cDNA library (March et al., 1985). Until recently, IL-1 family has been reported as composed of 11 members, including the most studied cytokines IL-1α, IL-1β, IL-1Ra, IL-18 and IL-33 (Dinarello, 2009). Despite only 25-30% of homology in their amino acid sequences, IL-1α and IL-1β present a similar three-dimensional structure and share similar functions (Graves et al., 1990b), (Dinarello, 1991). Both IL-1α and IL-1β are synthesized as pro-forms of 31 kDa (March et al., 1985; Mosley et al., 1987) and their cleaved forms, of both 17 kDa approximatively, interact with IL-1R family members and seem to trigger similar biological functions (Dinarello, 1991), (Carruth et al., 1991; Kobayashi et al., 1990). Although they share similar structure and act through the same receptors, IL-1α and IL-1β are distinct cytokines. Notably, IL-1β is only produced in the context of activation of hematopoietic cells while IL-1α is widely expressed in different subsets of cells over the organism *i.e* keratinocytes, epithelial cells and endothelial cells. Also, contrary to the precursor form of IL-1β (prec-IL-1β), the prec-IL-1α is biologically active (Kim et al., 2013). The prec-IL-1α contains a nuclear location signal (NLS) that allows its translocation towards the nucleus where it can interact with histone acetyltransferases and act as a DNA damage sensor (Idan et al., 2015). The prec-IL-1α requires Ca^{2+} intracellular influx to activate

proteases, such as calpain, or some NLRP3 inflammasome pathways to mature and release IL-1α during necroptosis cell death, but both the prec-IL-1α and IL-1α can bind IL1R1, whereas only the mature form of IL-1β, cleaved during pyroptosis by caspases of the inflammasome complex, allows its binding to IL1R1 (Groß et al., 2012). Importantly, IL-1α is ten times more affine for IL-1R1 and a hundred times less affine for IL-1R2 than IL-1β (M Bersudsky et al., 2014; McMahan et al., 1991). Actually, IL-1R2 acts as a decoy receptor and cannot transduce signal (Peters et al., 2013). Recent evidences have shown that in the context of inflammation precursor form of IL-1α (prec-IL1α) can be considered as an alarmin and IL-1β as an enhancer of inflammation. Indeed, IL-1α released by dying cells upon hypoxia can induce sterile inflammation and neutrophils recruitment, whereas IL-1β is produced upon the arrival of neutrophils, boost inflammation and promotes macrophages recruitment (Rider et al., 2011) (C.-J. Chen et al., 2007; I. Cohen et al., 2010) Thus, we will specifically focus on IL-1α.

2.4.2 IL-1α targeting in the context of CNS injuries

Although IL-1α has been detected in many cell types *in vitro* (Dinarello, 2009), only resident microglia and infiltrating platelets have been shown to be a potential source of IL-1α under inflammatory conditions in the CNS (Luheshi et al., 2011a; Thornton et al., 2010b). During CNS injuries, IL-1α is rapidly produced and precedes the expression of IL-1β acting as an alarmin, initiating sterile inflammation (Bastien et al., 2015; Luheshi et al., 2011a; Rider et al., 2011). IL-1α is released by resident microglia at the penumbra in stroke and in the surroundings of the epicenter in SCI (Bastien et al., 2015; Luheshi et al., 2011a).

2.4.3 IL-1α targeting in the context of SCI

IL-1α has been detected early in the injured spinal cord in mice (Bastien et al., 2015). While neither precursor and mature forms of IL-1α were detected by immunofluorescence in adult uninjured mice, it became detectable as early as 4 hours post-SCI in spinal cord of injured mice. IL-1α was still detectable 24 hours post-injury. Notably, at 4 hours post-injury, IL-1α was mainly localized at the lesion epicenter and the surrounding areas. At 24 hours the IL-1α expressing cells were specifically detected at the contusion site (Zhu et al., 2017).

The IL-1α knock out mice (IL-1a KO) showed reduced myeloid cell infiltration, i.e.

neutrophils and M1 monocytes, 24h post-SCI compare to wild-type (WT) mice, importantly IL-1a KO showed a prolonged motor recovery associated with a reduced lesion volume 35 days following SCI compare to IL-1b KO and WT mice (Bastien et al., 2015). The better outcome of IL-1a KO has been correlated with an increased number of CC1 oligodendrocytes compared to WT injured mice (Bastien et al., 2015). Additionally, Anakinra's intrathecal delivery, the commercially available antagonist of IL-1R1, significantly ameliorate functional recovery of mice 15 days after the injury (Bastien et al., 2015).

2.4.4 IL-1α targeting in the context of stroke

The IL-1 family members are constitutively expressed at a low level in a healthy brain but that after an insult cytokine level upregulation rapidly occurs which has detrimental effects and exacerbates post-stoke damages (Rothwell and Luheshi, 2000). As in spinal cord injury, IL-1α is expressed early in the context of stroke. The presence of IL-1α has been detected 4 hours after reperfusion following ischemia in a model of stroke, while no IL-1β was detected (Luheshi et al., 2011a). Additionally, a significant increase in IL-1α mRNA was observed at this time point. Elevated levels of IL-1a were still observed at 24h after ischemia and were mostly localized near the penumbra surrounding the infarct (Luheshi et al., 2011a). While IL-1α KO showed improved recovery following SCI, deleting IL-1a gene was not sufficient to obtain beneficial effect after ischemic brain damage (Boutin et al., 2001). In their study, Boutin *et al* showed that in mice lacking either IL-1α or IL-1β ischemic damage was similar to WT mice. Interestingly, ischemic infarct volumes were significantly reduced in mice lacking both forms of IL-1 compared to WT mice. Some studies also highlighted the potency of inhibiting IL-1 pathway using an IL-1 receptor agonist. The intracerebroventricularly administration of IL-1Ra reduced infarct volume in WT (-32%) and IL-1a KO (-48%) mice but not in IL-b KO or IL-1a/b KO mice(Boutin et al., 2001). Also, peripheral delivery of IL-1RA shows potential benefit in acute stroke patients(Simi et al., 2007). In fact, clinical trials have shown that IL-1Ra's administration contributes to the inflammation alleviating due to the reduction of IL-6 in the circulation and cerebrospinal fluid of patients with subarachnoid hemorrhage (SAH) (Galea et al., 2018; Ravanelli and Appel, 2015; Singh et al., 2014).

Altogether, these data suggest that targeting IL-1 pathway and specifically IL-1α in the context of CNS injuries has a huge potential for short-window therapies. However, considering the proximity between IL-1α and IL-1β signaling, it becomes a necessity to demystify the specific signaling of IL-1α to ensure efficient targeting.

2.5 IL-33

2.5.1 IL-33 protein

IL-33 is a member of the IL-1 cytokines family and is involved in immune response through interaction with its receptor ST2. Similarly to prec-IL-1α, prec-IL-33 has an NLS, that allows its translocation into nucleus where it can regulate some histones dimers, favoring chromatin compaction and it can bind NF-kB at the nucleus and cytoplasm in HEK293 cells (Ali et al., 2011). Meanwhile, prec-IL-33 does not require maturation to be active and can be released during necrosis or necroptosis cell death although, once in the milieu it can be cleaved by neutrophil proteases such as cathepsin G and elastase (Lefrançais and Cayrol, 2012). The only well-documented receptor for IL-33 is the specific subunit ST2. Once the IL-33 has bonded to ST2, the complex recruits the coreceptor IL-1 receptor accessory protein (IL-1RAcP) and transduce the signaling via MyD88, resulting in the activation of the NF-kB pathway (Molofsky et al., 2016).

2.5.2 IL-33 targeting in the context of SCI

IL-33 is extensively expressed in several tissues i.e. lungs, spleen, lymph nodes, vasculature, skin, stomach and at the CNS (Pichery et al., 2012). The brain expression varies during development and at least in the adult spinal cord IL-33 is found in mature CC1 oligodendrocytes of white matter tracts and in some astrocytes of the gray matter (Gadani et al., 2015). ST2 is expressed in microglia during CNS homeostasis. IL-33 peaks at 1 hour in the cerebro-spinal fluid (CSF) and ST2 expression switch from microglia to astrocytes 1 day after SCI. In addition, IL-33 KO showed impaired mobility when compare to WT mice after SCI, related with reduced recruitment of M1 monocyte at 1 day post-SCI that inhibits its capacity to switch into arginase 1 (Arg1), IL-10, Mrc M2 monocytes at 7 days post-SCI, which results in bigger lesion volume (Gadani et al., 2015). Importantly, intraperitoneal (I.P.)

IL-33 administration following stroke and SCI had better prognosis when compared to WT, these improvements were associated with an increase in the expression of IL-10 and Arg1 in several tissues (i.e. spleen and spinal cord or brain) and correlated with a reduced astrogliosis (reduced GFAP intensity) (Korhonen et al., 2015; Pomeshchik et al., 2015a).

2.5.3 IL-33 targeting in the context of stroke

As in the context of SCI, IL-33 showed beneficial effects in stroke via the activation of ST2 receptors (Yang et al., 2017) and regulation of microglial activities(Luo et al., 2018). In two models of stroke, Yang *et al* (Yang et al., 2017) showed that lesion volumes were larger in ST2 KO mice than in wild type, accompanied by neurobehavioral deficits. They showed that this phenomenon could explain the potency of IL-33 to polarize microglia in a protective phenotype via ST2. They investigated the expression as well of IL-33 overtime after a stroke (1,3,7 and 14 days post injury) and they noticed a significant augmentation of IL-33 in oligodendrocytes and astrocytes 1 day after stroke followed by a return to basal level. Interestingly, IL-33 could also be used as a potential prognostic biomarker in acute ischemic stroke. Indeed, in a clinical study conducted on two hundred and six patients, Li *et al* (Li et al., 2016) showed that levels of IL-33 in patients suffering from acute ischemic stroke patients were correlated with the severity of the stroke. Considering the beneficial potency of IL-33 in the context of CNS injuries, it would be an interesting way to reduce damages with a double targeted therapy. On the one hand, by decreasing the effects of the pro-inflammatory alarmins, such as IL-1α, and on the other hand by increasing the anti-inflammatory potency of IL-33.

2.6 ATP

Adenosine 5’ Triphosphate (ATP) is a purine nucleotide derived from adenosine and discovered in the 1920’ by Fiske and Subbarow (Fiske and Subbarow, 1929). In addition to its involvement in muscular contraction, ATP also plays a fundamental role in cellular energetic mechanisms, cellular signaling or neurotransmission (Abbracchio et al., 2009; Burnstock, 1999). In the nervous system, ATP is found in every neuronal and glial cell, as well in SNC as in SNP. The levels of ATP are mainly regulated by mitochondrial activity through the electron transport chain (Saraste et al., 1990)·(Kinnally et al., 2011) and the

oxidative phosphorylation mechanism. The dysfunction of this electron transport chain under pathological condition impairs ATP synthesis and more dramatically increases ROS levels (Turrens, 2003). ATP can activate two principal classes of receptors: P2X, which are described as ionotropic receptors (ligand gated), and P2Y, known as metabotropic receptors (G-protein coupled). Evidences support the idea that during CNS injuries, such as hypoxia or ischemia, ATP triggers an excitotoxic role through activation of P2 receptors. Considering the complexity of ATP signaling, we will especially focus on its signaling via P2X4 and P2X7 receptors. Indeed, many studies have reported an important role of ATP in neuroinflammation after CNS injuries by activating innate immune responses essentially through P2X4 and P2X7 receptors (Coull et al., 2005; Inoue et al., 2003; Wang et al., 2004). More precisely, the decrease of extracellular Ca2+ induced by CNS injuries trigger ATP release and Ca2+ signaling, resulting in cell death through P2X7 signaling (Nilsson et al., 1993; Stokes et al., 1983; Stout and Charles, 2003).

2.6.1 ATP in the context of SCI

In a study focusing on the expression of P2X4 following spinal cord injury in rats, Schwab *et al* (Schwab et al., 2005) have found that P2X4 accumulated in cells as early as 24 hours after SCI. This expression reached a peak 7 days after the injury, and then decreased but remain detectable 1-month post-SCI. P2X4 was mainly localized in activated microglia/macrophages and surviving neurons/neurites. Moreover, it has been shown that inflammasome signaling was impaired in the injured spinal cords of P2X4 KO mice, resulting in decreased levels of IL-1β and reduced infiltration of neutrophils and monocytes-derived M1 macrophages. Consequently, these mice showed better recovery after SCI accompanied by better tissue sparing. On the other hand, after SCI P2X7 receptors activate NLRP1 inflammasomes in neurons and astrocytes through a pannexin-1 dependent mechanism (Silverman et al., 2009). The blockade of P2X7 receptor using OxATP or PPADS, two antagonists of P2X7, significantly improved functional recovery after SCI and decreased cell death in the peritraumatic area (Wang et al., 2004). Additionally, it has been proven that knocking-out P2X4 receptor induced a decrease of P2X7-induced cell death by disrupting ATP-driven interaction (Pérez-Flores et al., 2015). Thus, P2X receptors, and in particularl

P2X4 and P2X7, represent potential therapeutic targets to reduce inflammation and improve recovery following SCI.

2.6.2 ATP in the context of stroke

In a study evaluating ATP responses in the context of *in vivo* ischemia in rats, Melani *et al* (Melani et al., 2005) showed that ATP extracellular levels doubled 220 min after middle cerebral artery occlusion (MCAO). ATP extracellular concentrations were even three-fold increased after ischemia when ATP metabolization to adenosine was blocked using ecto-5'-nucleotidase. Considering this increase in ATP outflow after ischemia, it is interesting to investigate whether the expression of P2X receptors concomitantly increases. In a model of permanent focal cerebral ischemia, Franke *et al* (Copyright and Vol, 2004) showed a time-dependent upregulation of P2X7 receptors at the peri-infarct region after MCAO. In particular, P2X7 became up-regulated by microglial cells after 1 and 4 days, in tubulin β-III neurons after 4 and 7 days and on astrocytes after 4 days. Interestingly, P2X7 has been reported to be expressed by both activated microglia in the infarcted area as well as reactive microglia in the remote regions (Melani et al., 2006). The delivery of Reactive Blue 2, a P2 unselective antagonist, blocked the function of activated microglia in the infarct area and promoted P2X7 expression in reactive microglia of the remote brain regions, developing defense and leading to improved sensorimotor deficit and restricted infarct volume (Melani et al., 2006). Additionally, Yanagisawa *et al* (Yanagisawa et al., 2008) showed that the injection of a P2X7 receptor antagonist 3'-3'-O-'-4-benzoylbenzoyl-adenosine 5'-triphosphate (BzATP) improved function after MCAO while the injection of an antagonist of the receptor exacerbated ischemic brain damages. That correlates with the fact that a deletion of P2X7 or treatment with P2X antagonists in the context of cerebral ischemia did not affect cell death (Feuvre et al., 2003). On the other hand, the expression of P2X7 receptors by oligodendrocytes after ischemia led to cell death (Domercq et al., 2010) which can be reversed by P2X7 receptor antagonists. Otherwise extracellular adenosine concentration increases, same as ATP concentration, after a stroke and can bind to its specific P1 receptor but contrariwise of ATP in the setting of brain damage adenosine is considered to be neuroprotective (Pedata et al., 2016). In summary, all these data suggest that P2X7 receptor can trigger both positive and detrimental effects depending on the cell type and that P2X7

therapy in the context of stroke should be specifically targeted.

2.7 HMGB1

2.7.1 HMGB1 protein

High-Mobility Group Box-1 (HMGB1), known as amphoterin, is a highly abundant and conserved non-histone DNA binding protein that belongs to HMGB protein group (Agresti and Bianchi, 2003; Štros, 2010),(Jantzen et al., 1990) and presents numerous function including maturation, proliferation and motility as well as inflammation, survey and cell death (Lotze and Tracey, 2005; Qiu et al., 2014; Yanai et al., 2009),(Wang et al., 1999),(Andersson et al., 2000). This protein is composed of two-DNA binding boxes (box A and box B) and an acid c-terminal sequence that directs the protein towards the nucleus(Kawase et al., 2008),(Stott et al., 2010),(Bianchi et al., 1992) where it binds to DNA and acts as a chaperon (Osmanov et al., 2013). Inside the nucleus, HMGB1 contributes to chromatin architecture (Kawase et al., 2008; Osmanov et al., 2013; Sapojnikova et al., 2005),(Yuan et al., 2004) and can modulate genetic expression by facilitating telomerase activity and DNA repair upon ROS or radiation exposure(Manuscript and Structures, 2009). HMGB1 can also be translocated into the cytoplasm where it regulates autophagy or apoptosis processes, depending on its post-translational modifications and redox status (Andersson et al., 2014; Yang et al., 2012),(Medsker et al., 2016b),(Hoppe et al., 2006). When a disulfide bond (oxidized status) is formed between the cysteine (C23) and C45 found at the B box, HMGB1 promotes autophagy via beclin-1(Yang et al., 2012),(Venereau et al., 2012). Under normal conditions, HMGB1 expression is mainly localized in the nucleus of a vast variety of cells, particularly stromal and immune cells (i.e monocytes, tissue macrophages) and also in neurons (Enokido et al., 2008),(Li et al., 2017; Shi et al., 2018), astrocytes (Enokido et al., 2008),(Xie et al., 2016) and microglia (Shi et al., 2018) in the CNS. In the context of CNS injuries, HMGB1 can be translocated from the nucleus to the cytoplasm and then secreted by reactive astrocytes,(Xie et al., 2016),(Hayakawa et al., 2013),(Li et al., 2014), microglia and neurons (Li et al., 2017; Shi et al., 2018). In the first few hours after injury, HMGB1 is also released by necrotic cells and leads to inflammatory responses (Scaffidi et al., 2002). It may also have a role in astrocytic swelling (L. Sun et al., 2017; Zhang et al.,

2011) and microglial priming (Medsker et al., 2016b), (Shi et al., 2018). Its signalization pathway involves a wild range of receptor, including TLR2, TLR4, TIM-3, RAGE, IL-1R1, CXRCR4 that leads to the activation of NF-kB and MAP kinase pathways and proinflammatory cytokines up-regulation (Balosso et al., 2014), (Scaffidi et al., 2002). Altogether, these elements underlie the potential of targeting HMGB1 in the context of central nervous system injuries (Xiwei Zheng, Cong Bi, Marissa Brooks, 2015), such as spinal cord injuries and stroke (Uezono et al., 2018; D. Wang et al., 2017; Zhang et al., 2011).

2.7.2 HMGB1 targeting in the context of SCI

HMGB1 has been detected in the plasma of human suffering from acute and chronic traumatic spinal cord injury (Papatheodorou et al., 2017) as well as in post-mortem tissues by proteomics approaches identifying specific matrix extracellular proteome after SCI (Didangelos et al., 2016). In mice, HMGB1 mRNA and protein level increased after SCI, reaching a peak at 24-72 hours post-injury (Kigerl et al., 2017). Moreover, the injection of 500 ng HMGB1 into an intact spinal cord ventral horn led to neuronal death (Kigerl et al., 2017). Different studies targeting HMGB1 pathway have been tested in the context of SCI. A majority of these studies was based on the use of anti-HMGB1 neutralizing antibodies and showed promising results, but also underlined the importance of the dose to inject and the optimal temporal window (Kigerl et al., 2017; Nakajo et al., 2018; Uezono et al., 2018). The group of Popovitch (Kigerl et al., 2017) performed a daily intraperitoneally injection of 50 µg/day/mouse of anti-HMGB1 antibody from 1 day before to 7 days after SCI. Despite unsuccessful neuroprotection using neutralizing antibody to block HMGB1 in the context of SCI, the authors suggest that identifying optimal concentrations of HMGB1 antagonists could be the key to SCI therapies based on the inhibition of HMGB1. Additionally, the other critical point of such approaches relies on determining the optimal therapeutic window to deliver anti-HMGB1 antagonists. Studies focusing on the specific time course expression of HMGB1 in rodent models of SCI have allowed to identify more precisely a specific window for potential therapies targeting HMGB (Didangelos et al., 2016; Kigerl et al., 2017). The group of Nakashima conducted preliminary studies using an anti-HMGB1 neutralizing antibody in the context of SCI. The intraperitoneal injection of 8mg/kg of anti-HMGB1 antibody mAb (IgG2a) at 5 minutes and 6 hours after injury reduced blood-spinal cord barrier

disruption and edema formation and improved neuronal survival (Uezono et al., 2018). To elaborate a more practical treatment of SCI, they performed additional experiments to identify the best therapeutic window for an anti-HMGB1 therapy (Nakajo et al., 2018). The best results were obtained when anti-HMB1 mAb was delivered 3 hours post-injury, with an improved functional recovery compared to an immediate injection after the injury. Improvements were lower when the injection was performed 6 hours post-injury and 9 hours after injury therapeutic effects were no more detectable (Kigerl et al., 2017; Nakajo et al., 2018). Other approaches to block the HMGB1 signaling pathway are based on the use of chemical compounds or surgical interventions (Kang et al., 2015). Bi *et al* (Bi et al., 2017) showed that the intraperitoneally of 100mg/kg of shikonin, a compound extracted from Zicao and used for its anti-bacterial, anti-inflammatory and anti-tumor activities in various diseases, 30 minutes post-injury decreased the inflammatory process and increased recovery by reducing HMGB1 in a rat model of SCI. However, other studies that targeted a downstream part of the HMGB1 signaling pathway did not show amelioration in the context of SCI (H. Wang et al., 2017), underlying the importance of targeting specifically HMGB1. Taken together, the blockade and neutralization of HMGB1 after a spinal cord injury has shown to improve locomotor functions and neuronal survival as well as alleviate edema formation and blood-spinal cord barrier permeability (Sun et al., 2019). Altogether, targeting HMBG1 in the context of SCI can be a potential and practical therapy, but need to be applied in the first few hours following the injury.

2.7.3 HMGB1 targeting in the context of stroke

Systemic levels of HMGB1 are significantly increased in patients suffering from stroke(Vogelgesang et al., 2010),(Goldstein et al., 2006). This alarmin is quickly released after the injury and can last for a long period of time(Schulze et al., 2013). It been reported that HMGB1 induces proinflammatory factors such as TNF-a, IL-1b, COX-2 and iNOS and promote ischemic neuronal death *in vitro*(Faraco et al., 2007) . Kim et al. showed that the neuronal death is prevented by transfection of a HMGB1 short hairpin RNA into MCAO rat model. They also report a repression of those proinflammatory cytokines in the injected area(Kim et al., 2006). Some studies also showed interesting results to inhibit HMGB1 using neutralizing antibodies in the context of strokes and, as for SCI, the dose and the therapeutic

window are crucial points to consider. The group of Nishibori showed that the intravenous injection of an anti-HMGB1 mAb (1mg/kg, i.v twice) immediately and 6 hours after injury improved results after IHC-injuries provoked by collagenase IV injections in rats striatum by decreasing HMGB1 levels, improving BBB integrity and decreasing brain edema(Zhang et al., 2011). Additionally, Wang *et al*(Wang et al., 2016) showed that the blockade of HMGB1 using a polyclonal anti-HMGB1 antibody (600µg/mouse, i.p) 1 hour before ischemia reversed the inflammatory response and the extent of brain damage in diabetic mice. The infarct size was also significantly reduced when a neutralizing anti-HMGB1 antibody (600µg/mouse) was injected 15 minutes before MCAO (Muhammad et al., 2008). Apart from therapies based on anti-HMGB1 antibodies, a vast variety of compounds were shown to have potential therapeutic properties in the context of stroke. Glycyrrhizin (Gong et al., 2014) has been reported to present protective effects on focal cerebral ischemia/reperfusion as a direct inhibitor of HMGB1. Apelin-13 (Xin et al., 2015), fetuin-A (H. Wang et al., 2010), dioscin (Tao et al., 2015), thrombomodulin and higenamine (Ha et al., 2012) are other examples of agents that have been tested in the context of stroke and showed promising results. However, in many of these studies anti-HMGB1 antibodies were injected before the injury. The late treatment with anti-HMGB1 seems to have a protective effect on the brain damage caused by stoke (Halder and Ueda, 2018). As an actor in the early pro-inflammatory cytokine production, HMGB1 can create a feedback loop and increase cytokine production. Nishibori et *al*. showed that an anti-HMGB1 mAb reduces the expression of those cytokines and hence may alter the secondary inflammatory pathway responses (D. Wang et al., 2017). Further experiments with post injury's injection should be performed before to confirm the neutralizing potential of anti-HMGB1 antibodies in the context of strokes. By inhibiting the HMGB1 activity with a HMGB1-binding heptamer peptide, Li et al also demonstrated an improvement in BBB leakage and a reduction in complication due to tPA treatment. In summary, HMGB1 has a detrimental effect in early ischemic stage and pharmacological strategies to neutralize HMGB1 might be beneficial.

2.8 Conclusion

Advances have been made in the past years highlighting the mechanisms underlying pathophysiological disorder of CNS injuries. It was put forward and it is now indisputable that alarmins are essential in the immune response upon tissue damage, though they also play a dichotomous role dependent on affection and lesions in which they are involved. Alarmins are released after insult and tissue damage and they can modulate inflammation and as a consequence, trigger the release of proinflammatory cytokine thereby they have an important role to play on the pathology outcomes. Here, we have reviewed IL-1a, IL-33, ATP and HMGB1 as DAMPs with a focus on CNS injuries specifically spinal cord injuries and strokes. However, targeting alarmins remains a challenge. The pharmacological targeting of DAMPs could be a benefit, but further studies are needed to understand how those alarmins may be modulated for the patient's advantage and well-being.

Chapitre 3 MICROGLIA ARE AN ESSENTIAL COMPONENT OF THE NEUROPROTECTIVE SCAR THAT FORMS AFTER SPINAL CORD INJURY

Victor Bellver-Landete[1], Floriane Bretheau[1], Benoit Mailhot[1], Nicolas Vallières[1], Martine Lessard[1], Marie-Eve Janelle[2], Nathalie Vernoux[1], Marie-Ève Tremblay[1], Tobias Fuehrmann[3], Molly S. Shoichet[3] and Steve Lacroix[1]*

[1]Axe Neurosciences du Centre de recherche du Centre hospitalier universitaire (CHU) de Québec–Université Laval et Département de médecine moléculaire de l'Université Laval, Québec, QC, G1V 4G2, Canada; [2] Département de biologie-biotechnologie du Cégep de Lévis-Lauzon, Lévis, QC, Canada, G6V 6Z9; [3]Department of Chemical Engineering & Applied Chemistry, University of Toronto, Toronto, ON, M5S 3E1, Canada

Keywords: Astrocytic scar, CSF1R, fibrotic scar, hydrogel, IGF-1, M-CSF, microglia depletion, neuroinflammation, PLX5622, secondary degeneration.

3.1 Résumé

Le rôle des microglies lors d'une lésion de la moelle épinière (LME) reste incompris et souvent confus avec celui des macrophages dérivés du sang (MDMs). Dans cet article, nous utilisons une lignée de souris transgéniques fluorescentes permettant de visualiser spécifiquement les microglies et des drogues servant à éliminer celles-ci afin de mieux comprendre leurs réactions et rôles à la suite d'une LME. Nous avons observé que la microglie est très dynamique et prolifère abondamment durant la première semaine, s'accumulant autour du site lésionnel. À cet endroit, les microglies actives se positionnent à la jonction entre les leucocytes dérivés du sang et les astrocytes qui prolifèrent et qui forment la cicatrice gliale en réponse aux facteurs relâchés par les microglies elles-mêmes, comme par exemple le facteur de croissance 1 ressemblant à l'insuline (IGF-1). L'élimination des microglies après une LME entraine une perturbation dans la formation de la cicatrice gliale, permettant du même coup la migration des MDMs hors de la zone lésée. Ceci a pour effet de réduire la survie des neurones et des oligodendrocytes et de perturber la récupération des fonctions locomotrices. Par ailleurs, une prolifération microgliale induite via un traitement local au M-CSF a pour effet de réduire la taille de la lésion et d'améliorer le recouvrement des fonctions motrices. Ainsi, nos résultats définissent la microglie comme un composant cellulaire important de la cicatrice qui se développe après une LME afin de protéger le tissu neuronal.

3.2 Abstract

The role of microglia in spinal cord injury (SCI) remains poorly understood and is often confused with the response of macrophages. Here, we use specific transgenic mouse lines and depleting agents to understand the response of microglia after SCI. We find that microglia are highly dynamic and proliferate extensively during the first two weeks, accumulating around the lesion. There, activated microglia position themselves at the interface between infiltrating leukocytes and astrocytes, which proliferate and form a scar in response to microglia-derived factors, such as IGF-1. Depletion of microglia after SCI causes disruption of glial scar formation, enhances parenchymal immune infiltrates, reduces neuronal and oligodendrocyte survival, and impairs locomotor recovery. Conversely, increased microglial proliferation, induced by local M-CSF delivery, reduces lesion size and enhances functional recovery. Altogether, our results identify microglia as a key cellular component of the scar that develops after SCI to protect neural tissue.

3.3 Introduction

Microglia derive from primitive yolk sac progenitors that arise during embryogenesis (Ginhoux et al., 2010; Kierdorf et al., 2013; Schulz et al., 2012) . They are maintained after birth and into adulthood by self-renewal (Askew et al., 2017; Tay et al., 2017), independently from bone marrow-derived hematopoietic stem cells (HSCs) and their differentiated progeny (e.g. monocyte-derived macrophages, MDMs) (Hoeffel et al., 2016; Sheng et al., 2015). After a CNS injury, blood-derived monocytes are massively recruited in the tissue where they differentiate into macrophages and adopt many of the markers and behaviors of microglia. These similarities have complicated the development of efficient prediction tools to discriminate between them. As a consequence, they are still referred to as microglia/macrophages in the neuroscience literature, and accordingly, their individual roles remain to be clarified.

Recent advances in genetic fate mapping and conditional gene targeting have allowed the study of the specific biology of microglia in various experimental contexts, including SCI . This, together with the newly-developed strategies to specifically eliminate microglia (Dagher et al., 2015), has moved forward knowledge about these cells substantially. For example, the application of some of these advances to a mouse model of stroke has led to the discovery that microglia can protect neurons through the regulation of calcium levels (Szalay et al., 2016). In contrast, the elimination of microglia in mouse models of Alzheimer's disease and Tau pathology reduced disease progression (Asai et al., 2015; Rice et al., 2015). Thus, depending on the context, microglia may exert diverging roles. Whether these cells are beneficial or deleterious after SCI remains unexplored.

Here, we took advantage of *Cx3cr1*^{creER} mice (Yona et al., 2013), a mouse line that allows with an adequate regimen of tamoxifen to label microglia while excluding nearly all MDMs. Our results show that microglia are highly dynamic and proliferate extensively during the first week post-SCI. Notably, we reveal that microglia form a dense cellular interface at the border of the lesion between reactive astrocytes and infiltrating MDMs, which we hereafter refer to as the "microglial scar". Microglia depletion experiments using PLX5622, a CSF1R inhibitor that crosses the blood-spinal cord barrier (BSCB), demonstrated that the absence of microglia in the context of SCI disrupts the organization of

the astrocytic scar, reduces the number of neurons and oligodendrocytes at the site of injury, and impairs functional recovery. The timing of the beneficial effects of microglia was estimated to be during the first week post-SCI. Accordingly, CNS delivery of M-CSF during that critical period boosted microglial proliferation and enhanced locomotor recovery. In light of these data, we conclude that microglia are an important component of the protective scar that forms after SCI.

3.4 Results

3.4.1 Microglia rapidly accumulate around the site of SCI

To distinguish microglia from MDMs, we took advantage of *Cx3cr1*^{creER}::*R26-TdT* mice, and the slow turnover of microglia (Askew et al., 2017; Tay et al., 2017). Mice received tamoxifen treatment one month before SCI to activate the inducible Cre for recombination of TdT floxed (Supplementary Figure 1a). As expected from our previous work (Lévesque et al., 2016), nearly all (99.6 ± 0.2 %) CD11b$^+$ cells in the spinal cord parenchyma expressed TdT (Supplementary Figure 1b-c). In contrast, only a few CD11b$^+$ cells in the blood, spleen and bone marrow were TdT$^+$, with average colocalization percentages of 3.8 ± 1.7 %, 6.7 ± 1.6 % and 2.4 ± 0.2 %, respectively (Supplementary Figure 1d-f). Thus, inducible *Cx3cr1*^{creER}::*R26-TdT* mice are a good tool to study microglia in SCI.

To understand the dynamics of the microglial response after SCI, we first quantified the total number of TdT$^+$ microglia both in normal conditions and at 1, 4, 7, 14 and 35 days post-injury (dpi) (Fig. 1a-g & Supplementary Figure 2). In the uninjured thoracic spinal cord of *Cx3cr1*^{creER}::*R26-TdT* mice, we counted an average of 85.9 ± 4.6 microglia per mm^2. Following a moderate contusive SCI, only 28.8 ± 1.9 microglia per mm^2 were left at the lesion epicenter at 1 dpi, which corresponds to a 67% reduction in cell numbers. Hardly any TdT$^+$ microglia were observed in the lesion core at this early time point, suggesting that they underwent rapid cell death. Despite the fact that the impactor tip measures 1.25 mm of diameter, microglia were lost across several spinal cord segments rostrocaudally. This microglial cell loss ranged from approximately 20% to 65% at rostrocaudal distances up to 6 mm from the lesion epicenter (Fig. 1g-h), and was mediated in part through apoptosis (Fig.

1i-k). At that time, residual microglia still expressed the purinergic receptor P2ry12 (Supplementary Figure 3), a receptor implicated in microglia recruitment during the early acute phase of CNS injury (Haynes et al., 2006). Accordingly, we noticed a retraction of microglial processes as early as day 1. Expression levels of the lysosome-associated glycoprotein CD68, a marker of phagocytosis, remained low in TdT^+ microglia at 1dpi (Supplementary Figure 4). However, the situation changed at day 4, as we counted 119.1 ± 15.0 microglia per mm^2 at the lesion epicenter, which represents a 4-fold increase in the number of TdT^+ microglia compared to day 1 (Fig. 1g). Microglia around the lesion epicenter exhibited a round morphology, downregulation of P2ry12 and a strong upregulation of CD68 (Supplementary Figures 3-4), which points to a potential increase in their phagocytic activity starting around 4 dpi. The number of microglia continued to increase at the lesion epicenter over time, reaching up to 1204.61 ± 137.8 cells/mm^2 at 14 dpi. Nearly all microglia observed in these areas were TdT^+ $CD68^{hi}$ $P2Y12^{neg}$ (Supplementary Figures 3-4). A similar trend was seen in the surrounding tissue (400-800 µm) of the lesion epicenter up to 35 dpi, after which the total number of microglia (i.e. 673.91 ± 62.4 cells/mm^2 at the lesion epicenter) started to decrease compared to day 14 (Fig. 1g). Interestingly, TdT^+ microglia started to gradually increase their expression of P2ry12 and decrease their expression of CD68 from day 14 up to day 35 (Supplementary Figures 3-4), suggesting a partial return to homeostasis. In sum, our data indicate that microglia are rapidly recruited around the site of SCI, where they accumulate extensively during the subacute phase and adopt an activated state that is eventually partially resolved during the intermediate/chronic phases.

3.4.2 Microglia proliferate extensively during the subacute phase of SCI

Under normal circumstances, the adult microglial population remains stable in the brain throughout life by coupled cell death and cell proliferation (Askew et al., 2017), but little is known about its dynamic in the spinal cord and how it reacts following SCI. Here, we report that 0.6 ± 0.1 microglia/mm^2 (0.58% of total) are proliferating in the normal thoracic spinal cord of *Cx3cr1*^{creER}::*R26-TdT* mice, as revealed by the co-expression of TdT and the cell proliferation marker Ki67. One day after SCI, no significant changes were observed in terms of microglial cell proliferation compared to the uninjured spinal cord (Fig. 1l-m). Strikingly, about 50% of microglia at the lesion epicenter expressed Ki67 at 4 dpi. As shown in

Supplementary Movie 1, proliferating TdT^+ $Ki67^+$ microglia were round-shaped. The peak proliferation of microglia, in terms of absolute numbers, was observed at day 7 (Fig. 1l, n-p). At 14 and 35 dpi, only a few (2-6%) microglia were still expressing Ki67, suggesting that microglial proliferation was mostly inhibited by then. Together, these results show that microglia are highly dynamic after SCI, not only through their recruitment and activation, but also through their ability to rapidly proliferate and surround the site of SCI during the subacute phase.

3.4.3 Depletion of microglia reduces locomotor recovery after SCI

Yolk sac progenitors are at the origin of specialized tissue-resident macrophages, including microglia, and depend on colony-stimulating factor 1 receptor (CSF1R) signaling for their survival (Perdiguero et al., 2015). Thus, to better understand the role of microglia and MDMs in SCI, we compared the effects of two novel CSF1R inhibitors from Plexxikon: 1) PLX5622, a drug that crosses the blood-brain barrier (BBB) and eradicates nearly all microglia in the brain (Cavnar et al., 2013; Dagher et al., 2015; Elmore et al., 2014; Rice et al., 2015; Szalay et al., 2016), and 2) PLX73086, a CSF1R inhibitor that does not deplete resident microglia because of its low BBB penetration (Dr. Andrey Rymar, Plexxikon, personal communication). Treatment of uninjured C57BL/6 mice with PLX5622 for 3 weeks resulted in depletion of 97.9 ± 0.6% of spinal cord microglia (Fig. 2a-d & Supplementary Figure 5). In contrast, PLX73086 did not affect the microglial population. To examine the effects of the two CSF1R inhibitors on peripheral immune cells, we next performed a cytometric analysis of leukocyte subsets in the blood, spleen and bone marrow. No changes were observed after 3 weeks of treatment with the different diets (Supplementary Figure 6a-c). Altogether, these data indicate that PLX5622 can be used to selectively and nearly completely eliminate spinal cord microglia without significantly affecting peripheral leukocyte counts under steady state in vivo conditions in mice.

To examine the long-term effect of continuous PLX5622 treatment on microglia depletion, we counted the number of microglia per mm^2 at 1, 7 and 14 days post-SCI (Fig. 2e-h). Mice were fed chow containing either PLX5622, PLX73086 or vehicle (without gavage) starting 3 weeks before SCI and until time of sacrifice. Again, treatment of C57BL/6 or *Cx3cr1*^{creER}::*R26-TdT* mice with PLX5622 eliminated virtually all microglia at each of the

above time points. Although no changes were observed at day 1 and day 14 between PLX73086-treated mice and those fed the control diet (Fig. 2e, g), we found that the total number of TdT^+ microglia at the lesion epicenter was reduced by nearly half at 7 dpi in animals that received PLX73086 (Fig. 2f). This might be due to a temporary breakdown of the BSCB, which allowed PLX73086 to enter the spinal cord parenchyma and to negatively affect microglial cell survival. In accordance, we detected an increased accumulation of fluorescein isothiocyanate (FITC)-conjugated Lycopersicon esculentum agglutinin (LEA) lectin from day 1 to day 7 post-SCI at the lesion site, but not at 14 dpi (Fig. 2i).

At 1 dpi, a slight neutropenia was observed in C57BL/6 mice treated with PLX5622 or PLX73086 compared to those fed with the control diet (Supplementary Figure 6d). However, the number of infiltrating neutrophils at the site of SCI was similar between all groups at this time (Fig. 2j). No changes in blood leukocyte numbers were observed between groups at 7 and 14 dpi (Supplementary Figure 6e-f), except for a slight and transient decrease in the B cell counts at day 7. Treatment of *LysM-eGFP* mice with CSF1R inhibitors highlighted a transient reduction in the number of myeloid cells at the lesion epicenter in PLX5622-treated mice that was overcome by day 14 (Fig. 2k). Treatment with PLX73086 had no impact on the number of neutrophils and $LysM^+$ cells at the lesion site compared to control treatment (Fig. 2j-k). We interpret that the delayed myeloid cell recruitment in the injured spinal cord of PLX5622-treated mice was caused by the absence of microglia rather than a direct effect on peripheral leukocytes. Overall, these results indicate that PLX5622 can be used to eradicate virtually all spinal cord microglia after SCI with minimal direct effects on leukocytes.

We next investigated the role of microglia in functional recovery after SCI. Chow containing either PLX5622, PLX73086 or no drug (control) was given to C57BL/6 mice starting 3 weeks prior to SCI and then maintained for an additional 5 weeks (Fig. 3a). Similar to uninjured mice that received the control diet, microglia-depleted uninjured animals showed no gross locomotor deficits at the beginning of behavioral testing, as illustrated by the perfect BMS scores and subscores at day 0. No difference was found in terms of BMS score between the PLX73086 and control groups at any of the time points analyzed after SCI (Fig. 3b). However, mice depleted in microglia (PLX5622) exhibited impaired locomotor recovery compared to mice treated with PLX73086 or the control diet at 3, 7, 14, 28 and 35

dpi (Fig. 3b). Statistical differences in the BMS subscores between PLX5622-treated mice and animals of the other groups were detected starting from day 7 up to day 35 (Fig. 3c). At 35 dpi, the average subscore of PLX5622-depleted mice was 2.9 ± 0.6 compared to 4.5 ± 0.2 for PLX73086-treated mice and 5.4 ± 0.2 for mice fed the control diet. These results indicate that microglia play an essential role in recovery from SCI.

3.4.4 The beneficial actions of microglia occur during week 1 post-SCI

Recent work has established that the microglia-depleted brain repopulates within one week through local proliferation of residual microglia (Huang et al., 2018). We reasoned that we could take advantage of this observation to study the time window during which the neuroprotective and/or neurorepair effects of microglia occur after SCI. We first evaluated the time course of repopulation of microglia in the spinal cord (Supplementary Figure 7). *Cx3cr1*^{creER}::*R26-TdT* mice were fed ad libitum for one week with the appropriate treatment. At this time, we counted 75.9 ± 7.9 TdT$^+$ microglia per mm^2 in the thoracic spinal cord of mice fed the control diet compared to 4 ± 0.6 in those treated with PLX5622 (94.7% depletion). The dynamic of the microglial repopulation was then assessed by switching the PLX5622 group to the control diet (Supplementary Figure 7a-m). The diet change resulted in a rapid increase in the number of microglia in the uninjured spinal cord, going from 4.0 ± 0.6 TdT$^+$ cells per mm^2 at day 0 to 15.8 ± 2.0 at day 2 and 35.3 ± 2.8 at day 3. By day 7 of withdrawal of CSF1R inhibition, the microglial population had completely recovered, with an average count of 99.5 ± 2.3 cells per mm^2, exceeding by ~30% the microglia numbers counted in control mice (Supplementary Figure 7m). Repopulated TdT$^+$ cells, observed after 7 days of drug withdrawal, had a ramified morphology and expressed CD11b and Iba1 (Supplementary Figure 7i-l, n), confirming that they are mature microglia. Only few (2.3 ± 1.7%) of the repopulated CD11b$^+$ Iba1$^+$ cells were TdT^{neg} at 7 days post-withdrawal. This indicates that microglia were repopulated from cells in which the Cx3cr1 gene promoter was active (i.e. TdT$^+$) at the time of tamoxifen treatment, confirming that adult spinal cord microglia are capable of self-renewal. A similar trend was also seen in C57BL/6 mice, in which the total number of P2ry12$^+$ microglia, after a repopulation period of 7 days, exceeded that of untreated mice by 54% (116.5 ± 5.4 P2ry12$^+$ cells/mm^2 compared to 75.7 ± 2.1 P2ry12$^+$ cells/mm^2).

As described above, spinal cord microglia of adult naïve mice are in low proliferative state (Supplementary Figure 7o). However, 2 and 3 days after PLX5622 removal, 93.5% and 87.4% of the TdT^{+} microglia, respectively, were actively proliferating based on Ki67 expression. Few TdT^{neg} cells also proliferated simultaneously to microglia proliferation but at a reduced rate. Multiple immunofluorescence labeling revealed that the non-microglia proliferating cells were mostly of the oligodendrocyte lineage, with 6.1 ± 0.9 and 6.7 ± 1.9 $Olig2^{+}$ TdT^{neg} $Ki67^{+}$ cells/mm^2 at 2 and 3 days, respectively (Supplementary Figure 7p). GFAP-positive astrocytes, $CD206^{+}$ perivascular macrophages, $CD13^{+}$ pericytes, and $CD45^{+}$ TdT^{-} blood-derived leukocytes accounted for less than 1% of the $Ki67^{+}$ cells. Therefore, our results indicate that residual microglia proliferate extensively and can repopulate the entire spinal cord microglial population within 7 days.

We next sought to determine when the beneficial effects of microglia occur after SCI, as this is critical for the development of a therapeutic approach targeting microglia. For that purpose, C57BL/6 mice were fed PLX5622 for 3 weeks, before switching to a control diet at the time of SCI (Fig. 3d), resulting in microglia depletion at the time of injury but not afterwards. No differences were found in behavioral outcomes between groups (Fig. 3e-f). As microglial repopulation requires about a week to be completed after cessation of treatment with the CSF1R inhibitor (Supplementary Figure 7i-m), we next hypothesized that the beneficial effects of microglia might take place during the first week post-SCI. Since injured mice eat significantly less during the first few days, separate groups of mice were force-fed with either PLX5622 or vehicle by gavage from the time of SCI up to day 7 (Fig. 3g), in addition to the ad libitum access to the drug-containing chow. Importantly, PLX5622-gavaged mice showed impaired locomotor recovery on the BMS scale compared to control mice (Fig. 3h-i). In contrast, SCI mice that were started on the PLX5622 diet at day 3 displayed locomotor scores similar to those observed in the PLX73086 and control groups (Fig. 3j-l). Altogether, these data indicate that activated, proliferating microglia are crucial for protecting/repairing the injured spinal cord and that their beneficial effects take place during the first week post-SCI.

3.4.5 A microglial scar forms at the astrocyte–immune cell interface

It was recently proposed that cytokines released by activated microglia in response to CNS injury or disease determine whether astrocytes will have neurotoxic or pro-survival effects (Liddelow et al., 2017b)

. Thus, we next investigated whether microglia play an important role in the formation of the astrocytic scar that develops during the subacute/chronic phases of SCI and which can influence axonal regeneration and functional recovery. As neutrophils and MDMs rapidly accumulate in the injured spinal cord and share common markers with microglia, *Cx3cr1*^{creER}::*R26-TdT*::*LysM-eGFP* reporter mice were initially used to perform an immunofluorescence and ultrastructural characterization of glial scar formation over time (Supplementary Figure 8a). We found that TdT^{+} microglia accumulate mainly around the lesion site, where they make direct contacts with GFAP^{+} astrocytes, especially their distal processes, and also with blood-derived LysM^{+} cells (Fig. 4a-g, Supplementary Figures 8b-e & 9). This microglial interaction with GFAP^{+} astrocytes and blood-derived LysM^{+} cells was most apparent starting at 14 dpi and persisted until at least day 35. As described above, nearly half of the microglia detected at the rim of the lesion were actively proliferating at day 7, a response that returned near baseline by day 14 (Fig. 4h). This translated into an increased number of TdT^{+} microglia at the lesion epicenter at 14 dpi (Fig. 4i). However, we noted that the lesion itself was predominantly occupied by LysM^{+} neutrophils/MDMs and PDGFR-ß$^{+}$ pericytes rather than TdT^{+} microglia (Fig. 4j-l). These results indicate that microglia synergize with reactive astrocytes, and perhaps as well with pericytes, to isolate infiltrating immune cells at the core of the lesion. We named this phenomenon “microglial scar” as an analogy to the astroglial-fibrotic scar that develops after SCI and limits the spread of inflammatory cells, and at the same time influences regeneration of the severed axons (Cregg et al., 2014; Sofroniew, 2015).

Since a residual fraction of peripheral myeloid cells express TdT in *Cx3cr1*^{creER}::*R26-TdT* (Supplementary Figure 1b), we further validated our microglial scar concept in chimeras resulting from the transplantation of *β-actin-eGFP* bone marrow cells into lethally irradiated *Cx3cr1*^{creER}::*R26-TdT* mice (Fig. 5a). Fourteen days after SCI, the microglial scar was still prominent and primarily consisted of TdT^{+} microglia, with infiltrating bone marrow-derived (eGFP^{+}) cells located at the core of the lesion (Fig. 5b-e). In contrast, very few TdT^{+} cells

were seen at the rim of the lesion when *Cx3cr1*^{creER}::*R26-TdT* mice were used as bone marrow donors for recipient C57BL/6 mice (Fig. 5f-h). Indeed, we found ~25 times less TdT^{+} cells in *Cx3cr1*^{creER}::*R26-TdT* → WT mice (49.5 ± 8.0 cells/mm^2) compared to *Cx3cr1*^{creER}::*R26-TdT* mice (1204.61 ± 137.8 TdT^{+} cells/mm^2, Fig. 1 e, g) at 14 dpi. This suggests that cells from the periphery contribute minimally (less than 4%) to the total TdT^{+} cell number in experiments using inducible *Cx3cr1*^{creER}::*R26-TdT* mice. Additionally, we inflicted SCI in *Flt3*^{cre}::*R26-TdT* mice (Supplementary Figure 8f), in which TdT is expressed in HSCs and their progeny (including MDMs and neutrophils), but not microglia (Perdiguero et al., 2015). At 14 dpi, a dense layer of CD11b^{+} TdT (Flt3)^{neg} cells was clearly detectable at the interface between GFAP^{+} astrocytic end-feet on the outside of the lesion and CD11b^{+} TdT (Flt3)$^{+}$ blood-derived myeloid cells inside the lesion (Supplementary Figure 8g-j). This once again indicates a minimal contribution of blood-derived myeloid cells to the microglial scar that rapidly forms after SCI.

To eliminate the possibility that long-living TdT^{+} perivascular and/or meningeal macrophages could be at the origin of the microglial scar, immunofluorescence staining was performed to detect the co-expression of TdT and markers of perivascular and meningeal macrophages. CNS border-associated macrophages were defined based on expression of macrophage mannose receptor (CD206) and major histocompatibility complex class II (MHCII) (Mrdjen et al., 2018; Zeisel et al., 2015). Although some TdT^{+} microglia at the rim of the lesion were CD206^{+} at 14 dpi, they weakly expressed CD206 compared to perivascular and meningeal macrophages (Fig. 5i-o & Supplementary Figure 10a-c). We failed to detect MHCII expression on TdT^{+} microglia (Fig. 5p & Supplementary Figure 10d-e). Instead, the MHCII signal was restricted to TdT^{neg} myeloid cells that infiltrated the lesion core, as well as perivascular and meningeal macrophages. In sum, our results demonstrate that a microglial scar, consisting of primarily proliferating microglia, forms at the border of the lesion after SCI.

3.4.6 Microglia induce astrocytic scar formation via IGF-1

Adequate astrocyte reactivity and glial scar formation have been shown to be vital for recovery of neurological functions after SCI (Faulkner, 2004; Okada et al., 2006). Strikingly, we observed that astrocytes located just outside of the lesion core formed a less compact scar

when microglia were depleted using PLX5622 compared to the control treatment at 14 dpi (Fig. 6a-d). Notably, $GFAP^+$ astrocytes were oriented randomly and not aligned in any particular direction in PLX5622-treated SCI mice. This disorganized astroglial scar was accompanied by an increased infiltration of blood-derived myeloid cells inside the spinal cord parenchyma, outside of the primary lesion. Since glial scar borders that surround the site of SCI are typically formed by newly proliferated astrocytes (Wanner et al., 2013), we next investigated whether microglial depletion was associated with changes in astrocytic proliferation. To enable accurate counting of proliferating ($BrdU^+$) astrocytes, these cells were identified based on expression of Sox9, a nuclear protein exclusively expressed by astrocytes in the adult CNS (except for ependymal cells) (W. Sun et al., 2017). As shown in Figure 6e-k, the number $Sox9^+$ $BrdU^+$ astrocytes at the lesion epicenter and in adjacent areas was reduced by ~40-55% in PLX5622-treated mice compared to the control group at 7 dpi. This suggests that, after SCI, microglia release molecules that trigger astrocyte proliferation and astrocyte scar formation.

Given the recent demonstration that the astrocyte response is determined by cytokines released by activated microglia in models of neuroinflammation (LPS) and CNS injury (optic nerve crush), we studied the expression of cytokines identified as confirmed or potential inducers of A1 (TNF, IL-1α, IL-1β, IL-6) and A2 (TGF-β1, IGF-1) phenotypes using in situ hybridization (ISH). From 7 to 14 dpi, the period during which we observed the greatest proliferation of astrocytes and formation of the astroglial scar, mRNA transcripts for the proinflammatory cytokines IL-1α, IL-1β, IL-6, and TNF-α were weakly expressed at the lesion epicenter (Fig. 7a-d). In contrast, we detected strong expression of TGF-β1 and IGF-1 mRNAs at these times (Fig. 7e-l). The spatial distribution of TGF-β1- and IGF-1-expressing cells correlated with the microglial scar, with more ISH signal at the lesion border than at the lesion center. Accordingly, selective depletion of microglia resulted in a decrease of TGF-β1 and IGF-1 mRNA signals. To further demonstrate the involvement of microglia-derived TGF-β1 and IGF-1 in the formation of the astrocytic scar, we treated primary astrocytes with recombinant forms of these proteins. As shown in Figure 7m-n, treatment with IGF-1, but not TGF-β1, induced the proliferation of astrocytes (BrdU incorporation) and their migration towards the site of injury (scratch assay). Immunolabeling for IGF-1 in tissue sections from *Cx3cr1*^{creER}::*R26-TdT* mice confirmed that scar-forming TdT^+ microglia

are the principal cellular source of this factor at 7 dpi (Fig. 7o-q). Accordingly, in vivo inhibition of the IGF-1 receptor using an antagonist, OSI-906 (Quail et al., 2017), resulted in reduced expression of the astrocyte-specific marker Sox9 in the injured spinal cord of C57BL/6 mice (Fig. 7r). Thus, microglia-derived IGF-1 triggers astrocyte proliferation and promotes astrocyte scar formation after SCI.

Since reactive astrocytes were previously shown to exert protective functions after SCI (Faulkner, 2004), we next aimed to determine whether microglial depletion affects tissue damage. Quantification revealed that disrupted glial scar formation in PLX5622-treated mice is correlated with an increase of the lesion core area at 7 days post-SCI (Fig. 8a-c). Although no significant differences were observed between groups regarding the lesion core area at 14 and 35 dpi, we detected the presence of several secondary satellite lesions outside of the primary lesion in the spinal cord parenchyma of microglia-depleted mice (Fig. 8d-i). Secondary satellite lesions were devoid of neuronal elements (NF-H$^+$) and instead filled by blood-derived myeloid cells (CD11b$^+$ LysM$^+$) and PDGFRβ$^+$ pericytes/fibroblasts (Fig. 8j-k). Together, these results indicate that microglia play an important role in the formation of the astroglial scar after SCI, which is at least partly mediated by IGF-1, and that failure to carry out this function results in widespread inflammation and the appearance of satellite lesions.

3.4.7 Microglia prevent death of neurons and oligodendrocytes after SCI

Having established that the lesion load was increased and functional recovery worse in microglia-depleted mice at 35 days post-SCI, we next determined whether microglial elimination would influence the survival of neurons and oligodendrocytes. No differences in numbers of HuC/HuD$^+$ neurons and Olig2$^+$ CC1$^+$ mature oligodendrocytes were seen between groups in the absence of injury (Fig. 8l, p). However, there were fewer neurons and oligodendrocytes in spinal cord sections spanning the lesion site in the PLX5622 group compared with the other groups at 35 dpi (Fig. 8m-o, q). As expected, this difference resolved at distances >1.0 mm from the lesion site, thus suggesting that microglia are necessary for the survival of neurons and oligodendrocytes following an insult. Altogether, our results indicate that microglia play a neuroprotective role during SCI.

3.4.8 Boosting microglial proliferation enhances recovery after SCI

The above results demonstrate the importance of the microglial response in scar formation, protection of neural tissue and functional recovery after SCI. We therefore asked whether an increased microglial population would be beneficial on the outcome of SCI. As we observed that 7 days after the end of PLX5622 regimen the microglial population exceeded the one observed in homeostatic conditions (Supplementary Figure 11a-c), we subjected microglia-repopulated C57BL/6 mice to SCI (Supplementary Figure 11d). Although these mice had ~50% more microglia in their spinal cord at the time of injury, they exhibited no motor benefit (Supplementary Figure 11e-f). These results suggest that microglial density at the time of injury is not the limiting factor in recovery.

Since we previously demonstrated that microglia exert their beneficial effects during the first week post-SCI, coinciding with their maximal proliferation rate (Fig. 1m), we hypothesized that artificially increasing their proliferative response right after the injury and continuously during the first week would lead to improvements. Given the importance of CSF1R signaling in microglia development, we tested whether M-CSF injection in the cisterna magna would induce microglial proliferation throughout the spinal cord. As shown in Figure 9a, treatment with M-CSF induced a dose-dependent effect on microglia proliferation, increasing by ~20-25% the number of $CD11b^{+}$ $P2ry12^{+}$ microglia in the thoracic spinal cord. Notably, this effect lasted for at least one week. To target the lesion site rather than the entire spinal cord, we incorporated M-CSF into a bioresorbable hydrogel that was injected into the intrathecal space at the site of SCI (Fig. 9b). Previous work has established that the hyaluronan-methyl cellulose hydrogel can provide sustained drug release for 3-7 days (Caicco et al., 2013; Elliott Donaghue et al., 2015; Kang et al., 2009). Despite the fact that treating *Cx3cr1*^{creER}::*R26-TdT* mice with the M-CSF-based hydrogel resulted in a non-significant trend towards a higher number of TdT^{+} microglia (Fig. 9c), it was sufficient to reduce the lesion area rostral to the epicenter at 7 dpi (Fig. 9d). In addition, the M-CSF-delivering hydrogels improved locomotor recovery from day 7 to day 21 after SCI when compared with PBS-based hydrogels (Fig. 9e-f). This suggests that enhancing the proliferation of microglia limits tissue loss and functional deficits following SCI through regulation of scar tissue formation. Altogether, our results demonstrate the importance of microglia in protecting the spinal cord after injury.

3.5 Discussion

The role of microglia in SCI has remained obscure for decades. Here, we took advantage of newly-developed genetic mouse models, in particular the *Cx3cr1*^{creER} mouse strain, and depletion strategies (e.g. the CSF1R inhibitor PLX5622) that allow us to target microglia specifically to study their role in the context of traumatic SCI. We found that microglia proliferate extensively and accumulate around the site of contusion at 7 days, forming a dense scar at the interface between the fibrotic scar and the yet-to-be-formed astrocytic scar. Notably, the near-complete elimination of spinal cord microglia by PLX5622 treatment led to a reduction in IGF-1 production, a disorganized astroglial scar and the appearance of satellite lesions filled with blood-derived inflammatory cells. This was accompanied by an increased loss of neurons and oligodendrocytes at the site of SCI, as well as greater tissue damage and impairment in locomotor function. The comparison of two CSF1R inhibitors with different BSCB permeability (given at various times before and after SCI) provided strong evidence that the protective function of microglia takes place during the first week post-SCI, matching the peak of proliferation of microglia. Accordingly, local delivery of the microglial proliferation factor, M-CSF, at the site of contusion significantly improved locomotor recovery compared to vehicle controls.

We initially predicted, based on previous SCI studies using radiation bone marrow chimeras, that MDMs would infiltrate almost exclusively the core of the lesion, while microglia would be found both within spared CNS tissue and the lesion itself (Donnelly et al., 2011; Popovich and Hickey, 2001). However, genetic fate mapping using *Cx3cr1*^{creER}::*R26-TdT* and *Cx3cr1*^{creER}::*R26-TdT*::*LysM-eGFP* mouse lines revealed that microglia at the site of trauma rapidly die after SCI. Additionally, we found that microglia that surround the lesion site rapidly become activated and proliferate extensively, forming a previously undescribed scar tissue, which we now refer to as the microglial scar. Our findings also contrast with those of Shecther and colleagues who reported that MDMs are restricted to the margins of the lesion and excluded from the center of the lesion (Shechter et al., 2009). Rather, the margins (borders) of the lesion are entirely occupied by microglia and pericytes/fibroblasts, whereas MDMs are confined to the center of the lesion. This once again shows that, although radiation bone marrow chimeras remain a useful tool, data generated

using them must be interpreted with care because: i) whole-body irradiation harms the blood-CNS barriers and impairs the proliferative capacity of microglia (Bruttger et al., 2015), and ii) HSCs and their progenitors are artificially introduced in the bloodstream as a result of the bone marrow transplant, thus creating a bias towards cells of the hematopoietic compartment (Ajami et al., 2007; Mildner et al., 2007). Using animal models that did not introduce such artifacts, we can conclude that blood-derived myeloid cells that infiltrate the injured spinal cord remain at the center of the lesion, where they are confined by surrounding tissue consisting of the microglial, fibrotic, and astrocytic scars.

As initially observed in the brain (Elmore et al., 2014), continuous treatment with the CSF1R inhibitor PLX5622 resulted in the depletion of spinal cord microglia (99.6%), that was in our hands more efficient than *Cx3cr1*^{creER}::*R26-iDTR* transgenic mice (77.9%), in which diphtheria toxin (DT) has to be injected to induce cell death (Parkhurst et al., 2013). The PLX5622 treatment also avoided the occurrence of the undesired cytokine storm described by Bruttger and colleagues using the iDTR model (Bruttger et al., 2015), thus making it a better model to study the role of microglia. We found that the recruitment of MDMs is delayed in the injured spinal cord of PLX5622-treated mice during the acute phase. This finding is consistent with our previous observation that physically injured microglia release damage-associated molecular patterns (DAMPs), such as IL-1α, that initiate sterile neuroinflammation after SCI (Bastien et al., 2015).

Historically, microglial activation in the injured CNS was generally perceived as harmful to both neurons and oligodendrocytes because of the release of high amounts of proinflammatory cytokines, proteases and reactive oxygen species. Supporting this view is the recent discovery that cytokines derived from activated microglia, such as IL-1α, TNF and C1q, determine whether astrocytes will have neurotoxic or pro-survival effects in various neurodegenerative disorders (Liddelow et al., 2017b). Accordingly, deletion of either of the genes encoding IL-1α, TNF and C1q in the context of SCI has been associated with an improved locomotor recovery (Bastien et al., 2015; Galvan et al., 2008; Kroner et al., 2014). However, the data here show that the elimination of microglia leads to aberrant growth factor production (e.g. IGF-1) and glial scar formation, increased neuronal and oligodendrocyte death, as well as reduced locomotor performance. In line with our results is a recent stroke study, where microglia depletion using PLX3397, a CSF1R inhibitor that also targets c-KIT

and FLT3, increased neuronal death and infarct size in the brain (Szalay et al., 2016). This once again reinforces the idea that the overall net effect of microglia after CNS injury is neuroprotection. Although the early infiltration of blood-derived myeloid cells at sites of SCI was previously associated with neurotoxicity (Blight, 1994; K. A. Kigerl et al., 2009; Popovich et al., 1999), we cannot rule out the possibility that these cells may have contributed to the functional recovery effect seen in PLX5622-treated mice. If it were to be the case, we argue that it would be under the positive influence of microglia as evidence here indicates that the reduction in myeloid cell infiltration was a direct cause of the absence of microglia. In the context of CNS injury, therapies targeting microglia should therefore be aimed at enhancing their neuroprotective function and/or reducing their neurotoxicity rather than complete microglia eradication.

We uncovered that microglia regulate the astrocytic response, in part, through IGF-1. The fact that activated, proliferating microglia are an important source of IGF-1 following a CNS insult is line with findings of Lalancette-Hébert et al. in a mouse model of ischemic stroke (Lalancette-Hébert et al., 2007). There is also ample in vitro evidence that IGF-1 modulates astrocyte proliferation and the migratory ability of these cells towards a lesion (Faber-Elman et al., 1996; P A Tranque, R Calle, F Naftolin, 1992). It should be noted, however, that TGF-β1 at the concentration tested in the present study and elsewhere was found not to be mitogenic for astrocytes (Hunter et al., 1993; Lindholm et al., 1992). Still, a role for microglia-derived TGF-β1 in scar formation remains plausible because this cytokine was found to influence astrocytes by acting in synergy with other cytokines and growth factors (Hunter et al., 1993), and as likely to occur in the complex *in vivo* setting of CNS injury where TGF-β1 neutralization reduces scarring (Hellal et al., 2011; Kohta et al., 2009; Logan et al., 1994). It will therefore be of interest in future work to validate the relevance of these cytokines and their receptors, individually or in combination, in animal models of SCI using cell-specific conditional gene targeting strategies.

In the absence of microglia, glial scar formation was perturbed, and this resulted in an increased presence of infiltrating blood-derived myeloid cells around the site of trauma. Satellite lesions filled with inflammatory cells have been reported before following depletion of reactive astrocytes (Faulkner, 2004), as well as in mice with conditional deletion of the *Stat3* gene from astrocytes after SCI (Herrmann et al., 2008; Okada et al., 2006). Given the

importance of astrocytic Stat3 activation in glial scar formation, we speculate that cytokines of the IL-10 families could be additional candidate upstream mediators of these effects (for review, see (Bastien and Lacroix, 2014)). Taken together with the finding that microglia-derived cytokines, such as IGF-1, regulate astrocyte function in pathological conditions (Liddelow et al., 2017b), our results indicate that activated microglia trigger scar formation after SCI.

The identification of the first week post-SCI as the time window for the beneficial effect of microglia suggests that treatments targeting these cells should be initiated promptly. This therapeutic time window is in line with clinical trials that focus on immunomodulators as potential treatments for SCI. We also provide evidence that microglia proliferate actively during this period, and that boosting their proliferative response during the early acute phase of SCI using a hydrogel-based M-CSF delivery system further enhances functional recovery.

In light of the current data, we conclude that activated, proliferating microglia play a key role in the formation of the scar that develops after SCI (Bracken et al., 1997, 1992; Casha et al., 2012), and that these multicellular interactions serve to sequester blood-derived immune cells in the lesion core, thus protecting non-injured neurons and oligodendrocytes from inflammation-mediated tissue damage.

3.6 Materials and methods

3.6.1 Animals

A total of 394 mice were used in this study. C57BL/6N mice were purchased from Charles River Laboratories at 8-10 weeks of age. *Cx3cr1*^{creER}::*Rosa26(R26)-TdT* transgenic mice were generated as before (Lévesque et al., 2016), and bred with *LysM*-eGFP knock-in mice created by Dr. T. Graf (Center for Genomic Regulation, Barcelona, Spain) to obtain *Cx3cr1*^{creER}::*R26-TdT*::*LysM-eGFP*. Breeders for Flt3-cre mice were obtained from Drs. Thomas Boehm and Conrad C. Bleul, Max Planck Institute, Freiburg, Germany. All mice were bred in-house at the Animal Research Facility of the Centre de recherche du Centre hospitalier universitaire de Québec–Université Laval. Mice had free access to food and water at all time. All animal procedures were approved by the Centre de recherche du CHU de Québec–Université Laval Animal Care Committee and conducted in compliance with relevant ethical regulations and guidelines of the Canadian Council on Animal Care.

3.6.2 Tamoxifen treatment

To induce recombination in *Cx3cr1*^{creER}::*R26-TdT* and *Cx3cr1*^{creER}::*R26-TdT*::*LysM*-eGFP mouse lines, mice were treated orally with 10 mg of tamoxifen (dissolved in 1:10 ethanol/corn oil) twice at 2-day intervals starting at postnatal day (P) 30-32. The animals were then allowed a resting period of 28 days prior to SCI to allow sufficient time for the turnover of MDMs and near disappearance of TdT^+ cells in the blood, spleen and bone marrow.

3.6.3 Spinal cord injury (SCI)

Mice were anesthetized with isoflurane and underwent a laminectomy at vertebral level T9-10, which corresponds to spinal segment T10-11. Briefly, the vertebral column was stabilized and a contusion of 50 kdyn was performed using the Infinite Horizon SCI device (Precision Systems & Instrumentation). Overlying muscular layers were then sutured and cutaneous layers stapled. Post-operatively, animals received manual bladder evacuation twice daily to

prevent urinary tract infections. Depending on the experiment performed, SCI mice were killed by transcardiac perfusion at 1, 4, 7, 14 and 35 days post-contusion.

3.6.4 Microglia depletion

To eliminate microglia, mice were fed PLX5622 (1200 ppm) or PLX73086 (200 ppm) provided by Plexxikon and formulated into AIN-76A chow from Research Diets Inc. For gavage experiments, mice received PLX5622 at 90 mg/kg once a day for 7 consecutive days, starting immediately after SCI. PLX5622 was diluted in 5% DMSO, 0.5 % hydroxypropyl methyl cellulose and 1% polysorbate 80. An equal volume of vehicle was used as control.

3.6.5 Systemic intravascular lectin injections

To visualize blood-perfused microvessels and determine the time course and magnitude of BSCB permeability after SCI, mice were injected in the tail vein with FITC-conjugated LEA lectin (100 µg/100 µl, Sigma-Aldrich Canada Ltd.) 10 minutes prior to transcardial perfusion.

3.6.6 Bromodeoxyuridine (BrdU) injections

To label proliferating cells, mice were intraperitoneally injected once daily with BrdU (50 mg/kg of body weight in 0.9% saline) for 6 consecutive days, starting on day 1 after SCI.

3.6.7 In vivo IGF-1R inhibition

To determine whether IGF-1/IGF-1R signaling is involved in astrocytic scar formation, mice were orally administered with OSI-906 (also known as Linsitinib, Selleckchem), a CNS-penetrant pharmacological inhibitor of IGF-1R. OSI-906 was formulated daily at 4 mg/ml in 25 mM tartaric acid with shaking and sonication for 15 min and then given by gavage once a day for 7 consecutive days at 40 mg/kg, starting immediately after SCI.

3.6.8 Intra-cisterna magna M-CSF injections

In the experiment in which we studied the effects of central M-CSF treatment on the proliferation of spinal cord microglia, mice were injected intra-cisterna magna (i.c.m.) with recombinant murine M-CSF (PreproTech) at various doses ranging from 25 to 250 ng/µl in

PBS. The i.c.m. treatment consisted of a single injection using a pulled-glass micropipette connected to a 10-µl Hamilton syringe.

3.6.9 Tissue processing

For the purpose of histology and immunofluorescence experiments, mice were overdosed with a mixture of ketamine-xylazine and transcardially perfused with PBS followed by 1% PFA, pH 7.4, in PBS. Spinal cords were dissected out and then immersed for two days in a PBS solution containing 20% sucrose for cryoprotection. For each animal, a spinal cord segment of 12 mm centered over the lesion site was cut in 7 series of 14 µm-thick coronal sections using a cryostat. For experiments involving ISH, mice were transcardially perfused with a 0.9% saline solution followed by 4% PFA, pH 9.5, in borax buffer. Spinal cords were post-fixed for an additional 2 days in 4% PFA, and then placed overnight in a 4% PFA-borax/10% sucrose solution. Thirty-µm-thick cryostat coronal sections were collected directly onto slides that have a permanent positive charged surface (Leica Biosystems) and stored at –20 °C until ISH was performed.

3.6.10 Immunofluorescence and confocal imaging

Immunofluorescence labeling was performed according to our previously published method. Primary antibodies used in this study are of the following sources (catalog numbers in parentheses) and were used at the indicated dilutions: rat anti-BrdU (1:750, Abcam, ab6326), mouse anti-CC1 (1:500, Abcam, ab16794), rat anti-CD11b (1:250, AbD Serotec, MCA711), goat anti-CD13 (1:100, R&D Systems, AF2335), rat anti-CD45 (1:500, BD Biosciences, 553076), rat anti-CD68 (1:2500, AbD Serotec, MCA1957), goat anti-CD206 (1:50, R&D Systems, AF2535), rabbit anti-cleaved caspase-3 (Asp175) (1:250, Cell Signaling Technology, 9661), rat anti-GFAP (1:1000, Invitrogen, 13-0300), rabbit anti-GFAP (1:750, Dako, Z0334), mouse anti-HuC/HuD (1:80, Thermo Fisher Scientific, A-21271), goat anti-iba1 (1:1000, Novus Biologicals, NB100-1028), goat anti-IGF-1 (1:10, R&D Systems, AF791), rabbit anti-Ki67 (1:200, Abcam, ab15580), rat anti-Ly6G *(1:2000, BD Biosciences, 551459)*, chicken anti-neurofilament H (NF-H, 1:500, EMD millipore, AB5539), goat anti-Olig-2 (1:400, R&D Systems, AF-2418), rabbit anti-P2ry12 (1:500, Anaspec, AS-55043A), rabbit anti-PDGFRβ (1:750, Abcam, ab32570), and rabbit anti-Sox9 (1:1000, Millipore,

AB5535). For Ki67 immunofluorescence, antigen retrieval was performed using sodium citrate buffer at 95ºC for 5 min. For BrdU, tissue sections were treated with HCl (2.0 N) for 30 min at 37 °C followed by 0.1M sodium borate (pH 8.5) for 10 min at room temperature. Alexa Fluor secondary antibodies from Thermo Fisher Scientific (1:250 dilution) or Vector Laboratories (1:500) were used for multicolor immunofluorescence imaging, whereas 4', 6-diamidino-2-phenylindole, dilactate (DAPI; 1 µg/ml, Thermo Fisher Scientific) was used for nuclear counterstaining. Sections were imaged on a Zeiss LSM 800 confocal microscope system equipped with 405, 488 nm, 561 nm, and 640 nm lasers. Confocal images were acquired using a Zeiss Axiocam 506 Mono camera and mosaics created using the Zen 2.3 software (Blue edition).

3.6.11 In situ hybridization (ISH)

ISH was carried out to detect mRNAs coding for IL-1α, IL-1ß, IL-6, TNF, TGF-β1 and IGF-1, following our previously published method. Primer pairs and enzymes used for riboprobe synthesis are listed in Supplementary Table 1.

3.6.12 Quantitative analyses

For the quantification of microglia (TdT^+ or $CD11b^+$ $P2yr12^+$ or $CD11b^+$ TdT^+), proliferating microglia ($Ki67^+$ TdT^+), neutrophils ($Ly6G^+$), blood-derived myeloid cells ($LysM^+$), astrocytes ($Sox9^+$), neurons (HuC/HuD^+), oligodendrocytes ($Olig\text{-}2^+$), proliferating oligodendrocytes ($Ki67^+$ $Olig\text{-}2^+$), proliferating astrocytes ($BrdU^+$ $Sox9^+$ or $Ki67^+$ $GFAP^+$), proliferating perivascular macrophages ($Ki67^+$ $CD206^+$), proliferating pericytes ($Ki67^+$ $CD13^+$), and proliferating leukocytes ($Ki67^+$ $CD45^+$ TdT^-), the total number of immunolabeled cells per cross section was counted at 20× magnification using mosaics created from 6-12 overlapping confocal images or images obtained using a Zeiss Slide Scanner Axio Scan.Z1. A threshold was applied to the resulting images to trace the contour of the coronal section and a grid of 50 µm × 50 µm positioned over the spinal cord either using ImageJ2 (version 1.51d) or BIOQUANT Life Science software (v. 18.5, Bioquant Image Analysis Corporation). Immunolabeled cells with a DAPI-stained nucleus were then manually counted. Results were presented as the total number of positive cells per cross-section, the average number of positive cells per mm^2 of tissue section, the percentage of

cells that expressed specific markers (Ki67), or the mean area under the curve (AUC) of the number of cells per mm^2 in a predetermined distance range (Sox9).

For the quantification of the BSCB permeability, the proportional area of tissue stained with the FITC-LEA lectin within the entire coronal section at the lesion epicenter was measured using images taken at 20× magnification with the Zeiss Slide Scanner Axio Scan.Z1. Thresholding values in Fiji (version 1.52h, National Institutes of Health, NIH) were chosen such that only labeled product resulted in measurable pixels on the digitized images. Contrast between positive signal and background was maximized and held constant between all images. Data were expressed as the proportional area of the tissue section occupied by FITC staining. Proportional area of tissue occupied by GFAP (astrocytes), TdT (microglia) and PDGFRβ (pericytes/fibroblasts) immunolabeling was measured in increments of 40 µm relative to the distance from astrocytic endfeet. The area of tissue occupied by immunostaining in each sampling region was measured using the BIOQUANT Life Science software on video images of tissue sections transmitted by a high-resolution Retiga QICAM fast color 1394 camera (1392 x 1040 pixels, QImaging) installed on a Nikon Eclipse 80i microscope. Thresholding values in BIOQUANT Life Science were chosen such that only immunolabeled product resulted in measurable pixels on the digitized image. Contrast between immunolabeling and background was maximized and held constant between all specimen. Data were presented as the proportional area of the sampling region occupied by immunolabeling.

The calculation of areas of tissue damage after SCI was performed on 1 series of adjacent sections within a predetermined spinal cord segment, including the lesion epicenter and surrounding sections in both directions (i.e., rostral and caudal). Fourteen-µm-thick coronal sections were first immunostained for GFAP as well as LysM, NF-H and/or PDGFRβ. Sections were then counterstained with DAPI and confocal mosaics prepared as described above. For each section, the outline of the core and satellite lesions were separately traced at 20× magnification and areas measured using ImageJ2. Both types of lesions were surrounded by GFAP-positive astrocytic processes. However, satellite lesions were adjacent to the lesion core and defined as the absence of normal spinal cord architecture and presence of blood-derived myeloid cells ($CD11b^+$) and pericytes ($PDGFR\beta^+$).

The average density of ISH signal was measured within the entire cross-section at the lesion epicenter. Mean grey values (MGV, ranging from 1 to 256 bits) were measured under dark-field illumination on video images of tissue sections transmitted by the Retiga camera, using the BIOQUANT Life Science software. Mean grey values were corrected for the average background signal, which was measured in three boxes of 50H x 50W µm (80H x 80W pixels) placed in regions where no positive signal was observed. ISH data were expressed as an average MGV of the section. All quantifications were done blind with respect to the identity of the animals.

3.6.13 Biological sample collection and processing for cytometry

Animals were anesthetized with a mixture of 400 mg/kg ketamine and 40 mg/kg xylazine. Blood was collected via cardiac puncture using a 22-gauge syringe and immediately transferred into EDTA-coated microtubes (Sarstedt). Blood samples were then put on slow rotation at room temperature until processing. Prior to collection of the spleen and femurs, animals were transcardially perfused with cold Hanks' balanced salt solution (HBSS) to remove blood from the vasculature.

Spleens were harvested from anesthetized animals and placed in HBSS (without Ca^{2+}/Mg^{2+}). Spleens were homogenized and passed through a 70-µm nylon mesh strainer (BD Biosciences). Erythrocyte lysis was performed using the ACK buffer. The cell suspension was passed on a second 70-µm nylon mesh strainer and the cell count measured.

For the bone marrow, animals were anesthetized and their left femurs isolated and flushed with HBSS (without Ca^{2+}/Mg^{2+}) + 2% FBS using a 25-gauge needle. Erythrocytes were lysed using the ACK buffer (NH_4Cl 150 mM, potassium bicarbonate 10 mM, EDTA 0.01 mM). Cells were manually counted with a hemocytometer (Hausser Scientific).

3.6.14 Flow cytometry

Cells freshly isolated from the blood, spleen and bone marrow of SCI mice were analyzed using flow cytometry. In brief, red blood cells were first lysed and the remaining cells incubated with Mouse Fc Block (i.e., purified anti-mouse CD16/CD32; BD Biosciences) for 15 min at 4°C to prevent nonspecific binding. Multicolor immunolabeling was then performed for 30 min at 4°C using the following fluorescently conjugated primary antibodies:

PerCP-conjugated anti-CD45 (1:50 dilution), Alexa 700-conjugated anti-CD11b (1:50), BD HorizonTM V450-conjugated anti-Ly6C (1:83), PE-Cy7-conjugated anti-Ly6G (1:50), APC-conjugated anti-CD3e (1:50) and Alexa 488-conjugated anti-B220 (1:50) (all from BD Biosciences; for a full description of these primary antibodies, please refer to our published work). Cells were analyzed using FlowJo software (v. 9.2; Tree Star Inc.) on a FACS LSRII flow cytometer (BD Biosciences). Cells were identified as follows: $CD45^{hi}$ $CD11b^{+}$ $Ly6C^{+}$ $Ly6G^{+}$ cells were considered as neutrophils, $CD45^{hi}$ $CD11b^{+}$ $Ly6C^{hi}$ $Ly6G^{-}$ cells as $Ly6C^{high}$ monocytes (also known as M1 monocytes or monocyte-derived M1 macrophages), $CD45^{hi}$ $CD11b^{+}$ $Ly6C^{lo}$ $Ly6G^{-}$ cells as $Ly6C^{low}$ monocytes (or M2 monocytes), $CD45^{hi}$ $CD11b^{-}$ $B220^{+}$ $CD3e^{-}$ cells as B cells, and $CD45^{hi}$ $CD11b^{-}$ $B220^{-}$ $CD3e^{+}$ cells as T cells.

3.6.15 Behavioral analysis

Recovery of locomotor function after SCI was quantified in an open field using the Basso Mouse Scale (BMS), according to the method developed by Basso and colleagues. All groups of mice exhibited similar parameters in terms of the impact force and spinal cord tissue displacement prior to BMS testing. All behavioral analyses were done blind with respect to the identity of the animals.

3.6.16 Immunoelectron microscopy

Mice were anesthetized with sodium pentobarbital (80mg/kg, intraperitoneally) and perfused with 3.5% acrolein followed by 4% PFA. Fifty-micrometer-thick coronal sections of the spinal cord were cut in sodium phosphate buffer (50 mM, pH 7.4) using a Leica VT1000S vibratome (Leica Biosystems) and stored at -20^{o}C in cryoprotectant until use. Spinal cord sections were rinsed in PBS (50 mM, pH 7.4) and then quenched with 0.3% hydrogen peroxide (H_2O_2) for 5 min followed by 0.1% sodium borohydride ($NaBH_4$) for 30 min. Afterwards, sections were rinsed three times in PBS and incubated for 1h in blocking buffer (5% fetal bovine serum, 3% bovine serum albumin, 0.01% Triton X-100) and then overnight with a primary anti-GFAP antibody (1:1000 dilution, Thermo Fisher Scientific). The next day, sections were rinsed three times in PBS and incubated for 2h with secondary antibody conjugated to biotin (1:500, Vector Laboratories) and for 1h with Vectastain® Avidin-Biotin Complex Staining kit (Vector Laboratories). Sections were developed in a Tris buffer

solution (TBS; 0.05M, pH 7.4) containing 0.05% diaminobenzidine and 0.015% H_2O_2 and then rinsed with PBS and incubated overnight with a primary anti-RFP antibody (1:1000, Rockland). The next day, sections were rinsed in TBS and incubated overnight with secondary antibody conjugated to gold (1.4 nm Nanogold goat anti-rabbit, 1:50, Nanoprobes). Then the sections were washed three times with TBS and twice with 3% sodium acetate. Using the HQ Silver Enhancement kit (Nanoprobes), the staining was revealed at room temperature for 1 min and rinsed quickly with sodium acetate followed by three 5-min washes with PBS. The sections were post-fixed with 1% osmium tetroxide, dehydrated using sequential alcohol baths followed by propylene oxide. Sections were embedded in Durcupan resin (Sigma-Aldrich Canada Ltd.) between ACLAR sheets at 55°C for 3 days. Ultrathin sections were generated at ~65 nm using a Leica UC7 ultramicrotome. Images were acquired at 1900× or 4800× magnification using a FEI Tecnai Spirit G2 transmission electron microscope (Thermo Fisher Scientific) operating at 80kV and equipped with a Hamamatsu ORCA-HR digital camera (10 MP).

3.6.17 Production of bone marrow chimeras

Recipient mice (*Cx3cr1*^{creER}::*R26-TdT* or C57BL/6 mice) were exposed to a total body γ-irradiation with a single dose of 7.5 Gy using a cesium-173 source (Gammacell 40 Exactor, MDS Nordion) to destroy hematopoietic stem cells. Recipients were then injected in the tail vein with a total of 9×10^6 bone marrow cells freshly isolated from either β-actin-GFP or *Cx3cr1*^{creER}::*R26-TdT* donors, as described before. Briefly, femurs and tibias were harvested from euthanized donor mice and flushed with HBSS (without Ca^{2+}/Mg^{2+}) + 2% FBS using a 25-gauge needle. After the bone marrow transplantation, mice were kept in sterile cages and treated for 2 weeks with antibiotics (2.5 mL of Septra (GlaxoSmithKline) in 200 mL of drinking water), and let to recover an additional 8 weeks (for a total of 70 days) before being subjected to SCI.

3.6.18 Proliferation and scratch wound assays

Primary cultures of mouse astrocytes were prepared from the cortex of P0-P1 pups, as described in, and used from passages 3 to 4. Cells were grown in complete Dulbecco's Modified Eagle Medium (DMEM) either on glass coverslips coated with poly-L-lysine (0.1

mg/ml) in 24-well plates (for the proliferation assay) or directly into 24-well plates (for the scratch wound assay) at a density of 200,000 cells/well. After 1 day in culture for the proliferation assay and two days for scratch wound assay, cells were starved for 18 hours after reaching a confluence level of ~70%. The proliferation assay was initiated by the addition of either recombinant mouse (rm) TGF-β1 (50 ng/ml, dissolved in PBS containing 4 mM HCl; R&D Systems), rmIGF-1 (760 ng/ml, dissolved in PBS; R&D Systems) or their respective vehicle. Six hours before the end of the experiment (48 hours after growth factor addition), a single dose of 10 µM bromodeoxyuridine (BrdU; Sigma-Aldrich Canada Ltd.) was added to each well. The BrdU labeling solution was then removed and cells washed several times with PBS. Cells were next fixed with 4% PFA for 15 min, permeabilized in PBS/0.1% Triton X-100 for 20 min, treated with HCl (2.0 N) for 20 min at 37 °C followed by 0.1M sodium borate (pH 8.5) for 30 min at room temperature, and then immunostained for BrdU. The total number of proliferating cells was counted on images taken at 10× magnification, using the "Co-localization and Analyze Particles" plugin in Fiji. Data were expressed as number of $BrdU^+$ YO-PRO-1^+ cells per mm^2. For the scratch wound assay, confluent cells were starved for 18 hours and a linear scratch made in the cell monolayer using a 10-µl sterile pipette tip. Complete DMEM was used to wash the cells three times, after which the growth factors identified above were added in 0.2% serum medium. The closure of the wound was monitored using a Zeiss Axio Observer.Z1 Inverted Microscope equipped with an AxioCam MRm digital camera and an incubation chamber by imaging each well every 4 hours over 48 hours. The phase-contrast images were analyzed by measuring the closure percentage of the scratch, relative to the initial width (t = 0), at various times following exposure to the factors under study.

3.6.19 Subdural hydrogel implantation

Hydrogels containing particular M-CSF were prepared as in. Briefly, methlycellulose (310 kDa, Shin-Etsu) and hyaluronan (1200-1900 kDa, FMC) were dissolved in ddH_2O, sterile filtered, lyophilized (Labconco) under sterile conditions, and stored at 4 °C until use. An initial particulate dispersion was produced by mixing M-CSF powder into 0.5% w/v methlycellulose solution. Drug loaded hydrogels were prepared by physical blending hyaluronan (HA, 1.6 x 10^6 g/mol), methylcellulose (3 x 10^5 g/mol), and methylcellulose

containing M-CSF in artificial cerebrospinal fluid (aCSF: 148 mM NaCl, 3 mM KCl, 0.8 mM $MgCl_2$, 1.4 mM $CaCl_2$, 1.5 mM Na_2HPO_4, 0.2 mM NaH_2PO_4 in ddH_2O, pH adjusted to 7.4, filter sterilized at 0.2 µm) for a final composition of 1.4% w/v HA, 3% w/v MC, and 0.5 µg/µl M-CSF. Components were dispersed in aCSF using a dual asymmetric centrifugal mixer (Flacktek Inc.) and dissolved overnight at 4 °C. On the day of the hydrogel implantation, a 5-µl Hamilton syringe (32-gauge needle with a pre-bent blunt tip) was filled with either M-CSF-loaded or PBS-loaded hydrogels. A needle was then used to gently puncture the dura at the level of the contusion injury and 2 µl of hydrogel injected subdurally immediately following SCI.

3.6.20 Statistical Analysis

Statistical evaluations were performed with one- or two-way ANOVA or repeated-measures ANOVA, as indicated in figure legends. Post-ANOVA comparisons were made using the Bonferroni correction. All statistical analyses were performed using the GraphPad Prism software (GraphPad Software Inc.). A p value < 0.05 was considered as statistically significant.

3.6.21 Data availability

The data that support the findings of this study are available from the corresponding author upon reasonable request.

3.7 Acknowledgments

This study was supported by grants from the International Foundation for Research in Paraplegia (P161 to S.L.), the Wings for Life Spinal Cord Research Foundation (WFL-CA-006/11 to S.L.), and the Canadian Institute of Health Research (Foundation Grant to M.S.S). M.E.J. is supported by the Research Support Program for College Teachers-Researchers of the Fonds de recherche en santé–Québec. We thank Nadia Fortin for her invaluable technical assistance and TransBIOTech–Centre de recherche et de transfert en biotechnologies for giving us access to their inverted fluorescence microscope. We also thank Plexxikon Inc. for

providing us with the PLX5622 and PLX73086 compounds, and Drs. Brian L. West and Andrey Rymar for their guidance on how to use these drugs effectively in rodents. We are grateful to Drs. Bleul and Boehm for providing the Flt3-Cre mice.

3.8 Author contributions

V.B.-L. conceived the study, designed and performed most of the experiments, analyzed the data, drafted the figures and wrote the manuscript. F.B. designed and performed in vitro experiments, performed immunofluorescence, microscopy imaging and quantitative analyses, and commented on the manuscript. B.M. performed the in vivo permeability assay and related quantitative analysis and commented on the manuscript. N.Vallières performed in situ hybridization, immunofluorescence and flow cytometry experiments, acquired microscopy images, performed quantitative analyses and edited all figures. M.L. generated bone marrow chimeras, performed in vitro and in vivo immunofluorescence, flow cytometry experiments and quantitative analyses. M.-E.J. performed in vitro assays and related analyses. N.Vernoux performed immunoelectron microscopy. M.-È.T. performed immunoelectron microscopy and commented on the manuscript. T.F. prepared the hydrogels, trained staff for the subdural implantation and commented on the manuscript. M.S.S. provided the hydrogels and commented on the manuscript. S.L. conceived the study, designed the experiments, supervised the overall project and wrote the manuscript.

3.9 Figures

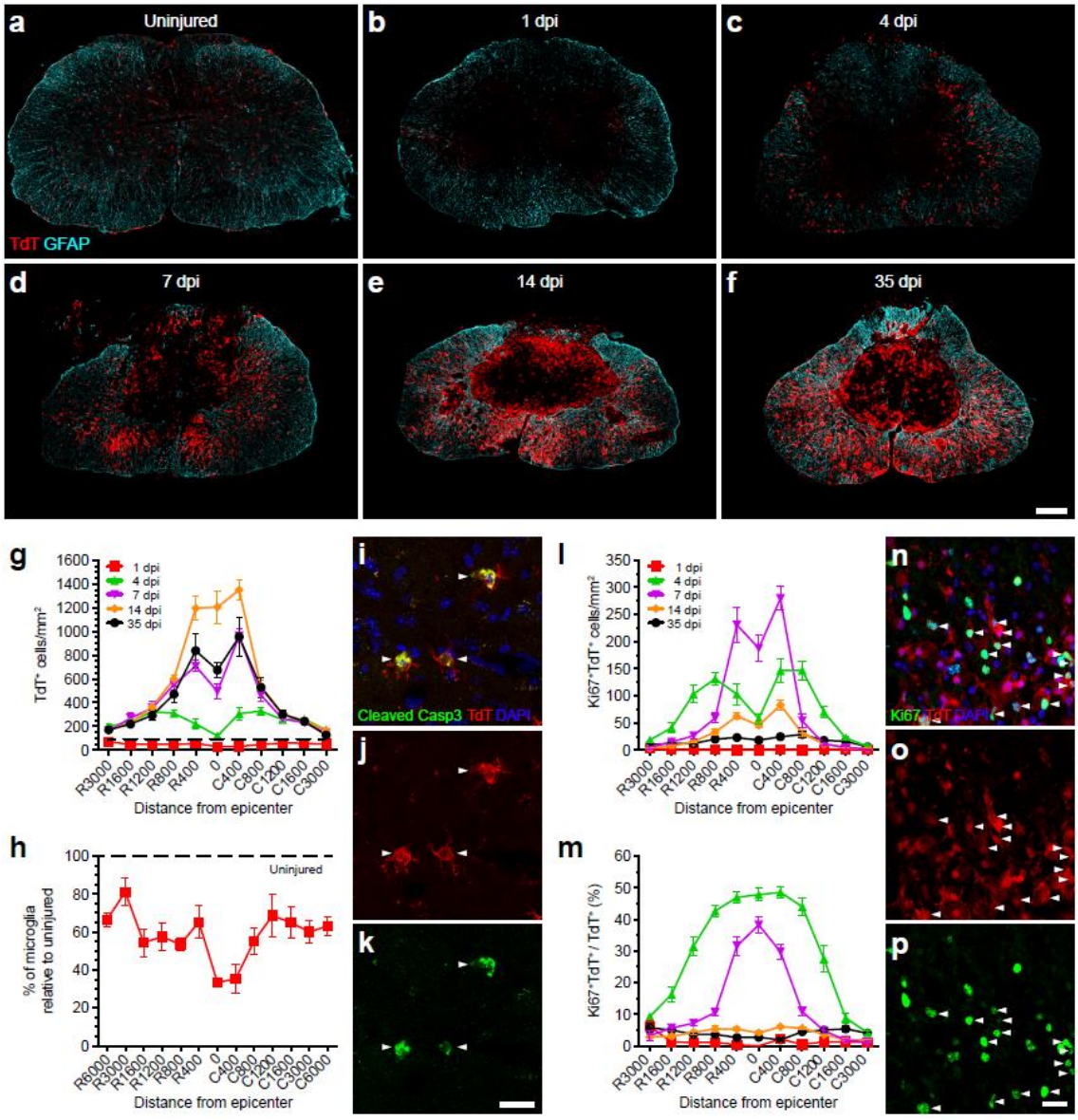

Figure 3.1 Microglia proliferate extensively and accumulate at the lesion border after SCI.

(**a-f**) Confocal immunofluorescence microscopy of representative spinal cord sections showing the spatio-temporal distribution of microglia (TdT, red) and astrocytes (GFAP, cyan) in an uninjured *Cx3cr1*^{creER}::*R26-TdT* transgenic mouse (**a**), as well as at the lesion epicenter at 1 (**b**), 4 (**c**), 7 (**d**), 14 (**e**), and 35 (**f**) days post-injury (dpi). (**g**) Quantification of

the total number of TdT^+ microglia per mm^2 of tissue in spinal cord sections taken both rostral (R) and caudal (C) to the lesion epicenter at 1 (red line), 4 (green), 7 (violet), 14 (orange) and 35 (black) dpi (n=6-8 mice per group/time point). Data from uninjured mice are shown with the dotted black line. (**h**) Percentage of surviving TdT^+ microglia at day 1 post-SCI relative to the uninjured group. (**i-k**) Confocal immunofluorescence images showing expression of the apoptotic marker cleaved caspase-3 (Casp3, green) in TdT^+ microglia (red) at 1 dpi. Nuclear staining (DAPI) is shown in blue, while white arrowheads indicate co-localization of cleaved Casp3, TdT and DAPI. (**l**) Quantification of the number of actively proliferating microglia (TdT^+ $Ki67^+$ cells) at 1, 4, 7, 14 and 35 dpi (n=7-8 mice per group). (**m**) Percentage of TdT^+ microglia undergoing proliferation after SCI (n=7-8 per group). (**n-p**) Confocal immunofluorescence microscopy showing that TdT^+ microglia (red) are actively proliferating at 7 dpi, as demonstrated by their expression of the proliferation marker Ki67 (green). DAPI is shown in blue, while white arrowheads indicate co-localization of TdT, Ki67 and DAPI staining. Data are expressed as mean ± SEM. Scale bars: (**a-f**, in **f**) 200 µm; (**i-k**, in **k**) 20 µm; (**n-p**, in **p**) 20 µm.

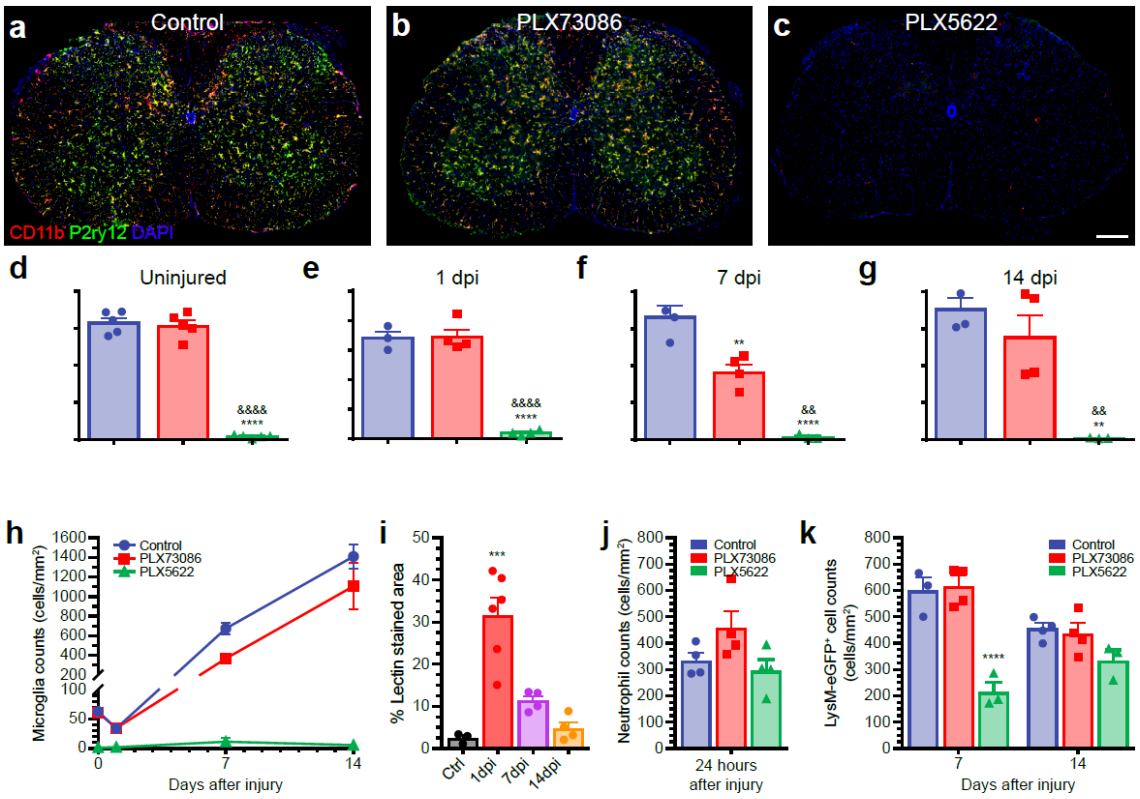

Figure 3.2 The CSF1R inhibitor PLX5622, but not PLX73086, crosses the blood-spinal cord barrier to deplete virtually all microglia.

(**a-c**) Representative confocal images of CD11b and P2ry12 immunostainings showing the almost complete elimination of microglia in the spinal cord of naïve (uninjured) C57BL/6 mice after treatment with the CSF1R inhibitor PLX5622 compared to those fed PLX73086 or the control diet. Mice were killed after 21 days of treatment. (**d-h**) Quantification of microglia in the spinal cord of uninjured C57BL/6 mice treated with PLX5622, PLX73086 or the control diet (**d**), as well as at the lesion epicenter in *Cx3cr1*^{creER}::*R26-TdT* mice killed at 1 (**e**), 7 (**f**), and 14 (**g**) days post-injury (dpi) (n=4-5 mice per group/time point). (**i**) Quantification of the proportional area of spinal cord tissue permeable to FITC-conjugated lectin injected intravenously prior to tissue fixation. (**j**) Quantification of Ly6G^{+} neutrophils at the lesion epicenter at day 1 post-SCI in mice treated with either PLX5622, PLX73086 or the control chow (n=4-5 per group). (**k**) Quantification of the number of granulo-myelomonocytic cells at the lesion epicenter at 7 and 14 dpi in *Cx3cr1*^{creER}::*R26-TdT*::*LysM*-eGFP mice treated with either PLX5622, PLX73086 or the control diet (n=4-5 mice per group/time point). For all injured mice, treatment was initiated 3 weeks before SCI and

continued until sacrifice. Data are expressed as mean ± SEM. ** $p < 0.01$, *** $p < 0.001$, **** $p < 0.0001$, PLX5622 or 1 dpi compared to the control group; and $^{\&\&}$ $p < 0.01$, $^{\&\&\&\&}$ $p < 0.0001$, PLX5622 compared with the PLX73086 group. Statistical analysis was performed using a one-way (**d-g, i-j**) or two-way (**k**) ANOVA followed by a Bonferroni's post hoc test. Scale bar: (**a-c**, in **c**) 200 µm.

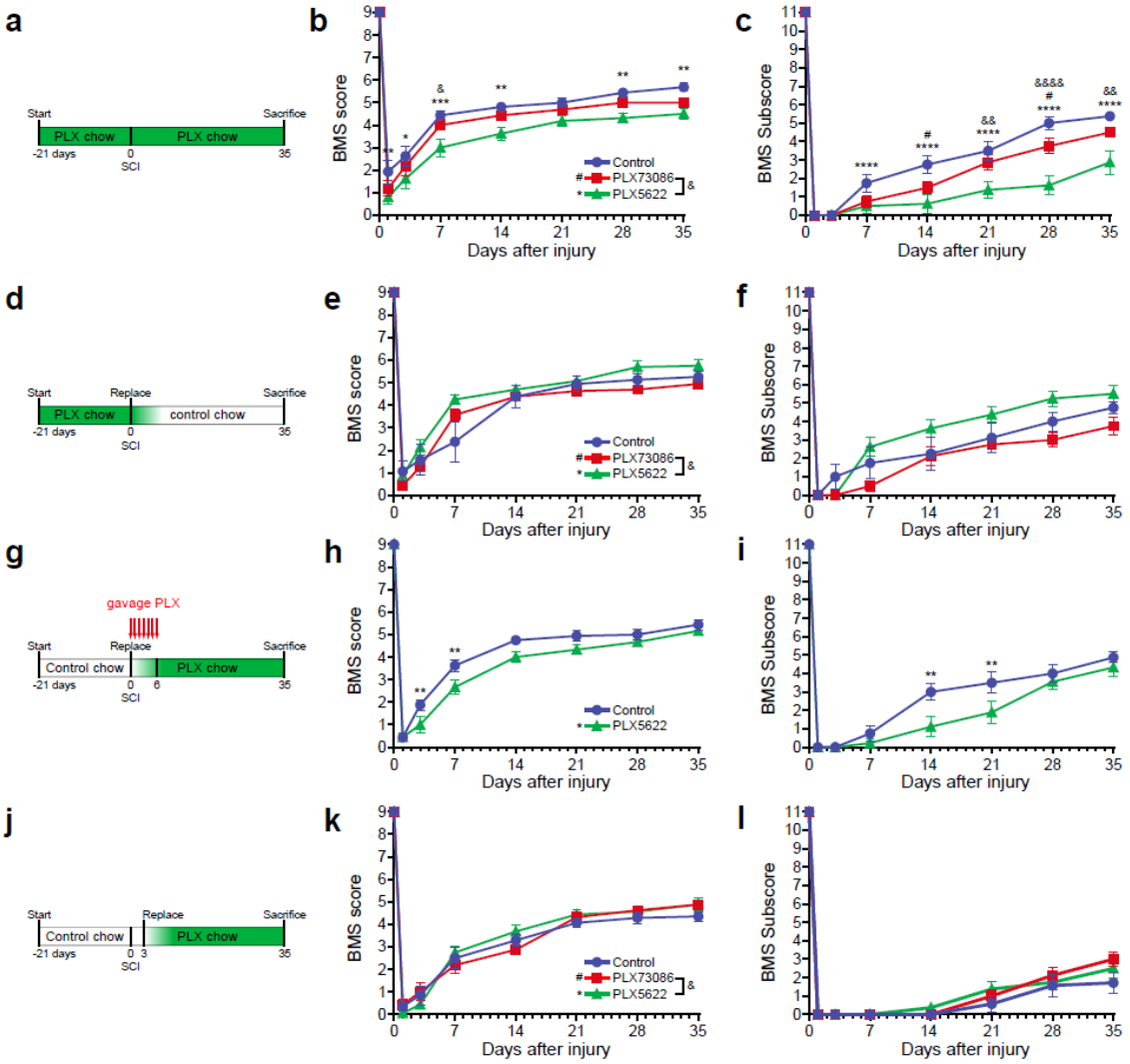

Figure 3.3 Microglia play a key role in recovery of locomotor function during the first week post-SCI.

(**a**, **d**, **g**, **j**) Schematics of experimental design showing the timeline of microglia depletion, spinal cord contusion, behavioral testing using the basso mouse scale (BMS), and sacrifice. CSF1R inhibitors and vehicle were administered in the diet or by oral gavage, as indicated. (**b-c**, **e-f**, **h-i**, **k-l**) Locomotor function was assessed using the BMS score (**b**, **e**, **h**, **k**) and BMS subscore (**c**, **f**, **i**, **l**) over a 35-day period after SCI (n=8 mice per group). Data are expressed as mean ± SEM. * $p < 0.05$, ** $p < 0.01$, *** $p < 0.001$, **** $p < 0.0001$, PLX5622 versus the control group; $^{\#}$ $p < 0.05$, PLX73086 versus the control group; and $^{\&}$ $p < 0.05$, $^{\&\&}$ $p < 0.01$, $^{\&\&\&\&}$ $p < 0.0001$, PLX5622 compared to PLX73086. Statistical analysis was

performed using a two-way repeated-measures ANOVA followed by a Bonferroni's post hoc test.

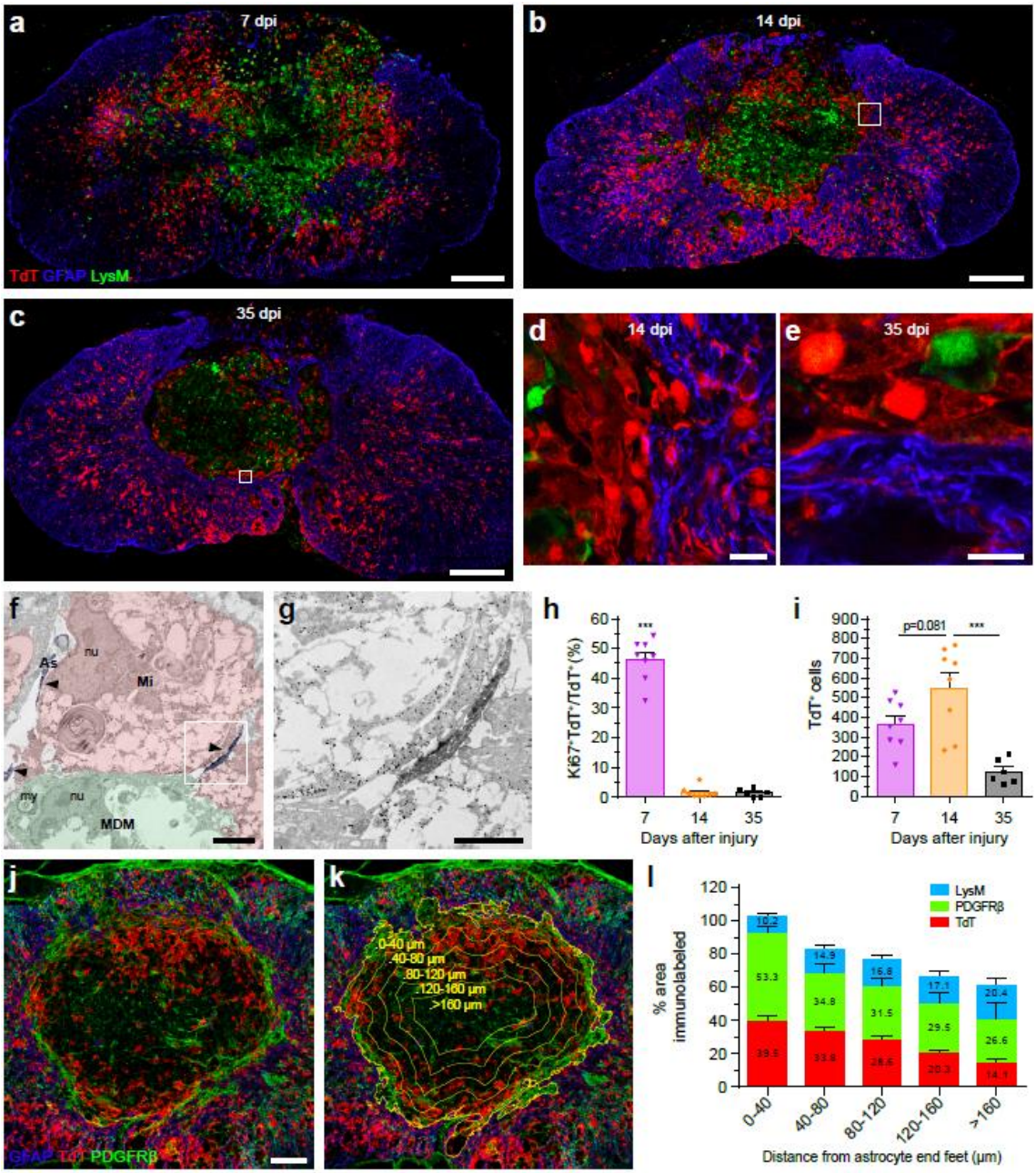

Figure 3.4 A microglial scar forms at the interface between the astrocytic and fibrotic scars.

(**a-e**) Confocal immunofluorescence microscopy of representative spinal cord sections taken at the lesion epicenter at 7 (**a**), 14 (**b**, **d**), and 35 (**c**, **e**) days post-injury (dpi) showing formation of the microglial scar, characterized by the accumulation of TdT^+ microglia (red) at the lesion borders, over time. The microglial scar is shown in relation to the infiltration of blood-derived myeloid cells (LysM-$eGFP^+$, green) and formation of the astroglial scar

(GFAP-immunoreactive astrocytes, blue). Panels (**d**) and (**e**) are insets of panels (**b**) and (**c**), respectively, showing close-ups of the microglial scar in *Cx3cr1*^{creER}::*R26-TdT*::*LysM*-eGFP mice at 14 and 35 dpi. (**f-g**) Immunoelectron microscopy images showing a gold-labeled microglia (Mi) (dense black dots, highlighted in red) located at the lesion border making direct contacts with immunolabeled astrocytic endfeet (As) (diffuse black, highlighted in blue and pointed by arrowheads) and a monocyte-derived macrophage (MDM, highlighted in green). The intimate relationship between the microglia and distal astrocytic processes is shown at high magnification in the inset (**g**). nu = nucleus, my = myelin debris. (**h**) Percentage of microglia (TdT^+) that are actively proliferating ($Ki67^+$ TdT^+) at the lesion epicenter at 7, 14 and 35 dpi. (**i**) Counts of microglia (TdT^+) at the lesion epicenter at 7, 14 and 35 dpi. (**j-k**) Confocal images showing the presence of TdT^+ microglia (red), PDGFRβ^+ pericytes/fibroblasts (green) and $GFAP^+$ astrocytes (blue) at the lesion epicenter at 14 dpi. The distance from astrocyte endfeet is depicted by the yellow lines and indicated (**k**). (**l**) Percentage area occupied by microglia (TdT^+, red bars in the histogram), pericytes/fibroblasts (PDGFRβ, green) and blood-derived myeloid cells (LysM-$eGFP^+$, blue) as a function of distance from astrocyte endfeet (n= 4-9 mice). Data are expressed as mean ± SEM. * $p < 0.05$, ** $p < 0.01$, *** $p < 0.001$, compared to the other time points. Statistical analysis was performed using a one-way ANOVA followed by a Bonferroni's post hoc test. Scale bars: (**a-c**) 200 µm; (**d-e**) 20 µm; (**f**) 5 µm; (**g**) 2 µm; (**j-k**) 100 µm.

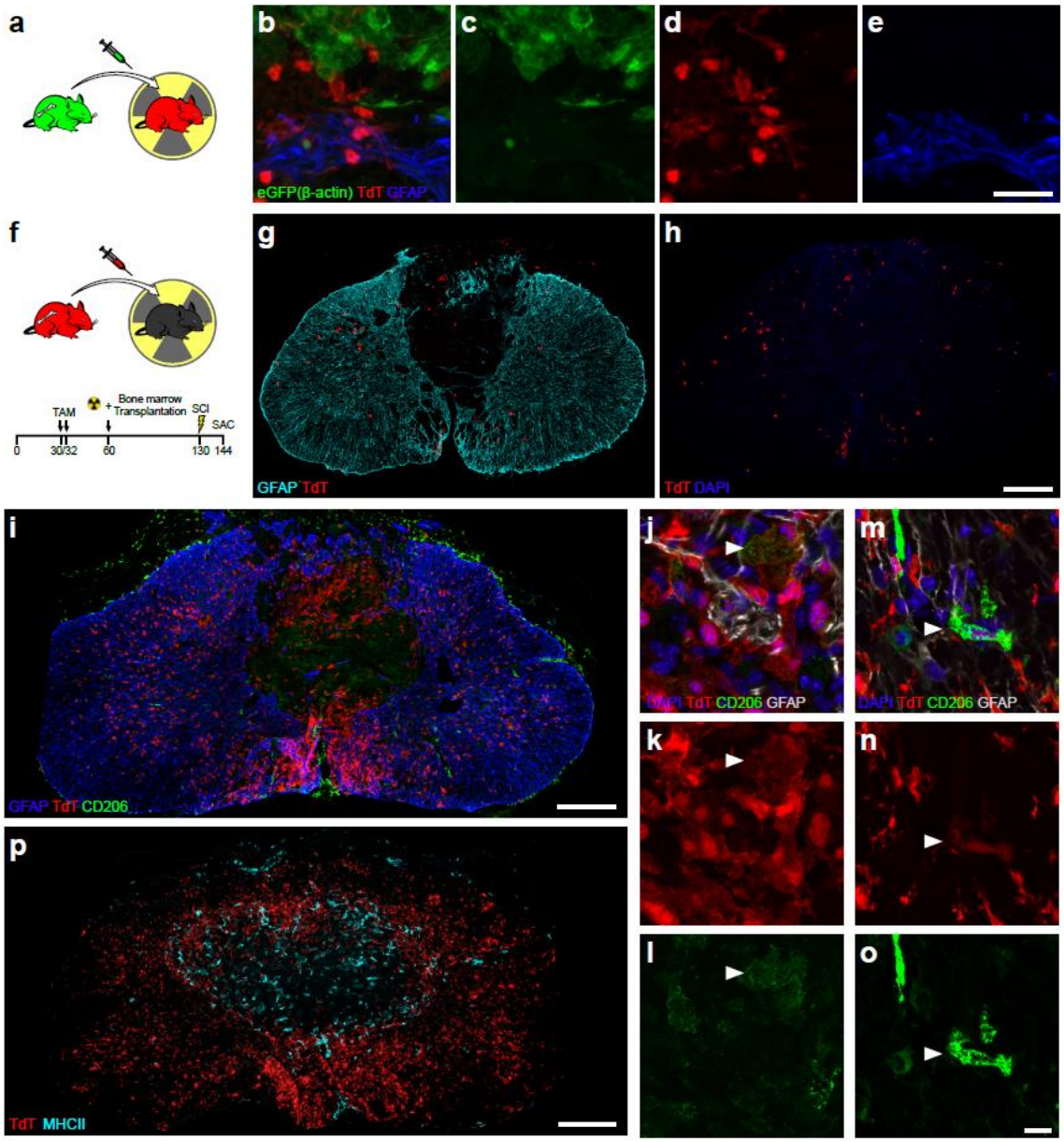

Figure 3.5 The microglial scar is mainly composed of microglia, with few scattered blood-derived myeloid cells and CNS border-associated macrophages.

(**a**) Schematic diagram showing the protocol used to generate radiation bone marrow chimeras in which microglia express TdT and bone marrow-derived cells the GFP reporter. (**b-e**) Representative confocal images showing the microglial scar formed of TdT^{+} microglia (red), some of which are in close apposition with GFAP-immunoreactive astrocyte endfeet (blue) on one side and bone marrow-derived cells ($eGFP^{+}$, green) on the other side at 14 days post-SCI. (**f**) Schematic of experimental procedure and timeline to generate bone marrow chimeras in which *Cx3cr1*^{creER}::*R26-TdT* mice were used as bone marrow donors for

irradiated recipient C57BL/6 mice. (**g-h**) Representative confocal images showing the virtual absence of bone marrow-derived TdT^+ cells (red) medial to the astrocytic scar (as defined by $GFAP^+$ astrocyte endfeet in blue), where the microglial scar normally develops, at 14 days post-SCI in *Cx3cr1*^{creER}::*R26-TdT* → WT chimeric mice. (**i-o**) Confocal images showing the absence (or very weak expression) of CD206 (green) in microglia (TdT^+, red) forming the microglial scar at the lesion borders at 14 days post-SCI. In contrast, border-associated macrophages express high levels of the CD206 protein. (**p**) Representative confocal image showing the absence of colocalization between TdT (red) and MHCII (cyan) in the injured spinal cord of a *Cx3cr1*^{creER}::*R26-TdT* mouse at 14 days. Scale bars: (**b-e**, in **e**) 20 µm, (**g-h**, in **h**) 200 µm, (**i**, **p**) 200 µm, (**j-o**, in **o**) 10 µm.

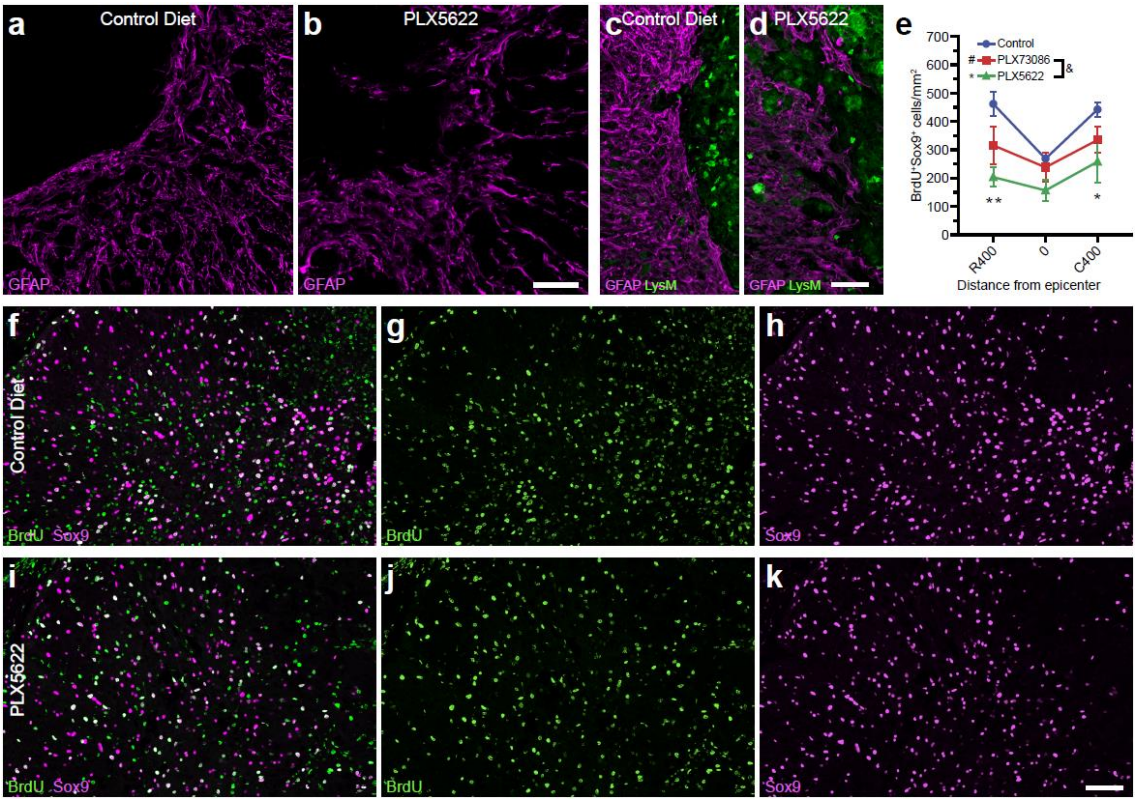

Figure 3.6 The elimination of microglia results in a reduced proliferation of astrocytes and disorganized astrocytic scar at the lesion border.

(**a-d**) Confocal immunofluorescence microscopy of astrocytes (GFAP, purple) in spinal cord sections taken at the lesion epicenter in *Cx3cr1*^{creER}::*R26-TdT*::*LysM*-eGFP mice at 14 days post-injury (dpi). In mice fed with the control diet (**a**, **c**), astrocytes adjacent to the site of SCI exhibit elongated processes oriented parallel to the lesion border, thus forming a compact scar. This astrocytic response was compromised in mice depleted of microglia *using* PLX5622 (b, d), and associated with clusters of blood-derived myeloid cells (*LysM-eGFP*$^{+}$, *green cells in **d***) spreading outside of the lesion core. (**e**) Total counts of Sox9^{+} BrdU^{+} cells at the epicenter and both rostral (R) and caudal (C) to the lesion at 7 dpi in mice fed the control diet (blue), PLX73086 (red) or PLX5622 (green) (n=4 mice per group). (**f-k**) Representative confocal images showing the proliferation of astrocytes (Sox9^{+}, purple cells), as demonstrated by their incorporation of BrdU (green cells), in mice treated with PLX5622 (**f-h**) or the control diet (**i-k**) and killed at 7 dpi. Data are expressed as mean ± SEM. * $p < 0.05$, ** $p < 0.01$, PLX5622 versus the control group. Statistical analysis was performed

using a two-way ANOVA followed by a Bonferroni's post hoc test. Scale bars: (**a**-**b**, in **b**) 50 µm, (**c**-**d**, in **d**) 50 µm, (**f**-**k**, in **k**) 50 µm.

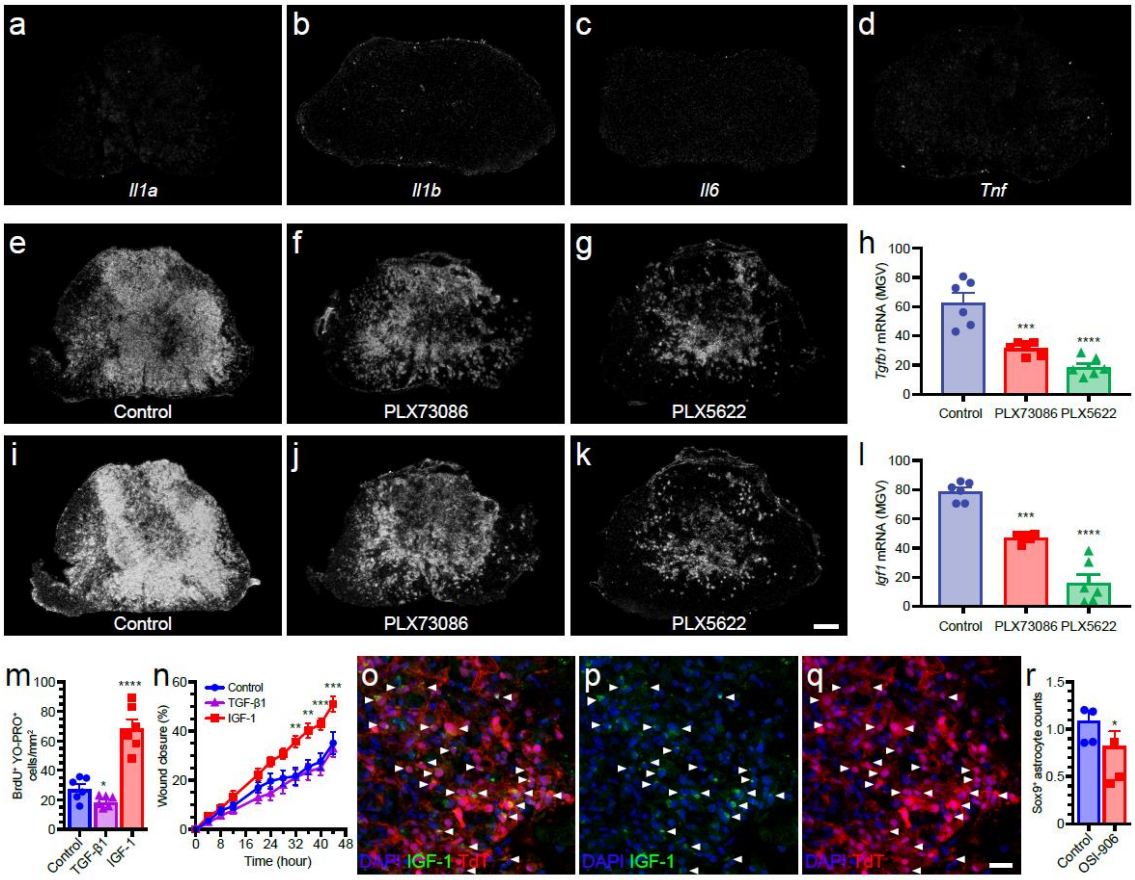

Figure 3.7 Microglia-derived IGF-1 is a potent mitogen for astrocytes and inducer of astrocytic migration towards an injured area.

(**a-d**) *In situ* hybridization (ISH) signal for the proinflammatory cytokines IL-1α, IL-1β, IL-6 and TNF in the injured mouse spinal cord (lesion epicenter) at 7 days post-SCI (dpi). (**e-g**, **i-k**) Representative darkfield photomicrographs showing expression of *Tgfb1* and *Igf1* mRNAs at the lesion epicenter at 7 dpi in C57BL/6 mice fed the control diet, PLX73086 or PLX5622. (**h**, **l**) Quantification of ISH signal (in mean grey values, MGV) for TGF-β1 (**h**) and IGF-1 (**l**) at the lesion epicenter in mice treated with vehicle (Control, blue bars), PLX73086 (red bars) or PLX5622 (green bars) (n=6 per group). (**m**) Quantification of the number of $BrdU^+$ $YO\text{-}PRO\text{-}1^+$ nuclear profiles following treatment of primary astrocyte cultures with either TGF-β1, IGF-1 or control solution (n=6 per group). (**n**) Quantification of the wound closure response in the different groups (n=6 per group). (**o-q**) Representative immunofluorescence images showing the expression of IGF-1 (green signal, **o-p**) by TdT^+ microglia (red cells, **o** and **q**) accumulating at the lesion border at 7 dpi. White arrowheads

indicate co-localization of IGF-1, TdT, and DAPI (blue). (**r**) Quantification of $Sox9^+$ astrocytes, expressed as the AUC of the total number of $Sox9^+$ cells (x 10^3 per mm^3) from 800 µm rostral to 800 µm caudal to the epicenter, in the injured spinal cord of C57BL/6 mice treated with the IGF-1R antagonist OSI-906 (red bar) or the vehicle solution (Control, blue bar) (n=4 per group). Data are expressed as mean ± SEM. * $p < 0.05$, ** $p < 0.01$, *** $p < 0.001$, **** $p < 0.0001$, compared to the control group. Statistical analysis was performed using either a one-way (**h**, **l-m**) or two-way (**n**) ANOVA followed by a Bonferroni's post hoc test, or a Student's t-test (**r**). Scale bars: (**a-g** & **i-k**, in **k**) 200 µm, (**o-q**, in **q**) 20 µm.

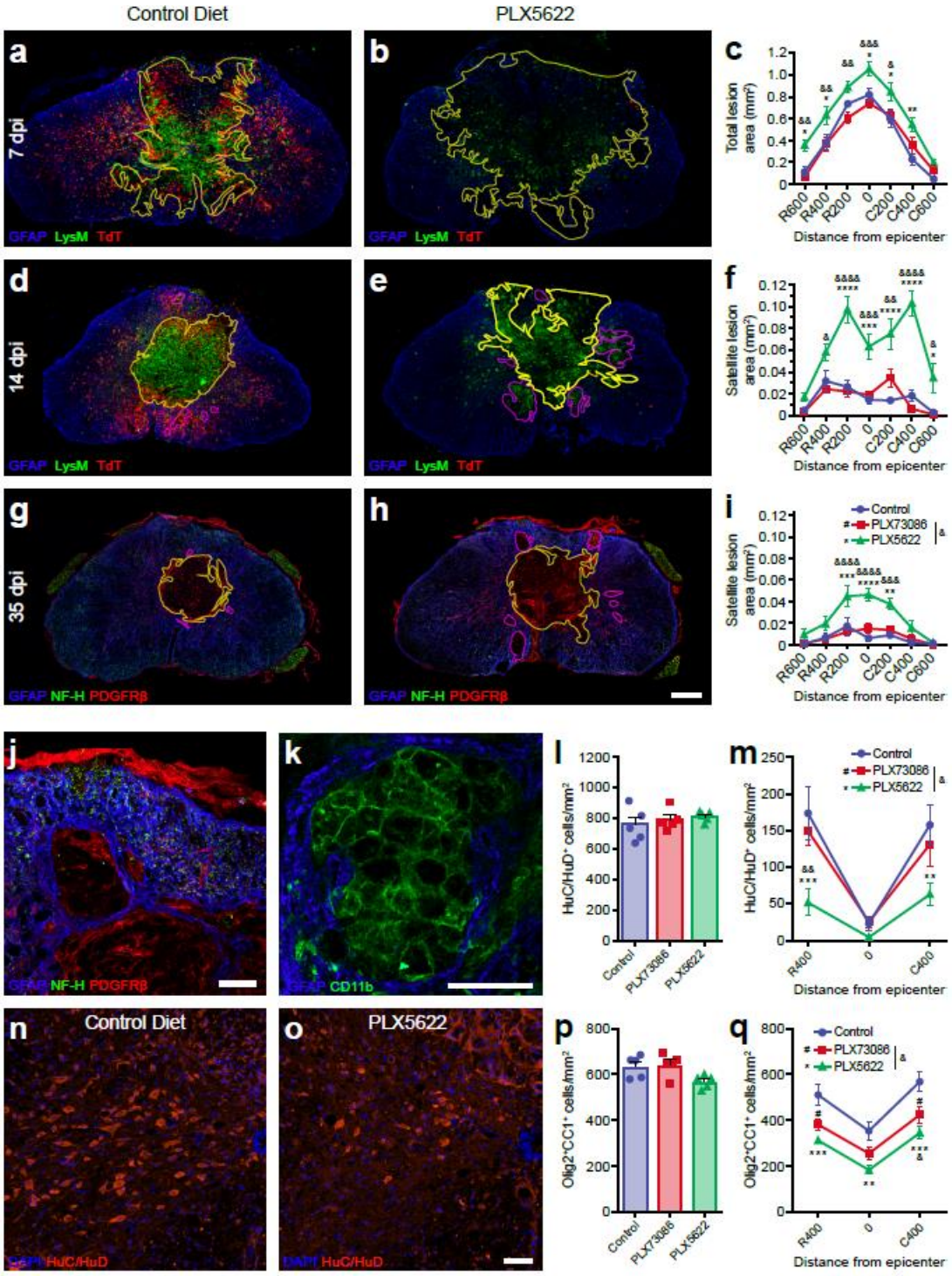

Figure 3.8 Microglial depletion results in an increased loss of neurons and oligodendrocytes leading to greater tissue damage after SCI.

(**a-b**, **d-e**, **g-h**, **j-k**) Confocal immunofluorescence of astrocytes (GFAP$^+$, blue), microglia (TdT$^+$, red cells in **a-b**, **d-e**), blood-derived myeloid cells (LysM-eGFP$^+$ or CD11b$^+$, green

cells in **a-b**, **d-e**, **k**), neurons/axons (NF-H$^+$, green in **g-h**, **j**) and pericytes/fibroblasts (PDGFRβ$^+$, red cells in **g-h**, **j**) at the lesion epicenter at 7 (**a-b**), 14 (**d-e**) and 35 (**g-h**) dpi. Yellow and purple lines respectively delineate the contours of the primary (core) and satellite lesions, which were surrounded by astrocytic endfeet and characterized by the absence of neuronal elements and presence of cells of non-CNS origin *(*blood-derived myeloid cells, pericytes and fibroblasts). Satellite lesions are shown in a microglia-depleted mouse at 35 dpi (j-k). (**c**) Quantification of the total lesion area at 7 dpi in mice fed the control diet (blue), PLX73086 (red) or PLX5622 (green) (n=5-6 mice/group). (**f**, **i**) Quantification of the total area occupied by satellite lesions at 14 (**f**) and 35 (**i**) dpi (n=5-7/group). (**l-m**) Quantification of the number of neurons (HuC/HuD$^+$) in the uninjured spinal cord (**l**), as well as rostral (R) and caudal (C) to the epicenter (**m**), in mice treated with PLX5622, PLX73086 or control at 35 dpi (n=5-8/group). (**n-o**) Representative confocal images taken at the lesion epicenter at 35 dpi immunostained for HuC/HuD (red). DAPI is shown in blue. (**p**, **q**) Quantification of the number of oligodendrocytes (Olig2$^+$ CC1$^+$) in the uninjured (**p**) and injured (**q**) spinal cord of mice treated with PLX5622, PLX73086 or control at 35 dpi (n=5-8/group). Data are expressed as mean ± SEM. * $p < 0.05$, ** $p < 0.01$, *** $p < 0.001$, **** $p < 0.0001$, PLX5622 versus control; $^{\#}$ $p < 0.05$, PLX73086 versus control; and $^{\&}$ $p < 0.05$, $^{\&\&}$ $p < 0.01$, $^{\&\&\&}$ $p < 0.001$, $^{\&\&\&\&}$ $p < 0.0001$, PLX5622 compared to PLX73086. Statistical analysis was performed using a two-way ANOVA followed by a Bonferroni's post hoc test. Scale bars: (**a-b, d-e, g-h** in **h**) 200 µm, (**j-k**) 50 µm, (**n-o**, in **o**) 50 µm.

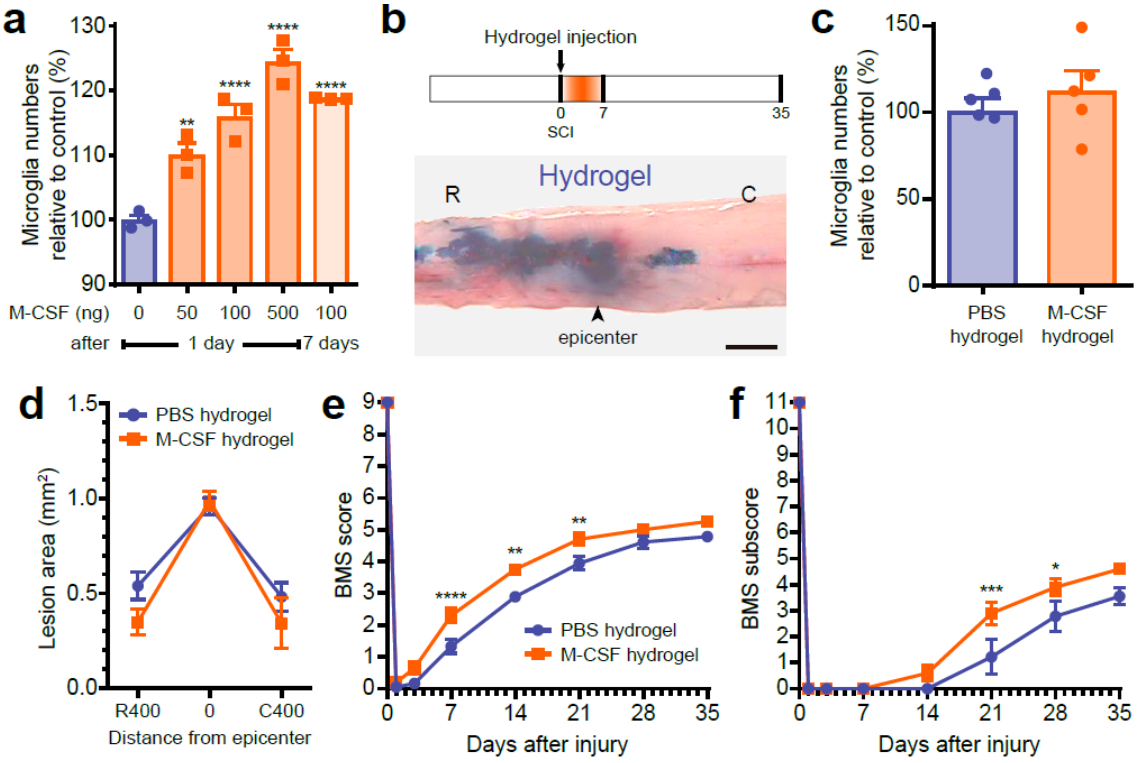

Figure 3.9 Hydrogel delivery of M-CSF at the site of SCI boosted microglial proliferation and enhanced functional recovery.

(**a**) Quantification of the number of microglia ($CD11b^+$ $P2ry12^+$) in the thoracic spinal cord following intra-cisterna magna injection of recombinant murine M-CSF at various doses (n=3 mice per group). (**b**) Schematic of the experimental design showing the timeline of spinal cord contusion (SCI), hydrogel injection, behavioral testing using the basso mouse scale (BMS), and sacrifice. Below the schematic is a picture showing how much a hydrogel loaded with Evans blue spreads following subdural injection at the site of SCI. (**c**) Quantification of the number of microglia (TdT^+) at the lesion epicenter at 7 days post-injury (dpi) in *Cx3cr1*^{creER}::*R26-TdT* mice treated with either M-CSF-based (orange bar) or PBS-based (blue) hydrogels (n=5 mice per group). (**d**) Quantitative analysis of the total lesion area at the lesion epicenter and both rostral (R) and caudal (C) at 7 dpi in mice treated with M-CSF (orange) or PBS (blue) in hydrogels (n= 9-15 mice per group). (**e-f**) Assessment of locomotor recovery using the BMS (**e**) and BMS subscore (**f**) showed that hydrogel delivery of M-CSF increased functional recovery after SCI (n=9-10 mice per group). Data are expressed as mean ± SEM. * $p < 0.05$, ** $p < 0.01$, *** $p < 0.001$, **** $p < 0.0001$, M-CSF-loaded hydrogel compared with PBS-loaded hydrogel. Statistical analysis was performed

using a one-way (**a**, **c**), two-way (**d**) or two-way repeated-measures (**e-f**) ANOVA followed by a Bonferroni's post hoc test.

Supplemental Figures

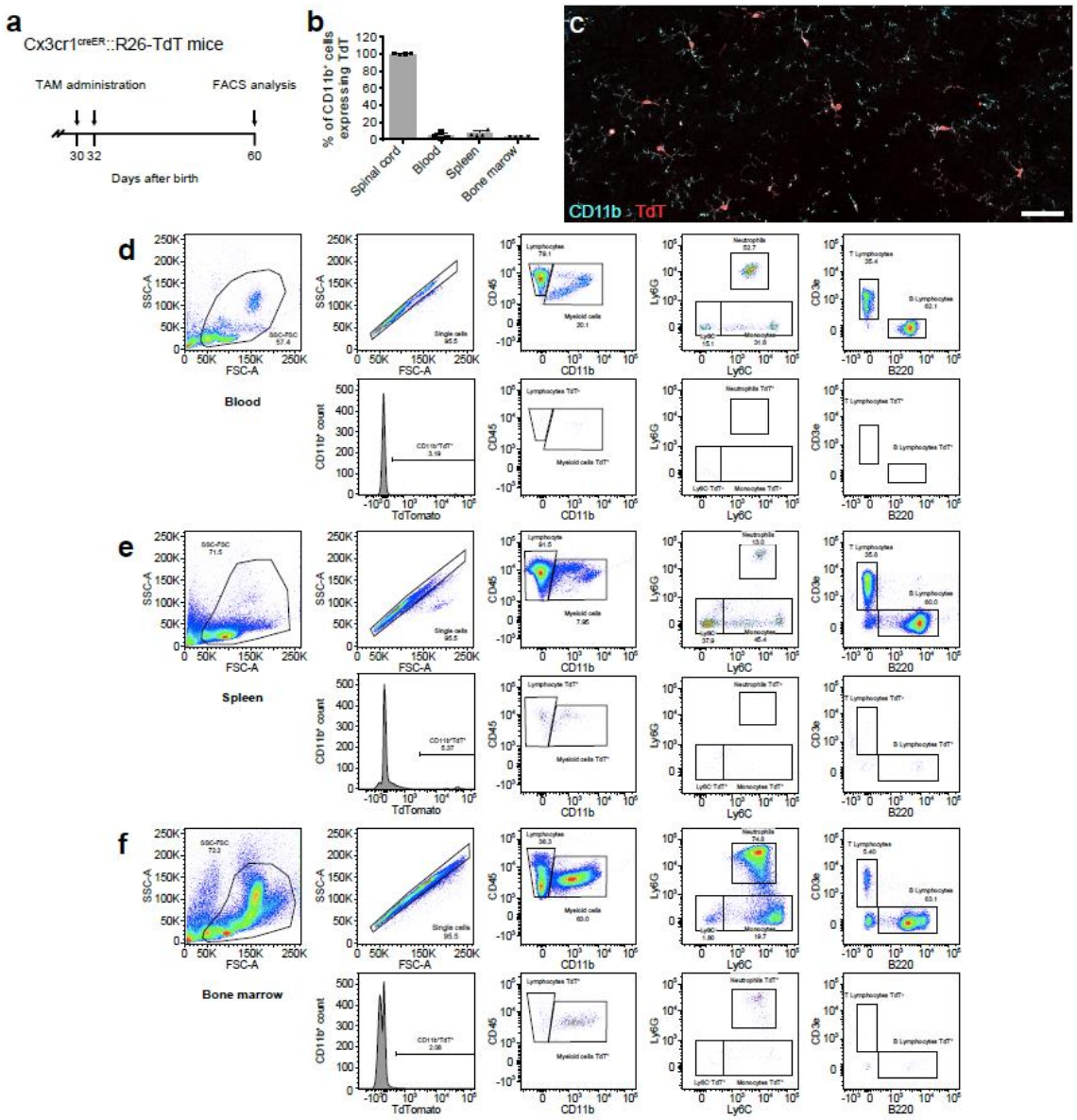

Figure 3.10 Adequate regimen of tamoxifen treatment in inducible Cx3cr1creER::R26-TdT mice allows to specifically target microglia, while leaving monocytes and tissue-resident macrophages almost unaffected.

(**a**) Schematic diagram of experimental design showing the timeline of tamoxifen (TAM) treatment and FACS analysis relative to the age of *Cx3cr1*c^{reER}::*R26-TdT* mice. Transgenic mice were administered tamoxifen at postnatal day (P) 30 and 32 and then allowed to recover for 28 days prior to SCI to allow sufficient time for the turnover of MDMs and near

disappearance of TdT+ cells in the blood, spleen and bone marrow. (**b**) Percentage of myeloid cells expressing the TdT fluorescent reporter 28 days following the last TAM injection. Note that virtually all CNS-resident myeloid cells are TdT+, while only few (if any) myeloid cells in the blood, spleen and bone marrow express TdT (n=4 mice). (**c**) Confocal image showing the colocalization of CD11b (green) and TdT (red) proteins in the spinal cord of a *Cx3cr1*^{creER}::*R26-TdT* mouse at 28 days post-tamoxifen treatment. (**d-f**) Gating strategy used to identify immune cell subsets in the blood (**d**), spleen (**e**) and bone marrow (**f**) of *Cx3cr1*^{creER}::*R26-TdT* mice. For each panel from (**d**) to (**f**), the second row of plots shows the gating strategy used to identify TdT+ cells. **** $p < 0.0001$, spinal cord versus peripheral fluids/tissues. Statistical analysis was performed using a one-way ANOVA followed by a Bonferroni's post hoc test. Scale bar: (**c**) 200 μm.

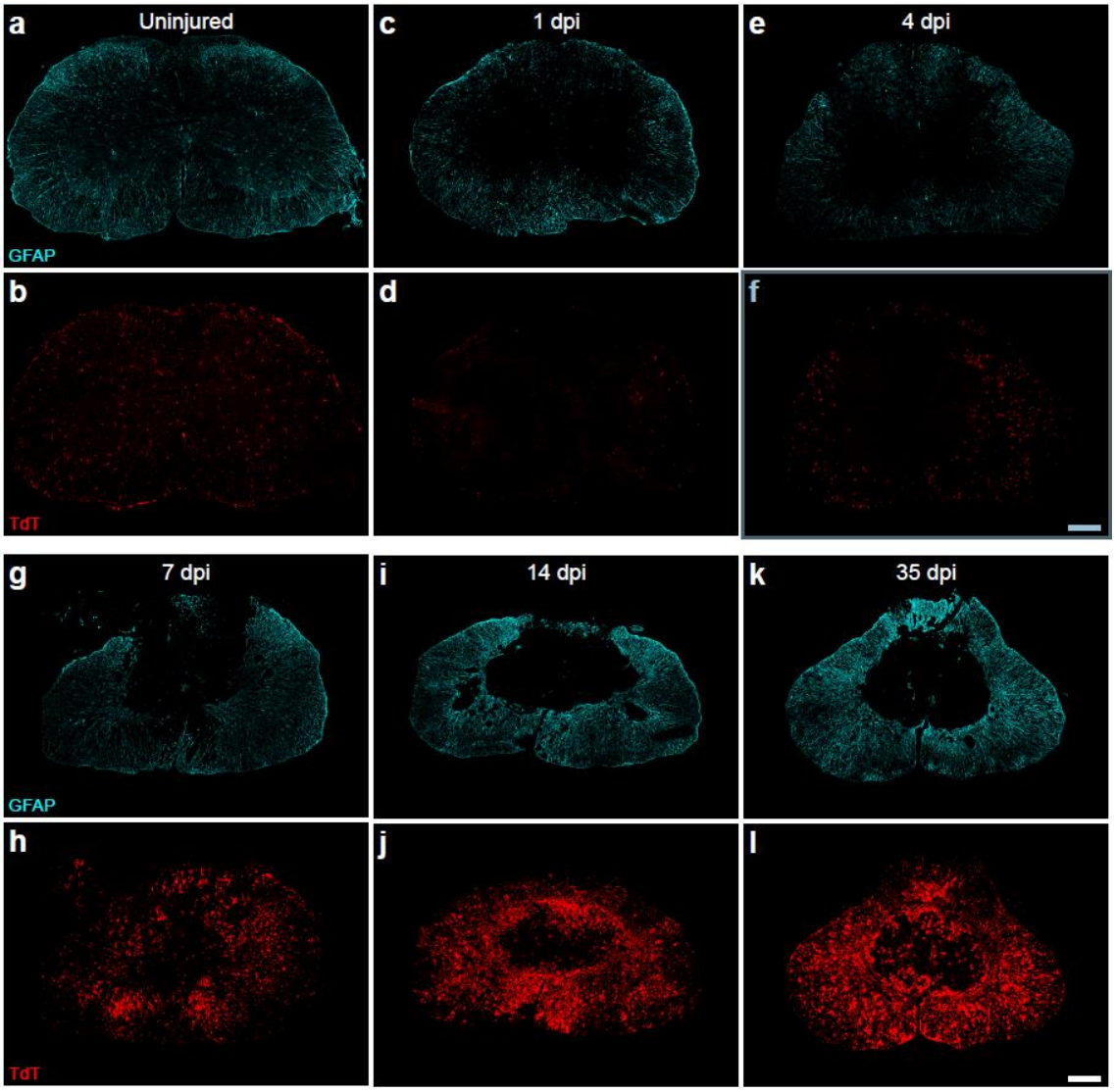

Supplementary Figure 3.11. Microglia proliferate extensively and accumulate at the lesion border after SCI.

(**a-l**) Individual color channels are displayed for the merged confocal images shown in Fig. 1a-f. Depicted are representative confocal immunofluorescence photomicrographs of spinal cord sections showing the spatio-temporal distribution of microglia (TdT, red) and astrocytes (GFAP, cyan) in an uninjured *Cx3cr1*^{creER}::*R26-TdT* transgenic mouse (**a-b**), as well as at the lesion epicenter at 1 (**c-d**), 4 (**e-f**), 7 (**g-h**), 14 (**i-j**), and 35 (**k-l**) days post-injury (dpi). Scale bars: (**a-l**, in **f** and **l**) 200 μm.

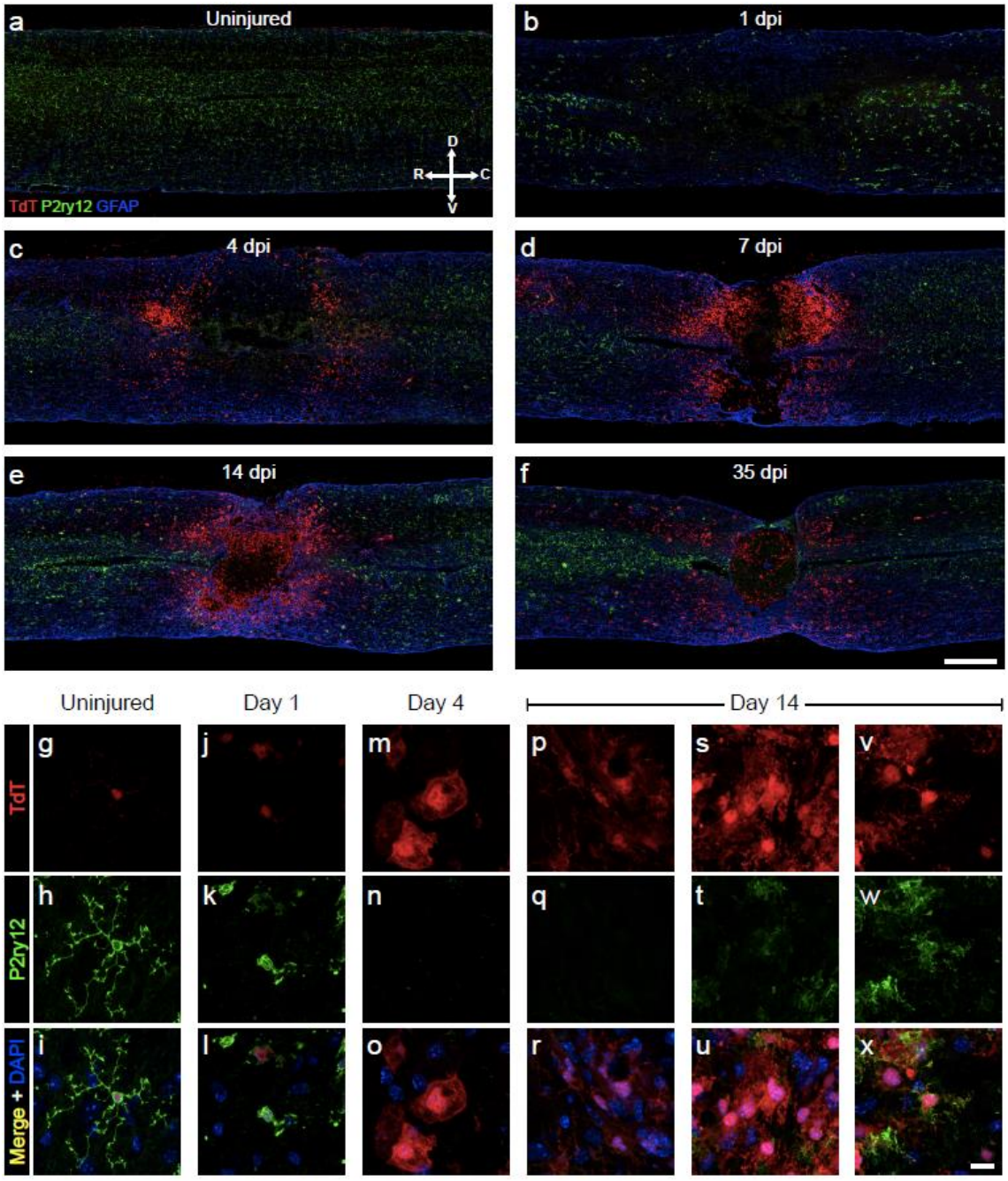

Supplemental Figure 3.12 Microglia rapidly downregulate P2ry12 after SCI and regain expression over time.

(**a-r**) Confocal immunofluorescence microscopy of representative sagittal sections showing the expression of P2ry12 (green) by TdT+ microglia (red) in the uninjured spinal cord of *Cx3cr1*^{creER}::*R26-TdT* transgenic mice (**a, g-i**), as well as at the lesion epicenter in *Cx3cr1*^{creER}::*R26-TdT* mice killed at 1 (**b, j-l**), 4 (**c, m-o**), 7 (**d**), 14 (**e, p-x**), and 35 (**f**) days post-injury (dpi). Astrocytes (GFAP+) are shown in blue in panels (**a-f**), while DAPI (blue)

is shown instead in panels (**g-x**). Note the re-expression of the P2ry12 protein in some TdT+ microglia at the lesion epicenter starting at day 14 post-SCI. Scale bars: (**a-f,** in **f**) 400 μm, (**g-x,** in **x**) 10 μm.

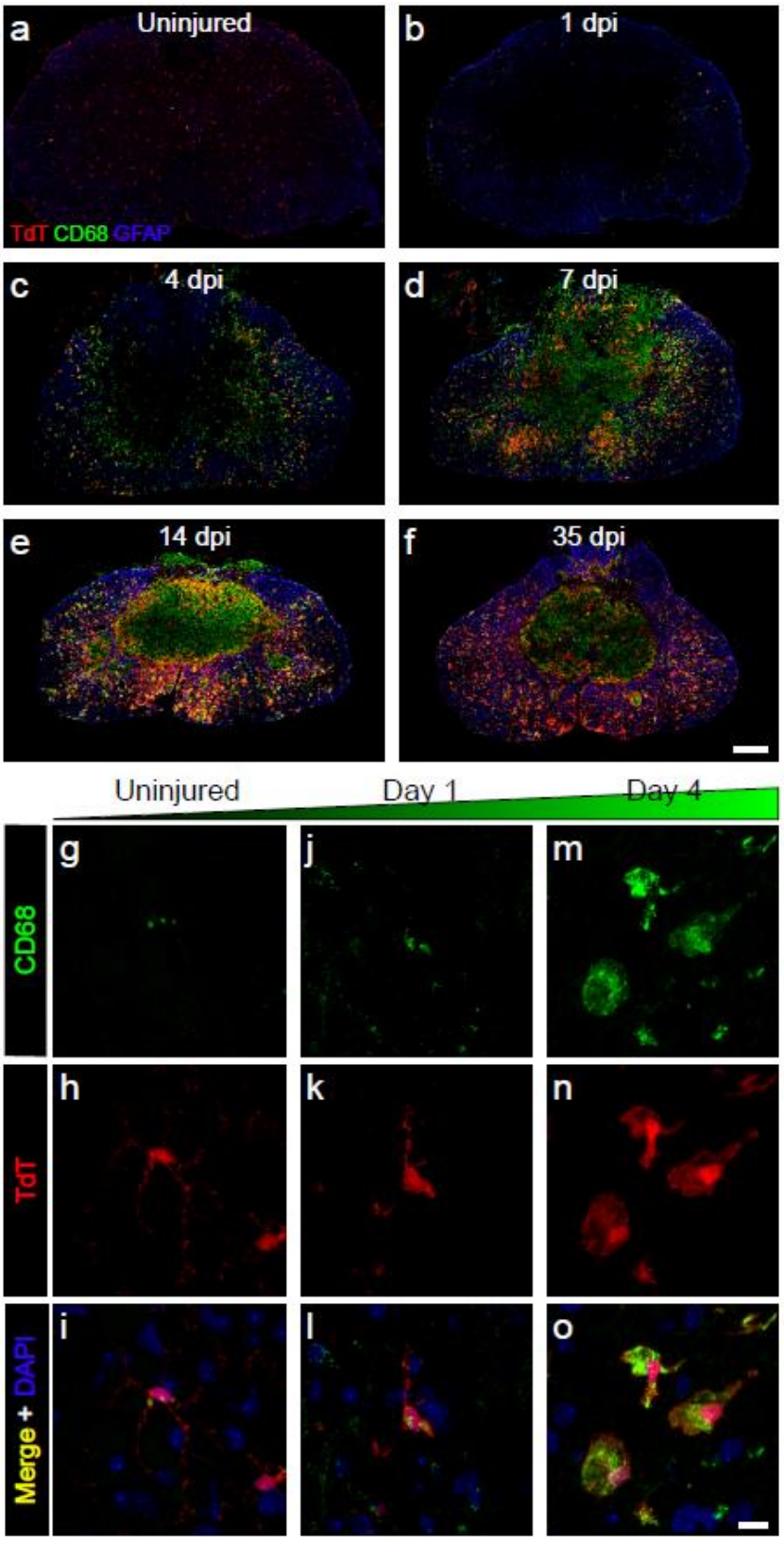

Supplementary Figure 3.12. Microglia rapidly upregulate CD68 after SCI.

Supplemental Figure 3.13 Microglia rapidly upregulate CD68 after SCI.

(**a-o**) Confocal immunofluorescence microscopy of representative spinal cord sections showing the expression of CD68 (green) by TdT+ microglia (red) in the uninjured spinal cord of *Cx3cr1*^{creER}::*R26-TdT* transgenic mice (**a, g-i**), as well as at the lesion epicenter in *Cx3cr1*^{creER}::*R26-TdT* mice killed at 1 (**b, j-k**), 4 (**c, m-o**), 7 (**d**), 14 (**e**), and 35 (**f**) days post-injury (dpi). Astrocytes (GFAP+) are shown in blue in panels (**a-f**), while DAPI (blue) is shown instead in panels (**g-o**). Scale bars: (**a-f,** in **f**) 200 μm, (**g-o**, in **o**) 10 μm.

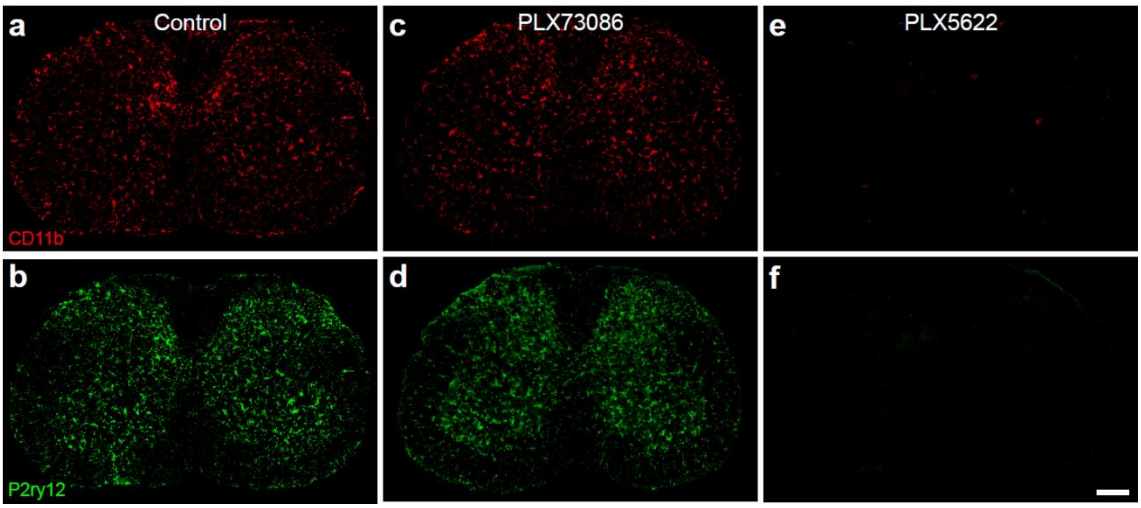

Supplementary Figure 3.14 The CSF1R inhibitor PLX5622, but not PLX73086, crosses the intact blood-spinal cord barrier to deplete virtually all microglia.

(**a-c**) Individual color channels are displayed for the merged confocal images shown in Fig. 2a-c. Depicted are representative confocal images of CD11b and P2ry12 immunostainings showing the almost complete elimination of microglia in the spinal cord of naïve (uninjured) C57BL/6 mice after treatment with the CSF1R inhibitor PLX5622 compared to those fed PLX73086 or the control diet. Mice were killed after 21 days of treatment. Scale bar: (**a-f**, in **f**) 200 μm.

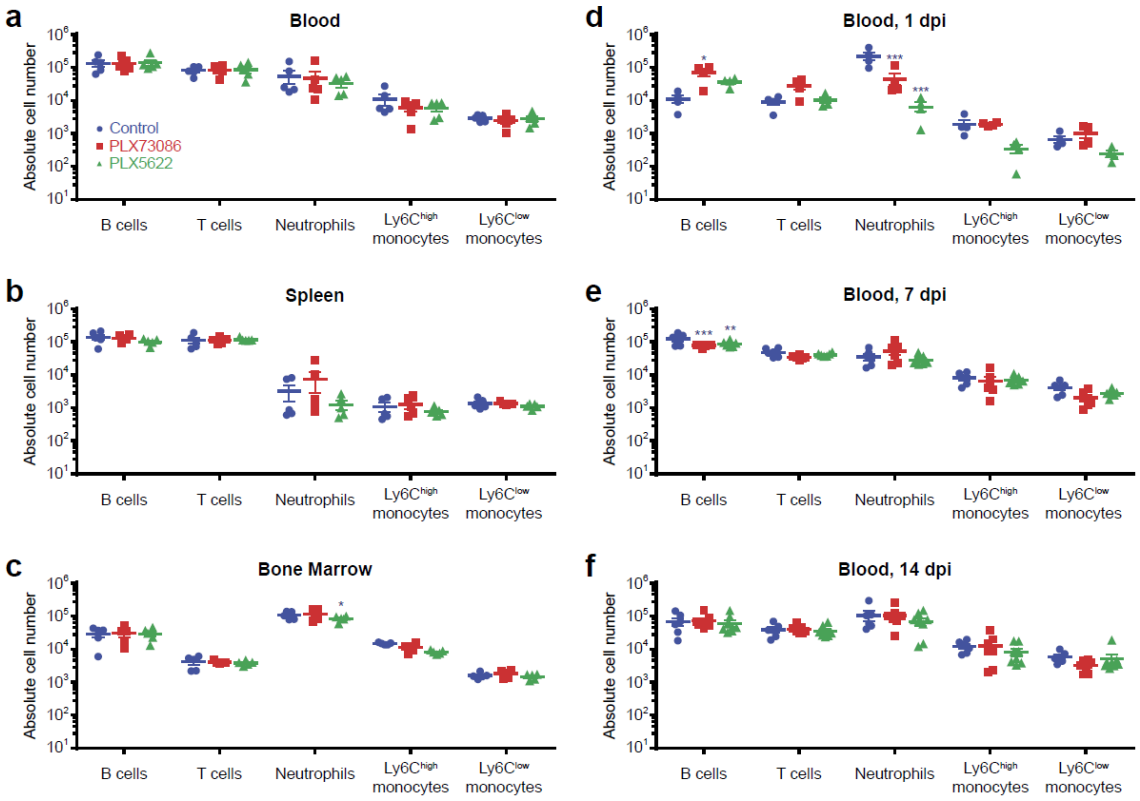

Supplementary Figure 3.15 Treatment with CSF1R inhibitors barely affects the number of peripheral immune cells.

(**a-f**) Absolute numbers of immune cells in the blood (**a, d-f**), spleen (**b**), and bone marrow (**c**) of uninjured (**a-c**) and spinal cord injured (**d-f**) mice following 3 weeks of treatment with either PLX5622, PLX73086 or control diet (n=4-8 mice per group per time point). No changes in cell numbers were detected, except a small and transient blood neutropenia at day 1 post-SCI in mice fed CSF1R inhibitors. Note that treatments were continued until the time of sacrifice. Data are expressed as mean ± SEM. * $p < 0.05$, *** $p < 0.001$, compared to the control group. Statistical analysis was performed using a two-way ANOVA followed by a Bonferroni's post hoc test.

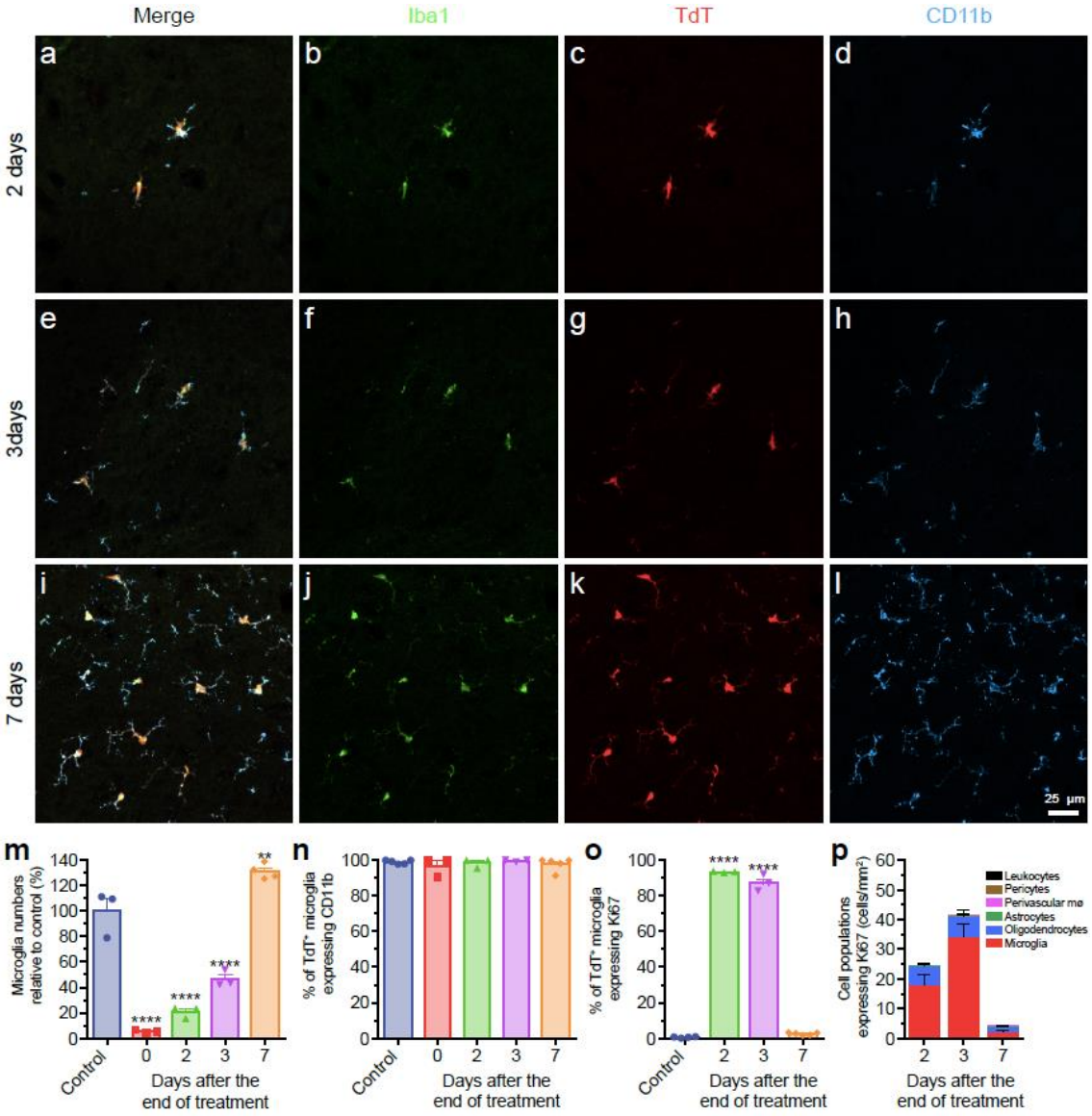

Supplementary Figure 3.16 Microglia proliferate extensively and repopulate the entire spinal cord after one week of cessation of PLX5622.

(**a-l**) Representative confocal images showing CD11b (blue), Iba1 (green), and TdT (red) signals in the uninjured spinal cord of *Cx3cr1*^{creER}::*R26-TdT* mice at 2 (**a-d**), 3 (**e-h**), and 7 (**i-l**) days after cessation of treatment with PLX5622. Nuclear staining (DAPI) is shown in turquoise. (**m**) Quantification of the number of TdT+ microglia in the normal thoracic spinal cord (control, blue bar), after 1 week of continuous treatment with PLX5622 (referred to as day 0 in the graph, (red), as well as 2 (green), 3 (purple) and 7 (orange) days after cessation of PLX5622 treatment (n=3-5 mice per group and per time point). (**n-o**) Percentage of spinal cord microglia (TdT+) expressing CD11b (**n**) and the proliferation marker Ki67 (**o**) at various

times after cessation of PLX5622 treatment. (**p**) Number of microglia (TdT+, red bars), oligodendrocytes (Olig2+, blue), astrocytes (GFAP+, green), perivascular macrophages (perivascular mø, CD206+; purple), pericytes (CD13+, brown), and blood-derived leukocytes (CD45+ TdTneg, black) expressing Ki67 at various times after cessation of PLX5622 treatment. * $p < 0.05$, ** $p < 0.01$, *** $p < 0.001$, **** $p < 0.0001$, compared to the control group. Statistical analysis was performed using a one-way ANOVA followed by a Bonferroni's post hoc test. Scale bar: (**a-l**, in **l**) 200 μm.

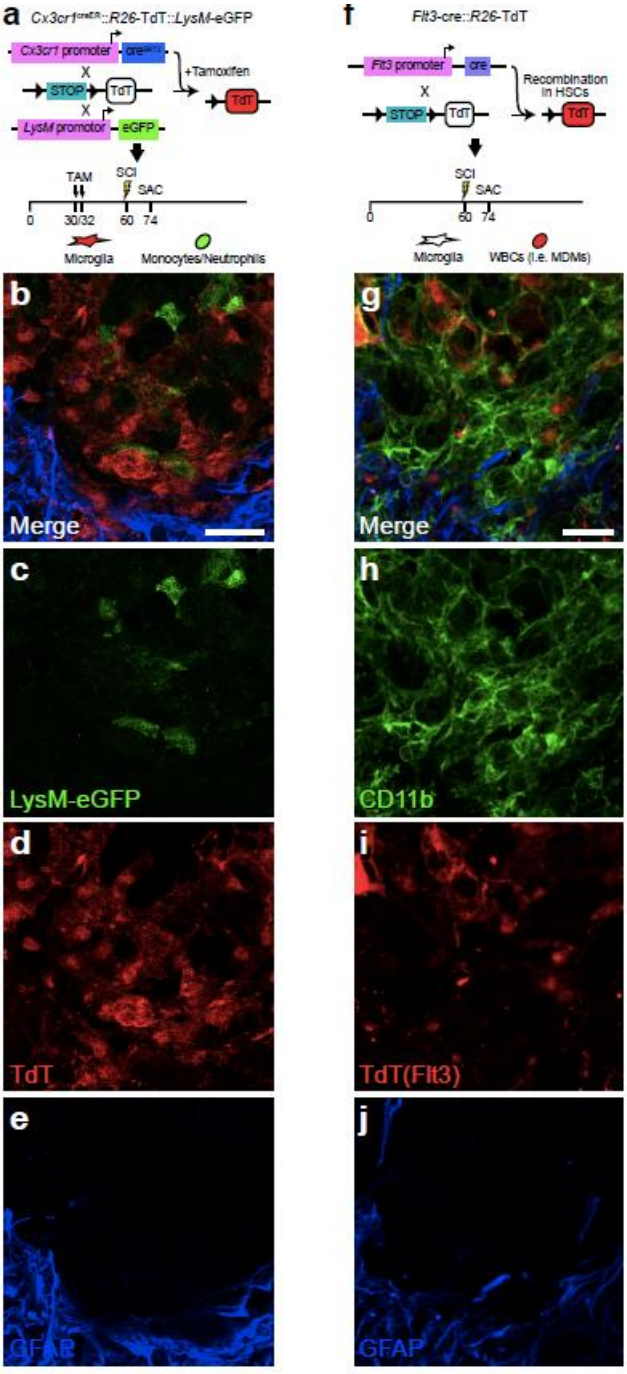

Supplementary Figure 3.17 Fate-mapping analysis reveals that microglia form a scar between reactive astrocytes and infiltrated peripheral immune cells after SCI.

(**a**) Schematic diagram showing the strategy of breeding to obtain *Cx3cr1*^{creER}*::R26-TdT*::*LysM-eGFP* mice, and the timeline of tamoxifen treatment, spinal cord contusion (SCI) and sacrifice (SAC). (**b-e**) Representative confocal images showing the microglial scar formed of TdT+ microglia (red cells), some of which are in direct contact with GFAP-

immunoreactive astrocyte endfeet (blue) on one side and LysM-eGFP+ blood-derived myeloid cells (green cells) on the other side at 14 days post-SCI. (**f**) Schematic diagram showing the breeding strategy to obtain *Flt3^{cre}::R26-TdT* mice, in which TdT is expressed in hematopoietic stem cells (HSCs) and their progeny (e.g. monocyte-derived macrophages, MDMs), but not microglia. (**g-j**) Representative confocal images showing the microglial scar formed of CD11b+ Flt3neg microglia (green cells), making close contact with astrocyte endfeet (GFAP+, blue) and infiltrating MDMs (CD11b+ Flt3+, green cells with red nuclei) at 14 days post-SCI. Scale bars: (**b-e**, in **e**) 20 μm, (**g-j**, in **j**) 20 μm.

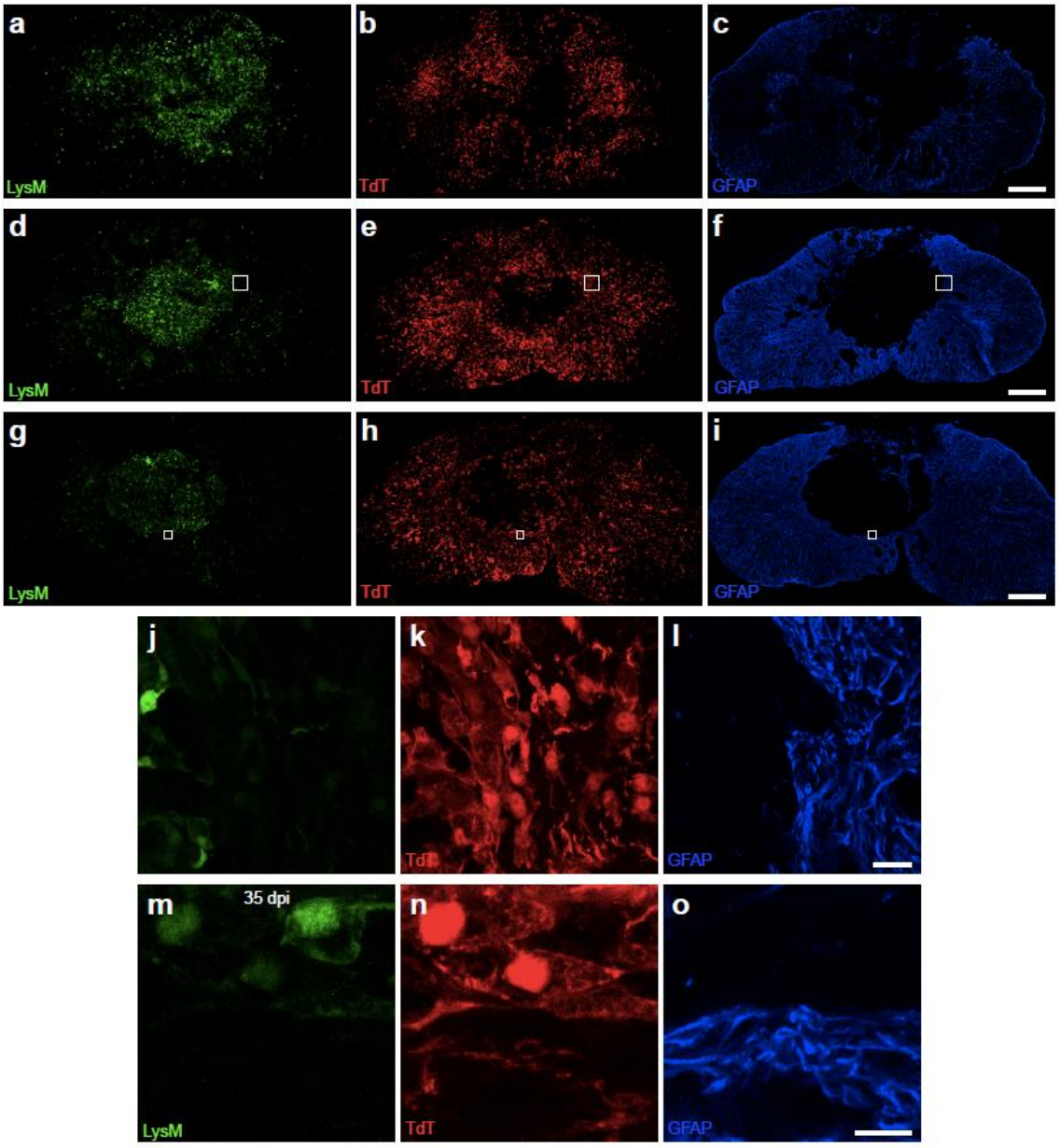

Supplementary Figure 3.18 A microglial scar forms at the interface between reactive astrocytes and blood-derived myeloid cells that infiltrate the lesion site.

(**a-o**) Individual color channels are displayed for the merged confocal images shown in Fig. 4a-e. Depicted are representative confocal immunofluorescence photomicrographs of spinal cord sections taken at the lesion epicenter at 7 (**a-c)**, 14 (**d-f, j-l)**, and 35 (**g-i, m-o**) days post-injury (dpi) showing formation of the microglial scar, characterized by the accumulation of TdT+ microglia (red) at the lesion borders, over time. The microglial scar is shown in relation to the infiltration of blood-derived myeloid cells (LysM-eGFP+, green) and formation of the

astroglial scar (GFAP-immunoreactive astrocytes, blue). Panels (**j**-**l**) and (**m**-**o**) are insets of panels (**d**-**f**) and (**g**-**i**), respectively, showing close-ups of the microglial scar in *Cx3cr1*^{creER}::*R26-TdT*::*LysM-eGFP* mice at 14 and 35 dpi. Scale bars: (**a**-**i**) 200 μm; (**j**-**o**) 20 μm.

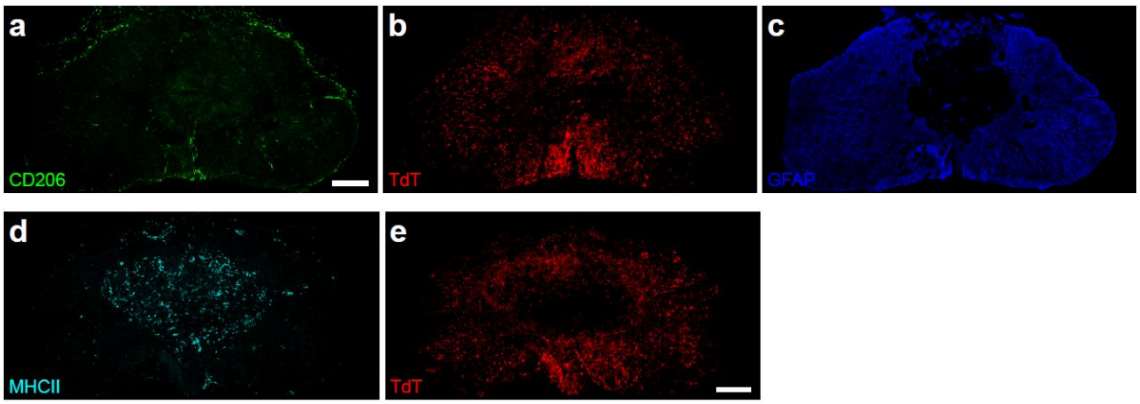

Supplementary Figure 3.19 The microglial scar is mainly composed of microglia with the presence of only few scattered CNS border-associated macrophages.

(**a-c**) Individual color channels are displayed for the merged confocal image shown in Fig. 5i. Depicted are representative confocal immunofluorescence photomicrographs showing the absence (or very weak expression) of CD206 (green) in microglia (TdT+, red) forming the microglial scar at the lesion borders at 14 days post-SCI. In contrast, border-associated macrophages express high levels of the CD206 protein. (**d-e**) Individual color channels are displayed for the merged confocal image shown in Fig. 5p. Depicted are representative confocal image showing the absence of colocalization between TdT (red) and MHCII (cyan) in the injured spinal cord of a *Cx3cr1*^{creER}::*R26-TdT* mouse at 14 days. Scale bars: **(a-c**, in **c**) 200 μm, (**d-e**, in **e**) 200 μm.

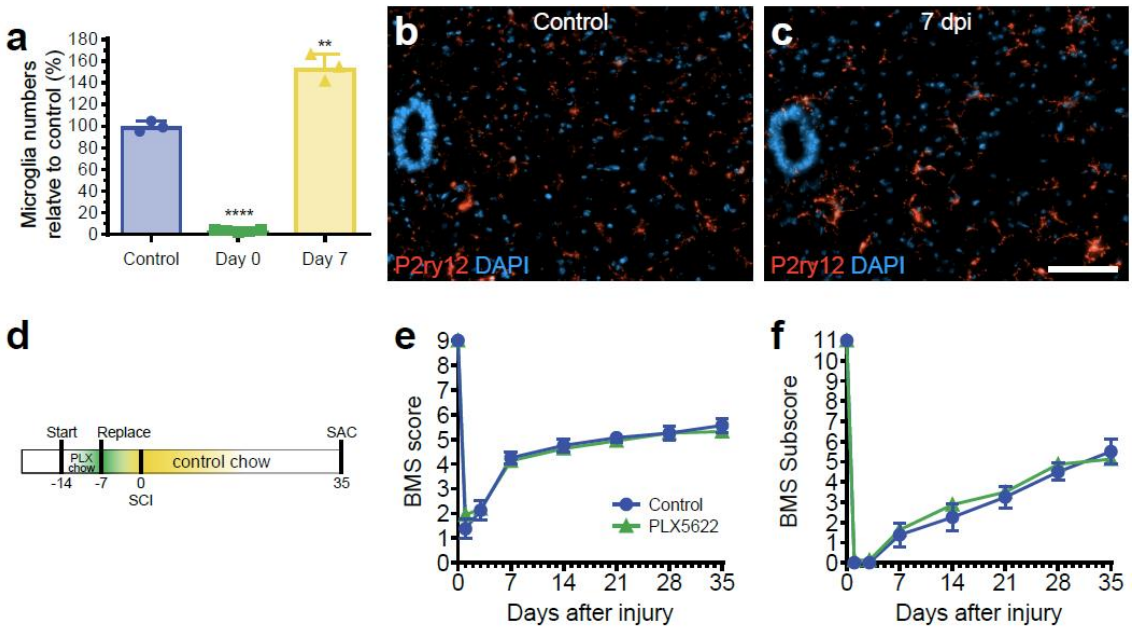

Supplementary Figure 3.20 Mice with more microglia in their spinal cord at the time of injury recover locomotor function similar to that of SCI mice on the control diet.

(**a**) Quantification of the number of microglia (P2ry12+) in the uninjured thoracic spinal cord of C57BL/6 mice (control, blue bar in the histogram), as well as in mice treated with PLX5622 for 1 week and then switched to the control diet for 0 (green) or 7 (yellow) days (n=3-5 mice per group). (**b-c**) Representative confocal images of P2ry12 immunostaining showing the increased number of spinal cord microglia after switching C57BL/6 mice from the PLX5622 diet to control chow for 7 days. (**d**) Schematic diagram of experimental design showing the timeline of treatment (PLX5622 versus control chow), spinal cord contusion (SCI) and sacrifice (SAC). (**e-f**) Assessment of locomotor recovery using the BMS (**e**) and BMS subscore (**f**) (n=8 mice per group). ** p <0.01, **** p <0.0001, compared to the control group. Statistical analysis was performed using a one-way ANOVA (**a**) or a two-way repeated-measures ANOVA (**e-f**) followed by a Bonferroni's post hoc test. Scale bar: (**b-c,** in **c**) 50 μm.

Table 3.1 List of cDNA used for *in situ* hybridization

Symbol	Gene Name	Genbank Accession Numbers	Position	Size (bp)	Linearization		Transcription	
					Antisense	Sense	Antisense	Sense
Igf1	Insulin-like growth factor 1	NM_184052	1338-1856	868	HindIII	XhoI	T7	SP6
Il1a	Interleukin 1 alpha	NM_010554	270-1985	1715	XhoI	BamHI	SP6	T7
Il1b	Interleukin 1 beta	M15131	1-1339	1358	KpnI	XhoI	T7	SP6
Il6	Interleukin 6	J03783		600	KpnI	HindIII	T3	T7
Tnf	Tumor necrosis factor	NM_013693	426-844	419	XhoI	HindIII	SP6	T7
Tgfb1	Transforming growth factor, beta 1	BC013738	315-1487	1173	EcoRI	XhoI	T3	T7

Chapitre 4 RELEASE OF THE ALARMIN INTERLEUKIN-1 ALPHA BY SPINAL CORD INJURED MICROGLIA TRIGGERS SECONDARY DEGENERATION THROUGH REACTIVE ASTROCYTES AND ENDOTHELIAL CELLS

Floriane Bretheau[1], Benoit Mailhot[1], Martine Lessard[1], Nicolas Vallières[1], Ning Quan[2] and Steve Lacroix[1*]

[1]Axe neurosciences du Centre de recherche du Centre hospitalier universitaire (CHU) de Québec–Université Laval et Département de médecine moléculaire de l'Université Laval, Québec, QC, Canada, G1V 4G2;

[2]Charles E. Schmidt College of Medicine, Florida Atlantic University, Jupiter, FL, USA, 33458.

Keywords: Cytokine, danger signal, endothelial cell, interleukin-1, neutrophil, neuroinflammation.

4.1 Résumé

Les dommages infligés aux cellules du système nerveux central (SNC) à la suite d'une lésion de la moelle épinière (LME) entraînent la mort des neurones et des cellules gliales. Dans cette étude, nous avons mis en évidence que l'IL-1α est relâchée par les microglies réactives dans les premières heures suivant la lésion. D'autre part, nous avons montré que l'injection *intra cisterna magna* (i.c.m) d'IL-1α entraîne une forte infiltration de neutrophiles ainsi qu'une perte importante des oligodendrocytes de la moelle épinière. De manière intéressante, les effets de l'injection de l'IL-1α disparaissent complètement lorsque les souris sont co-traitées avec l'antagoniste de l'IL-1R1, l'anakinra, de même que chez des souris Il-1R1-knockout. Nous avons ensuite mis en évidence que la présence exclusive de l'IL-1R1 chez les astrocytes ou les cellules endothéliales, mais pas chez les microglies ou les oligodendrocytes, rétablissent une partie des effets médiés par l'IL-1α. De plus, la délétion de l'*Il1r1* spécifiquement chez les astrocytes ou les cellules endothéliales permet de limiter les effets de la cytokine sur la neuroinflammation et les Ols. La déplétion des neutrophiles et des monocytes nous a permis de mettre en évidence que ces cellules ne semblent pas être impliquées dans ces mécanismes. Finalement, nous avons découvert que l'IL-1α stimule la production de *reactive oxygen species* (ROS) chez les astrocytes et que bloquer les ROS chez des souris traitées à l'IL-1α prévient la perte des Ols. Ainsi, cette étude suggère que l'IL-1α relâchée par la microglie à la suite d'une LME régule la dégénérescence secondaire des Ols via les astrocytes et les cellules endothéliales.

4.2 Abstract

Spinal cord injury (SCI) causes direct damage to cell bodies of neurons and glial cells. This leads to neuroinflammation and a second wave of tissue degeneration characterized by the death of oligodendrocytes (OLs). We report that the alarmin interleukin (IL)-1α is rapidly released by damaged microglia after SCI. When injected intra-cisterna magna to mice, IL-1α induces neutrophil infiltration and death of mature OLs throughout the spinal cord within 24 hours, thus mimicking what is seen at sites of SCI. Importantly, this effect was completely abrogated by co-treatment with the IL-1 receptor 1 (IL-1R1) antagonist anakinra, as well as in IL-1R1-knockout mice which showed greater locomotor recovery than wild-type mice after SCI. Conditional restoration of IL-1R1 expression in either astrocytes or endothelial cells (ECs), but not in OLs or microglia, of IL-1R1-knockout mice restored IL-1α-mediated neuroinflammation and OL loss. Deletion of the Il1r1 gene specifically in astrocytes or ECs compromised neuroinflammation and OL loss in IL-1α-injected mice. Depletion of neutrophils and monocytes however failed to affect these responses, reinforcing the idea that IL-1α-mediated OL cell death is indirect. Primary cell culture experiments revealed that conditioned medium derived from IL-1α-stimulated astrocytes is toxic for OLs. Finally, we discovered that IL-1α-stimulated astrocytes generate an important amount of reactive oxygen species (ROS), and that blocking ROS production in IL-1α-treated mice prevented OL death. Altogether, our data suggest that release of the alarmin IL-1α by microglia after SCI regulates secondary degeneration of OLs through the intermediary of reactive astrocytes and ECs.

4.3 Introduction

The pathophysiology of spinal cord injury (SCI) is divided into two distinct phases: the primary damage and the secondary damage (Tator, 1995; Tator and Fehlings, 1991). The initial mechanical trauma caused by SCI, characterized by the impact with possible persisting compression, leads to a reduced spinal cord blood flow and ischemia, an increased permeability of the blood-spinal cord barrier (BSCB), and the development of hemorrhages at the lesion site, conditions leading to cell death in the first few minutes to hours following the injury. These processes rapidly lead to a series of biochemical changes, characterized by the production of excitatory amino acids, free radicals, eicosanoids, cytokines and other inflammatory molecules, ultimately culminating in a progressive wave of secondary damage (David, 2005). The transition from primary to secondary damage is triggered, at least in part, by the release of the intracellular content of necrotic cells, in particular danger-associated molecular patterns (DAMPs). Most prevalent among DAMPs in the injured CNS are nucleic acids, nucleotide derivatives and chromatin-associated proteins, including ATP, high-mobility group box (HMGB) proteins, interleukin (IL)-33 and IL-1α (Bastien et al., 2015; Davalos et al., 2005; de Rivero Vaccari et al., 2012; Gadani et al., 2015; Kigerl et al., 2017; Nimmerjahn et al., 2005). Thus, DAMPs released after SCI drive neuroinflammation and secondary tissue damage, but the relationship between these processes remains poorly understood.

We recently established that microglia at sites of SCI rapidly produce the danger signal IL-1α, which in return triggers neuroinflammation and locomotor deficits (Bastien, 2015). The presence of DAMPs at sites of SCI has also been associated with the production and release of inflammatory mediators, such as the proinflammatory cytokines IL-1β and tumor necrosis factor (TNF). Of particular interest is the fact that CNS endothelial cells (ECs) abundantly express both IL-1R1 and TNF receptor 1 (TNFR1) and are readily activated by this inflammatory environment (Nadeau and Rivest, 1999). Activation of endothelial IL-1R1 and TNFR1 typically results in multiple responses, including cytokine and chemokine release (Lévesque et al., 2016; McCandless et al., 2009), expression of cell adhesion molecules (Li et al., 2011; Paré et al., 2018), disruption of vascular permeability (Proebstl et al., 2012; Qian et al., 2012), and leukocyte trafficking (Paré et al., 2018). Astrocytes, which are major

contributors to glial scar formation after SCI (Sofroniew, 2009), also react quickly to these inflammatory mediators. Using rodent primary CNS cell cultures and post-mortem brain tissue from patients with various neurodegenerative diseases, Liddelow and colleagues recently found that microglia-derived cytokines and growth factors determine whether astrocytes will have neurotoxic or pro-survival effects (Liddelow et al., 2017b). Notably, a subtype of reactive astrocytes, termed A1 astrocytes, activated by microglia-derived IL-1α (but not IL-1ß), TNF and complement component 1q (C1q), was suggested to play a role in the mechanisms leading to the death of OLs and neurons in diseases such as Alzheimer's, Huntington's and Parkinson's disease, amyotrophic lateral sclerosis and multiple sclerosis. However, not all forms of microglia and astrocyte responses have a detrimental impact on functional recovery in the context of SCI, as depletion of these cells caused disruption of scar formation, enhanced parenchymal immune infiltrates, as well as reduced OL and neuronal survival (Bellver-Landete et al., 2019; Faulkner, 2004). To what extent, and though which signals, microglia, astrocytes, ECs and blood-derived immune cells are driving secondary degeneration after SCI therefore remains an open question.

The mechanisms underlying secondary tissue damage after SCI generate an environment particularly toxic for OLs (Almad et al., 2011; Plemel et al., 2013). In mice, the number of OLs rapidly decreases during the first 24 hours post-SCI, with a maximum loss at 1 week post-injury (Lytle and Wrathall, 2007). Apoptotic death of OLs has been detected in degenerating white matter tracts of rodents, monkeys and humans until at least 2 to 3 weeks post-SCI (Casha et al., 2001; Crowe et al., 1997; Emery et al., 1998; Li et al., 1999; Liu et al., 1998). Whether this loss of OLs is directly responsible for the demyelination and conduction failure observed in axons that survived the initial trauma (Blight, 1985, 1983; Siegenthaler et al., 2007), and perhaps some of the behavioral deficits detected after SCI, remains however uncertain. Although the inflammatory response that takes place following an injury to non-CNS tissue often leads to repair, a similar response in the injured CNS could cause secondary damage (David, 2005). As mentioned, the neuroimmune response that develops after SCI is initiated by the release of DAMPs from disrupted glial cells, neurons and ECs, leading to the recruitment of leukocytes from the blood. Given the dichotomic nature of the neuroimmune response and its overall complexity, it is therefore critical to identify the cells that release the most important DAMPs during the acute phase of SCI.

Equally important is to study the effects of DAMPs on the CNS environment and the periphery.

Following up on our recent discovery that deletion of the *Il1a* gene protects OLs and reduces tissue damage after SCI, we investigated the cellular and molecular mechanisms that underlie IL-1α-dependent effects in the normal and injured mouse spinal cord. We found that microglia-derived IL-1α induces death of OLs through the intermediary of astrocytes. More specifically, activation of astrocytic IL-1R1 by IL-1α triggered the generation and release of reactive oxygen species (ROS) that are toxic to OLs. Accordingly, blocking ROS production in IL-1α-injected mice and SCI mice prevented OL death. Thus, blocking IL-1R1 signaling or ROS production may be a promising therapeutic avenue to prevent loss of OLs following a CNS insult.

4.4 Results

4.4.1 IL-1α is released by injured and stressed microglia during the early acute phase of SCI

We previously showed that microglia and/or macrophages are the main producers of IL-1α after SCI (Bastien, 2015). To clarify which of these two cell types is the major contributor to the production of IL-1α, we performed immunofluorescence staining against IL-1α on spinal cord tissue sections from *Cx3cr1*^{CreER}::*R26-TdT* mice killed at 4 hours post-SCI (Fig. 1A-F), which corresponds to the peak of IL-1α protein expression. *Cx3cr1*^{CreER}::*R26-TdT* mice received tamoxifen treatment one month prior to SCI to drive TdT expression specifically in microglia, but not in peripheral myeloid cells, as established before (Bellver-Landete, 2019). Quantification revealed that nearly all (95% ± 5%) IL-1α-positive (+) cells also express TdT, suggesting that they are microglia (Fig. 1G). To confirm this finding, microglia were depleted *in vivo* using PLX5622, a CSF1R inhibitor from Plexxikon. As shown in Fig. 1D-G, very few IL-1α$^+$ cells were detected in the injured spinal cord of *Cx3cr1*^{CreER}::*R26-TdT* mice fed PLX5622 chow (44,8 ± 7,4 IL-1α$^+$ cells/mm^2) compared to those fed the control diet (0.7% ± 0.3% IL-1α$^+$ cells/mm^2). Thus, our results show that microglia located at the lesion epicenter and surrounding damaged areas are the main cellular source of IL-1α production after SCI.

Since IL-1α is typically synthesized as a precursor protein and constitutively stored in the nucleus of cells, consistent with its role as an alarmin, we next sought to determine the health status of IL-1α-producing microglia in the injured mouse spinal cord. Most IL-1α$^+$ microglia had both damaged cell bodies and processes or exhibited retracted, swollen processes, indicative of an activated status (Fig. 1H-S). Confocal microscopy images revealed a homogenous distribution of the IL-1α protein within the whole microglia (nucleus and cytoplasm). Together, these results show that damaged and stressed microglia release the alarmin IL-1α during the early acute phase of SCI.

4.4.2 Acute central delivery of IL-1α in mice induces activation of glia throughout the spinal cord

Trauma-induced necrotic cell death, as it occurs after SCI, is likely to induce the release of several different alarmins at roughly the same time, as it was suggested for IL-1α, HMGB1, IL-33, and ATP (Bastien et al., 2015; Kigerl et al., 2017; Pomeshchik et al., 2015b). To be able to study the effect of IL-1α in a relatively simpler *in vivo* model, we injected murine recombinant IL-1α (rmIL-1α) intra-cisterna magna (i.c.m) to naïve C57BL/6 mice and examined the effects of the alarmin on the activation of glial cells and neurons in the spinal cord at different time points. Expression of the transcription factors Fos was used as marker of cell activation (Mailhot, 2020). Immunolabeling for Fos in spinal cord tissue sections from mice injected with rmIL-1α revealed that astrocytes and oligodendrocytes (OLs) are activated as early as 1-hour post-injection (Fig. 2). The peak of activation for OLs and astrocytes was observed at 4 hours, with a total of 265,3 ± 49,8 Fos^+ $Olig2^+$ cells/mm² and 131,3 ± 15,9 Fos^+ $Sox9^+$ astrocytes/mm² in the thoracic spinal cord white matter (Fig. 2H, O). The number of activated astrocytes and OLs decreased afterward to 16,0 ± 5,5 cells/mm² and 45,0 ± 13,0 cells/mm², respectively, at 24 hours post-injection. For all time points examined, nearly zero Fos^+ cells were detectable in the spinal cord white matter of PBS-injected mice.

4.4.3 Acute central delivery of IL-1α induces neutrophil infiltration into the neurovascular space and parenchyma of the spinal cord

Knowing that IL-1α initiates sterile inflammation by recruiting neutrophils in Matrigel plugs supplemented with necrotic cell products (Rider et al., 2011), we next examined whether IL-1α injection resulted in the recruitment of $Ly6G^+$ neutrophils along the rostro-caudal spinal cord axis. From 1 to 4 hours after the injection of IL-1α, no $Ly6G^+$ cells were observed in the spinal cord (Fig. 3A). However, the situation drastically changed at 24 hours, a time at which we observed a massive influx of neutrophils into the spinal cord. As shown in Fig. 3B-C, neutrophils were found both in the neurovascular space and parenchyma of the spinal cord following i.c.m. injection of IL-1α. The neutrophil recruitment was transient, as 3 days after IL-1α injection, neutrophil numbers were back to baseline (*data not shown*). Thus, also

implicated in the cascade of cellular events elicited by IL-1α are infiltrating innate immune cells such as neutrophils, whose recruitment occurs after the activation of glial cells.

4.4.4 IL-1α induces the death of mature oligodendrocytes in the mouse spinal cord

Neuroinflammation has been pointed out to be a major cause of the secondary degeneration that occurs after SCI. Thus, we next evaluated whether the presence of IL-1α in the spinal cord would affect cell health and homeostasis, with a special focus on cells of the OL lineage as this cell population was found to be particularly vulnerable to secondary damage after SCI (Casha et al., 2001; Li et al., 1999). Mature OLs were identified as cells that are immunopositive for both Olig2 and CC1 and specifically quantified in the spinal cord white matter. At 4 hours post-injection, no differences in numbers of $Olig2^+$ $CC1^+$ mature OLs were seen between mice injected with either PBS or IL-1α (Fig. 3D). However, the total number of mature OLs was reduced by approximately 40% in mice that received IL-1α i.c.m. compared to PBS-injected control mice at 24 hours (Fig. 3D-F). We counted on average 512,3 ± 24,2 $Olig2^+$ $CC1^+$ cells/mm² in the spinal cord white matter of mice injected with PBS compared to 302,6 ± 32,6 $Olig2^+$ $CC1^+$ cells/mm² in mice injected with IL-1α ($p = 0,0068$). Notably, the decrease in the number of mature OLs at 24 hours post-IL-1α injection was amplified at higher concentrations of the cytokine (*data not shown*), thus suggesting a dose-response effect.

4.4.5 Mature oligodendrocytes are rapidly replaced following death by increased proliferation of oligodendrocyte lineage cells

Mature OLs are a highly diverse cell population, but they all originate from a common oligodendrocyte precursor cell (OPC) whose proliferation and differentiation are regulated by extrinsic signals present in the cell microenvironment (Floriddia et al., 2020). Considering that mature OLs are decimated during the early acute phase of SCI (Bastien et al., 2015), an effect that was mimicked by acute central delivery of IL-1α in the current study, we next investigated whether the OL cell population is restored upon death by performing *in vivo* BrdU experiments. As shown in Fig. 4D, the number of $Olig2^+$ $BrdU^+$ cells was increased by

~6,4 fold in the spinal cord white matter of IL-1α-injected mice compared to the control group at 3 days post-injection. This finding was confirmed by immunofluorescence staining that showed the proliferative marker Ki67 to be augmented by ~4,6-fold in the Olig2 cell population in response to IL-1α administration (Fig. 4E). Importantly, the number of mature OLs in the IL-1α group returned back to baseline values after 3-5 days (Fig. 4F). Altogether, these results suggest that the death of mature OLs induced by IL-1α is compensated by the rapid proliferation of OL lineage cells.

4.4.6 IL-1α induces neuroinflammation and OL cell death through IL-1R1 signaling

As evidence suggests that IL-1R1 is the main signaling receptor for IL-1α, we postulated that IL-1R1 blockade using anakinra, a recombinant IL-1 receptor antagonist with greater affinity for IL-1R1 than IL-1α itself (Abbate et al., 2020), would reduce the central effects of the cytokine. When anakinra was administered concomitantly with rmIL-1α, the infiltration of neutrophils in the mouse spinal cord was completely blocked (Fig. 5A-C). Moreover, treatment with anakinra protected from IL-1α-induced OL cell death (Fig. 5D-F). Thus, blockade of IL-1R1 signaling is sufficient to abolish the potential pathophysiological effects of IL-1α in the spinal cord.

4.4.7 Early signs of secondary degeneration and recovery of locomotor function are improved in mice lacking IL-1R1 after SCI

Based on the previous findings, we postulated that mice deficient in IL-1R1 would exhibit reduced neuropathology and improved functional recovery after SCI. Therefore, we next investigated whether the absence of the *Il1r1* gene positively affects locomotor recovery after SCI, as previously reported for *Il1a*$^{-/-}$ mice (Bastien et al., 2015). Naïve *Il1a*$^{-/-}$, *Il1r1*$^{-/-}$ and WT mice all performed flawlessly and received perfect scores on the 9-point Basso Mouse Scale for locomotion (BMS) and the 11-point BMS subscore. The situation was however different after a moderate (50 kdyn) traumatic SCI. As shown in Suppl. Fig. 1, *Il1r1*$^{-/-}$ mice recovered significantly better than WT mice at 1 and 3 days post-SCI, mimicking the neurological improvements observed in *Il1a*$^{-/-}$ mice. At the end of behavioral assessment (day

35), *Il1r1*$^{-/-}$ mice were mostly coordinated and had parallel paw position at initial contact (score ≥ 7 on the BMS), compared to WT mice. The average BMS subscore of *Il1a*$^{-/-}$ and *Il1r1*$^{-/-}$ mice was 8.3 ± 0.4 and 8.3 ± 0.4, respectively, compared with 5.4 ± 0.3 for WT mice at 35 days post-SCI (Suppl. Fig. 1). Together, these results suggest that global deficiency in IL-1R1 signaling contributes to better functional recovery after SCI by reducing early signs of secondary degeneration.

4.4.8 IL-1R1 is expressed by both glial and endothelial cells in the mouse spinal cord

Next, we assessed IL-1R1 protein expression in the main cell types that reside in the spinal cord. For this, we opted for an immunoblotting approach using membrane protein extracts derived from either specific primary cell types isolated from the normal CNS or cell lines. Immunoblot analysis revealed that IL-1R1 is expressed by CNS-ECs, OPCs, astrocytes and microglia (Suppl. Fig. 2). Intriguingly, the protein detected using the anti-IL-1R1 polyclonal antibody in OPCs and astrocytes was of a slightly lower molecular weight than the predicted 75-kDa IL-1R1 protein, suggesting the possibility that cells of the glial-restricted lineage could express a different form of the receptor. Along this line, we point out that IL-1R3 is identical to IL-1R1 at the C terminus, but with a shorter extracellular domain and a predicted molecular weight of about 66 kDa (Qian, 2012).

4.4.9 Oligodendrocyte cell death is not directly mediated by IL-1α

To investigate the mechanisms by which IL-1α mediates its effects, we took advantage of the IL-1R1-restored mouse line developed by Liu *et al.* (Liu et al., 2015). IL-1R1-restored mice, designed hereafter to as *Il1r1*$^{r/r}$ mice, exhibit an IL-1R1 (and IL-1R3) knockout phenotype that can be reversed in a cell-specific manner by Cre-mediated recombination. First, we asked whether OL cell death could be mediated by a direct effect of IL-1α on OLs. To address this question *in vivo*, we crossed *Il1r1*$^{r/r}$ mice to mice expressing an inducible Cre recombinase under the control of the *Pdgfra* promoter, thus restoring *Il1r1* gene expression specifically in OPCs and their cell derivatives. To measure the efficiency of Cre-mediated IL-1R1 restoration in OL lineage cells, qPCR was used to amplify the floxed *Neo* cassette causing

disruption of the *Il1r1* gene in PDGFRα^{+} OPCs and O4^{+} pro-OLs immunopanned from the adult mouse spinal cord. We estimated the restoration of *Il1r1* gene expression to be around 20% and 25% of normal levels in PDGFRα^{+} OPCs and O4^{+} pro-OLs, respectively, in *Pdgfra*^{CreER}::*Il1r1*$^{r/r}$ mice (Fig. 6A). Based on Olig2 immunolabeling, the purity of the OPC and pro-OL cell populations used for total DNA extraction was estimated at 50% and 60%, respectively (*data not shown*). Thus, this translates into a recombination rate of approximately 40% in both OL cell populations. As expected, no restoration of the wild-type *Il1r1* allele was observed in OL lineage cells of *Il1r1*$^{r/r}$ mice. Despite partial restoration of *Il1r1* gene expression in OLs of *Pdgfra*^{CreER}::*Il1r1*$^{r/r}$ mice, we failed to restore the infiltration of neutrophils and death of mature OLs in response to i.c.m. delivery of IL-1α (Fig. 6B-C). The total number of mature OLs in the spinal cord white matter of *Pdgfra*^{CreER}::*Il1r1*$^{r/r}$ mice injected with IL-1α was similar to that of *Il1r1*$^{r/r}$ mice and animals injected with PBS (Fig. 6C). Finally, we did not observe any significant effect of IL-1α on the death of primary mature OLs *in vitro* (*see data presented below*). Altogether, these results suggest that IL-1α does not cause OL cell death by a direct mechanism of action.

4.4.10 IL-1α mediates OL cell death independently from microglial IL-1R1 signaling

As we previously established that IL-1α is released by microglia in the first few hours post-SCI and that these cells express IL-1R1, we next aimed to investigate whether IL-1α could have autocrine effects on microglia, promoting in return neuroinflammation and the death of mature OLs. To test this, we crossed *Cx3cr1*^{CreER} and *Il1r1*$^{r/r}$ mice to restore IL-1R1 expression specifically in microglia in otherwise null mice. The efficiency of IL-1R1 restoration was estimated at approximately 65% in microglia isolated from the normal spinal cord of adult *Cx3cr1*^{CreER}::*Il1r1*$^{r/r}$ mice (Fig. 7A). We next conducted an experiment in which a single dose of rmIL-1α was injected i.c.m. in either WT, *Il1r1*$^{r/r}$ or *Cx3cr1*^{CreER}::*Il1r1*$^{r/r}$ mice. As shown in Fig. 7B, neutrophils infiltrated the spinal cord of WT mice, but not *Il1r1*$^{r/r}$ or *Cx3cr1*^{CreER}::*Il1r1*$^{r/r}$ mice, within 24 hours of the injection. Similarly, only WT mice responded to IL-1α treatment with a significant decrease in OL cell number (Fig. 7C), suggesting that microglial IL-1R1 signaling does not mediate the central effects of IL-1α. However, when microglia were depleted using PLX5622, the number of neutrophils that

infiltrated the spinal cord in response to acute i.c.m. delivery of IL-1α increased from 165,0 ± 22,3 to 301,0 ± 39,5 $Ly6G^+$ cells/mm² (Fig. 7D-J). In parallel, the number of mature OLs further decreased in mice that received IL-1α and PLX5622, passing from 353,3 ± 22,5 $Olig2^+CC1^+$/mm² in the spinal cord white matter of PBS-injected WT mice, to 114,3 ± 29,4 $Olig2^+CC1^+$/mm² in IL-1α-injected WT mice, and finally to 56,7 ± 25,7 $Olig2^+CC1^+$/mm² in IL-1α-injected WT mice fed the PLX5622 diet (Fig. 7K). This indicates that the central effects of IL-1α are amplified in the absence of microglia, with nearly two times more infiltrating neutrophils and half the number of mature OLs in the spinal cord of microglia-depleted mice. Considering the existence of a decoy IL-1 receptor, IL-1R2, we next hypothesized that the protection conferred by microglia could have been provided by an upregulation of this receptor. To test this possibility, we took advantage of tamoxifen-inducible *Cx3cr1*^{CreER}::*R26-TdT* mice to isolate microglia specifically, with minimal contamination by blood-derived immune cells (Bellver-Landete et al., 2019). We then extracted total RNA from microglia at 24 hours post-injection of either PBS or rmIL-1α and measured *Il1r2* mRNA levels using quantitative real-time PCR. Data showed that IL-1R2 is undetectable at the mRNA level in microglia of PBS-injected mice, but that its expression is dramatically increased in microglia following i.c.m. injection of IL-1α (Fig. 7L). Together, these results suggest that the mechanism by which IL-1α induces OL cell death in the spinal cord occurs independently of microglial IL-1R1 signaling. Rather, microglia appear to protect OLs by sequestering IL-1 cytokines within the extracellular compartment through the decoy IL-1R2.

4.4.11 IL-1R1 signaling in CNS endothelial cells drives neuroinflammation

The expression of IL-1R1 by CNS ECs is well described in the literature. In previous studies, we and others have described the importance of endothelial IL-1R1 signaling in the neuroinflammatory processes that take place at the blood-brain barrier (BBB) and BSCB in the experimental autoimmune encephalomyelitis (EAE) mouse model of multiple sclerosis (Li, 2011; Levesque, 2016; Pare, 2018; Hauptmann, 2020). To investigate the functional role of endothelial IL-1R1 in the central effects of IL-1α, *Cdh5*^{CreER} mice were crossed with *Il1r1*$^{r/r}$ or *Il1r1*$^{fl/fl}$ mice to restore or delete, respectively, IL-1R1 expression specifically in

CNS ECs (Fig. 8). We determined that *Il1r1* gene expression was restored to 90% of normal levels in CNS ECs of *Cdh5*^{CreER}::*Il1r1*$^{r/r}$ mice at 1 month post-tamoxifen treatment (Fig. 8B). This restoration of endothelial IL-1R1 function was sufficient to restore about 36,6% of the neutrophil infiltration observed after i.c.m. injection of rmIL-1α (Fig. 8C & Suppl. Fig. 3A-B). As shown in Fig. 8D and Suppl. 3C-D, the average number of mature OLs in the spinal cord of *Cdh5*^{CreER}::*Il1r1*$^{r/r}$ mice was statistically higher than the one observed for the WT group after central administration of IL-1α, but still reduced compared to IL-1R1-deficient (*Il1r1*$^{r/r}$) mice. Restoration of IL-1R1 expression in CNS ECs was, however, insufficient to restore locomotor deficits to the levels observed in SCI WT mice using the BMS score (Fig. 8E-F). These results suggest that endothelial IL-1R1 signaling only partially contributes to the global effects of IL-1α in the pathogenesis of SCI. This prompted us to investigate the potential contribution of endothelial IL-1R1 in another transgenic mouse model, namely *Cdh5*^{CreER}::*Il1r1*$^{fl/fl}$ mice. In these mice, expression levels of the *Il1r1* gene were reduced by nearly half in CNS ECs when compared to *Il1r1*$^{fl/fl}$ control mice (Fig. 8G-H). In agreement with data presented in Fig. 8C, conditional knockout (cKO) of IL-1R1 specifically in CNS ECs also proved that endothelial IL-1R1 is at least in part responsible for the recruitment and infiltration of neutrophils in the spinal cord of mice at 24 hours post-i.c.m. injection of IL-1α (Fig. 8I & Suppl. Fig. 3E-F). Notably, the IL-1α-mediated decrease in the number of mature spinal cord OLs was prevented by genetic deletion of the *Il1r1* gene in *Cdh5*^{CreER}::*Il1r1*$^{fl/fl}$ mice (Suppl. Fig. 3G-H). We counted on average 538.9 ± 45.6 Olig2^{+}CC1^{+}cells/mm² in the spinal cord white matter of *Cdh5*^{CreER}::*Il1r1*$^{fl/fl}$ mice injected with PBS compared to 469.2 ± 30.7 Olig2^{+}CC1^{+}cells/mm² in those injected with IL-1α (Fig. 8J & Suppl. Fig. 3G-H). This decrease was not statistically significant and did not recapitulate the magnitude of the OL cell loss detected in the two control mouse lines in response to IL-1α (i.e. 45-50% decrease). These loss-of-function effects caused by cKO of IL-1R1 in CNS ECs did not translate into any changes in terms of locomotor recovery (Fig. 8K-L). Thus, endothelial IL-1R1 signaling is at least partially responsible for the infiltration of neutrophils and death of mature OLs induced by IL-1α.

4.4.12 IL-1α induces OL cell death in part through activation of IL-1R1 signaling in astrocytes

In light of the recent studies reporting the existence of neurotoxic A1 astrocytes in various CNS disorders (Liddelow et al., 2017a), we next investigated the contribution of astrocytic IL-1R1 signaling in IL-1α-mediated OL cell death. To examine this, *Gfap*^{Cre} mice were crossed with either *Il1r1*$^{r/r}$ or *Il1r1*$^{fl/fl}$ mice to restore or delete, respectively, IL-1R1 expression specifically in astrocytes (Fig. 9). In brain astrocytes of neonate *Gfap*^{Cre}::*Il1r1*$^{r/r}$ mice, *Il1r1* gene expression was restored to approximately 30% of normal levels (Fig. 9B). A partial restoration of IL-1R1 expression in astrocytes was however not sufficient to reestablish IL-1α-mediated neutrophil infiltration, as virtually no Ly6G^{+} cells were observed in the spinal cord of *Gfap*^{Cre}::*Il1r1*$^{r/r}$ at 24 hours post-injection (Fig. 9C & Suppl. Fig. 4A-B). Despite the absence of neutrophil recruitment, this level of restoration of IL-1R1 expression in astrocytes partially restored OL cell death induced by IL-α (Suppl. Fig. 4C-D). Indeed, the number of mature OLs decreased by 35% in *Gfap*^{Cre}::*Il1r1*$^{r/r}$ mice following central injection of IL-1α, passing from 476.4 ± 50.8 to 308.2 ± 16.6 Olig2^{+}CC1^{+} cells/mm² (Fig. 9D & Suppl. Fig. 4C-D). In comparison, 55% of the population of mature OLs died in response to central delivery of IL-α in WT mice, passing from 489.0 ± 225.1 to 225.6 ± 34.0 Olig2^{+}CC1^{+}cells/mm² in the spinal cord white matter. While WT mice performed significantly worse than IL-1R1-deficient (*Il1r1*$^{r/r}$) mice on the BMS open-field locomotor scale after SCI, *Gfap*^{Cre}::*Il1r1*$^{r/r}$ mice performed identical to *Il1r1*$^{r/r}$ mice. Importantly, the above findings were confirmed in another transgenic mouse model, namely *Gfap*^{Cre}::*Il1r1*$^{fl/fl}$ mice (Fig. 9G). Astrocyte-specific knockdown of *Il1r1* expression significantly reduced neutrophil infiltration and prevented OL cell death in response to IL-α administration compared to WT and *Il1r1*$^{fl/fl}$ controls (Fig. 9H-J & Suppl. Fig. 4E-H). However, partial deletion of the *Il1r1* gene in astrocytes alone did not promote functional recovery in the context of SCI (Fig. 9K-L). Therefore, combining targeting of both astrocytic and endothelial IL-1R1, or their common downstream effector molecules, could prove synergistic and produce better outcomes in terms of preventing secondary degeneration and locomotor deficits after SCI.

4.4.13 Myeloid cells are not responsible for the killing of mature OLs

To determine whether immune cells of the myeloid lineage could play a role in OL cell death induced by i.c.m. delivery of IL-1α, we depleted neutrophils and monocytes by repeated i.p. injections of high doses of the anti-Ly6C/Ly6G (Gr-1) antibody (Suppl. Fig. 5A). Mice presented with a significant decrease in granulocyte and monocyte counts in blood 1 day after the last injection of the Gr-1-depleting antibody regimen, regardless of whether they received IL-1α or PBS i.c.m. (Suppl. Fig. 5B-C). As treatment with the anti-Gr-1 antibody could have resulted in the masking of surface Ly6C/Ly6G antigens, thus preventing their subsequent detection by flow cytometry, the effectiveness of the depletion strategy was also validated in *LysM*^{GFP} transgenic mice, which express the eGFP fluorescent protein in cells of granulo-myelomonocytic lineage. As shown in Suppl. Fig. 5D, the number of LysM-GFP$^+$ cells per mm^3 of blood was reduced by approximately 95% compared with saline-treated and isotype control-treated animals 1 day after the last injection of three high doses of anti-Gr-1. Importantly, the efficacy of the myeloid cell depletion strategy was also confirmed using blood and spinal cord tissue of *LysM*^{GFP} mice injected in the CSF with rmIL-1α. Flow cytometry analysis revealed a decrease of roughly 60% in blood circulating LysM-GFP$^+$ cells in fluorescent transgenic mice treated with the anti-Gr-1 antibody. Immunostaining showed about 70% fewer LysM-GFP$^+$ cells in the spinal cord of *LysM*^{GFP} mice treated with the anti-Gr-1 antibody (32.4 ± 9.0 cells/mm²) compared to saline- and isotype control-treated mice (101.8 ± 43.1 and 102.4 ± 31.0 cells/mm², respectively). Despite this important decrease in myeloid cell infiltration, the anti-Gr-1 treatment did not prevent or reduce the OL cell loss induced by IL-1α. We counted similar numbers of mature OLs in the saline, isotype control and anti-Gr1 groups, with 322.5 ± 15.4, 353.4 ± 44.7 and 282.2 ± 33.1 Olig2$^+$CC1$^+$ cells/mm², respectively. Altogether, these results suggest that immune myeloid cells did not play a role in the death of mature spinal cord OLs observed after central IL-1α administration.

4.4.14 IL-1α triggers an A1 astrocytic response that leads to the killing of mature OLs through the release of reactive oxygen species

We next performed cell culture experiments using primary murine astrocytes and OLs to determine whether OL cell death is induced by toxic factors that are released from astrocytes upon IL-1α stimulation, rather than toxicity induced through cell-cell contact mediated

mechanisms (Fig. 10A). Consistent with findings discussed earlier that i.c.m. delivery of IL-1α to *Pdgfra*^{CreER}::*Il1r1*$^{r/r}$ mice did not lead to death of mature spinal cord OLs (Fig. 6), we found that the addition of rmIL-1α to the control medium was not cytotoxic for OLs *in vitro* (Fig. 10B). However, the transfer of conditioned medium from IL-1α-stimulated astrocytes to cultured primary OLs was sufficient to evoke their death, as assessed using the LDH cytotoxicity assay. No significant cytotoxicity was detected on primary mature OLs when incubated with astrocyte-conditioned medium from untreated astrocytes. This indicates that IL-1α-stimulated astrocytes release factors that are lethal to mature OLs. Thus, we next aimed to determine the identity of the molecules that could harm OLs. Considering the susceptibility of OLs and neurons (axons) to reactive oxygen species (ROS) (Juurlink, 1997; Nikic, 2011), we hypothesized that ROS could be implicated in this cell death mechanism. To assess the potential involvement of ROS in cell death of mature spinal cord OLs, we first examined whether IL-1α can trigger the production of ROS by astrocytes *in vitro*. For this, we cultured primary murine astrocytes in the presence of rmIL-1α or vehicle and then measured the production of ROS using the CellRox assay. We found that stimulation of astrocytes with IL-1α significantly increased the number ROS-producing cells (Fig 10C). Next, we attempted to validate this the theoretical proposition *in vivo* using IL-1α-injected C57BL/6 mice pretreated or not with N-acetyl-L-cysteine (NAC), a potent antagonist of ROS activity. Pretreatment with the NAC compound was sufficient to neutralize part of the effect of IL-1α on neutrophil infiltration (Suppl. Fig. 6A-C). More importantly, the NAC pretreatment completely prevented the loss of mature spinal cord OLs normally caused by central IL-1α administration (Fig 10D-F). Inhibition of ROS may therefore be a good target to mitigate inflammation and block secondary degeneration of mature OLs after SCI. We thus tested this hypothesis in a mouse model of contusion SCI. Although the NAC pretreatment failed to reduce neutrophil infiltration after SCI (Suppl. Fig. 6AD-F), it did reduce the death of mature OLs at the lesion epicenter and both rostral and distal to the site of contusion injury when compared to saline-treated animals (Fig. 10G-I). This shows, once more, that neutrophils are not the cause of OL cell death observed in mice injected i.c.m. with IL-1α or those subjected to SCI. Together, these data show that IL-1α activates astrocytes that in return release toxic ROS that contribute to secondary pathogenesis after SCI.

4.5 Discussion

It has long been recognized that the release of DAMPs initiate inflammation following tissue injury, but their identity and effects are only beginning to be understood in the injured CNS. Here, we further investigated the role of the alarmin IL-1α in the context of SCI. We found that IL-1α is released by microglia located in the lesion core, most of which are dead as early as 24 hours post-SCI. Importantly, deletion of the *Il1a* or *Il1r1* gene in mice not only reduced the infiltration of innate immune cells, but significantly diminished the death of mature OLs at sites of SCI. Delivery of IL-1α i.c.m. in an attempt to mimic SCI conditions triggered the recruitment and infiltration of neutrophils and led to a dramatic loss of mature OLs throughout the spinal cord. Using sophisticated transgenic mouse lines in which we induced cell-specific restoration or deletion of the gene coding for IL-1R1 in CNS-resident cell populations, we found that OL cell death was indirect and involved astrocytes and ECs. Last but not least, we uncovered that OL loss was caused by the release of ROS by activated A1 astrocytes.

IL-1α is a proinflammatory cytokine that contributes to inflammation in various disorders through activation of its cell-surface receptor IL-1R1 (Cavalli, 2021). In addition, IL-1α is ubiquitously expressed as a precursor protein of about 31 kDa (pro-IL-1α) that is translocated from the cytoplasm to the cell nucleus under inflammatory conditions, where it acts as a proinflammatory activator of transcription (Buryskova, 2004; Werman, 2013). Pro-IL-1α does not require proteolytic cleavage to be active (Kim, 2013), despite the fact that proteolysis augments its biological potency (Afonina, 2011). Accordingly, the rapid release of IL-1α from necrotic cells, but not apoptotic cells, following sterile injury to peripheral tissues makes it an ideal DAMP (Rider, 2011; Chen, 2007; Cohen, 2010). We recently reported that IL-1α triggers neuroinflammation after SCI, being produced by myeloid cells that either reside in or infiltrate the spinal cord from the bloodstream in response to the injury (Bastien, 2015). Taking advantage of Cre-inducible *Cx3cr1*^{CreER}::*Rosa26-TdT* transgenic mice which, with an adequate regimen of tamoxifen, allow to specifically label microglia but not monocyte-derived macrophages, we have extended these data to show that dead and damaged microglia are the main source of IL-1α in the early acute phase of SCI.

It is known that IL-1α can bind to at least three specific cell-surface receptors, namely IL-1R1, IL-1R2 and IL-1R3 (Qian, 2012). However, the identity of the CNS resident cells that express each type of receptor has been hampered by the low *in situ* levels of the proteins and difficulties related to the purification of cell types purely. Although there is no doubt that IL-1R1 is strongly expressed by CNS ECs and some types of neurons, as shown by immunofluorescence microscopy (Levesque, 2016; Mailhot, 2020), the evidence supporting that microglia, astrocytes, OL lineage cells, and perivascular macrophages express IL-1 receptors has often been indirect and linked to the overall response of these cells to IL-1 treatment (Vela, 2002; Serrats, 2010; Basu, 2002; Bruttger, 2015). Here, the expression of IL-1R1 was analyzed by immunoblotting of membrane proteins extracted from specific primary cell cultures derived from the normal mouse brain. Our immunoblotting findings confirm that IL-1R1 is expressed by microglia, astrocytes and OLs, despite our failure to detect the IL-1R1 protein in these cells by way of immunofluorescence staining using PFA-fixed brain and spinal cord tissue sections. We interpret this to mean that IL-1R1 is weakly expressed in glial cells. Supporting this, Pinteaux et al. have previously reported that murine microglial cell cultures express low levels of IL-1R1 mRNA, but high levels of the decoy IL-1R2, conferring to these cells a high resistance to IL-1 cytokines (Pinteaux, 2002). This could explain why we failed to detect expression of the transcription factor Fos, a marker of cell activity, in microglia after central administration of IL-1α. In contrast, both astrocytes and mature OLs were activated throughout the mouse spinal cord as early as 1 hour post-injection, thus pointing towards those cells as potential direct or indirect targets of IL-1α.

We previously found that IL-1α plays a critical role in SCI in mice. First, we showed that IL-1R1/MyD88 signaling is essential for the expression of CXCL1, CXCL2 and CCL2 chemokines by astrocytes and the subsequent recruitment of neutrophils and proinflammatory Ly6C^{hi} monocytes at sites of SCI (Pineau, 2010). Accordingly, deficiency in IL-1α or IL-1R1 led to a reduction in the infiltration of innate immune myeloid cells, reduced lesion volume and improved functional recovery after SCI, effects that were correlated with an increased survival of mature OLs (Bastien, 2015). Until now, however, a direct causal effect relationship had yet to be demonstrated and the *in vivo* mechanisms underlying the effects of IL-1α on OL loss remained obscure. Our findings shed light on these issues by revealing that IL-1α by itself is sufficient to trigger a cascade of cellular and

molecular events leading to the rapid death (within 24 hours) of nearly 40% of the population of mature OLs in the mouse spinal cord. Using a diphtheria toxin (DT) receptor-based strategy to selectively ablate mature OLs, Oluich et al. demonstrated that a loss of approximately 25% and 40% of mature OLs in the brain and spinal cord, respectively, resulted in severe clinical dysfunction with an ascending spastic paralysis ultimately leading to fatal respiratory impairment within 3 weeks of DT administration (Oluich, 2012). No evidence was found that OPCs compensate for the loss of mature OLs in that study. While two other groups also independently showed that genetically-induced death of mature OLs is associated with severe ataxia and tremor that correlates with signs of demyelination, impaired axonal conduction and even sometimes death, they found that surviving mice recovered from their neurological deficits and displayed OL replenishment and remyelination (Traka, 2010; Pohl, 2011). The replenishment of the OL population was determined to occur between 5 and 10 weeks following the toxin-mediated death of mature OLs, followed by complete attenuation of motor deficits by week 11 (Traka, 2010). Likewise, targeted laser-induced ablation of a single mature cortical OL resulted in the emergence of a newly matured OL within an approximate turnaround time of 11 weeks (Snaidero, 2020). This prompted us to investigate in our model whether OPCs proliferate and differentiate to replace the original OLs and, if yes, what is the timing of this process. Strikingly, we found that the number of mature OLs came back to baseline after 3-5 days post-injection of IL-1α. BrdU pulse experiments and Ki67 immunostaining confirmed the proliferation of OPCs and their differentiation into newly matured $Olig2^+$ $CC1^+$ OLs. This rapid turnover is reminiscent of changes observed in the acutely injured spinal cord, where robust replacement of mature OLs by OPCs is taking place (Lytle, 2007; Hesp, 2015). Although whether remyelination positively influences locomotor recovery after SCI remains a question of debate (Duncan, 2018), a better understanding of the mechanisms of replacement of lost OLs and myelin has a far more reach than the field of SCI alone. Collectively, these data suggest that SCI triggers a local response characterized by the release of alarmins, such as IL-1α, that induce the death of mature OLs and their rapid replacement by newly matured OLs, which are presumably more efficient at remyelinating the injured spinal cord.

We discovered that concomitant injection of IL-1α and anakinra, an IL-1 receptor antagonist, was sufficient to abolish the effects of IL-1α on neutrophil infiltration and OL

cell death. Accordingly, our data demonstrated that OLs were protected and functional recovery improved in *Il1a*$^{-/-}$ and *Il1r1*$^{-/-}$ mice compared to WT mice after SCI. This prompted us to further investigate the mechanism behind IL-1α-mediated OL loss using various cell-specific IL-1R1 restored and knockout mouse lines. Our *in vivo* experiments revealed that the effects of IL-1α on neutrophils and mature OLs are indirect and mediated through activation of IL-1R1 signaling in CNS ECs and astrocytes. That endothelial IL-1R1, but not microglial IL-1R1, is necessary for mediating the central effects of IL-1ß on sickness behavior and leukocyte recruitment was recently proposed by the Quan laboratory (Liu, 2019). Moreover, Liddelow and colleagues recently found that microglia-derived cytokines, including IL-1α, determine whether astrocytes will exert toxic or pro-survival effects on differentiated OLs (but not OPCs) and neurons in culture (Liddelow, 2017). This implies that astrocytic IL-1R1 may contribute to some form of degeneration in variety of neurodegenerative diseases and CNS injuries. Under all activation conditions tested, microglia were found insufficient by themselves to induce neuronal death (Liddelow, 2017). Whether microglia are protective or pathologic is also a matter of intense debate and most likely context-dependent. Depletion of microglia in mice injected i.c.m. with IL-1α increased inflammation and OL loss, an effect that we associated to the overexpression of the decoy IL-1R2. In a mouse model of contusion SCI, microglia were proved to be a key cellular component of the scar that develops after SCI to protect neural tissue (Bellver-Landete, 2019). Using a mouse model of ischemic SCI, neuroprotection conferred by repeated LPS treatment was partly reversed by specific deletion of microglial or endothelial IL-1R1 (Freria, 2020). It is important to keep in mind, however, that Cre-reporter mouse lines have some limitations despite being a powerful tool to decipher molecular mechanisms *in vivo*. Perhaps the most important being that recombination in a specific cell type is often incomplete, which is particularly true in the case of tamoxifen-inducible CreER mice. This is especially limiting when one aims to knockout a gene of interest, rather than restoring it, in a specific cell type *in vivo*. As the knockout will only be partial, it cannot be determined with certainty whether the response observed is due to the receptors that are still expressed by the targeted cell population or another cell type. Here, we circumvented part of this problem by using restored and knockout mouse models as well as primary cell lines, thus ensuring an additional level of confidence and reproducibility to our results. Therefore, it appears that IL-1α released by

spinal cord injured microglia triggers myeloid cell recruitment and secondary degeneration of OLs through IL-1R1 expressed by cells forming the neurovascular unit, namely ECs and astrocytes.

The role of astrocytes in SCI, and more generally in CNS injury and diseases, has recently been a hot topic of discussion (Escartin, 2021). While some studies suggest that reactive astrocytes protect the injured spinal cord via their role in glial scar formation (Faulkner, 2004; Okada, 2006), evidence suggests that they may also inhibit axonal regeneration and exacerbate secondary tissue damage (Brambilla, 2005; Brambilla, 2009; Bradbury, 2002; McKeon, 1991). The fact of the matter is that, pending the right conditions of activation and/or given the right molecular cues, astrocytes can adopt an axon growth-supporting phenotype despite their contribution to scar formation (Anderson, 2016). Overall, our results support the idea that astrocytes are plastic cells that adapt to their constantly changing microenvironment. When activated by IL-1α, we found that astrocytes produce and release ROS that in return induce death of mature OLs. Accordingly, treatment with the antioxidant NAC prevented the loss of OLs induced by either i.c.m. delivery of IL-1α or SCI in mice. That cells of the OL lineage are particularly vulnerable to oxidative damage after CNS injury has been suggested before (Giacci, 2018). Some studies reported improved functional recovery in NAC-treated rodents after traumatic brain or spinal cord injury (Patel, 2014; Eakin, 2014; Guo, 2015). Collectively, these findings suggest that IL-1α-activated astrocytes release toxic ROS that play a crucial role in secondary degeneration of OLs after SCI.

Recently, Liddelow et al. described a subtype of reactive astrocytes, termed A1 astrocytes, capable of inducing neurotoxicity by a still unknow mechanism (Liddelow, 2017). More specifically, they found that the supernatant of astrocytes activated by a cocktail of microglia-derived proteins, namely IL-1α, TNF and C1q, was sufficient to induce cell death in primary cultures of neurons and mature OLs, but not OPCs or other CNS cell types. In an LPS model of systemic inflammation, each individual global knockout mouse line for either IL-1α, TNF or C1q showed a significant decrease in the A1 astrocytic response, but only the triple-knockout (*Il1a*$^{-/-}$ *Tnf*$^{-/-}$ *C1qa*$^{-/-}$) mice had no sign of astrocyte reactivity. Since TNF and C1q are also produced at sites of SCI during the early acute phase (Anderson, 2004; Pineau, 2007), it is possible that the loss of mature OLs detected in our transgenic mouse models

would have been further prevented by targeting these three genes at the same time. It will therefore be of interest in future work to validate the relevance of these immune molecules and their receptors, individually or in combination, in animal models of SCI using cell-specific conditional gene targeting strategies. Likewise, it will be important to identify other downstream effector molecules like ROS that directly mediate CNS cell toxicity.

In addition to reactive astrocytes, another possible source of ROS could be the innate immune cells that infiltrate the spinal cord during the early acute phase of SCI. Activated neutrophils have long been recognized to produce large amounts of ROS that, for example, increase vascular permeability and their subsequent infiltration of tissues (Harlan, 1987). Neutrophils have also been suspected to promote neurotoxicity through the release of ROS, TNF and proteases (Nguyen, 2007). Of particular relevance here is the fact that neutrophils acquire neurotoxic properties following transmigration across IL-1-stimulated CNS endothelium (Allen, 2012). Monocyte-derived proinflammatory (M1) macrophages should also be considered as another potential source of ROS in the injured spinal cord (David, 2011). Like neutrophils, M1 macrophages were shown to be neurotoxic when co-cultured with primary neurons (Kigerl, 2009). To answer the question of whether neutrophils and proinflammatory M1 monocytes have contributed to OL loss in response to central IL-1α delivery, we therefore had to turn to a depletion strategy that would deplete both types of myeloid cells simultaneously. Taking advantage of *Ly6g*$^{\text{Cre-TdT}}$ mice, Faget et al. recently showed that both neutrophils and proinflammatory M1 monocytes can be efficiently depleted by repeated injections of anti-Gr-1 (Ly6C/G) antibodies, clone RB6-8C5, but not anti-Ly6G (1A8) antibodies (Faget, 2018), a finding that we confirmed here both in blood and SCI tissue. Another key new finding of our study is that neutrophils and proinflammatory M1 monocytes are not implicated in the OL loss observed after i.c.m. injection of IL-1α. Also supporting this statement is the fact that restoring IL-1R1 expression in astrocytes of *Gfap*$^{\text{Cre}}$::*Il1r1*$^{\text{r/r}}$ mice did not restore the infiltration of neutrophils in response to IL-1α, yet restored OL cell death near to WT levels. Taken together with our previous work, this study suggests that endothelial IL-1R1 is required for neutrophil recruitment in the spinal cord under sterile inflammatory conditions, but that these innate immune cells do not contribute to OL loss during neuroinflammation. Instead, astrocytes and CNS endothelial cells appear

to drive OL cell death via an IL-1R1-dependent release of ROS and other yet to be identified molecules.

In summary, our results show that the alarmin IL-1α released by damaged microglia drives neuroinflammation and OL loss after SCI. These responses are mediated in part through activation of endothelial and astrocytic IL-1R1 signaling, the end result of which is the release of toxic ROS. Thus, IL-1α inhibition may prove to be a valuable strategy to prevent secondary degeneration after SCI.

4.6 Materials and methods

4.6.1 Mice

A total of 421 mice of both sexes were used in this study. Male and/or female C57BL/6N mice were purchased from Charles River Laboratories at 8-10 weeks of age. *Cx3cr1*^{CreER} mice were obtained from the European Mouse Mutant Archive, with prior authorization from Dr. Steffen Jung (Rehovot, Israel), and genotyped as described (Yona, 2013). Breeders for *Rosa26-tdTomato* (also known as Ai9, JAX stock #007905 (Madisen, 2010), *Pdgfra*^{CreER} (JAX stock #018280, (Kang, 2010)), *Gfap*^{Cre} (JAX stock #024098 (Gregorian, 2009)), and *Il1r1*$^{fl/fl}$ (JAX stock #028398, (Robson, 2016)) mice were purchased from The Jackson Laboratory. *Cdh5*^{CreER} (line #13073) mice were obtained from the Cancer Research Technology Repository at Taconic, with prior consent of the creator of the mouse line (Sorensen, 2009), Dr. Ralf Adams (London Research Institute, UK). *Il1r1*$^{r/r}$ mice were obtained from Dr. Ning Quan (Ohio State University, Columbus, OH) (Liu, 2015). *Cx3cr1*^{CreER}, *Pdgfra*^{CreER}, *Gfap*^{Cre} and *Cdh5*^{CreER} mice were bred in-house and crossed with either *Rosa26-tdTomato* (*R26-TdT*), *Il1r1*$^{r/r}$ or *Il1r1*$^{fl/fl}$ mice at the Animal Facility of the Centre de recherche du Centre hospitalier universitaire (CRCHU) de Québec–Université Laval. Wild-type littermates generated from heterozygous mating were used as controls. Mice had free access to food and water at all time. All animal procedures were approved by the CRCHU de Québec–Université Laval Animal Care Committee and conducted in compliance with relevant ethical regulations and guidelines of the Canadian Council on Animal Care.

4.6.2 Tamoxifen treatment

To induce Cre-mediated recombination in *Cx3cr1*^{CreER}::*R26-TdT*, *Cx3cr1*^{CreER}::*Il1r1*$^{r/r}$, *Cdh5*^{CreER}::*Il1r1*$^{r/r}$, and *Cdh5*^{CreER}::*Il1r1*$^{fl/fl}$ mouse lines, mice were treated orally with 10 mg of tamoxifen (dissolved in 1:10 ethanol/corn oil) twice at 2-day intervals starting at postnatal day (P) 30-32. To induce recombination in *Pdgfra*^{CreER}::*Il1r1*$^{r/r}$ mice, animals were treated intraperitoneally with 2 mg of tamoxifen twice at 2-day intervals starting at P12-14.

4.6.3 Spinal cord injury (SCI)

Mice were anesthetized with isoflurane and underwent a laminectomy at vertebral level T9-10, which corresponds to spinal segment T10-11. Briefly, the vertebral column was stabilized and a contusion of 50 kdyn was performed using the Infinite Horizon SCI device (Precision Systems & Instrumentation). Overlying muscular layers were then sutured and cutaneous layers stapled. Post-operatively, animals received manual bladder evacuation twice daily to prevent urinary tract infections.

4.6.4 Behavioral analysis

Recovery of locomotor function after SCI was quantified in an open field using the Basso Mouse Scale (BMS), according to the method developed by Basso and colleagues. All groups of mice exhibited similar parameters in terms of the impact force and spinal cord tissue displacement prior to BMS testing. All behavioral analyses were done blind with respect to the identity of the animals.

4.6.5 Intra-cisterna magna (i.c.m.) injections

Mice were injected i.c.m. with either recombinant murine (rm) IL-1α (doses ranging from 20 to 100 ng/µL diluted in PBS, 5 µL injected per mouse, Prepotech catalog #211-11A), rmIL-1β (20 to 100 ng/µL diluted in PBS, 5 µL injected per mouse, Prepotech catalog #211-11B), anakinra (also known as Kineret®, 100 µg/µL, 5 µL injected per mouse) or PBS. The i.c.m treatment consisted of a single injection using a pulled-glass micropipette connected to a 10-µL Hamilton syringe.

4.6.6 Bromodeoxyridine (BrdU) injections

To label proliferating cells, mice were intraperitoneally injected once daily with BrdU (50 mg/kg of body weight in 0.9% saline) for 3 consecutive days, starting on day 1 post-i.c.m. injection of either IL-1α or PBS.

4.6.7 Microglia depletion

To eliminate microglia, mice were fed PLX-5622, a CSF1R inhibitor provided by Plexxikon and formulated at a dose of 1200 mg/kg in AIN-76A chow from Research Diets Inc., for 21 consecutive days.

4.6.8 Myeloid cell depletion

Neutrophils and monocytes were depleted through repeated i.p. injections of anti-mouse Ly-6C/Ly-6G antibody, clone RB6-8C5, purchased from BioXCell. Rat IgG2a isotype (clone 2A3; BioXCell) and PBS served as controls. Mice were injected with 100 µl of antibody at 0.2 µg/µl or PBS at 1 and 2 days prior to and immediately after central IL-1α administration.

4.6.9 In vivo inhibition of ROS production

Mice received 4 injection of saline or NAC (150 mg/kg) intraperitoneally at 12 hours before, 1 hour before, 12 hours after and 24 hours after i.c.m injection of either PBS or rmIL-1α. Mice were perfused 1 hour after the last injection of NAC.

4.6.10 Tissue processing

Mice were overdosed with a mixture of ketamine (400 mg/kg) and xylazine (40 mg/kg) and intracardially perfused with 1% paraformaldehyde (PFA), pH 7.4, in PBS. Spinal cords were dissected out from vertebral columns, post-fixed for an additional 48 hours in 1% PFA at 4°C, and then transferred into PBS + 20% sucrose for at least 24 hours before tissue sectioning. Spinal cords were then blocked into 4-mm segments, corresponding to the upper cervical, mid-thoracic and upper lumbar levels. Therefore, for each animal, a total of three spinal cord segments were embedded in Shandon™ M-1 Embedding Matrix (Thermo Fisher Scientific) and tissue sections cut at a thickness of 14 µm using a cryostat (model CM3050S; Leica Biosystems). All sections were collected directly onto Surgipath X-tra® slides having a permanent positive charged surface (Leica Microsystems Canada) and stored at -20°C until use.

4.6.11 Immunostaining and quantification

Immunofluorescence labeling was performed according to our previously published method {Pineau, 2007 #1242}. Primary antibodies used in this study are of the following sources (catalog numbers in parentheses) and were used at the indicated dilutions: rat anti-BrdU (1:750, Abcam, ab6326), mouse anti-CC1 (1:500, Abcam, ab16794), rat anti-CD11b (1:250, AbD Serotec, MCA711), goat anti-sox9 (1:250, R&D Systems, AF3075), rabbit anti-cfos (1:500, Cell signaling, 2250), mouse anti-GalC (1:800, Millipore, MAB242), goat anti-Iba1 (1:1500, Novus Biologicals, NB100-1028), goat anti-IL-1α (1:100 dilution, R&D Systems, catalog #AF-400-NA), rabbit anti-Ki67 (1:200, Abcam, ab15580), rabbit anti-laminin (1:1000, Dako, Z0097), rat anti-Ly6G (1:2000, BD Biosciences, 551459), rat anti-NG2 (1:200, R&D Systems, MAB6689), mouse anti-O4 (1:400, R&D Systems, MAB1326), goat anti-Olig2 (1:400, R&D Systems, AF2418), and rabbit anti-P2ry12 (1:500, AnaSpec, AS-55043A). For Ki67 immunofluorescence, antigen retrieval was performed using sodium citrate buffer at 95°C for 5 min. For BrdU, tissue sections were treated with HCl (2.0 N) for 30 min at 37°C followed by 0.1M sodium borate (pH 8.5) for 10 min at room temperature. Primary antibodies were visualized with appropriate Alexa Fluor®-conjugated secondary antibodies from Thermo Fisher Scientific (1:250 dilution). DAPI (1µg/ml, Thermo Fisher Scientific) was used for nuclear counterstaining. Sections were imaged on a Zeiss LSM 800 confocal microscope system equipped with 405, 488, 561, and 640nm lasers. Confocal images were acquired using a Zeiss Axiocam 506 Mono camera and mosaics created using the Zen 2.3 software (Blue edition).

All stereological counts were performed using the BIOQUANT Life Science software (v. 18.5, Bioquant Image Analysis Corporation). For the quantification of OLs ($Olig2^+$ or $NG2^+Olig2^+$ or $CC1^+Olig2^+$), the total number of immunolabeled cells in the spinal cord white matter per cross section was counted at 40× magnification. For the quantification of neutrophils, the total number of $Ly6G^+$ cells into the spinal cord blood vessels or parenchyma, delineated using pan-laminin immunostaining, was counted at 20× magnification in the entire spinal cord cross section. Only immunolabeled cells with a DAPI-stained nucleus were counted and results presented as the total number of immunolabeled cells per mm^2. All quantifications were done blind with respect to the identity of the animals.

4.6.12 Isolation of specific CNS cell types

OPCs and late OL progenitors (pro-OLs): OPCs were isolated from the neonatal (P7-P9) mouse brain to perform cell culture studies, whereas pro-OLs were isolated from adult brains (6-8 weeks old mice) to assess the efficiency of Cre-mediated recombination. Mouse pups were anesthetized on ice and sacrificed by decapitation according to institutional guidelines. Adult mice were anesthetized and perfused intracardially with ice cold Hanks' balanced salt solution (HBSS) without Ca^{2+}/Mg^{2+} to remove blood from the vasculature. Brains were extracted and cerebral cortices dissected and diced into small pieces, which were then incubated in a mixture of papain (0.9 mg/mL), cysteine (0.2 mg/mL) and DNase I (39 U/ml) at 37°C for 20 min on an orbital shaker. The digestion was stopped by adding trypsin inhibitor to a final concentration of 5 mg/mL, and tissue dissociated into a single-cell suspension by gentle mechanical trituration. OPCs and pro-OLs were isolated by immunopanning at room temperature using antibodies directed against PDGFRα (CD140a) and O4 cell surface markers, respectively, following the methods of Emery and Dugas {Emery, 2013 #2722}.

Microglia: Microglia were isolated from the adult mouse spinal cord at 8 weeks of age to determine the efficiency of Cre-mediated recombination or to assess gene expression by qRT-PCR. In brief, mice were transcardially perfused with cold HBSS (without Ca^{2+}/Mg^{2+}) to remove immune cells from the vasculature, their spinal cords dissected out and gently mechanically homogenized on ice. Cells were next filtered through a 70-µm nylon mesh cell strainer (BD Biosciences), fractionated using 37-70% Percoll density gradient centrifugation and microglia-enriched fractions purified by cell sorting according to the methods and cell surface markers described below.

Endothelial cells (ECs): ECs were isolated from brain capillaries of 6-8 weeks old mice. In brief, mouse brain tissue, free of meninges, was minced, homogenized and digested in a mixture of 0.7 mg/ml collagenase type II and 39 U/ml DNase I in DMEM for 75 min at 37°C. Myelin was removed by centrifugation at 1,000 g for 20 min in 20% BSA-DMEM. The cell pellet was then incubated for another hour at 37°C with a mixture of 1 mg/ml collagenase-

dispase and 39 U/ml DNAse I in DMEM. Microvascular ECs were separated on a 33% continuous Percoll gradient.

Astrocytes: Astrocytes were isolated from the cortex of P0-P2 mouse pups, as described by Schildge and colleagues (Schildge, 2013). In brief, meninges were removed and cortex isolated, minced and incubated for 40 minutes in a collagenase IV solution (750 U/mL) at 37°C under occasional agitation. The suspension was centrifuged, resuspended in complete DMEM supplemented with 10% FBS, dissociated into a single-cell-suspension and then seeded on T75 flasks coated with poly-D-lysine in a 37°C, 5% CO2 humidified incubator. After 7-8 days, cells were agitated on an orbital shaker at 37°C at 180 rpm for 30 min to remove microglia. Medium was removed and replaced by fresh medium. Cells were again agitated at 37°C at 240 rpm for 6 hours to remove OPCs. Medium was removed and astrocytes were collected by trypsinization.

4.6.13 Primary cell culture

Oligodendrocytes: OPCs were seeded on poly-L-lysine-coated cell culture plates in the presence of DMEM-Sato Base Growth Medium and their proliferation induced by adding platelet-derived growth factor-AA (PDGF-AA,10 ng/mL) and basic fibroblast growth factor (bFGF, 20 ng/mL) in the absence of the T3 thyroid hormone, following a protocol adapted from Haines and colleagues {Haines, 2015 #2461}. Once in sufficient numbers, OPCs were differentiated into mature OLs by adding the T3 hormone to the DMEM-Sato Base Growth Medium, in the absence of PDGF and bFGF. The differentiation of OPCs into mature OLs was confirmed by immunostaining against O4 marker and assed according cell morphology.

Endothelial cells: Primary brain microvascular endothelial cells (BMECs) were plated on culture dishes coated with 10 µg/ml collagen type IV and 5 mg/ml gelatin and cultured in DMEM supplemented with 20% FBS, 1 ng/mL basic fibroblast growth factor, 100 µg/mL heparin, 1.4 µM hydrocortisone with antibiotics and antimycotics. Medium was supplemented with puromycin (10 µg/mL) for the first 2 days of culture, after which the concentration was adjusted to 4 µg/mL.

Astrocytes: Primary cultures of mouse astrocytes were prepared from the cortex of P0-P1 pups, as described in (Schildge S, Bohrer C, Beck K, Schachtrup C. Isolation and culture of mouse cortical astrocytes. Journal of visualized experiments: JoVE, (2013))., and used from passages 3 to 4. Cells were grown in complete Dulbecco's Modified Eagle Medium (DMEM) either) in 6-well plates (to generate astrocytes-conditioned medium) or directly into 96-well plates (for the ROS assay) at a density of 200,000 cells/well or 20 000 cells/well coated with poly-L-lysine (0.1 mg/ml) respectively.

4.6.14 Automated blood cell count, flow cytometry and cell sorting

Mice were overdosed with a mixture of ketamine-xylazine and their blood collected via cardiac puncture using a 22-gauge heparinized syringe. Blood samples were immediately transferred into EDTA-coated microtubes (Sarstedt) and put on slow rotation at 5 rpm (using the Mini LabRoller^{TM} Rotator) until processing. Automated complete blood cell count was performed using the Scil Vet abc Plus+^{TM} analyzer (Scil Animal Care Company), following manufacturer's instructions. For flow cytometry, red blood cells were lysed and the remaining cells incubated with Mouse Fc Block (i.e., purified anti-mouse CD16/CD32; BD Biosciences) for 15 minutes at 4°C to prevent nonspecific binding. Multicolor labeling was then performed using the LIVE/DEAD™ Fixable Yellow Dead Cell Stain Kit (Thermo Fisher Scientific) and the following fluorescently conjugated primary antibodies: PerCP-conjugated anti-CD45 (1:50 dilution), Alexa 700-conjugated anti-CD11b (1:50), BD HorizonTM V450-conjugated anti-Ly6C (1:83), and PE-Cy7-conjugated anti-Ly6G (1:50) (all from BD Biosciences). Cells were analyzed using FlowJo software (v. 9.2; Tree Star Inc.) on a FACS LSRII flow cytometer (BD Biosciences).

For the purification of microglia needed for DNA and mRNA analyses by means of quantitative real-time PCR (qPCR) and RT-PCR (qRT-PCR), respectively, microglia were isolated from the adult spinal cord as described above and then sorted using a BD FACSAria II (BD Biosciences). The following primary antibodies were used: PerCP-conjugated anti-CD45 (1:50 dilution), Alexa 700-conjugated anti-CD11b (1:50), FITC-conjugated anti-Ly6C (1:83), and PE-Cy7-conjugated anti-Ly6G (1:50) (all from BD Biosciences). Microglia were identified as $CD45^{int}$ $CD11b^{+}$ $Ly6C^{-}$ $Ly6G^{-}$ cells.

4.6.15 Assessment of Cre-mediated recombination using qPCR

Genomic DNA was extracted from pro-OLs, microglia, ECs or astrocytes isolated from the mouse CNS using the GenElute Mammalian Genomic DNA Miniprep Kit (Sigma-Aldrich Canada Ltd.), according to the manufacturer's instructions. The following primers were used to determine the extent of Cre-mediated deletion of the inserted sequence, which contained a neocassette (Neo) and other interfering elements (flanked by *loxP* sites) causing disruption of *Il1r1* gene expression, and whose deletion restored the normal coding frame of the *Il1r1* gene in *Il1r1*$^{r/r}$ mice crossed with cell-specific Cre mice: *Neo*, 5'-gcttgggtggagaggctattc-3' and 5'-gcctcgtcttgcagttcattca-3' and *Il1r1* (intron 7), 5'-gccctttttcttacattctatttggtgc-3' and 5'-caagaaggagttaaccgggacatc-3'. Primers designed to amplify intron 7 of the *Il1r1* gene were used to normalize gene expression between animals, and data expressed as fold change relative to the WT group. To determine the extent of deletion of the floxed *Il1r1* alleles in *Cdh5*^{CreER}::*Il1r1*$^{fl/fl}$ and *Gfap*^{Cre}::*Il1r1*$^{fl/fl}$ mice, qPCR amplification was conducted using primers spanning intron 2 and exon 3 of the *Il1r1* gene: *Il1r1* (intron 2-exon 3), 5'-cattgcttctccttttctctctttaa-3' and 5'-gccgtgcattttatttggagta-3'. As above, intron 7 was amplified to normalize data. The sequences chosen were selected to match only the intended gene using the GeneTool software (v. 2.0, BioTools Inc.), and verified by BLAST analysis in GenBank. Amplification was performed using reagents of the KAPA SYBR ® FAST qPCR Master Mix Kit (Kapa Biosystems Ltd.) optimized for the LightCycler 480 (Roche Diagnostics), and by following these conditions for PCR reactions: 45 cycles, denaturation at 95°C for 30 sec, annealing/elongation and reading at either 62°C (for amplification of the *Neo* sequence) or 58°C (intron 2-exon 3 of the mouse *Il1r1* gene) for 30 sec. A melting curve was performed to assess non-specific signal. Relative quantity was calculated using the delta Ct method. Quantitative real-time PCR measurements were performed by the CRCHU de Québec–Université Laval Gene Expression Platform and were compliant with MIQE guidelines.

4.6.16 Assessment of gene expression using real time qRT-PCR

FACS-isolated spinal cord microglia were homogenized using Qiazol Lysis Reagent (Qiagen) and total RNA extracted using the miRNeasy Micro Kit On-column DNase (Qiagen), following the manufacturer's instructions. The quantity of total RNA was measured using a NanoDrop ND-1000 Spectrophotometer (NanoDrop Technologies). First-

strand cDNA synthesis was accomplished using 0.1-0.2 µg of isolated RNA in a reaction containing 200 U of Superscript IV RNase H-RT (Thermo Fisher Scientific), 300 ng of oligo-dT_{18}, 50 ng of random hexamers, 50 mM Tris-HCl pH 8.3, 75 mM KCl, 3 mM $MgCl_2$, 500 µM deoxynucleotides triphosphate, 5 mM dithiothreitol, and 40 U of Protector RNase Inhibitor (Roche Diagnostics) in a final volume of 50 µl. The reaction was incubated at 25°C for 10 min and then at 50°C for 20 min, followed by inactivation by incubation at 80°C for 10 min. A PCR Purification Kit (Qiagen) was used to purify cDNA. cDNA corresponding to 10-18 ng of total RNA was used to perform fluorescent-based real-time PCR quantification using the LightCycler 480 (Roche Diagnostics). Reagents of the KAPA SYBR ® FAST qPCR Master Mix Kit (Kapa Biosystems Ltd.) optimized for the LightCycler 480 were used as described by the manufacturer. The primer pairs were: *Il1r2*, 5'-gagaccccacacgcctattga-3' and 5'-ggttccgtggttgttcctttga-3' and *Gapdh*, 5'-ggctgcccagaacatcatccct-3' and 5'-atgcctgcttcaccaccttcttg-3'. Once again, primer pairs were designed using the GeneTool 2.0 software (Biotools Inc.) and their specificity verified by blast in the GenBank database. The conditions for PCR reactions were: 45 cycles, denaturation at 95°C for 30 sec, annealing/elongation and reading at 60°C for 30 sec. A melting curve was performed to assess non-specific signal. Relative quantity was calculated using the delta Ct method. Normalization was performed with the delta-delta Ct method using the PBS group and the *Gapdh* gene used as a reference. Real time qRT-PCR measurements were performed by the CRCHU de Québec–Université Laval Gene Expression Platform and were compliant with MIQE guidelines.

4.6.17 Immunoblotting analysis

For protein extraction, cells were washed twice with ice cold PBS and then incubated in ice cold RIPA lysis buffer (100 µL for 1.10^6 cells; 20 mM Tris-HCl pH 8.0, 2 mM EDTA, 10 mM EGTA, 1% Triton X-100) containing Protease and Phosphatase Inhibitor Cocktail (Sigma-Aldrich Canada Ltd.). Cells were scraped off the plate and the lysate immediately transferred to a microcentrifuge tube on ice. Homogenates were sonicated and incubated for 20 min at 4°C under rotation to complete cell lysis. Tubes were centrifuged at 13,000 *g* for 20 min at 4°C and supernatant collected into new microtubes. Protein levels were determined using the BCA Protein Assay Kit (Sigma-Aldrich Canada Ltd.).

For quantification of protein levels, 3 to 10 µg of proteins were boiled and electrophoresed on SDS-acrylamide gel, followed by blotting on PVDF or nitrocellulose membranes (PerkinElmer). Membranes were blocked for 1 hour with 5% dry milk in TBST buffer (50 mM Tris-HCl pH 8.0, 150 mM NaCl, 0.05% Tween-20) and then incubated overnight in 5% milk/TBST solution containing primary antibody. The following antibodies were used: mouse anti-actin (1:75000, EMD Millipore, MAB1501), rabbit anti-GFAP (1:8000, Agilent Technologies (Dako), Z0334), and goat anti-IL-1R1 (1:1500, R&D Systems, AF-771). Membranes were incubated with secondary antibodies conjugated to horseradish peroxidase (1:2500, Vector Laboratories) and cross-reactive bands visualized by chemiluminescence (PerkinElmer).

4.6.18 Detection of ROS *in vitro*

Production of ROS was assessed in living cells by using the fluorogenic probe CellROX® Green Reagent (Molecular Probe), a cell-permeable dye that is non-fluorescent while in a reduced state but upon oxidation exhibits strong fluorescent signal with excitation/emission maxima of ~485/520 nm. Astrocytes primary cells, seeded in 96 well plates at 20 000 cells/well, were exposed to vehicle or rmIL-1α (10 ng/mL) for 24h. Cells were loaded with 5 µM CellROX® Green Reagent and 1 µg/ml Hoechst 33342, for nuclear counterstain, for 30 min and then rinsed three times with PBS and finally fixed with PFA 4% for 15 minutes at room temperature. Imaging was then performed using the EVOS® FL Auto Imaging System (Thermo Fisher) and further analysed with Image J.

4.6.19 *In vitro* cytotoxic assay

To study the effect of conditioned medium derived from astrocytes or ECs stimulated with either IL-1α or PBS on the survival of mature OLs, cell viability was measured using the Pierce Lactate Dehydrogenase (LDH) Cytotoxicity Assay Kit (Thermo Fisher Scientific), according to the manufacturer's instructions. In brief, primary astrocytes were plated in 6-well plates at a density of 100 000 cells/well and treated with either rmIL-1α (10 ng/mL) or PBS. Following a 24-hour incubation period, the conditioned medium was removed and immediately transferred onto mature OLs plated at a density of 20,000 cells/well in 96-well plates for 24 hours. The LDH reaction mixture was then added to the culture medium for 30

minutes at room temperature, the reactions stopped and absorbances measured at 490 nm and 680 nm (background signal from the instrument) using the SpectraMax i3 (Molecular Devices).

4.6.20 Statistical analysis

Statistical evaluations were performed using one- or two-way ANOVA or repeated-measures ANOVA where appropriate. The multiple comparisons adjustment was made using the Bonferroni correction. All statistical analyses were performed using the GraphPad Prism software (v.7, GraphPad Software Inc.). A p value < 0.05 was considered as statistically significant. All data in graphs are expressed as means ± SEM.

4.7 Acknowledgments

This study was supported by grants from the Canadian Institutes of Health Research (PJT-168852 to S.L.) and Natural Sciences and Engineering Research Council of Canada (RGPIN-2015-05281 to S.L.). Salary support to F. B. was in part provided by the Fondation du CHU de Québec and the Centre thématique de recherche en neurosciences (CTRN). We thank Nadia Fortin for her invaluable technical assistance.

4.8 Author contributions

F.B. conceived the study, designed and performed most of the *in vivo* and *in vitro* experiments, analyzed the data, drafted the figures and wrote the manuscript. B.M participated to the design and commented on the manuscript. M.L. performed immunofluorescence and some of the *in vitro* experiments. N.V. performed acquired microscopy images and edited figures. N.Q. commented on the manuscript. S.L. conceived the study, designed the experiments, supervised the overall project and wrote the manuscript.

4.9 Figures

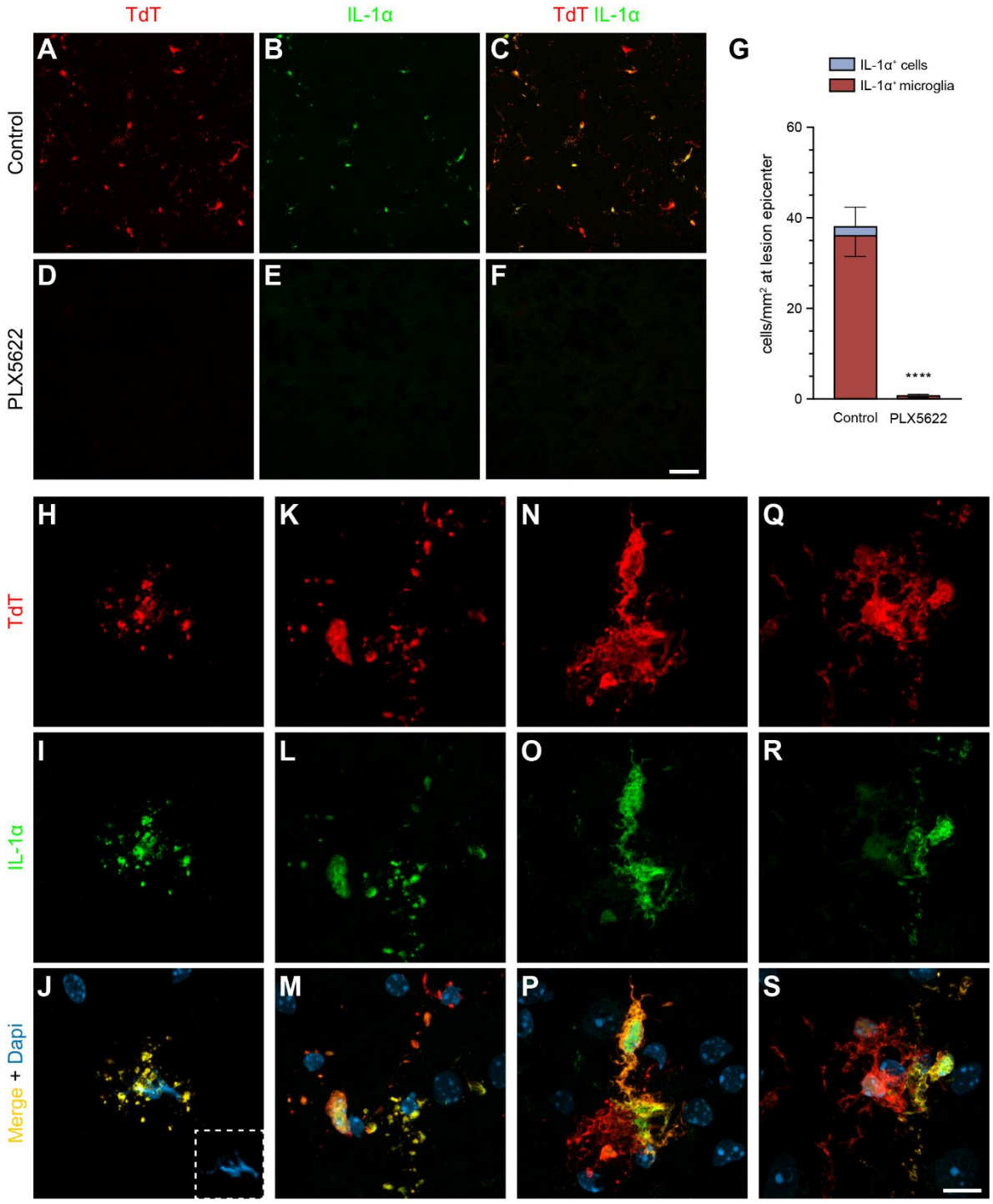
TdT
IL-1α
TdT IL-1α
Control
PLX5622
A
B
C
D
E
F
G
IL-1α⁺ cells
IL-1α⁺ microglia
cells/mm² at lesion epicenter
60
40
20
0
****
Control
PLX5622
H
K
N
Q
I
L
O
R
J
M
P
S
TdT
IL-1α
Merge + Dapi

Figure 4.1. Damaged or stressed microglia rapidly release IL-1α at the site of spinal cord contusion in mice.

(**A**-**F**) Representative confocal images showing IL-1α immunostaining (green) in the spinal cord of an injured *Cx3cr1*^{Cre}::*Rosa26*^{TdT} transgenic mouse, in which microglia express the fluorescent reporter Td-Tomato (TdT, red), at 4 hours post-SCI. Note that immunostaining for IL-1α in panels **D**-**F** disappeared after elimination of microglia from the injured spinal cord of *Cx3cr1*^{Cre}::*Rosa26*^{TdT} mice treated with the CSF1R inhibitor PLX5622. (**G**) Quantification of IL-1α-positive (+) cells at the lesion epicenter in *Cx3cr1*^{Cre}::*Rosa26*^{TdT} mice treated with PLX5622 or the control diet and killed at 4 hours post-SCI (n=4 mice/group). (**H**-**S**) High magnification confocal images of IL-1α^{+} TdT^{+} microglia revealed that these cells often exhibit damaged cell bodies and processes (**H**-**M**) or have retracted, swollen processes, indicative of an activated status (**N**-**S**). Nuclear staining (DAPI) is shown in blue (**J**, **M**, **P**, **S**) in the merged images. Data are expressed as mean ± SEM. *** $p < 0.001$, PLX5622 compared to the control diet group; one-way ANOVA with Bonferroni's post-hoc test. Scale bars: (**A**-**F**, in **F**) 50 µm, (**H**-**S**, in **S**) 50 µm.

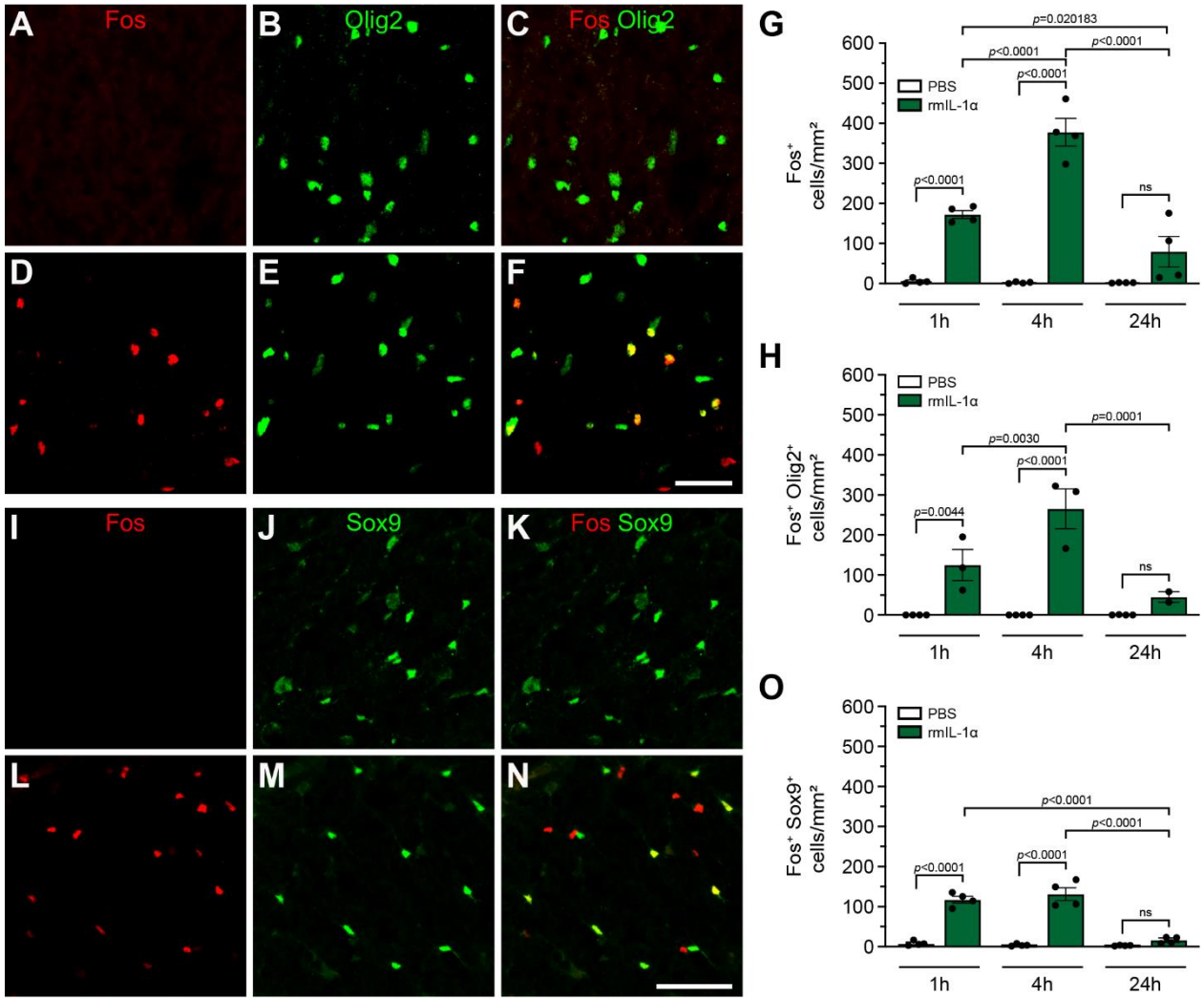

Figure 4.2. Intra-cisterna magna delivery of IL-1α in mice induces rapid activation of astrocytes, oligodendrocytes throughout the spinal cord.

(**A-F**, **I-N**, **P-U**) Representative confocal images of the spinal cord showing expression of the cell activation markers Fos (red signal in **A-F**, **I-N**), Olig2-positive (+) oligodendrocyte (OL) lineage cells (green cells in **A-F**) and $Sox9^{+}$ astrocytes (green cells in **I-N**) 4 hours after a single intra-cisterna magna (i.c.m.) injection of either PBS (**A-C**, **I-K**), or recombinant mouse (rm) IL-1α (**D-F**, **L-N**). (**G-H**) Quantification of the total number of Fos^{+} cells (**G**) and $Fos^{+}Olig2^{+}$ double-labeled OLs (**G**) in the spinal cord white matter of C57BL/6 mice injected with either PBS or rmIL-1α and killed at 1, 4 or 24 hours post-injection (n=4-7 mice/group). (**O**) Quantification of the total number of $Fos^{+}Sox9^{+}$ double-labeled astrocytes

in the spinal cord white matter (n=4-7 mice/group). Data are expressed as mean ± SEM. Statistical significance was determined by a two-way ANOVA followed by a Bonferroni post-hoc test. Scale bars: (**A**-**F**, in F) 50 µm, (**I**-**N**, in **N**) 50 µm, (**P**-**U**, in **U**) 50 µm.

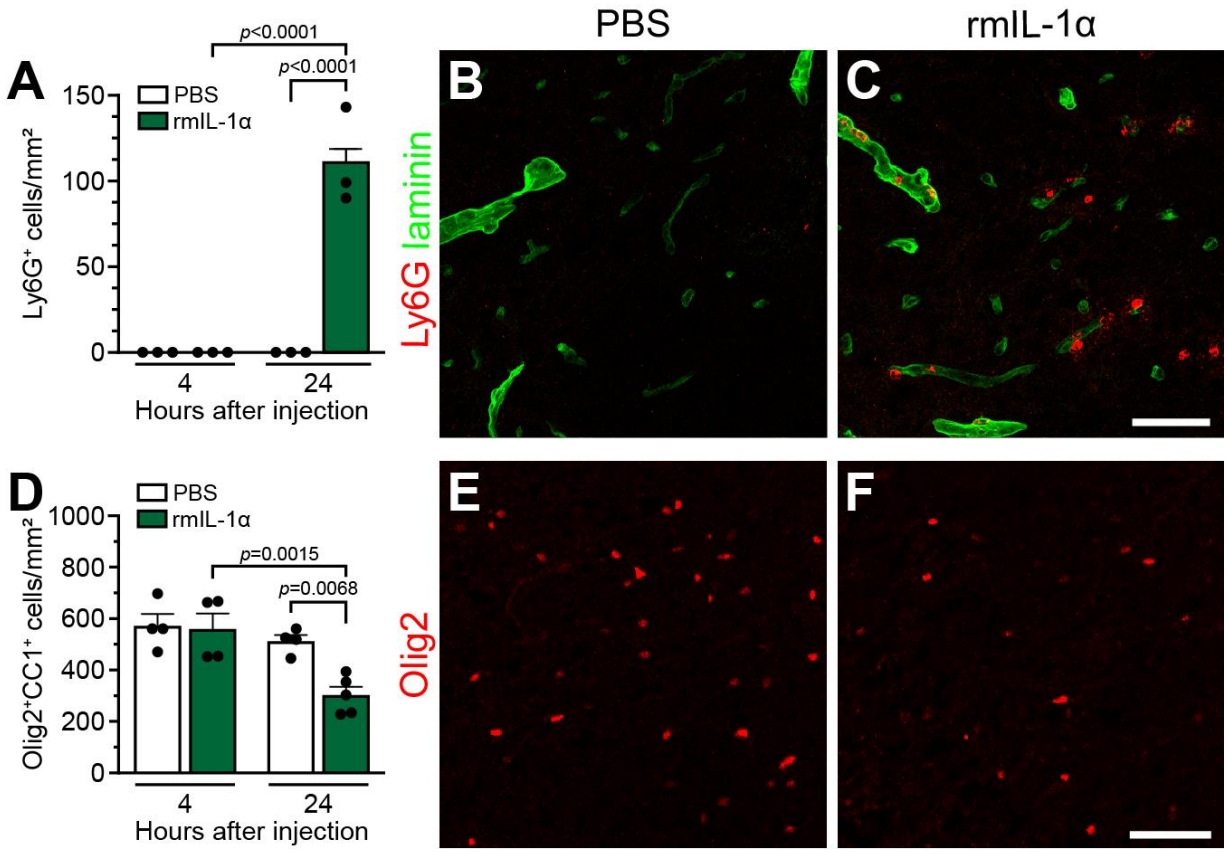

Figure 4.3. Intra-cisterna magna delivery of IL-1α in mice induces innate immune cell infiltration and loss of mature oligodendrocytes throughout the spinal cord.

(**A**) Quantification of the total number of $Ly6G^+$ neutrophils that infiltrated the spinal cord at 4 and 24 hours post-injection of PBS or recombinant mouse (rm) IL-1α intra-cisterna magna (i.c.m.) (n=5 mice/group). (**B-C**) Representative confocal images showing Ly6G (a marker of neutrophils, red) and laminin (a marker of blood vessel basement membranes, green) immunostainings in the spinal cord of C57BL/6 mice injected with either PBS (**B**) or rmIL-1α (**C**) at 24 hours post-injection. (**D**) Quantification of the total number of $Olig2^+CC1^+$ mature oligodendrocytes in the spinal cord white matter of C57BL/6 mice at 4 and 24 hours post-i.c.m. injection of either PBS or rmIL-1α (n=5 mice/group/time). (**E-F**) Representative confocal images showing immunostaining for the oligodendrocyte transcription factor 2 (Olig2, red cells), a nuclear marker of oligodendrocyte lineage cells, in the spinal cord of C57BL/6 mice at 24 hours post-injection of either PBS (**E**) or rmIL-1α (**F**). Data are

expressed as mean ± SEM. Statistical significance was determined by a two-way ANOVA followed by a Bonferroni post-hoc test. Scale bars: (**B-C**, in **C**) 50 µm, (**E-F**, in **F**) 50 µm.

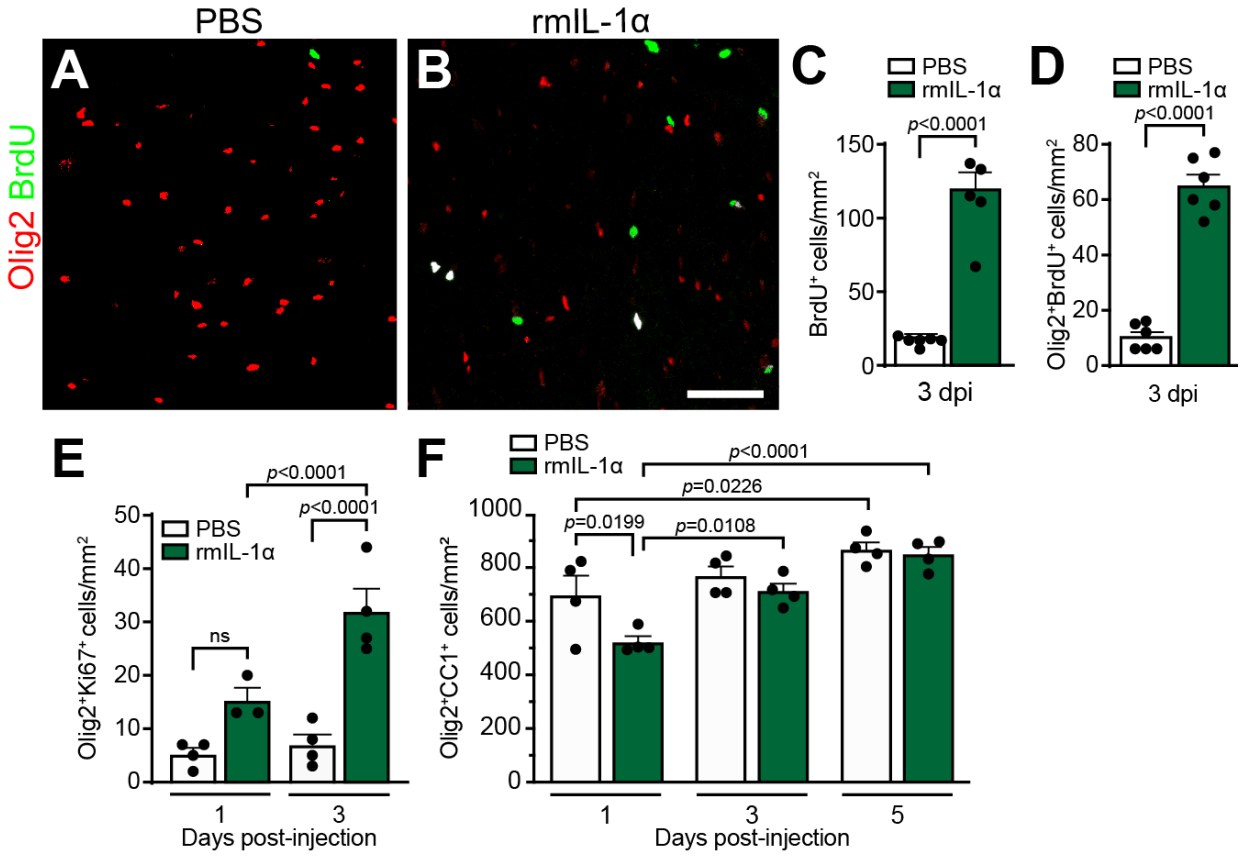

Figure 4.4. Proliferating Olig2+ cells rapidly restore the number of mature oligodendrocytes in mice injected centrally with IL-1α.

(**A-B**) Representative confocal images showing Olig2 (red) and BrdU (a marker of cell proliferation, green) immunostainings in the spinal cord white matter of C57BL/6 mice injected with either PBS (**A**) or recombinant mouse (rm) IL-1α (**B**) at 3 days post-injection. (**C-D**) Quantification of the total number of $BrdU^+$ cells (**C**) and $Olig2^+$ $BrdU^+$ double-positive cells (**D**) in the spinal cord white matter at 3 days post-injection of PBS or rmIL-1α intra-cisterna magna (i.c.m.) (n=5 mice/group). (**E**) Quantification of the total number of $Olig2^+Ki67^+$ double-positive cells in the spinal cord white matter of C57BL/6 mice at 1 and 3 days post-i.c.m. injection of either PBS or rmIL-1α (n=5 mice/group/time). (**F**) Quantification of the total number of $Olig2^+$ $CC1^+$ mature oligodendrocytes in the spinal cord white matter at 1, 3 and 5 days post-i.c.m. treatment (n=5 mice/group). Data are expressed

as mean ± SEM. Statistical significance was determined by a two-way ANOVA followed by a Bonferroni post-hoc test. Scale bars: (**A-B**, in **B**) 50 µm.

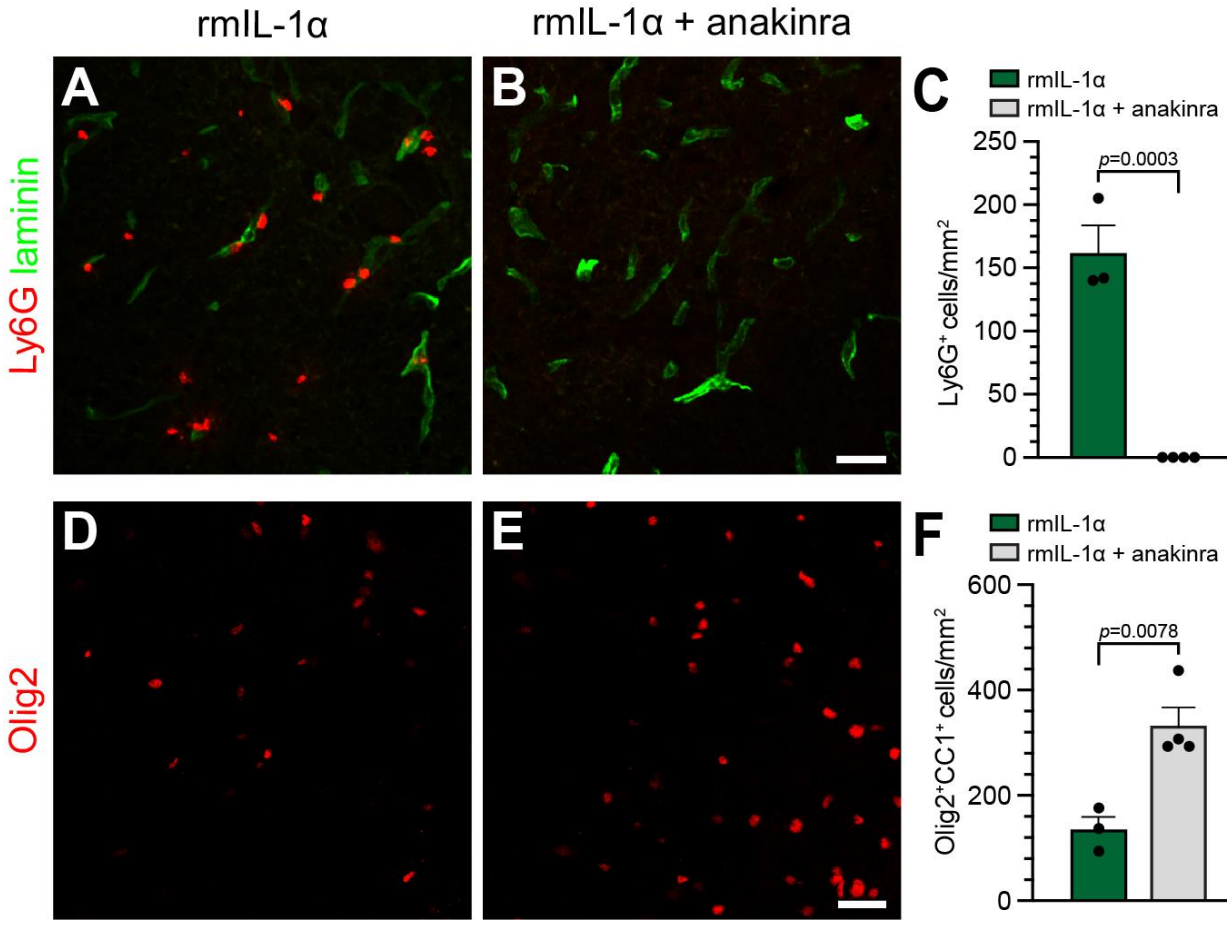

Figure 4.5. Delivery of the IL-1 receptor antagonist anakinra in the cerebrospinal fluid blocks the effects of IL-1α on neutrophil infiltration and oligodendrocyte loss.

(**A-B**) Representative confocal images showing the presence (or absence) of $Ly6G^+$ neutrophils (red cells) in the spinal cord of C57BL/6 mice injected intra-cisterna magna (i.c.m.) with either recombinant mouse (rm) IL-1α alone (**A**) or rmIL-1α + anakinra (**B**), a recombinant human IL-1R antagonist. All mice were killed at 24 hours post-injection. An anti-pan-laminin antibody was used to stain blood vessel basement membranes (green staining). (**C**) Quantification of the total number of $Ly6G^+$ neutrophils that infiltrated the spinal cord of mice (n=3-4 mice/group). (**D-E**) Representative confocal images showing immunostaining for the Olig2 transcription factor, a marker of cells of the oligodendrocyte lineage, in the spinal cord of C57BL/6 mice injected with either rmIL-1α (**D**) or rmIL-1α + anakinra (**E**). All mice were killed at 24 hours post-injection (n = 3-4 mice/group). (**F**) Quantification of the total number of $Olig2^+$ $CC1^+$ mature oligodendrocytes in the spinal cord

white matter at 24 hours post-i.c.m. treatment (n = 3-4 mice/group). Data are expressed as mean ± SEM. Statistical significance was determined by a two-way ANOVA followed by a Bonferroni post-hoc test. Scale bars: (**A**-**B**, in **B**) 25 µm, (**D**-**E**, in **E**) 25 µm.

.

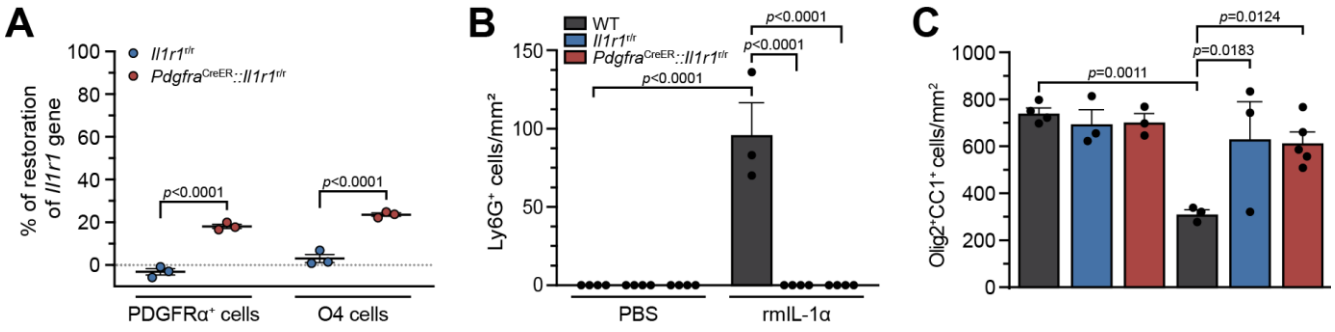

Figure 4.6. Restoration of the Il1r1 gene in oligodendrocyte lineage cells does not allow for IL-1α-mediated neuroinflammation and oligodendrocyte loss.

(**A**) Quantification of restoration of *Il1r1* gene expression in primary PDGFRα^{+} and O4^{+} oligodendrocyte lineage cells isolated by immunopanning from the uninjured spinal cord of adult *Il1r1*$^{r/r}$ mice, which express an IL-1R1-knockout phenotype, and *Pdgfra*^{CreER}::*Il1r1*$^{r/r}$ mice at 50 days post-tamoxifen treatment. (**B**) Quantification of the number of Ly6G^{+} neutrophils that infiltrated the spinal cord of WT, *Il1r1*$^{r/r}$ and *Pdgfra*^{CreER}::*Il1r1*$^{r/r}$ mice at 24 hours post-injection of either PBS or rmIL-1α (n=3-5 mice/group). (**C**) Quantification of the total number of Olig2^{+} CC1^{+} mature oligodendrocytes in the spinal cord white matter of WT, *Il1r1*$^{r/r}$ and *Pdgfra*^{CreER}::*Il1r1*$^{r/r}$ mice at 24 hours post-injection of either PBS or rmIL-1α (n=3-5 mice/group). Data are expressed as mean ± SEM. Statistical significance was determined by a two-way ANOVA followed by a Bonferroni post-hoc test.

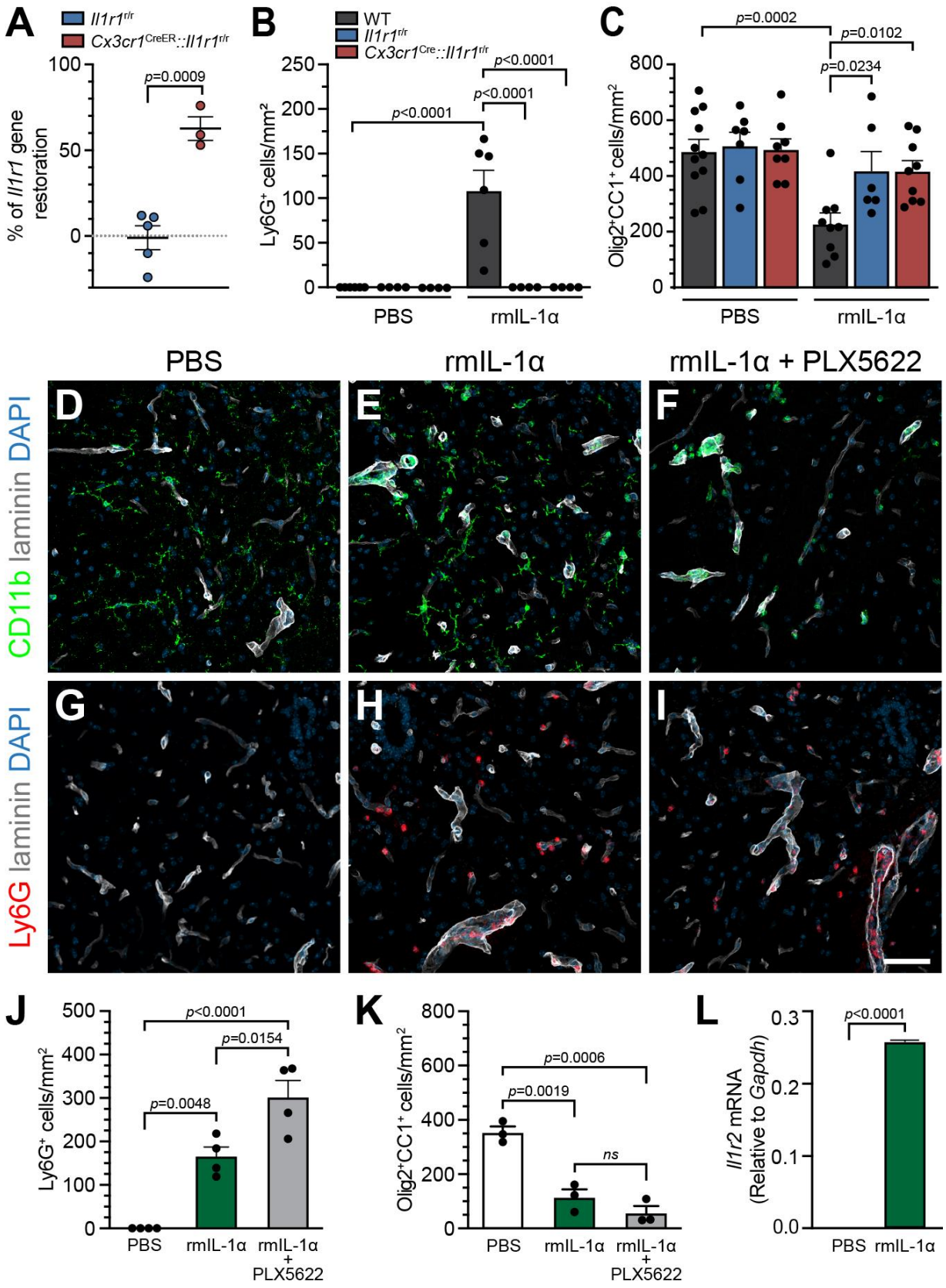
A
Il1r1r/r
Cx3cr1CreER::Il1r1r/r
% of Il1r1 gene restoration
p=0.0009
B
WT
Il1r1r/r
Cx3cr1Cre::Il1r1r/r
Ly6G+ cells/mm2
p<0.0001
p<0.0001
p<0.0001
PBS
rmIL-1α
C
Olig2+CC1+ cells/mm2
p=0.0002
p=0.0102
p=0.0234
PBS
rmIL-1α
PBS
rmIL-1α
rmIL-1α + PLX5622
CD11b laminin DAPI
Ly6G laminin DAPI
D
E
F
G
H
I
J
Ly6G+ cells/mm2
p<0.0001
p=0.0154
p=0.0048
PBS
rmIL-1α
rmIL-1α + PLX5622
K
Olig2+CC1+ cells/mm2
p=0.0006
p=0.0019
ns
PBS
rmIL-1α
rmIL-1α + PLX5622
L
Il1r2 mRNA (Relative to Gapdh)
p<0.0001
PBS
rmIL-1α

Figure 4.7. Microglia alleviate IL-1α-mediated neuroinflammation and oligodendrocyte loss independently of their expression of IL-1R1.

(**A**) Quantification of restoration of *Il1r1* gene expression in primary microglia isolated from the uninjured spinal cord of adult *Il1r1*$^{r/r}$ mice, which express an IL-1R1-knockout phenotype (set to 0%), and *Cx3cr1*^{CreER}::*Il1r1*$^{r/r}$ mice at 30 days post-tamoxifen treatment. (**B**) Quantification of the number of Ly6G^{+} neutrophils that infiltrated the spinal cord of WT, *Il1r1*$^{r/r}$ and *Cx3cr1*^{CreER}::*Il1r1*$^{r/r}$ mice at 24 hours post-injection of either PBS or rmIL-1α (n=6-11 mice/group). (**C**) Quantification of the total number of Olig2^{+} CC1^{+} mature oligodendrocytes (OLs) in the spinal cord white matter of WT, *Il1r1*$^{r/r}$ and *Cx3cr1*^{CreER}::*Il1r1*$^{r/r}$ mice at 24 hours post-injection of either PBS or rmIL-1α (n=6-11 mice/group). (**D-I**) Representative confocal images showing the presence of CD11b^{+} cells (green cells in **D-F**; CD11b stains microglia, macrophages and neutrophils) and Ly6G^{+} neutrophils (red cells in **G-I**) in the spinal cord of C57BL/6 mice injected with either PBS (**D**, **G**), rmIL-1α (**E**, **H**) or rmIL-1α + PLX5622 (a CSF1R inhibitor from Plexxikon; **F**, **I**) at 24 hours post-injection. (**J**) Quantification of the total number of Ly6G^{+} neutrophils that infiltrated the spinal cord of C57BL/6 mice at 24 hours post-injection of either PBS or rmIL-1α (n=3-4 mice/group). (**K**) Quantification of the total number of Olig2^{+} CC1^{+} mature OLs in the spinal cord white matter of C57BL/6 mice at 24 hours post-injection of either PBS or rmIL-1α (n=3-4 mice/group). For all experiments involving PLX5622 (**F-M**), mice were fed the PLX5622 diet for 3 weeks before the experimentation to deplete all microglia. (**L**) Relative expression of *Il1r2* gene, as determined by quantitative real-time PCR. *Gapdh* expression levels were used to normalize data. Data are expressed as mean ± SEM. Statistical significance was determined by a two-way ANOVA followed by a Bonferroni post-hoc test. Scale bars: (**D-I**, in **I**) 50 µm.

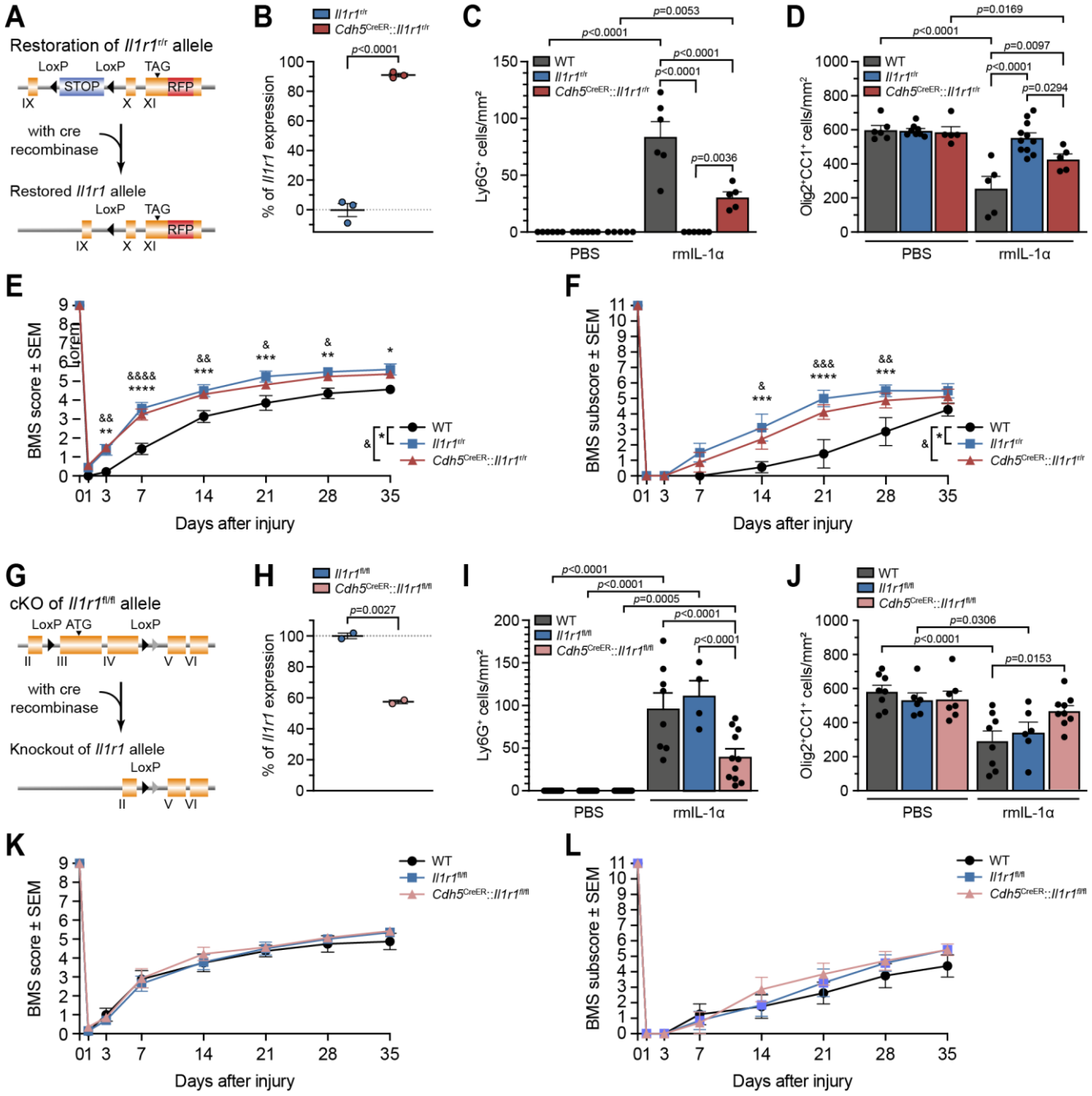
A
Restoration of Il1r1r/r allele
LoxP
LoxP
TAG
STOP
RFP
IX
X
XI
with cre recombinase
Restored Il1r1 allele
B
Il1r1r/r
Cdh5CreER::Il1r1r/r
p<0.0001
% of Il1r1 expression
C
p=0.0053
p<0.0001
p<0.0001
p<0.0001
p=0.0036
WT
Il1r1r/r
Cdh5CreER::Il1r1r/r
Ly6G+ cells/mm2
PBS
rmIL-1α
D
p=0.0169
p<0.0001
p=0.0097
p<0.0001
p=0.0294
Olig2+CC1+ cells/mm2
E
BMS score ± SEM
Days after injury
F
BMS subscore ± SEM
Days after injury
G
cKO of Il1r1fl/fl allele
LoxP ATG
LoxP
II
III
IV
V
VI
with cre recombinase
Knockout of Il1r1 allele
H
Il1r1fl/fl
Cdh5CreER::Il1r1fl/fl
p=0.0027
% of Il1r1 expression
I
p<0.0001
p<0.0001
p=0.0005
p<0.0001
p<0.0001
J
p=0.0306
p<0.0001
p=0.0153
K
L

Figure 4.8. IL-1α-induced neuroinflammation and oligodendrocyte loss is partly mediated by endothelial IL-1R1.

(**A**) Schematic diagram showing the genetic design of the *Cdh5*^{CreER}::*Il1r1*$^{r/r}$ mouse line. (**B**) Quantification of restoration of *Il1r1* gene expression in primary endothelial cells isolated from the brain of naïve adult *Il1r1*$^{r/r}$ mice, which express an IL-1R1-knockout phenotype (set to 0%), and *Cdh5*^{CreER}::*Il1r1*$^{r/r}$ mice at 30 days post-tamoxifen treatment. (**C**) Quantification of the total number of Ly6G^{+} neutrophils that infiltrated the spinal cord of WT, *Il1r1*$^{r/r}$ and *Cdh5*^{CreER}::*Il1r1*$^{r/r}$ mice at 24 hours post-injection of either PBS or recombinant mouse (rm) IL-1α intra-cisterna magna (n=5-11 mice/group). (**D**) Quantification of the total number of Olig2^{+} CC1^{+} mature OLs in the spinal cord white matter of WT, *Il1r1*$^{r/r}$ and *Cdh5*^{CreER}::*Il1r1*$^{r/r}$ mice at 24 hours post-injection of either PBS or rmIL-1α (n=5-11 mice/group). **(E-F)** Locomotor function was assessed using the BMS score (**E**) and BMS subscore (**F**) over a 35-day period after SCI in C57BL/6, *Il1r1*$^{r/r}$ and *Cdh5*^{CreER}::*Il1r1*$^{r/r}$ mice (n=8 mice per group). (**G**) Schematic diagram showing the genetic design of the *Cdh5*^{CreER}::*Il1r1*$^{fl/fl}$ mouse line. (**H**) Quantification of *Il1r1* gene expression in primary endothelial cells isolated from the spinal cord of *Il1r1*$^{fl/fl}$ mice, which normally express the *Il1r1* gene (set to 100%), and *Cdh5*^{CreER}::*Il1r1*$^{fl/fl}$ mice at 30 days post-tamoxifen treatment. (**I**) Quantification of the total number of Ly6G^{+} neutrophils that infiltrated the spinal cord of WT, *Il1r1*$^{fl/fl}$, and *Cdh5*^{CreER}::*Il1r1*$^{fl/fl}$ mice at 24 hours post-injection of either PBS or rmIL-1α (n=6-9 mice/group). (**J**) Quantification of the total number of Olig2^{+} CC1^{+} mature OLs in the spinal cord white matter of WT, *Il1r1*$^{fl/fl}$, and *Cdh5*^{CreER}::*Il1r1*$^{fl/fl}$ mice at 24 hours post-injection of either PBS or rmIL-1α (n=6-9 mice/group). **(K-L)** Locomotor function was assessed using the BMS score (**K**) and BMS subscore (**L**) over a 35-day period after SCI in WT, *Il1r1*$^{fl/fl}$, and *Cdh5*^{CreER}::*Il1r1*$^{fl/fl}$ mice (n=7-8 mice per group). Data are expressed as mean ± SEM. Statistical significance was determined by a two-way ANOVA followed by a Bonferroni post-hoc test.

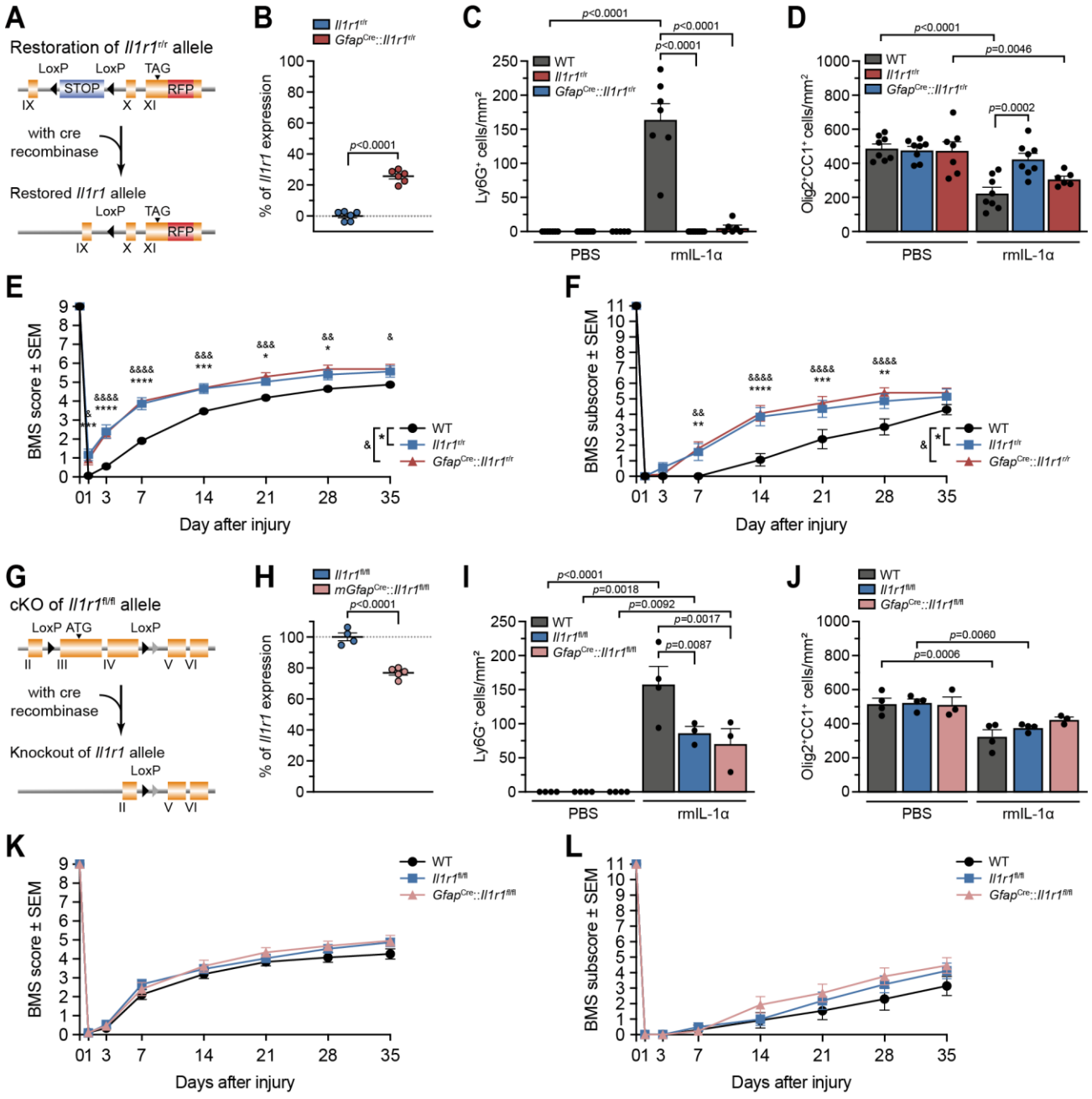
A
Restoration of Il1r1r/r allele
LoxP
LoxP
TAG
STOP
RFP
IX
X
XI
with cre recombinase
Restored Il1r1 allele
B
Il1r1r/r
Gfap Cre::Il1r1r/r
% of Il1r1 expression
p<0.0001
C
p<0.0001
p<0.0001
p<0.0001
WT
Il1r1r/r
Gfap Cre::Il1r1r/r
Ly6G+ cells/mm2
PBS
rmIL-1α
D
p<0.0001
p=0.0046
p=0.0002
WT
Il1r1r/r
Gfap Cre::Il1r1r/r
Olig2+CC1+ cells/mm2
PBS
rmIL-1α
E
BMS score ± SEM
Day after injury
WT
Il1r1r/r
Gfap Cre::Il1r1r/r
F
BMS subscore ± SEM
Day after injury
WT
Il1r1r/r
Gfap Cre::Il1r1r/r
G
cKO of Il1r1fl/fl allele
LoxP ATG
LoxP
II
III
IV
V
VI
with cre recombinase
Knockout of Il1r1 allele
H
Il1r1fl/fl
mGfap Cre::Il1r1fl/fl
% of Il1r1 expression
p<0.0001
I
p<0.0001
p=0.0018
p=0.0092
p=0.0017
p=0.0087
WT
Il1r1fl/fl
Gfap Cre::Il1r1fl/fl
Ly6G+ cells/mm2
PBS
rmIL-1α
J
p=0.0060
p=0.0006
WT
Il1r1fl/fl
Gfap Cre::Il1r1fl/fl
Olig2+CC1+ cells/mm2
PBS
rmIL-1α
K
BMS score ± SEM
Days after injury
WT
Il1r1fl/fl
Gfap Cre::Il1r1fl/fl
L
BMS subscore ± SEM
Days after injury
WT
Il1r1fl/fl
Gfap Cre::Il1r1fl/fl

Figure 4.9. IL-1α-induced neuroinflammation and oligodendrocyte loss is partly mediated by astrocytic IL-1R1.

(**A**) Schematic diagram showing the genetic design of the *Gfap*^{Cre}::*Il1r1*$^{r/r}$ mouse line. (**B**) Quantification of restoration of *Il1r1* gene expression in primary astrocytes isolated from the brain of neonate *Il1r1*$^{r/r}$ mice, which express an IL-1R1-knockout phenotype (set to 0%), and *Gfap*^{Cre}::*Il1r1*$^{r/r}$ mice. (**C**) Quantification of the total number of Ly6G^{+} neutrophils that infiltrated the spinal cord of WT, *Il1r1*$^{r/r}$ and *Gfap*^{Cre}::*Il1r1*$^{r/r}$ mice at 24 hours post-injection of either PBS or recombinant mouse (rm) IL-1α intra-cisterna magna (n=7-9 mice/group). (**D**) Quantification of the total number of Olig2^{+} CC1^{+} mature OLs in the spinal cord white matter of WT, *Il1r1*$^{r/r}$ and *Gfap*^{Cre}::*Il1r1*$^{r/r}$ mice at 24 hours post-injection of either PBS or rmIL-1α (n=7-9 mice/group). **(E-F)** Locomotor function was assessed using the BMS score (**E**) and BMS subscore (**F**) over a 35-day period after SCI in WT, *Il1r1*$^{r/r}$ and *Gfap*^{Cre}::*Il1r1*$^{r/r}$ mice (n=15-16 mice per group). (**G**) Schematic diagram showing the genetic design of the *Gfap*^{Cre}::*Il1r1*$^{fl/fl}$ mouse line. (**H**) Quantification of *Il1r1* gene expression in primary astrocytes isolated from the brain of neonate *Il1r1*$^{fl/fl}$ mice, which normally express the *Il1r1* gene (set to 100%), and *Gfap*^{Cre}::*Il1r1*$^{fl/fl}$ mice. (**I**) Quantification of the total number of Ly6G^{+} neutrophils that infiltrated the spinal cord of WT, *Il1r1*$^{fl/fl}$ and *Gfap*^{Cre}::*Il1r1*$^{fl/fl}$ mice at 24 hours post-injection of either PBS or rmIL-1α (n=3-4 mice/group). (**J**) Quantification of the total number of Olig2^{+} CC1^{+} mature OLs in the spinal cord white matter of WT, *Il1r1*$^{fl/fl}$ and *Gfap*^{Cre}::*Il1r1*$^{fl/fl}$ mice at 24 hours post-injection (n=3-4 mice/group). **(K-L)** Locomotor function was assessed using the BMS score (**K**) and BMS subscore (**L**) over a 35-day period after SCI in WT, *Il1r1*$^{fl/fl}$ and *Gfap*^{Cre}::*Il1r1*$^{fl/fl}$ mice (n=13-16 mice per group). Data are expressed as mean ± SEM. Statistical significance was determined by a two-way ANOVA followed by a Bonferroni post-hoc test.

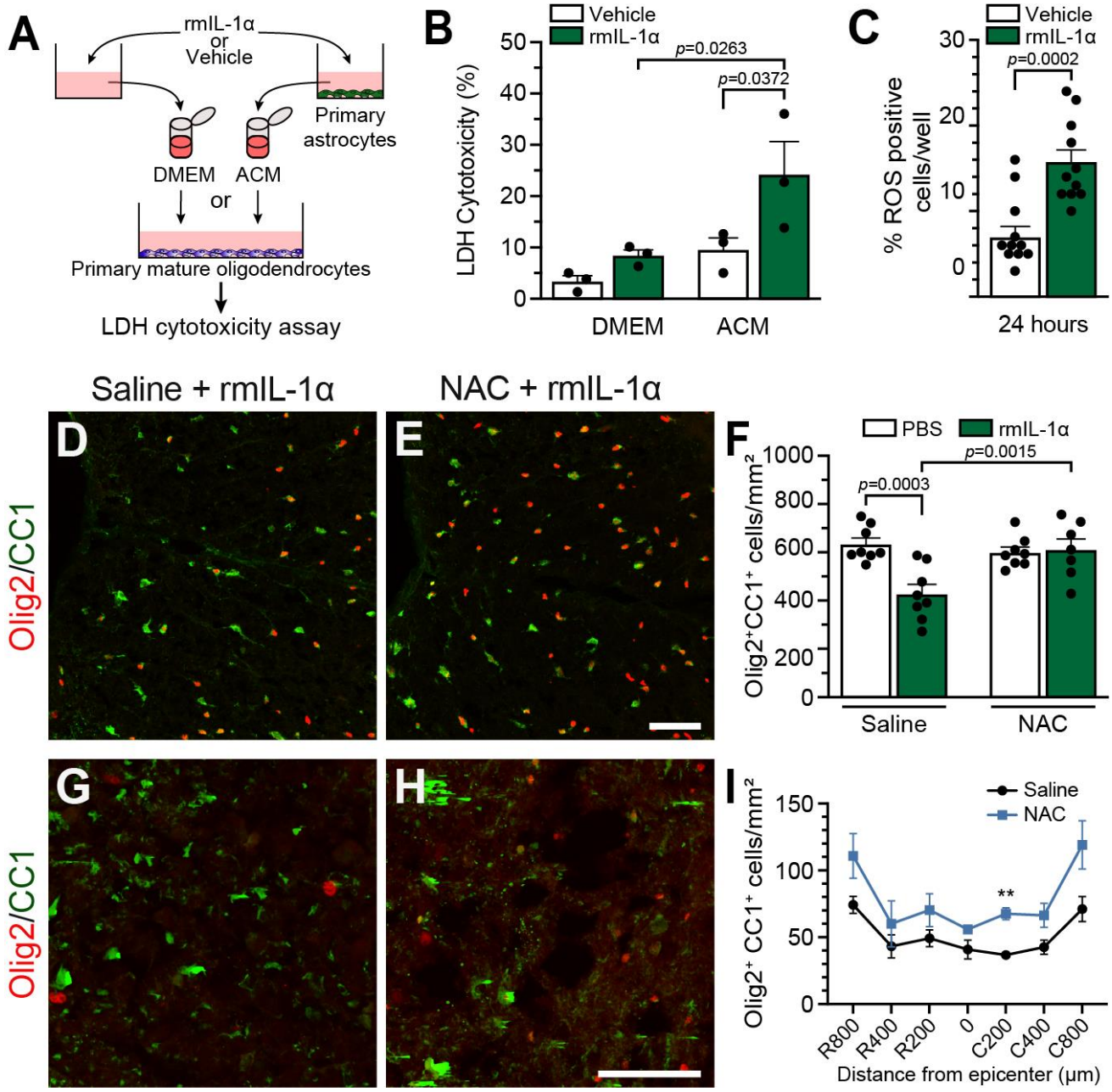
A
rmIL-1α
or
Vehicle
Primary
astrocytes
DMEM
ACM
or
Primary mature oligodendrocytes
LDH cytotoxicity assay
B
Vehicle
rmIL-1α
p=0.0263
p=0.0372
LDH Cytotoxicity (%)
DMEM
ACM
C
Vehicle
rmIL-1α
p=0.0002
% ROS positive cells/well
24 hours
Saline + rmIL-1α
NAC + rmIL-1α
D
E
Olig2/CC1
F
PBS
rmIL-1α
p=0.0015
p=0.0003
Olig2⁺CC1⁺ cells/mm²
Saline
NAC
G
H
Olig2/CC1
I
Saline
NAC
**
Olig2⁺ CC1⁺ cells/mm²
R800
R400
R200
0
C200
C400
C800
Distance from epicenter (μm)

Figure 4.10. Reactive oxygen species released by astrocytes in response to IL-1α induce oligodendrocyte death. (**A**) Schematic diagram showing the experimental design for the lactate dehydrogenase (LDH) assay used to determine the cytotoxicity of primary oligodendrocytes (OLs) *in vitro*. Primary astrocytes were cultured in the presence of either PBS (vehicle) or rmIL-1α. Primary mature OLs were then incubated in control DMEM medium containing (or not) rmIL-1α, or in conditioned medium derived from astrocytes (ACM) stimulated with either PBS (vehicle) or IL-1α. (**B**) Quantification of OL loss using the LDH cytotoxicity assay. (**C**) Quantification of reactive oxygen species (ROS) production in primary astrocytes stimulated with either PBS (vehicle) or rmIL-1α (10 ng/mL). The detection of ROS was performed using the CellROX Green Reagent (green). (**D-E**) Representative confocal images showing immunostaining for the Olig2 transcription factor, a marker of cells of the OL lineage, in the spinal cord of C57BL/6 mice injected intra-cisterna magna (i.c.m.) with rmIL-1α and treated i.p. with either N-acetyl-L-cysteine (NAC, an antagonist of ROS activity) or saline. Mice were killed at 24 hours post-i.c.m. injection. (**F**) Quantification of the total number of $Olig2^+$ $CC1^+$ mature OLs in the spinal cord white matter of PBS- and IL-1α-injected mice following treatment with either NAC or saline (n=5 mice/group). (**G-H**) Representative confocal images taken at the lesion epicenter showing immunostaining for Olig2 (green) and CC1 (red) at day 1 post-SCI in C57BL/6 mice treated with either NAC or saline. (**I**) Quantification of the number of $Olig2^+$ $CC1^+$ oligodendrocytes in the injured spinal cord of mice treated with NAC or saline and killed at day 1 post-SCI (n=3-5/group). Data are expressed as mean ± SEM. Statistical significance was determined by a two-way ANOVA followed by a Bonferroni post-hoc test. Scale bars: (**D-E**, in **E**) 50 µm, (**G-H**, in **H**) 50 µm.

SUPPLEMENTARY FIGURE LEGENDS

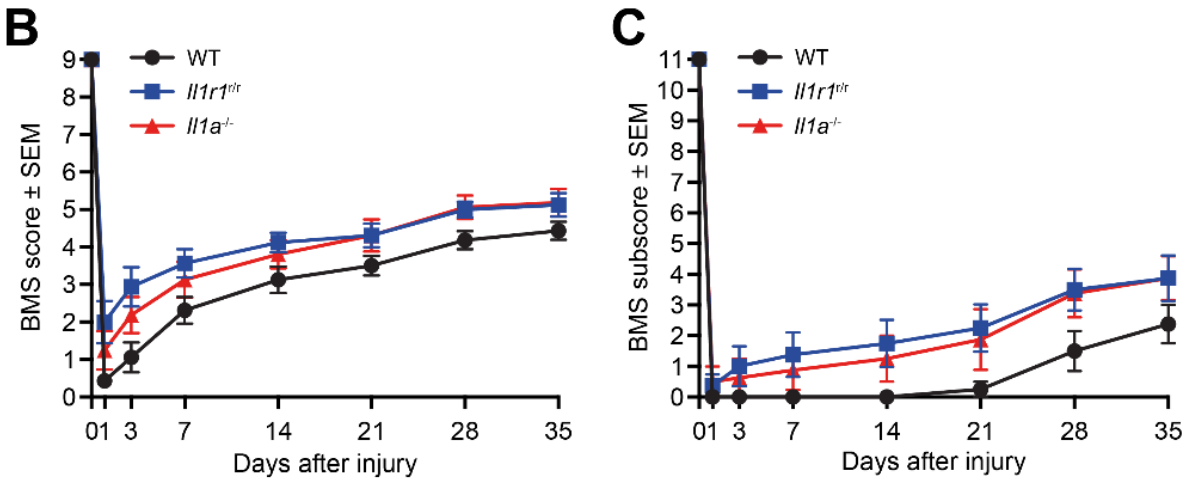

Supplementary Figure 1. Early signs of secondary degeneration and recovery of locomotor function are improved in mice lacking IL-1R1 after SCI. (A) Quantification of the number of $Olig2^{+}CC1^{+}$ oligodendrocytes in the injured spinal cord of C57BL/6 and IL-1R1-deficient (*Il1r1*$^{r/r}$) mice at day 1 post-SCI (n=4-5/group). **(B-C)** Locomotor function was assessed using the BMS score (**B**) and BMS subscore (**C**) over a 35-day period after SCI in C57BL/6, *Il1r1*$^{r/r}$ or *Il1a*$^{-/-}$ mice (n=8 mice per group). Statistical significance was determined by either a two-way ANOVA (**A**) or two-way repeated measures ANOVA (**B-C**) followed by a Bonferroni post-hoc test. *** $p < 0.001$, ** $p < 0.01$, * $p < 0.05$, compared to the WT group.

A

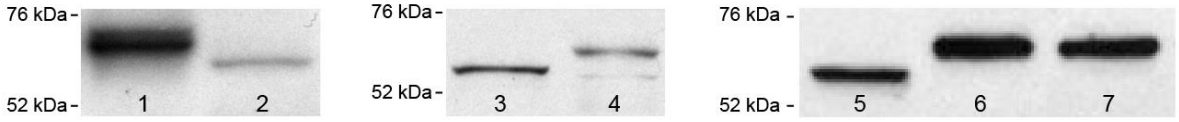

Supplementary Figure 2. The IL-1 receptor is expressed by various cell types in the mouse central nervous system. Detection by immunoblotting of IL-1R1 in various murine primary and immortalized cells including: (1) primary brain microvascular endothelial cells (ECs), (2) primary oligodendrocyte progenitor cells, (3) primary astrocytes, (4) immortalized bEnd.3 ECs, (5) primary astrocytes, (6) primary brain microvascular ECs, and (7) primary microglia.

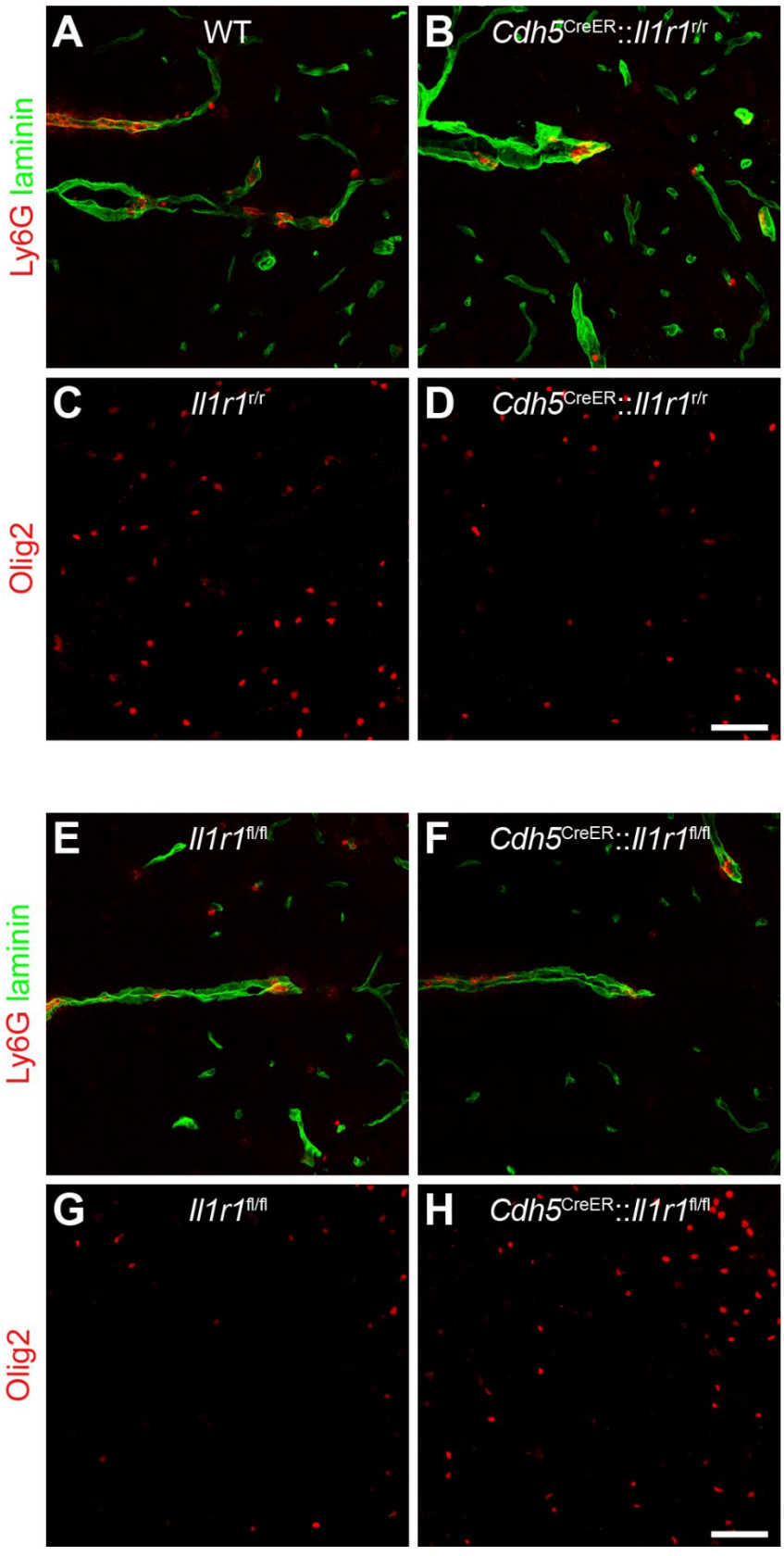
A
WT
B
Cdh5CreER::Il1r1r/r
Ly6G laminin
C
Il1r1r/r
D
Cdh5CreER::Il1r1r/r
Olig2
E
Il1r1fl/fl
F
Cdh5CreER::Il1r1fl/fl
Ly6G laminin
G
Il1r1fl/fl
H
Cdh5CreER::Il1r1fl/fl
Olig2

Supplementary Figure 3. Endothelial IL-1R1 partly mediates neutrophil infiltration and oligodendrocyte cell loss after intra-cerebrospinal administration of IL-1α. (**A-B**) Representative confocal images showing the infiltration of $Ly6G^+$ neutrophils (red cells) in the spinal cord of wild-type (WT) mice (**A**) and *Cdh5*^{CreER}::*Il1r1*$^{r/r}$ mice (**B**) 24 hours following intra-cisterna magna (i.c.m.) injection with recombinant mouse (rm) IL-1α. An anti-pan-laminin antibody was used to stain blood vessel basement membranes (green staining). (**C-D**) Representative images showing immunostaining for the Olig2 transcription factor, a marker of cells of the oligodendrocyte lineage, in the spinal cord of *Il1r1*$^{r/r}$ mice (**C**), which express an IL-1R1-knockout phenotype, and *Cdh5*^{CreER}::*Il1r1*$^{r/r}$ (**D**) mice at 24 hours post-injection of rmIL-1α. (**E-F**) Representative images showing $Ly6G^+$ neutrophils (red cells) in the spinal cord of *Il1r1*$^{fl/fl}$ mice (**E**), which normally express the *Il1r1* gene, and *Cdh5*^{CreER}::*Il1r1*$^{fl/fl}$ mice (**F**) injected i.c.m. with rmIL-1α and killed at 24 hours post-injection. Laminin immunostaining is shown in green. (**G-H**) Representative confocal images showing immunostaining for Olig2 (red cells) in the spinal cord of *Il1r1*$^{fl/fl}$ (**G**) and *Cdh5*^{CreER}::*Il1r1*$^{fl/fl}$ (**H**) mice at 24 hours post-injection of rmIL-1α. Scale bars: (**A-D**, in **D**) 50 µm, (**E-H**, in **H**) 50 µm.

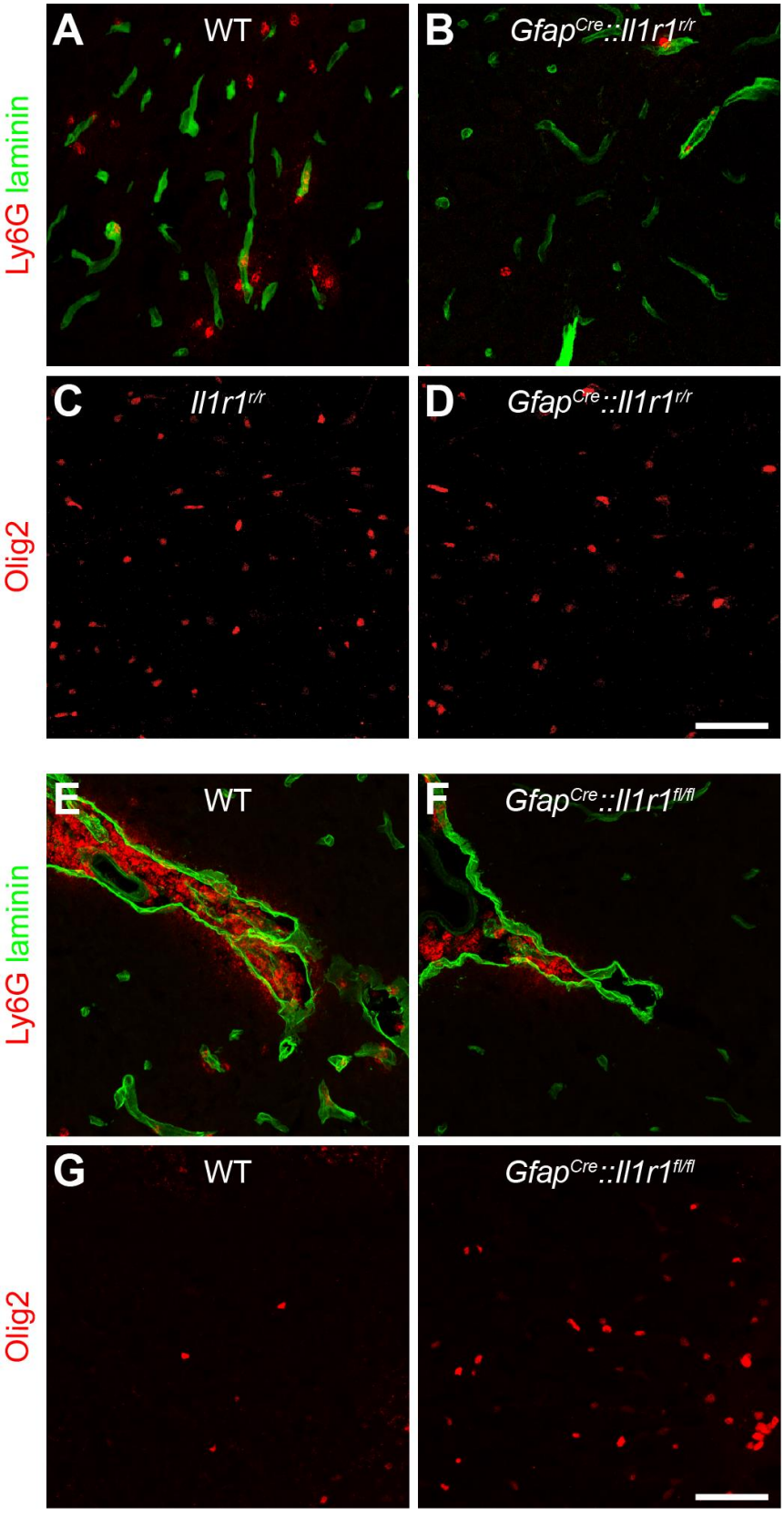
A
WT
B
Gfap^Cre::Il1r1^r/r
Ly6G laminin
C
Il1r1^r/r
D
Gfap^Cre::Il1r1^r/r
Olig2
E
WT
F
Gfap^Cre::Il1r1^fl/fl
Ly6G laminin
G
WT
Gfap^Cre::Il1r1^fl/fl
Olig2

Supplementary Figure 4. Astrocytic IL-1R1 partly mediates neutrophil infiltration and oligodendrocyte cell loss after intra-cerebrospinal administration of IL-1α. (**A-B**) Representative confocal images showing $Ly6G^+$ neutrophils (red cells) in the spinal cord of WT (**A**) and $Gfap^{Cre}$::$Il1r1^{r/r}$ (**B**) mice injected intra-cisterna magna (i.c.m.) with recombinant mouse (rm) IL-1α and killed at 24 hours post-injection. An anti-pan-laminin antibody was used to stain blood vessel basement membranes (green staining). (**C-D**) Representative images showing immunostaining for the Olig2 transcription factor, a marker of cells of the oligodendrocyte lineage, in the spinal cord of $Il1r1^{r/r}$ mice (**C**), which express an IL-1R1-knockout phenotype, and $Gfap^{Cre}$::$Il1r1^{r/r}$ mice (**D**) at 24 hours post-injection of rmIL-1α. (**E-F)** Representative images showing $Ly6G^+$ neutrophils (red cells) in the spinal cord of WT (**E**) and $Gfap^{Cre}$::$Il1r1^{fl/fl}$ (**F**) mice injected i.c.m. with rmIL-1α and killed at 24 hours post-injection. Laminin immunostaining is shown in green. (**G-H**) Representative images showing Olig2 immunostaining in the spinal cord of WT (**G**) and $Gfap^{Cre}$::$Il1r1^{fl/fl}$ (**H**) mice at 24 hours post-injection of either PBS or rmIL-1α. Scale bars: (**A-D**, in **D**) 50 μm, (**E-H**, in **H**) 50 μm.

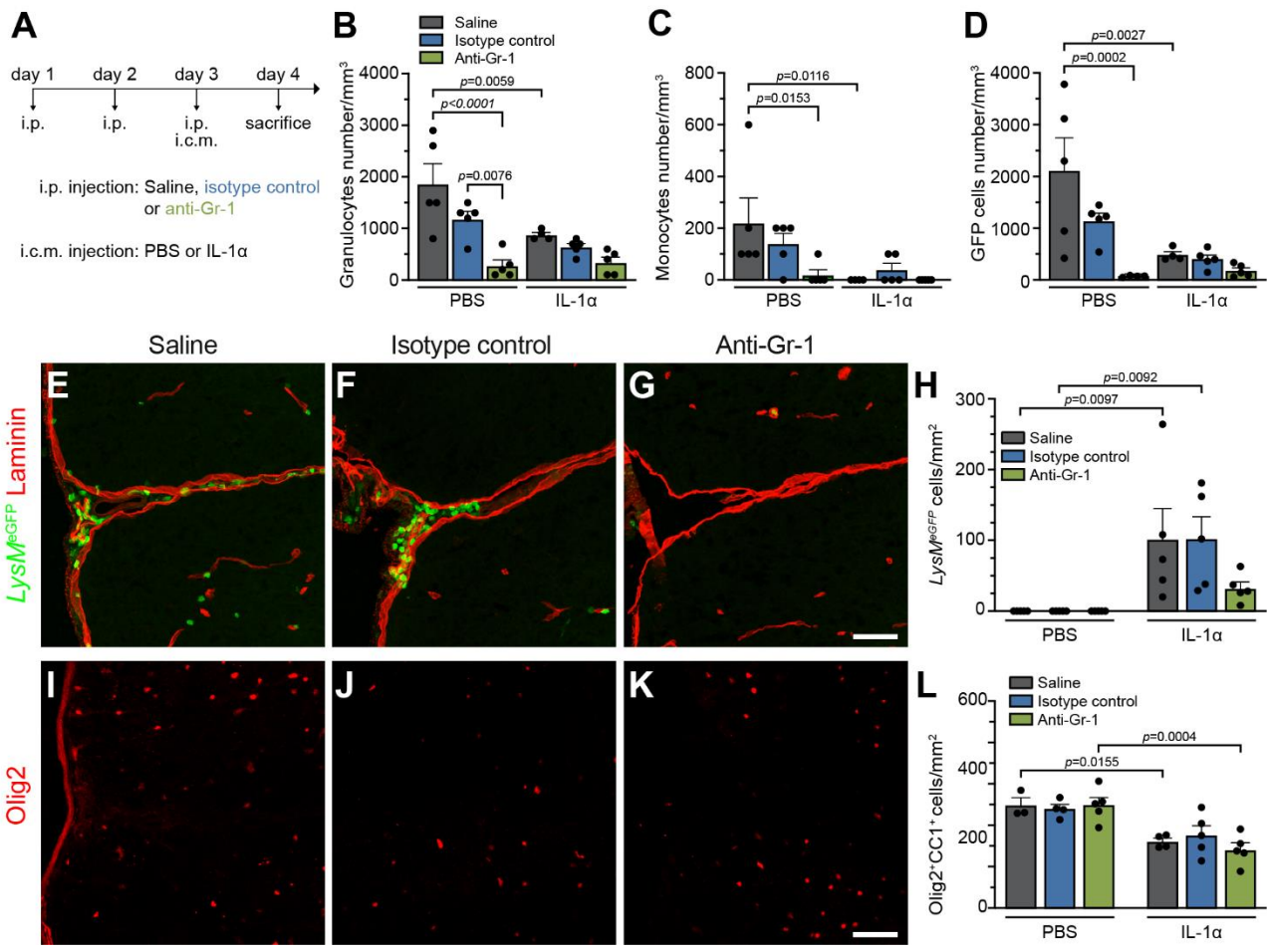
A
day 1
day 2
day 3
day 4
i.p.
i.p.
i.p.
i.c.m.
sacrifice
i.p. injection: Saline, isotype control or anti-Gr-1
i.c.m. injection: PBS or IL-1α
B
Saline
Isotype control
Anti-Gr-1
Granulocytes number/mm3
p=0.0059
p<0.0001
p=0.0076
PBS
IL-1α
C
Monocytes number/mm3
p=0.0116
p=0.0153
D
GFP cells number/mm3
p=0.0027
p=0.0002
Saline
Isotype control
Anti-Gr-1
LysMeGFP Laminin
Olig2
E
F
G
H
LysMeGFP cells/mm2
p=0.0092
p=0.0097
I
J
K
L
Olig2+CC1+ cells/mm2
p=0.0004
p=0.0155

Supplementary Figure 5. Depletion of Ly6C/G$^+$ (Gr-1) neutrophils and monocytes does not alter IL-1α-mediated oligodendrocyte loss. (**A**) Schematic diagram showing the experimental design and timeline of the depletion study. Abbreviations: i.c.m., intra-cisterna magna; i.p., intraperitoneal. (**B-C**) Quantification of the number of granulocytes (**B**) and monocytes (**C**) in the blood of PBS- and IL-1α-injected C57BL/6 mice pretreated with either anti-Gr-1 (Ly6C/G) antibodies, isotype control antibodies or PBS, as determined by automated complete blood cell count using the Scil Vet ABC PlusTM analyzer. (**D**) Quantification by flow cytometry of the number of granulo-myelomonocytic cells in the blood of *LysM*^{GFP} transgenic mice at the day of sacrifice. (**E-G**) Representative confocal images showing Ly6G (a marker of neutrophils, red cells) and laminin (a marker of blood vessel basement membranes, green) immunostainings in the spinal cord of C57BL/6 mice injected i.c.m. with recombinant mouse IL-1α and pretreated i.p with either PBS (**E**), isotype control antibodies (**F**) or anti-Gr-1 depleting antibodies (**G**). Mice were killed at 24 hours post-i.c.m. injection (n=5 mice/group). (**H**) Quantification of the total number of Ly6G$^+$ neutrophils that infiltrated the spinal cord at 24 hours post-i.c.m. injection of IL-1α or PBS and treatment with either PBS, isotype control antibodies or anti-Gr-1 depleting antibodies (n=5 mice/group). (**I-K**) Representative confocal images showing Olig2 immunostaining in the spinal cord white matter of C57BL/6 mice injected i.c.m. with either IL-1α or PBS, combined with treatment with either Gr-1-depleting antibodies, control antibodies or vehicle (PBS). (**L**) Quantification of the total number of Olig2$^+$ CC1$^+$ mature OLs in the spinal cord white matter of these mice. Data are expressed as mean ± SEM. Statistical significance was determined by a two-way ANOVA followed by a Bonferroni post-hoc test. Scale bar: (**E-G**, in **G**) 50 µm, (**I-K**, in **K**) 50 µm.

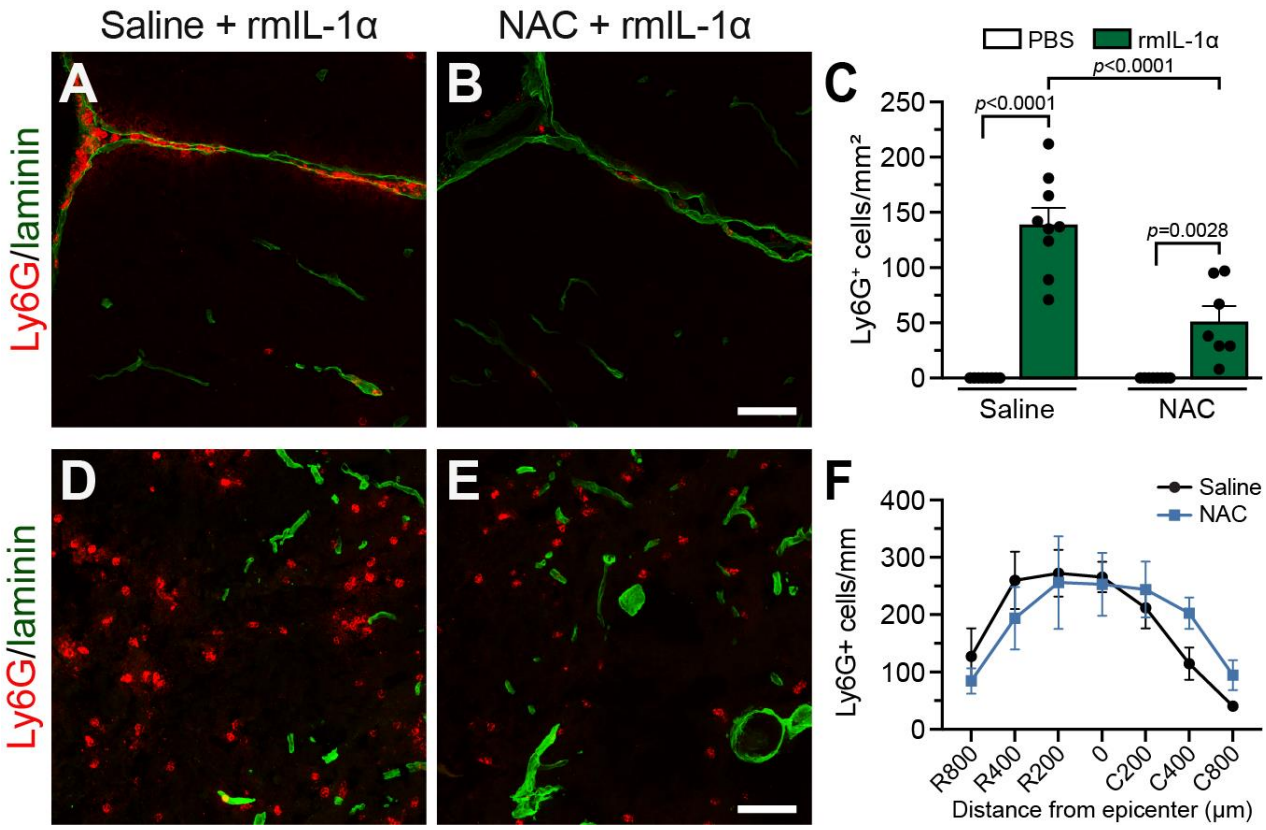

Supplementary Figure 6. *In vivo* neutralization of reactive oxygen species with the antioxidant N-acetyl-L-cysteine partially reverses neutrophil infiltration after central IL-1α delivery, but not SCI, in mice. (**A-B**) Representative confocal images showing Ly6G$^+$ neutrophils (red cells) in the spinal cord of C57BL/6 mice injected intra-cisterna magna (i.c.m.) with rmIL-1α and treated intraperitoneally (i.p.) with either N-acetyl-L-cysteine (NAC, an antagonist of ROS activity) or saline. All mice were killed at 24 hours post-i.c.m. injection. (**C**) Quantification of the total number of Ly6G$^+$ neutrophils that infiltrated the spinal cord of PBS- and IL-1α-injected mice following treatment with either NAC or saline (n=5 mice/group). (**D-E**) Representative confocal images taken at the lesion epicenter showing immunostaining Ly6G$^+$ neutrophils (red cells) at day 1 post-SCI in C57BL/6 mice treated with either NAC or saline. (**F**) Quantification of the number of Ly6G$^+$ neutrophils that infiltrate the injured spinal cord of mice treated with NAC or saline and killed at day 1 post-SCI (n=3-5/group). Data are expressed as mean ± SEM. Statistical significance

was determined by a two-way ANOVA followed by a Bonferroni post-hoc test. Scale bars: (**A**-**B**, in **B**) 50 µm, (**D**-**E**, in **E**) 50 µm.

5. DISCUSSION

Les LME peuvent engendrer des conséquences dramatiques sur la vie des personnes qui les subissent puisque celles-ci peuvent finir paralysées, en partie ou voire même totalement. À l'heure actuelle, il n'existe pas de traitement pour « soigner » ces lésions et réparer les dommages qui ont été fait à la moelle épinière. Ainsi, différentes études sont menées à l'international afin d'améliorer la locomotion des patients et tenter de diminuer les comorbidités associées aux LME, dont plus particulièrement la douleur. Parmi ces études, beaucoup d'entre elles s'intéressent aux thérapies cellulaires, dont le but est de remplacer les cellules qui ont péri par des cellules saines, entre autres des cellules souches. Toutefois, si l'on s'intéresse aux avancées les plus récentes et les plus prometteuses, il va sans dire que les travaux menés par le Dr. Grégoire Courtine à l'École Polytechnique Fédérale de Lausanne (EPFL) apparaissent en première ligne (Wagner et al., 2018). Son équipe est en effet l'une des premières à avoir permis à des patients paralysés de marcher de nouveau. Ces études, très axées sur la biophysique et l'informatique, ont permis de développer un implant reliant les deux parties de la moelle entre la zone lésée afin de rétablir artificiellement un contact. Aux vues des avancées très prometteuses, il reste toutefois essentiel de mieux comprendre la pathophysiologie des LME afin de permettre d'améliorer les traitements apportés aux patients. Il est d'ailleurs reconnu depuis longtemps que les DAMPs, de par leur rôle dans l'initiation de la neuroinflammation mais également dans le développement de dommages sur le long terme, ont une importance majeure dans la pathophysiologie des LME (Thundyil and Lim, 2015). Les travaux effectués au cours de cette thèse ont ainsi pour objectif de mieux comprendre les évènements se déroulant lors d'une LME. En particulier, une meilleure identification et compréhension des facteurs impliqués dans la dégénérescence secondaire pourrait permettre de développer différentes thérapies afin de réduire les dommages associés à cette phase. La revue de littérature présentée au chapitre 1 s'intéresse plus particulièrement aux nouvelles stratégies thérapeutiques visant ces DAMPs. Le reste de la thèse fait suite aux travaux antérieurs du laboratoire qui ont montré que parmi les DAMPs jouant un rôle critique au cours des LME, l'IL-1α constitue probablement le joueur le plus important (Bastien et al., 2015). En effet, cette étude a démontré que les souris n'exprimant pas l'IL-1α présentent des lésions moins sévères, accompagnées d'une meilleure récupération motrice et d'un volume lésionnel plus faible.

5.1 Effets de l'IL-1α au niveau de la moelle épinière

L'objectif général de cette thèse était d'étudier le mécanisme d'action de l'IL-1α au niveau de la moelle épinière et plus précisément de comprendre pourquoi l'absence de cette cytokine pro-inflammatoire confère une meilleure protection contre les LME. Nous avons tout d'abord développé une approche permettant d'étudier les effets de l'IL-1α *in vivo*. Pour ce faire, nous avons injecté ladite cytokine dans la *cisterna magna* puis évalué ses effets à différents niveaux spinaux et temps post-injection.

5.1.1 Effets sur l'inflammation

l'IL-1α étant une cytokine pro-inflammatoire, notre attention s'est donc tournée de prime abord vers l'inflammation. Tel qu'attendu, nous avons observé une très forte inflammation caractérisée par la présence de neutrophiles et monocytes à travers l'ensemble de la moelle épinière, un signe que l'effet n'est pas seulement localisé au site d'injection. Ces résultats concordent avec ce qui se déroule lors d'une LME. En effet, dans un modèle murin de LME, une augmentation des neutrophiles circulants est observée dès 12 heures post-lésion, alors que la densité sanguine des monocytes est quant à elle augmentée 24 heures post-lésion (Stirling and Yong, 2008b). Le nombre de lymphocytes circulants est pour sa part fortement diminué à 24 heures post-lésion (Stirling and Yong, 2008b). Dans notre étude, l'analyse sanguine a également révélé une augmentation des neutrophiles et des monocytes circulants, accompagnée d'une légère diminution du nombre de lymphocytes 24 heures suivant l'injection d'IL-1α. Au niveau du tissu, quelques neutrophiles commencent à adhérer aux vaisseaux sanguins de la moelle épinière dès 3 heures post-LME et un très grand nombre de ces cellules sont détectées à 6 heures (Bartholdi and Schwab, 1997) (K. Kigerl et al., 2009). Le nombre de neutrophiles infiltrants continue à augmenter à 24 heures post-lésion (Bartholdi and Schwab, 1997; Tjoa et al., 2003), pour finalement atteindre un pic à 3 jours (K. Kigerl et al., 2009). Un second pic d'infiltration de neutrophiles fut observé à 14 jours post-LME dans différentes lignées murines (K. Kigerl et al., 2009). Leur présence reste encore détectable plusieurs semaines après la lésion. Les macrophages pro-inflammatoires commencent quant à eux à s'accumuler dans la moelle épinière lésée à 12 heures post-lésion pour atteindre un maximum aux temps 1 et 3 jours (Thawer et al., 2013). Les macrophages dits anti-inflammatoires sont quant à eux présents au niveau de la moelle épinière aux jours 7 et 14

post-LME (Stirling and Yong, 2008b; Thawer et al., 2013). Pour notre part, nous avons pu observer par imagerie 2-photons que les premières cellules immunitaires dérivées du sang commencent à s'accumuler dans les vaisseaux de la moelle entre 4 et 6 heures après l'injection d'IL-1α. L'infiltration des leucocytes dans le parenchyme de la moelle commence à 6 heures post-injection et un pic de recrutement de neutrophiles est observé au temps 24 heures. Ainsi, la dynamique de la réponse inflammatoire observée après l'injection d'IL-1α dans notre étude partage des similarités avec ce qui se passe *in vivo* dans le contexte d'une lésion, aussi bien au niveau sanguin qu'au niveau tissulaire avec l'infiltration de neutrophiles et de monocytes. En effet, nous savons que suite à une LME, l'IL-1α est relâchée très rapidement après la lésion (Bastien et al., 2015). Ce faisant, le délai d'infiltration des leucocytes dans le tissu, d'une durée approximative de 6 heures, est donc identique dans les deux cas. Toutefois, alors qu'un pic d'infiltration de neutrophiles est observé à 3 jours post-lésion, aucun leucocyte n'est détectable au temps 48 heures après l'injection de l'IL-1α. On peut soulever là une des limites du modèle d'injection, dont l'effet sur l'inflammation est beaucoup plus transitoire que ce qui se passe lors d'une LME. Dans le contexte d'une LME, la libération précoce d'IL-1α initie une succession d'évènements, dont les effets, additionnés aux dommages de la lésion en elle-même, font perdurer le processus inflammatoire, ce qui n'est pas observé dans le modèle d'injection. Une des conséquences de cette inflammation chronique spécifique aux LME est la production de grandes quantités de radicaux libres par les cellules myéloïdes infiltrantes (Colton and Gilbert, 1987; Lewén et al., 2000; Liu et al., 2000; Xiong et al., 2007). Cela promeut une oxydation irréversible du tissus et entraîne la mort de nombreuses cellules résidentes du SNC, telles que les oligodendrocytes (Lewén et al., 2000).

5.1.2 Effets sur les oligodendrocytes

Notre attention s'est ensuite portée aux réactions des cellules de la lignée des Ols en réponse à la présence d'IL-1α. En effet, cette population cellulaire est particulièrement affectée lors des LME, en particulier les Ols matures. Nos résultats ont montré que l'IL-1α n'affecte pas les progéniteurs d'oligodendrocytes (OPCs). Toutefois, nous avons observé un effet très important de l'IL-1α sur les Ols matures. En effet, suite à l'injection d'IL-1α, le nombre d'Ols matures a diminué de manière très significative, avec un nombre minimal atteint à 24 heures

post-injection. Fait intéressant, ce nombre est revenu à sa valeur initiale dès le temps 3 jours post-injection, une réponse que nous avons corrélée avec une prolifération importante des Ols dès le jour 2.

En mettant de l'avant le rôle de l'IL-1α dans le processus de perte des Ols matures, ces résultats apportent des éléments de réponse en faveur de notre hypothèse initiale. En effet, cette cytokine étant responsable de la mort des Ols, son absence permet de préserver ces cellules. Cela permet donc de justifier que l'absence d'IL-1α dans un contexte de LME a pour effet de prévenir la mort des Ols matures. Compte tenu des différentes études montrant les effets bénéfiques de la transplantation de précurseurs d'Ols dans un contexte de LME (Fu et al., 2018; Mhatre V. Ho and Kelsey C. Martin, 2012; Yang et al., 2018), permettant de remplacer les Ols perdus suite à la lésion, nous pourrions nous attendre à ce que prévenir la perte de ces cellules puisse également être bénéfique dans un contexte de LME. En permettant une meilleure compréhension du mécanisme par lequel l'IL-1α régule la mort des Ols, cette thèse permet d'envisager différentes stratégies thérapeutiques visant à limiter la perte de ces cellules dans divers contextes pathologiques où la démyélinisation est mise en cause. Ces différentes possibilités seront discutées à la section Directions futures, ci-dessous.

5.2 Mécanismes d'action de l'IL-1α

Afin d'identifier les mécanismes exacts qui sous-tendent les effets de l'IL-1α *in vivo*, nous avons opté pour l'utilisation de nouveaux modèles transgéniques murins qui nous ont permis d'identifier spécifiquement les cellules impliquées et les mécanismes moléculaires en cause. Cette stratégie nous a permis de déterminer que les effets sur les cellules immunitaires sanguines et les Ols sont distincts.

5.2.1 Effets de l'IL-1α sur l'inflammation

Nous avons observé que l'injection d'IL-1α a pour effet d'entraîner l'infiltration de cellules de l'immunité innée (e.g. monocytes, neutrophiles) à travers l'entièreté de la moelle épinière avec un pic de recrutement au temps 24 heures. Comme précédemment observé dans le laboratoire en réponse à l'IL-1β (Lévesque et al., 2016), l'activation par l'IL-1α du récepteur IL-1R1 à la surface des cellules endothéliales entraîne une diminution de l'étanchéité de la BSCB concomitante à la surexpression des récepteurs d'intégrines ICAM1 et VCAM1. Chez

les souris *Cdh5*^{CreER}::*Il1r1*$^{r/r}$, dans lesquelles l'expression de l'IL-1R1 est restreinte aux cellules endothéliales, nous avons pu observer l'infiltration de cellules myéloïdes suite à l'injection d'IL-1α. Au contraire, chez les souris *Il1r1*$^{r/r}$ chez qui le récepteur est invalidé dans toutes les cellules, de même que chez les souris *Pdgfra*^{CreER}::*Il1r1*$^{r/r}$, *Cx3cr1*^{CreER}::*Il1r1*$^{r/r}$ et *mGfap*^{Cre}::*Il1r1*$^{r/r}$ chez qui l'IL-1R1 est restauré spécifiquement dans les OPCs/Ols matures, les microglies et les astrocytes, respectivement, nous n'avons observé aucun leucocyte dans le parenchyme de la moelle épinière en réponse à l'injection de l'IL-1α. Ainsi, l'expression du récepteur de l'IL-1, IL-1R1, par les cellules endothéliales est une condition suffisante et nécessaire à l'entrée des cellules myéloïdes dans le parenchyme.

Les cellules endothéliales étant nécessaires à l'infiltration des cellules immunitaires, on peut naturellement s'interroger sur le rôle de ces cellules dans la perte des Ols. De manière intéressante, chez les souris *Cdh5*^{CreER}::*Il1r1*$^{r/r}$, le récepteur IL-1R1 est présent uniquement à la surface des cellules endothéliales. Nous avons observé chez ces souris l'infiltration de cellules immunitaires dans le parenchyme nerveux de même qu'une perte des Ols suite à l'injection d'IL-1α. Ces deux effets, puisque moins prononcés que chez les souris sauvages, suggèrent qu'une partie de la perte des Ols pourrait être liée soit à la présence du récepteur sur les cellules endothéliales, soit à la présence des cellules immunitaires. Il est connu que les Ols sont des cellules très sensibles au stress oxydatif, ce dernier pouvant causer leur mort (Bao and Liu, 2004; Simon et al., 2000; Yang et al., 2013). Il est également connu que les cellules immunitaires, en particulier les neutrophiles, constituent une source importante de ROS (Nguyen et al., 2017; Robinson, 2008). Nous pourrions donc penser que les cellules immunitaires qui infiltrent la moelle épinière à la suite d'une injection d'IL-1α pourraient jouer un rôle direct dans la perte des Ols. Cependant, la déplétion des cellules immunitaires à l'aide de l'anticorps déplétant Anti-Gr1 n'a pas eu d'effet sur la perte des Ols suivant l'injection de l'IL-1α. En effet, alors que nous avons observé une déplétion quasiment totale des cellules immunitaires, aussi bien au niveau sanguin qu'au niveau spinal, la perte en Ols était similaire à celle mesurée chez les animaux non déplétés. L'importance des cellules immunitaires dans le cadre des LME reste également sujet à controverse. Alors que Lee et ses collaborateurs ont rapporté que la déplétion concomitante des neutrophiles et des monocytes à l'aide d'anticorps anti-Ly6G et de liposomes au chlodronate, améliorait les fonctions sensori-motrices, diminuait le stress oxydatif et réduisait l'étanchéité de la BSCB

(Lee et al., 2011), pointant du même coup à un rôle délétère des cellules immunitaires, d'autres études vont dans le sens complètement inverse. En effet, Stirling et ses collaborateurs ont montré que la déplétion des neutrophiles à l'aide du même anticorps altérait la cicatrisation et aggravait les effets neurologiques à la suite d'une LME (Stirling et al., 2009). D'ailleurs, un article récemment publié met en évidence l'existence d'un sous-type de neutrophiles immatures qui favoriseraient la survie des neurones et la repousse axonale à la suite d'une hémisection dorsale à la moelle épinière, notamment via la production de NGF et d'IGF-1 (Sas et al., 2020). L'existence de différents sous-types de neutrophiles, comme suggéré dans l'étude de Sas et collaborateurs, pourrait expliquer la différence des résultats obtenus dans le cadre des études de déplétion chez les modèles animaux de LME. En effet, les neutrophiles étant présents depuis les premières heures jusqu'à plusieurs semaines post-LME, il est possible qu'en fonction du moment où la déplétion est effectuée et de sa durée, le type de neutrophiles déplétés ne soit pas le même, entraînant donc des effets différents.

D'autre part, il est possible que l'activation des cellules endothéliales et des cellules immunitaires par l'IL-1α puisse conduire à la perte des Ols matures de manière indirecte. Une fois activées, ces cellules pourraient libérer des médiateurs autres que l'IL-1α capables d'activer les astrocytes A1 responsables de la mort des Ols. Une façon de vérifier cette hypothèse sera présentée à la section Directions futures.

5.2.2 Effets de l'IL-1α sur la mort des oligodendrocytes

Nos travaux suggèrent que les astrocytes seraient directement impliqués dans cette perte d'Ols médiée par l'IL-1α. Cette possibilité a d'ailleurs déjà été avancée par l'équipe du Dr. Ben Barres suite à leurs travaux effectués à l'aide de cultures primaires dérivées des populations cellulaires du cerveau (Liddelow et al., 2017), dans lesquels son équipe a rapporté que des astrocytes stimulés avec un cocktail de facteurs dérivés des microglies, incluant l'IL-1α, le TNF et la protéine C1q, pouvaient médier la mort des neurones et des Ols. Les résultats *in vivo* que nous avons obtenus dans notre étude confirment ceux obtenus *in vitro* par Liddelow et collaborateurs. En effet, nous avons observé qu'une injection unique d'IL-1α est suffisante pour induire la perte des Ols et que cet effet requiert l'expression du récepteur IL-1R1. En particulier, l'expression de l'IL-1R1 uniquement par les astrocytes est

suffisante à engendrer la majeure partie de l'effet observé sur les Ols, confirmant l'implication directe de ces cellules dans le processus de perte des Ols.

En plus des évidences *in vivo* que nous avons apportées, nos analyses *in vitro* démontrent que le surnageant d'astrocytes primaires murins stimulés à l'IL-1α est en mesure d'induire la mort d'Ols matures, renforçant du même coup le niveau de confiance en nos résultats et interprétations. Dans l'objectif de développer une stratégie thérapeutique pour bloquer la mort des Ols médiée par les astrocytes, nous avons donc investigué quel pouvait être le ou les facteurs toxiques libérés par les astrocytes stimulés à l'IL-1α. En se basant sur la littérature, nous avons émis l'hypothèse que les ROS pouvaient être impliqués. En effet, les dérivés oxygénés sont très présents à la suite d'une LME et la vulnérabilité des Ols à de tels composés a été rapportée à plusieurs reprises dans la littérature (Fan et al., 2019; Liu et al., 2004, 2000; Simon et al., 2000; Zong et al., 2012). Nous avons dans un premier temps validé que la cytokine entraîne bel et bien la production de ces dérivés oxygénés dans des cultures primaires d'astrocytes murins. Par la suite, nous avons validé ces effets *in vivo* en optant pour une stratégie d'inhibition des ROS. Pour ce, nous avons choisi d'injecter le NAC, reconnu pour être un puissant anti-oxydant capable de bloquer l'effet des ROS (Jiao et al., 2016). En réponse à l'injection d'IL-1α, l'administration de NAC s'est avérée suffisante pour inhiber complètement les effets toxiques de l'IL-1α sur les Ols. Nous avons observé que lorsque le NAC est injecté de façon concomitante à l'IL-1α, aucune diminution du nombre d'Ols n'est observée. Ces résultats laissent croire à la possibilité d'une thérapie ciblant l'IL-1α dans un contexte de LME. Toutefois, l'injection de NAC ne fut pas suffisante pour induire une amélioration de la récupération motrice chez des souris ayant subi une LME. Nous avons malgré tout observé que le nombre d'Ols est préservé au temps 24 heures post-LME chez les souris traitées au NAC. Il va sans dire que le modèle de LME est beaucoup plus complexe que le modèle d'injection de l'IL-1α puisque ce dernier ne reproduit qu'une infime partie de ce qui se passe suite à une lésion. En tenant compte qu'une LME est une série d'évènements qui se suivent et s'enchaînent, il pourrait être pertinent d'injecter le NAC de manière continue, ceci sera discuté dans la section Directions futures, ci-dessous.

Évoquer l'idée d'un traitement qui permettrait de limiter la perte des Ols afin de limiter les dommages et améliorer la récupération motrice soulève toutefois la question de l'efficacité d'une telle thérapie. Les Ols sont les cellules produisant la myéline, une

composante indispensable au bon fonctionnement du SNC. Nous pourrions donc nous attendre à ce que préserver les Ols et, de ce fait, la myéline, ou encore augmenter la remyélinisation post-lésion, pourrait contribuer à améliorer la récupération motrice après une LME. L'idée de faciliter la régénération de la myéline est d'ailleurs considérée comme un enjeu dans le développement de traitements post-LME. Cependant, bien que plusieurs études aient montré que la remyélinisation ait un effet bénéfique sur la récupération motrice (Cao et al., 2010; Karimi-Abdolrezaee et al., 2006; Keirstead et al., 2005), d'autres études ont au contraire rapporté que la récupération motrice suite à une LME serait en fait indépendante du processus de remyélinisation (Duncan et al., 2018; Papastefanaki and Matsas, 2015). En effet, Duncan et collaborateurs ont montré qu'induire une délétion du *myelin regulatory factor* (Myrf) dans le cadre d'une LME réduisait de 44% le nombre d'axones myélinisés à l'épicentre de la lésion. Cette inhibition du processus de remyélinisation ne fut toutefois pas associée à baisse de la récupération motrice spontanée qui survient normalement post-LME. Cependant, dans l'étude de Cao et collaborateurs et celle de Karimi-Abdolrezaee et collaborateurs, le processus de remyélinisation ne fut pas directement modulé. En effet, les deux équipes ont respectivement réalisé des greffes de précurseurs d'Ols matures exprimant le facteur neurotrophique cilaire ou de précurseurs de cellules neurales. Ainsi, l'augmentation de la remyélinisation qu'ils ont observée serait une conséquence de la greffe de ces précurseurs, mais n'aurait pas d'effet direct sur la récupération motrice. L'amélioration de cette fonction pourrait en fait s'expliquer par la greffe des précurseurs.

5.3 Utilisation des modèles Cre

Tout étude n'est pas parfaite, est c'est aussi ce qui fait la beauté de la science et rend le défi plus intéressant. Une des premières critiques qui pourrait être amenée sur mes travaux, et j'en suis la première à le faire valoir, concerne les modèles transgéniques. Ces modèles sont d'une très grande utilité mais comportent aussi leurs limitations. Sans s'étendre trop longuement sur le sujet, la première chose qu'il est important de souligner sur ce point concerne la spécificité des modèles Cre permettant de cibler des populations cellulaires spécifiques. Bien que nous ayons utilisé, dans la mesure du possible, les modèles Cre les plus spécifiques, il reste un pourcentage de non-spécificité propre à chacune des lignées. C'est pourquoi nous avons, pour la majorité de nos lignées, opté pour des modèles inductibles qui permettent de

limiter la non-spécificité grâce à l'ajout d'un niveau de régulation additionnel, c'est-à-dire le temps, par l'entremise du traitement au tamoxifène. Par exemple, concernant la souris *Cx3cr1*^{CreERT2}, l'expression de la recombinase Cre est régulée par le promoteur du gène codant pour le récepteur de la fractalkine, exprimé à la fois par les microglies et les monocytes. Cependant, afin d'écarter la composante monocytaire de l'équation, les souris *Cx3cr1*^{CreERT2} sont gavées au tamoxifène à 1 mois d'âge. Dès lors, la recombinaison s'effectue à la fois dans les microglies et les monocytes. Mais en laissant aux souris une période de repos d'une durée d'un mois avant de les utiliser, les monocytes qui ont été recombinés seront remplacés par de nouveaux monocytes dérivant de progéniteurs de la lignée myéloïde n'exprimant pas le transcrit *Cx3cr1*, donc des monocytes non-recombinés.

Toutefois, les modèles Cre-inductibles présentent également certains inconvénients. En particulier, le taux de recombinaison est plus faible chez les modèles inductibles en comparaison aux modèles constitutifs. Il est donc essentiel d'optimiser le protocole de recombinaison, que ce soit en fonction de la dose de tamoxifène, de la durée du traitement ou de l'âge à laquelle débute le traitement. Prendre en considération ces différents éléments permet de maximiser la recombinaison. Il reste toutefois quasiment impossible d'obtenir une recombinaison efficace à 100%. Cela peut être particulièrement problématique dans le cas de knockout induits. En effet, à partir du moment où le knockout n'est pas de 100%, comme par exemple chez nos souris *Cdh5*^{CreER}::*Il1r1*$^{fl/fl}$, il n'est pas possible d'assumer avec certitude si l'effet observé est dû à la présence du récepteur sur un autre type cellulaire, ou si l'effet est médié par des cellules endothéliales dans lesquelles la délétion du gène n'a pas été efficace.

5.4 Différences entre l'IL-1α et l'IL-1β

Bien que l'IL-1α et l'IL-1β appartiennent à la même famille et présentent des propriétés très similaires, il est intéressant de noter les différences d'effets obtenus avec ces deux cytokines. Dans le cas où les cytokines sont injectées dans la *cisterna magna* à doses équivalentes (100 ng/souris), nous avons observé des effets similaires en termes d'inflammation, c'est-à-dire un nombre équivalent de neutrophiles infiltrés dans la neurovasculature et le parenchyme nerveux. Cependant, l'effet sur la perte des Ols n'a été observé qu'en présence d'IL-1α, ce qui pourrait laisser penser que les deux cytokines possèdent des effets distincts. Toutefois,

nous avons observé qu'un effet similaire sur la perte en Ols peut être observé avec l'IL-1β lorsque la dose injectée est multipliée par 5, en l'occurrence une dose de 500 ng/souris. Ceci pourrait s'expliquer par la différence d'affinité des cytokines avec les récepteurs de l'IL-1 (McMahan et al., 1991). En effet, il a été montré que l'IL-1α est plus affin pour l'IL-1R1, qui médie les effets cellulaires, alors que l'IL-1β est plus affin pour le récepteur de type II de l'IL-1 (IL-1RII) qui n'exerce aucune signalisation intracellulaire. Or, nous avons démontré que l'IL-1R2 est surexprimé par les microglies suite à l'injection d'IL-1α. Cela peut donc expliquer que les deux cytokines aient un effet similaire sur l'inflammation, mais pas sur les Ols. En effet, le recrutement des leucocytes est médié par l'IL-1R1 présent à la surface des cellules endothéliales, or, ces cellules ne sont pas situées à proximité des cellules exprimant des hauts taux d'IL-1R2, en l'occurrence les microglies. Au contraire, les astrocytes, qui expriment fortement IL-1R1 et entraînent la perte des Ols une fois activés par l'IL-1, sont situés à proximité des microglies exprimant l'IL-1R2. Ainsi, en raison de leur différence d'affinité, l'IL-1β se fixerait préférentiellement sur l'IL-1R2 des microglies plutôt que l'IL-1R1 exprimé par les astrocytes, contrairement à l'IL-1α.

De manière intéressante, la surexpression de l'IL-1R2 par les microglies pourrait limiter les effets de l'IL-1α en abrogeant ses actions sur les autres types cellulaires. Cela pourrait également expliquer pourquoi la déplétion des microglies a pour conséquence d'accroitre les effets de l'IL-1α sur le recrutement et l'infiltration des cellules immunitaires innées et la mort des Ols. Augmenter l'expression de l'IL-1R2 dans la phase initiale des LME pourrait d'ailleurs constituer une possibilité intéressante afin de bloquer les effets de l'IL-1α dans ce contexte. Cette possibilité sera évoquée à la section Directions futures.

5.5 Directions futures

Nos travaux ont montré l'importance de la signalisation de l'IL-1α sur l'inflammation et la perte des Ols. Nos résultats ont permis de montrer que la perte des Ols est une conséquence directe de l'activation des astrocytes par l'IL-1α. Ce projet permet ainsi d'imaginer des pistes prometteuses quant à l'élaboration de nouveaux traitements dans le cadre des LME. Toutefois, ce mécanisme soulève certaines interrogations auxquelles il serait pertinent de répondre pour donner suite à ce projet. Ces différentes perspectives seront développées dans la présente section.

5.5.1 Démystifier l'importance des cellules endothéliales et des cellules immunitaires

Ce projet soulève la question à savoir si les cellules endothéliales et/ou les cellules immunitaires pourraient jouer un rôle direct ou indirect dans la perte des Ols. Cette question pourrait être investiguée par des expériences *in vitro*. Par exemple, nous pourrions mettre en culture des cellules endothéliales ou des cellules immunitaires, les stimuler avec de l'IL-1α et récupérer le surnageant. D'une part, l'effet potentiellement cytotoxique du surnageant pourrait être testé sur des cultures primaires d'Ols matures par essai LDH. D'autre part, des cultures primaires d'astrocytes pourraient également être incubées avec ce surnageant. Le surnageant subséquent serait alors récupéré et mis en présence d'Ols pour tester sa toxicité et l'effet cytotoxique comparé à celui d'un surnageant d'astrocytes stimulés directement à l'IL-1α. Ces expériences permettraient de déterminer si : 1) les cellules endothéliales ou les cellules immunitaires stimulées directement à l'IL-1α peuvent être toxiques pour les Ols, 2) les astrocytes peuvent adopter des effets toxiques suite à leur stimulation par des cellules endothéliales ou immunitaires activées à l'IL-1α.

Également, compte tenu de l'existence de différents sous-types de neutrophiles et de macrophages dans un contexte de LME (Sas et al., 2020;Thawer et al., 2013), il serait intéressant de caractériser avec exactitude les types cellulaires présents dans la moelle épinière à différents temps suivant l'injection d'IL-1α. Une façon d'identifier les différents sous-types de macrophages présents dans la moelle épinière serait de dissocier les cellules à l'échelle unitaire puis de les analyser par single-cell RNA-sequencing. Cette technique permet d'accéder à l'information génétique à l'échelle d'une seule cellule et permet donc de discriminer avec précision les différents types cellulaires.

5.5.2 Élaboration de stratégies visant à assurer la protection des Ols suite à une LME

Particulièrement affectés par les LME, les Ols matures sont pourtant des cellules essentielles au bon fonctionnement du SNC. Cette thèse a permis d'apporter de nouvelles connaissances quant aux mécanismes d'action impliqués dans la perte de ces cellules, notamment en lien avec l'IL-1α et son récepteur de type 1. En disséquant de manière précise les mécanismes par

lesquels cette cytokine, libérée dès les premières minutes/heures post-lésion, entraîne la mort des Ols matures, nous croyons dorénavant être en mesure d'agir à différents niveaux afin de préserver ces cellules.

5.5.2.1 Stratégies visant à bloquer l'IL-1α

L'IL-1α joue un rôle critique dans les premières heures suivant une LME. L'absence d'IL-1α est suffisante pour obtenir des effets significativement bénéfiques sur la récupération motrice chez la souris et cette cytokine constitue, de ce fait, une cible de choix pour l'élaboration de stratégies thérapeutiques dans un contexte de LME. Tout d'abord, il serait intéressant de tester si l'utilisation d'un anticorps neutralisant l'IL-1α pourrait permettre de bloquer directement la cytokine et, ainsi, d'interrompre sa signalisation. Pour tester cette hypothèse, il s'agirait d'injecter l'anticorps neutralisant anti-IL-1α dans les premières heures post-lésion dans un modèle murin de LME et d'évaluer les effets sur la récupération motrice (score BMS) et sur les conséquences pathophysiologiques des LME (inflammation, activation gliale, cicatrice gliale, volume lésionnel,…).

D'autre part, en lien avec le rôle de l'IL-1R2 comme récepteur « decoy », il serait pertinent d'étudier si l'injection du recombinant murin de l'IL-1R2, dans les premières heures suivant une LME, permettrait de bloquer les effets de l'IL-1α. Si tel est le cas, nous pourrions nous attendre à des résultats similaires à ceux observés chez les souris invalidées pour l'*Il1a*. A postériori, ces expériences pourraient même permettre de développer des thérapies axées sur l'utilisation d'anti-IL-1α ou d'IL-1R2 afin de réduire les dommages tissulaires qui surviennent de la phase aiguë post-LME.

5.5.2.2 Agir sur les astrocytes

Cette thèse a également permis de mettre en évidence le rôle clé des astrocytes dans le processus de perte des Ols *in vivo*. En effet, ces cellules sont extrêmement sensibles à l'IL-1α. Lorsque l'IL-1α est relâchée dans le milieu extracellulaire, comme suite à une LME, les astrocytes sont stimulés puis polarisés en un phénotype toxique. Il serait donc pertinent de développer une approche qui consisterait à bloquer cette transformation des astrocytes naïfs (ou A2) en A1 ou bien d'inhiber l'activité des astrocytes A1, ce qui permettrait de réduire la perte d'Ols. Liddlelow et collaborateurs ont récemment effectué des expériences de

séquençages d'ARN qui leur ont permis d'établir les profils d'expression génique des astrocytes A1 et A2. En se basant sur leurs résultats, il serait possible d'identifier des cibles potentielles qui pourraient permettre de bloquer l'activité des astrocytes A1 grâce à des inhibiteurs biologiques (anticorps neutralisant, antagonistes,…). Ces inhibiteurs pourraient ensuite être validés *in vitro* puis testés *in vivo* chez des souris lésées afin d'évaluer leur potentiel.

5.5.2.3 Bloquer les ROS

Suite aux résultats prometteurs obtenus en termes de préservation des Ols avec le traitement au NAC dans les modèles murins d'injection centrale d'IL-1α et la contusion de la moelle épinière, il serait intéressant d'optimiser la méthode de délivrance du NAC afin d'élaborer une thérapie pour les LME et autres types de traumatismes nerveux. L'utilisation d'une pompe osmotique apposée directement sur la moelle lésée permettrait de délivrer de manière contrôlée et continue le NAC afin d'optimiser ses effets bénéfiques. Il serait cependant plus difficile, voire impossible, d'évaluer le score locomoteur dû à la présence de la pompe sur le dos de l'animal, et ce même si l'administration en continue du NAC pourrait avoir des effets bénéfiques en préservant le nombre d'Ols et en réduisant l'étendu des dommages tissulaires secondaires suite à la LME.

5.5.3 Étude des effets de l'IL-1α sur les neurones et incidence sur la sensation douloureuse

Suite aux recherches menées au sein de notre laboratoire, établissant un lien direct entre le récepteur IL-1R1 et le phénomène douloureux dans diverses pathologies, nous avons débuté des expériences visant à investiguer le lien entre l'IL-1R1et la douleur dans un contexte de LME. Bien que la grande majorité des études menées dans un contexte de LME visent à réparer les dommages et améliorer la récupération des fonctions motrice chez le patient, il ne faut surtout pas négliger que plus de 60% ceux-ci souffrent de douleur chronique. Il est donc extrêmement pertinent de trouver des solutions afin de réduire le phénomène douloureux chez les lésés médullaires. En ce sens, nous avons obtenu des résultats préliminaires intéressants en injectant l'IL-1α chez des souris WT et en évaluant par le test Von Frey la sensation douloureuse. Nous avons en effet observé que l'injection d'IL-1α est suffisante

pour déclencher une allodynie à 24 heures chez les femelles. Il serait donc intéressant de pousser l'investigation de ce mécanisme dans un contexte de LME. Tout d'abord, en évaluant s'il existe une différence de réponse douloureuse entre des souris WT et des souris *Il1r1*$^{r/r}$ (knockout) lésées. Comme il a été démontré que la sensation douloureuse passe par les neurones TRPV1^{+}, il serait aussi pertinent d'étudier le comportement douloureux chez des souris *Trpv1*^{Cre} ::*Il1r1*$^{fl/fl}$ chez qui le récepteur IL-1R1 est invalidé dans les neurones TRPV1^{+}. Si l'IL-1α induit bel et bien un effet douloureux via ce type de neurones, alors ces souris devraient être moins sensibles à la douleur que des souris WT suite à l'injection d'IL-1α. Enfin, si les résultats sont prometteurs, il serait judicieux de vérifier si l'administration d'anakinra, un antagoniste de l'IL-1R1, pourrait diminuer la sensation de douleur chez des souris lésées. Si tel est le cas, cela permettrait d'offrir une solution pour diminuer la douleur chez les patients LME.

Conclusion

Bien que l'immunologie soit un des domaines les plus anciens de la biologie, de nombreux mystères restent encore à résoudre. Notre compréhension du système immunitaire et de l'inflammation ne cesse d'évoluer, et leurs liens étroits avec les autres systèmes du corps humain, en particulier le système nerveux, les rendent fascinant de complexité.

Les LME constituent un exemple parfait du lien qui existe entre le système nerveux et le système immunitaire. Le processus inflammatoire qui fait suite aux LME est à la base de la dégénérescence secondaire, entraînant des dommages non négligeables. Cependant, chaque élément y joue un rôle important et il ne s'agit pas d'inhiber complètement, ou au contraire d'exacerber l'inflammation, mais plutôt de trouver l'équilibre parfait afin d'optimiser à la fois le nettoyage des débris cellulaires causés par le traumatisme et la réparation tissulaire. L'IL-1α est au cœur de ce processus inflammatoire, jouant un rôle critique dans la phase aiguë qui est déclenchée post-LME mais dont les effets se répercutent sur le long terme. Mieux comprendre les effets et mécanismes d'action de l'inflammation pourrait permettre d'identifier de nouvelles cibles thérapeutiques qui pourraient permettre de diminuer la gravité des LME.

Bibliographie

Abbate, A., Toldo, S., Marchetti, C., Kron, J., Van Tassell, B.W., Dinarello, C.A., 2020. Interleukin-1 and the Inflammasome as Therapeutic Targets in Cardiovascular Disease. Circ. Res. 126, 1260–1280. https://doi.org/10.1161/CIRCRESAHA.120.315937

Abbott, N.J., Rönnbäck, L., Hansson, E., 2006. Astrocyte–endothelial interactions at the blood–brain barrier. Nat. Rev. Neurosci. 7, 41–53. https://doi.org/10.1038/nrn1824

Abbracchio, M.P., Burnstock, G., Verkhratsky, A., Zimmermann, H., 2009. Purinergic signalling in the nervous system: an overview. Trends Neurosci. 32, 19–29. https://doi.org/10.1016/j.tins.2008.10.001

Ackery, A., Tator, C., Krassioukov, A., 2004. A global perspective on spinal cord injury epidemiology. J. Neurotrauma 21, 1355–1370. https://doi.org/10.1089/neu.2004.21.1355

Afonina, I.S., Tynan, G.A., Logue, S.E., Cullen, S.P., Bots, M., Lüthi, A.U., Reeves, E.P., McElvaney, N.G., Medema, J.P., Lavelle, E.C., Martin, S.J., 2011. Granzyme B-dependent proteolysis acts as a switch to enhance the proinflammatory activity of IL-1α. Mol. Cell 44, 265–278. https://doi.org/10.1016/j.molcel.2011.07.037

Afsar, B., Covic, A., Ortiz, A., Afsar, R.E., Kanbay, M., 2018. The Future of IL-1 Targeting in Kidney Disease. Drugs 78, 1073–1083. https://doi.org/10.1007/s40265-018-0942-2

Agresti, A., Bianchi, M.E., 2003. HMGB proteins and gene expression. Curr. Opin. Genet. Dev. 13, 170–178. https://doi.org/10.1016/S0959-437X(03)00023-6

Ajami, B., Bennett, J.L., Krieger, C., Tetzlaff, W., Rossi, F.M.V., 2007. Local self-renewal can sustain CNS microglia maintenance and function throughout adult life. Nat. Neurosci. 10, 1538–1543. https://doi.org/10.1038/nn2014

Ali, S., Mohs, A., Thomas, M., Klare, J., Ross, R., Schmitz, M.L., Martin, M.U., 2011. The

dual function cytokine IL-33 interacts with the transcription factor NF-κB to dampen NF-κB-stimulated gene transcription. J. Immunol. https://doi.org/10.4049/jimmunol.1003080

Allan, S.M., Tyrrell, P.J., Rothwell, N.J., 2005. Interleukin-1 and neuronal injury. Nat. Rev. Immunol. 5, 629–640. https://doi.org/10.1038/nri1664

Almad, A., Sahinkaya, F.R., McTigue, D.M., 2011. Oligodendrocyte Fate after Spinal Cord Injury. Neurotherapeutics 8, 262–273. https://doi.org/10.1007/s13311-011-0033-5

Anderson, M.A., Burda, J.E., Ren, Y., Ao, Y., O'Shea, T.M., Kawaguchi, R., Coppola, G., Khakh, B.S., Deming, T.J., Sofroniew, M. V, 2016. Astrocyte scar formation aids central nervous system axon regeneration. Nature 532, 195–200. https://doi.org/10.1038/nature17623

Andersson, U., Antoine, D.J., Tracey, K.J., 2014. The functions of HMGB1 depend on molecular localization and post-translational modifications. J. Intern. Med. 276, 420–424. https://doi.org/10.1111/joim.12309

Andersson, U., Wang, H., Palmblad, K., Aveberger, A.C., Bloom, O., Erlandsson-Harris, H., Janson, A., Kokkola, R., Zhang, M., Yang, H., Tracey, K.J., 2000. High mobility group 1 protein (HMG-1) stimulates proinflammatory cytokine synthesis in human monocytes. J. Exp. Med. 192, 565–70. https://doi.org/10.1084/jem.192.4.565

Anthes, D.L., Theriault, E., Tator, C.H., 1995. Characterization of axonal ultrastructural pathology following experimental spinal cord compression injury. Brain Res. 702, 1–16. https://doi.org/10.1016/0006-8993(95)01028-6

Arakawa, M., Ito, Y., 2007. N-acetylcysteine and neurodegenerative diseases: Basic and clinical pharmacology. Cerebellum 6, 308–314. https://doi.org/10.1080/14734220601142878

Asai, H., Ikezu, S., Tsunoda, S., Medalla, M., Luebke, J., Wolozin, B., Butovsky, O., Ikezu, T., Therapeutics, E., 2015. Depletion of microglia and inhibition of exosome synthe. Nat. Neurosci. 18, 1584–1593. https://doi.org/10.1038/nn.4132.Depletion

Askew, K., Li, K., Olmos-Alonso, A., Garcia-Moreno, F., Liang, Y., Richardson, P., Tipton, T., Chapman, M.A., Riecken, K., Beccari, S., Sierra, A., Molnár, Z., Cragg, M.S., Garaschuk, O., Perry, V.H., Gomez-Nicola, D., 2017. Coupled Proliferation and Apoptosis Maintain the Rapid Turnover of Microglia in the Adult Brain. Cell Rep. 18, 391–405. https://doi.org/10.1016/j.celrep.2016.12.041

Assmann, J.C., Körbelin, J., Schwaninger, M., 2016. Genetic manipulation of brain endothelial cells in vivo. Biochim. Biophys. Acta - Mol. Basis Dis. 1862, 381–394. https://doi.org/10.1016/j.bbadis.2015.10.006

Attwell, D., Mishra, A., Hall, C.N., O'Farrell, F.M., Dalkara, T., 2016. What is a pericyte? J. Cereb. Blood Flow Metab. 36, 451–455. https://doi.org/10.1177/0271678X15610340

Auron, P.E., Webb, A.C., Rosenwasser, L.J., Mucci, S.F., Rich, A., Wolff, S.M., Dinarello, C.A., 1984. Nucleotide sequence of human monocyte interleukin 1 precursor cDNA. Proc. Natl. Acad. Sci. U. S. A. 81, 7907–7911. https://doi.org/10.1073/pnas.81.24.7907

Badhiwala, J.H., Ahuja, C.S., Fehlings, M.G., 2019. Time is spine: A review of translational advances in spinal cord injury. J. Neurosurg. Spine 30, 1–18. https://doi.org/10.3171/2018.9.SPINE18682

Balosso, S., Liu, J., Bianchi, M.E., Vezzani, A., 2014. Disulfide-Containing High Mobility Group Box-1 Promotes *N* -Methyl- <scp>d</scp> -Aspartate Receptor Function and Excitotoxicity by Activating Toll-Like Receptor 4-Dependent Signaling in Hippocampal Neurons. Antioxid. Redox Signal. 21, 1726–1740. https://doi.org/10.1089/ars.2013.5349

Bandman, O., Coleman, R.T., Loring, J.F., Seilhamer, J.J., Cocks, B.G., 2002. Complexity of inflammatory responses in endothelial cells and vascular smooth muscle cells determined by microarray analysis. Ann. N. Y. Acad. Sci. 975, 77–90. https://doi.org/10.1111/j.1749-6632.2002.tb05943.x

Bao, F., Chen, Y., Schneider, K.A., Weaver, L.C., 2008. An integrin inhibiting molecule decreases oxidative damage and improves neurological function after spinal cord injury. Exp. Neurol. 214, 160–167. https://doi.org/10.1016/j.expneurol.2008.09.006

Bao, F., Liu, D., 2004. Hydroxyl radicals generated in the rat spinal cord at the level produced by impact injury induce cell death by necrosis and apoptosis: Protection by a metalloporphyrin. Neuroscience 126, 285–295. https://doi.org/10.1016/j.neuroscience.2004.03.054

Barrette, B., Hébert, M.-A., Filali, M., Lafortune, K., Vallières, N., Gowing, G., Julien, J.-P., Lacroix, S., 2008. Requirement of myeloid cells for axon regeneration. J. Neurosci. 28, 9363–9376. https://doi.org/10.1523/JNEUROSCI.1447-08.2008

Bartholdi, D., Schwab, M.E., 1997. Expression of pro-inflammatory cytokine and chemokine mRNA upon experimental spinal cord injury in mouse: An in situ hybridization study. Eur. J. Neurosci. 9, 1422–1438. https://doi.org/10.1111/j.1460-9568.1997.tb01497.x

Bastien, D., Bellver Landete, V., Lessard, M., Vallieres, N., Champagne, M., Takashima, a., Tremblay, M.-E., Doyon, Y., Lacroix, S., 2015. IL-1 Gene Deletion Protects Oligodendrocytes after Spinal Cord Injury through Upregulation of the Survival Factor Tox3. J. Neurosci. 35, 10715–10730. https://doi.org/10.1523/JNEUROSCI.0498-15.2015

Bastien, D., Lacroix, S., 2014. Cytokine pathways regulating glial and leukocyte function after spinal cord and peripheral nerve injury. Exp. Neurol. 258, 62–77. https://doi.org/10.1016/j.expneurol.2014.04.006

Basu, A., Krady, J.K., Levison, S.W., 2004. Interleukin-1: A master regulator of neuroinflammation. J. Neurosci. Res. 78, 151–156. https://doi.org/10.1002/jnr.20266

Beeson, P.B., 1948. Temperature-elevating effect of a substance obtained from polymorphonuclear leucocytes. J. Clin. Invest. 27, 524.

Bell, R.D., Winkler, E.A., Sagare, A.P., Singh, I., Larue, B., Deane, R., Zlokovic, B. V,

2011. Pericytes control key neurovascular functions and neuronal. Neuron. 68, 409–427. https://doi.org/10.1016/j.neuron.2010.09.043.Pericytes

Bellver-Landete, V., Bretheau, F., Mailhot, B., Lessard, M., Shoichet, M.S., Vallières, N., Janelle, M.-E., Tremblay, M.-È., Vernoux, N., Fuehrmann, T., Tremblay, M.-È., Shoichet, M.S., Lacroix, S., 2019. Microglia are an essential component of the neuroprotective scar that forms after spinal cord injury. Nat. Commun. 10. https://doi.org/10.1038/s41467-019-08446-0

Ben-Neriah, Y., Karin, M., 2011. Inflammation meets cancer, with NF-κB as the matchmaker. Nat. Immunol. 12, 715–23. https://doi.org/10.1038/ni.2060

Benson, M.D., Romero, M.I., Lush, M.E., Lu, Q.R., Henkemeyer, M., Parada, L.F., 2005. Ephrin-B3 is a myelin-based inhibitor of neurite outgrowth. Proc. Natl. Acad. Sci. U. S. A. 102, 10694–10699. https://doi.org/10.1073/pnas.0504021102

Bergles, D.E., Richardson, W.D., 2016. Oligodendrocyte development and plasticity. Cold Spring Harb. Perspect. Biol. 8, 1–27. https://doi.org/10.1101/cshperspect.a020453

Berk, M., Kapczinski, F., Andreazza, A.C., Dean, O.M., Giorlando, F., Maes, M., Yücel, M., Gama, C.S., Dodd, S., Dean, B., Magalhães, P.V.S., Amminger, P., McGorry, P., Malhi, G.S., 2011. Pathways underlying neuroprogression in bipolar disorder: Focus on inflammation, oxidative stress and neurotrophic factors. Neurosci. Biobehav. Rev. 35, 804–817. https://doi.org/10.1016/j.neubiorev.2010.10.001

Bersudsky, Marina, Luski, L., Fishman, D., White, R.M., Ziv-Sokolovskaya, N., Dotan, S., Rider, P., Kaplanov, I., Aychek, T., Dinarello, C.A., Apte, R.N., Voronov, E., 2014. Non-redundant properties of IL-1α and IL-1β during acute colon inflammation in mice. Gut 63, 598–609. https://doi.org/10.1136/gutjnl-2012-303329

Bersudsky, M, Luski, L., Fishman, D., White, R.M., Ziv-Sokolovskaya, N., Dotan, S., Rider, P., Kaplanov, I., Aychek, T., Dinarello, C.A., Apte, R.N., Voronov, E., 2014. Non-redundant properties of IL-1alpha and IL-1beta during acute colon inflammation in mice. Gut 63, 598–609. https://doi.org/gutjnl-2012-303329 [pii]\r10.1136/gutjnl-

2012-303329

Bi, Y., Zhu, Y., Zhang, M., Zhang, K., Hua, X., Fang, Z., Zhou, J., Dai, W., Cui, Y., Li, J., You, T., 2017. Effect of Shikonin on Spinal Cord Injury in Rats Via Regulation of HMGB1/TLR4/NF-κB Signaling Pathway. Cell. Physiol. Biochem. 43, 481–491. https://doi.org/10.1159/000480474

Bianchi, M.E., Falciola, L., Ferrari, S., Lilley, D.M., 1992. The DNA binding site of HMG1 protein is composed of two similar segments (HMG boxes), both of which have counterparts in other eukaryotic regulatory proteins. Embo J 11, 1055–1063.

Blakemore, W.F., Keirstead, H.S., 1999. The origin of remyelinating cells in the central nervous system. J. Neuroimmunol. 98, 69–76. https://doi.org/10.1016/S0165-5728(99)00083-1

Blight, A.R., 1994. Effects of silica on the outcome from experimental spinal cord injury: Implication of macrophages in secondary tissue damage. Neuroscience 60, 263–273. https://doi.org/10.1016/0306-4522(94)90220-8

Blight, A.R., 1985. Delayed demyelination and macrophage invasion: a candidate for secondary cell damage in spinal cord injury. Cent. Nerv. Syst. Trauma 2, 299–315. https://doi.org/10.1089/cns.1985.2.299

Blight, A.R., 1983. Cellular morphology of chronic spinal cord injury in the cat: Analysis of myelinated axons by line-sampling. Neuroscience 10. https://doi.org/10.1016/0306-4522(83)90150-1

Borregaard, N., 2010. Neutrophils, from Marrow to Microbes. Immunity 33, 657–670. https://doi.org/10.1016/j.immuni.2010.11.011

Bouhy, D., Malgrange, B., Multon, S., Poirrier, A.-L., Scholtes, F., Schoenen, J., Franzen, R., 2006. Delayed GM-CSF treatment stimulates axonal regeneration and functional recovery in paraplegic rats via an increased BDNF expression by endogenous macrophages. FASEB J. 20, 1239–1241. https://doi.org/10.1096/fj.05-4382fje

Boutin, H., LeFeuvre, R. a, Horai, R., Asano, M., Iwakura, Y., Rothwell, N.J., 2001. Role of IL-1alpha and IL-1beta in ischemic brain damage. J. Neurosci. 21, 5528–5534. https://doi.org/21/15/5528 [pii]

Bracken, M.B., Shepard, M.J., Collins, W.F., Holford, T.R., Baskin, D.S., Eisenberg, H.M., Flamm, E., Leo-Summers, L., Maroon, J.C., Marshall, L.F., Perot, P.L., Piepmeier, J., Sonntag, V.K.H., Wagner, F.C., Wilberger, J.L., Winn, H.R., Young, W., 1992. Methylprednisolone or naloxone treatment after acute spinal cord injury: 1-year follow-up data: Results of the second National Acute Spinal Cord Injury Study. J. Neurosurg. 76, 23–31. https://doi.org/10.3171/jns.1992.76.1.0023

Bracken, M.B., Shepard, M.J., Holford, T.R., Leo-Summers, L., Aldrich, E.F., Fazl, M., Fehlings, M., Herr, D.L., Hitchon, P.W., Marshall, L.F., Nockels, R.P., Pascale, V., Perot, P.L., Piepmeier, J., Sonntag, V.K.H., Wagner, F., Wilberger, J.E., Winn, H.R., Young, W., 1997. Administration of methylprednisolone for 24 or 48 hours or tirilazad mesylate for 48 hours in the treatment of acute spinal cord injury: Results of the Third National Acute Spinal Cord Injury randomized controlled trial. J. Am. Med. Assoc. 277, 1597–1604. https://doi.org/10.1001/jama.277.20.1597

Bradbury, E.J., Moon, L.D.F., Popat, R.J., King, V.R., Bennett, G.S., Patel, P.N., Fawcett, J.W., McMahon, S.B., 2002. Chondroitinase ABC promotes functional recovery after spinal cord injury. Nature 416, 636–40. https://doi.org/10.1038/416636a

Brady, S.T., Siegel, G.J., 2012. Characteristic composition of myelin. Basic Neurochem. Princ. Mol. Cell. Med. Neurobiol. 1096.

Brambilla, R., Bracchi-Ricard, V., Hu, W.H., Frydel, B., Bramwell, A., Karmally, S., Green, E.J., Bethea, J.R., 2005. Inhibition of astroglial nuclear factor κB reduces inflammation and improves functional recovery after spinal cord injury. J. Exp. Med. 202, 145–156. https://doi.org/10.1084/jem.20041918

Brinkmann, V., Reichard, U., Goosmann, C., Fauler, B., Uhlemann, Y., Weiss, D.S., Weinrauch, Y., Zychlinsky, A., 2004. Neutrophil Extracellular Traps Kill Bacteria. Science (80-.). 303, 1532–1535. https://doi.org/10.1126/science.1092385

Brown, B.N., Sicari, B.M., Badylak, S.F., 2014. Rethinking regenerative medicine: A macrophage-centered approach. Front. Immunol. 5, 1–11. https://doi.org/10.3389/fimmu.2014.00510

Bruttger, J., Karram, K., Wörtge, S., Regen, T., Marini, F., Hoppmann, N., Klein, M., Blank, T., Yona, S., Wolf, Y., Mack, M., Pinteaux, E., Müller, W., Zipp, F., Binder, H., Bopp, T., Prinz, M., Jung, S., Waisman, A., 2015. Genetic Cell Ablation Reveals Clusters of Local Self-Renewing Microglia in the Mammalian Central Nervous System. Immunity 43, 92–106. https://doi.org/10.1016/j.immuni.2015.06.012

Bujalka, H., Koenning, M., Jackson, S., Perreau, V.M., Pope, B., Hay, C.M., Mitew, S., Hill, A.F., Lu, Q.R., Wegner, M., Srinivasan, R., Svaren, J., Willingham, M., Barres, B.A., Emery, B., 2013. MYRF Is a Membrane-Associated Transcription Factor That Autoproteolytically Cleaves to Directly Activate Myelin Genes. PLoS Biol. 11. https://doi.org/10.1371/journal.pbio.1001625

Burnstock, G., 1999. Current status of purinergic signalling in the nervous system. Nucleotides Their Recept. Nerv. Syst. 120, 3–10.

Buryskova, M., Pospisek, M., Grothey, A., Simmet, T., Burysek, L., 2004. Intracellular Interleukin-1α Functionally Interacts with Histone Acetyltransferase Complexes. J. Biol. Chem. 279, 4017–4026. https://doi.org/10.1074/jbc.M306342200

Bush, T.G., Puvanachandra, N., Horner, C.H., Polito, A., Ostenfeld, T., Svendsen, C.N., Mucke, L., Johnson, M.H., Sofroniew, M. V, 1999. Leukocyte Infiltration, Neuronal Degeneration, and Neurite Outgrowth after Ablation of Scar-Forming, Reactive Astrocytes in Adult Transgenic Mice provision of metabolic substrates for neurons, and inter-actions with endothelia to create and maintain the b. Neuron 23, 297–308.

Buss, A., Pech, K., Kakulas, B.A., Martin, D., Schoenen, J., Noth, J., Brook, G.A., 2008. TGF-β1 and TGF-β2 expression after traumatic human spinal cord injury. Spinal Cord 46, 364–371. https://doi.org/10.1038/sj.sc.3102148

Buttgereit, A., Lelios, I., Yu, X., Vrohlings, M., Krakoski, N.R., Gautier, E.L.,

Nishinakamura, R., Becher, B., Greter, M., 2016. Sall1 is a transcriptional regulator defining microglia identity and function. Nat. Immunol. 17, 1397–1406. https://doi.org/10.1038/ni.3585

Cabal-Hierro, L., Lazo, P.S., 2012. Signal transduction by tumor necrosis factor receptors. Cell. Signal. 24, 1297–1305. https://doi.org/10.1016/j.cellsig.2012.02.006

Cai, J., Qi, Y., Hu, X., Tan, M., Liu, Z., Zhang, J., Li, Q., Sander, M., Qiu, M., 2005. Generation of oligodendrocyte precursor cells from mouse dorsal spinal cord independent of Nkx6 regulation and Shh signaling. Neuron 45, 41–53. https://doi.org/10.1016/j.neuron.2004.12.028

Caicco, M.J., Cooke, M.J., Wang, Y., Tuladhar, A., Morshead, C.M., Shoichet, M.S., 2013. A hydrogel composite system for sustained epi-cortical delivery of Cyclosporin A to the brain for treatment of stroke. J. Control. Release 166, 197–202. https://doi.org/10.1016/j.jconrel.2013.01.002

Carroll, W.M., Jennings, A.R., Ironside, L.J., 1998. Identification of the adult resting progenitor cell by autoradiographic tracking of oligodendrocyte precursors in experimental CNS demyelination. Brain 121, 293–302. https://doi.org/10.1093/brain/121.2.293

Carruth, L.M., Demczuk, S., Mizel, S.B., 1991. Involvement of a calpain-like protease in the processing of the murine interleukin la precursor. J. Biol. Chem.

Casha, S., Yu, W.R., Fehlings, M.G., 2001. Oligodendroglial apoptosis occurs along degenerating axons and is associated with FAS and p75 expression following spinal cord injury in the rat. Neuroscience 103, 203–218. https://doi.org/10.1016/S0306-4522(00)00538-8

Casha, S., Zygun, D., McGowan, M.D., Bains, I., Yong, V.W., John Hurlbert, R., 2012. Results of a phase II placebo-controlled randomized trial of minocycline in acute spinal cord injury. Brain 135, 1224–1236. https://doi.org/10.1093/brain/aws072

Casper, K.B., McCarthy, K.D., 2006. GFAP-positive progenitor cells produce neurons and

oligodendrocytes throughout the CNS. Mol. Cell. Neurosci. 31, 676–684. https://doi.org/10.1016/j.mcn.2005.12.006

Cavnar, M.J., Zeng, S., Kim, T.S., Sorenson, E.C., Ocuin, L.M., Balachandran, V.P., Seifert, A.M., Greer, J.B., Popow, R., Crawley, M.H., Cohen, N.A., Green, B.L., Rossi, F., Besmer, P., Antonescu, C.R., DeMatteo, R.P., 2013. KIT oncogene inhibition drives intratumoral macrophage M2 polarization. J. Exp. Med. 210, 2873–2886. https://doi.org/10.1084/jem.20130875

Chen, C.-J., Kono, H., Golenbock, D., Reed, G., Akira, S., Rock, K.L., 2007. Identification of a key pathway required for the sterile inflammatory response triggered by dying cells. Nat. Med. 13, 851–6. https://doi.org/10.1038/nm1603

Chen, C.J., Kono, H., Golenbock, D., Reed, G., Akira, S., Rock, K.L., 2007. Identification of a key pathway required for the sterile inflammatory response triggered by dying cells. Nat. Med. https://doi.org/10.1038/nm1603

Chen, G.Y., Nuñez, G., 2010. Sterile inflammation: Sensing and reacting to damage. Nat. Rev. Immunol. 10, 826–837. https://doi.org/10.1038/nri2873

Chen, M.J., Yokomizo, T., Zeigler, B.M., Dzierzak, E., Speck, N.A., 2009. Runx1 is required for the endothelial to haematopoietic cell transition but not thereafter. Nature 457, 887–91. https://doi.org/10.1038/nature07619

Chen, Q., Zhang, H., Li, Q., An, Y., Herkenham, M., Lai, W., Popovich, P., Agarwal, S., Quan, N., 2009. Three promoters regulate tissue- and cell type-specific expression of murine interleukin-1 receptor type I. J. Biol. Chem. 284, 8703–8713. https://doi.org/10.1074/jbc.M808261200

Chen, Y., Balasubramaniyan, V., Peng, J., Hurlock, E.C., Tallquist, M., Li, J., Lu, Q.R., 2007. Isolation and culture of rat and mouse oligodendrocyte precursor cells. Nat. Protoc. 2, 1044–1051. https://doi.org/10.1038/nprot.2007.149

Chen, Y., Swanson, R.A., 2003. Astrocytes and brain injury. J. Cereb. Blood Flow Metab. 23, 137–149. https://doi.org/10.1097/01.WCB.0000044631.80210.3C

Chizzonite, R., Truitt, T., Kilian, P.L., Stern, A.S., Nunes, P., Parker, K.P., Kaffka, K.L., Chua, A.O., Lugg, D.K., Gubler, U., 1989. Two high-affinity interleukin 1 receptors represent separate gene products. Proc. Natl. Acad. Sci. U. S. A. 86, 8029–8033. https://doi.org/10.1073/pnas.86.20.8029

Chung, W.-S., Clarke, L.E., Wang, G.X., Stafford, B.K., Sher, A., Chakraborty, C., Joung, J., Foo, L.C., Thompson, A., Chen, C., Smith, S.J., Barres, B.A., 2013. Astrocytes mediate synapse elimination through MEGF10 and MERTK pathways. Nature 504, 394–400. https://doi.org/10.1038/nature12776

Clarke, L.E., Barres, B.A., 2013. Emerging roles of astrocytes in neural circuit development : Article : Nature Reviews Neuroscience. Nat Rev Neurosci. 14, 311–321. https://doi.org/10.1038/nrn3484.Emerging

Cohen, I., Rider, P., Carmi, Y., Braiman, A., Dotan, S., White, M.R., Voronov, E., Martin, M.U., Dinarello, C.A., Apte, R.N., 2010. Differential release of chromatin-bound IL-1 discriminates between necrotic and apoptotic cell death by the ability to induce sterile inflammation. Proc. Natl. Acad. Sci. https://doi.org/10.1073/pnas.0915018107

Cohen, Idan, Rider, P., Carmi, Y., Braiman, A., Dotan, S., White, M.R., Voronov, E., Martin, M.U., Dinarello, C.A., Apte, R.N., 2010. Differential release of chromatin-bound IL-1α discriminates between necrotic and apoptotic cell death by the ability to induce sterile inflammation. Proc. Natl. Acad. Sci. U. S. A. 107, 2574–2579. https://doi.org/10.1073/pnas.0915018107

Colton, C.A., Gilbert, D.L., 1987. Production of superoxide anions by a CNS macrophage, the microglia. FEBS Lett. 223, 284–288. https://doi.org/10.1016/0014-5793(87)80305-8

Copyright, E.N., Vol, N., 2004. P2X 7 Receptor Expression after Ischemia in the Cerebral Cortex of Rats 63, 686–699.

Coull, J.A.M., Beggs, S., Boudreau, D., Boivin, D., Tsuda, M., Inoue, K., Gravel, C., Salter, M.W., De Koninck, Y., 2005. BDNF from microglia causes the shift in

neuronal anion gradient underlying neuropathic pain. Nature 438, 1017–1021. https://doi.org/10.1038/nature04223

Cregg, J.M., DePaul, M.A., Filous, A.R., Lang, B.T., Tran, A., Silver, J., 2014. Functional regeneration beyond the glial scar. Exp. Neurol. 253, 197–207. https://doi.org/10.1016/j.expneurol.2013.12.024

Crowe, M.J., Bresnahan, J.C., Shuman, S.L., Masters, J.N., Beattie, M.S., 1997. Apoptosis and delayed degeneration after spinal cord injury in rats and monkeys. Nat. Med. 3, 73–6. https://doi.org/10.1038/nm0197-73

Dagher, N.N., Najafi, A.R., Kayala, K.M.N., Elmore, M.R.P., White, T.E., Medeiros, R., West, B.L., Green, K.N., 2015. Colony-stimulating factor 1 receptor inhibition prevents microglial plaque association and improves cognition in 3xTg-AD mice. J. Neuroinflammation 12, 1–14. https://doi.org/10.1186/s12974-015-0366-9

Davalos, D., Grutzendler, J., Yang, G., Kim, J. V., Zuo, Y., Jung, S., Littman, D.R., Dustin, M.L., Gan, W.B., 2005. ATP mediates rapid microglial response to local brain injury in vivo. Nat. Neurosci. 8, 752–758. https://doi.org/10.1038/nn1472

David, S., Lacroix, S., 2003. Molecular approaches to spinal cord repair. Annu. Rev. Neurosci. 26, 411–440. https://doi.org/10.1146/annurev.neuro.26.043002.094946

de Rivero Vaccari, J.P., Bastien, D., Yurcisin, G., Pineau, I., Dietrich, W.D., De Koninck, Y., Keane, R.W., Lacroix, S., 2012. P2X4 Receptors Influence Inflammasome Activation after Spinal Cord Injury. J. Neurosci. 32, 3058–3066. https://doi.org/10.1523/JNEUROSCI.4930-11.2012

De Souza, L.E.B., Malta, T.M., Kashima Haddad, S., Covas, D.T., 2016. Mesenchymal Stem Cells and Pericytes: To What Extent Are They Related? Stem Cells Dev. 25, 1843–1852. https://doi.org/10.1089/scd.2016.0109

Dejardin, E., Droin, N.M., Delhase, M., Haas, E., Cao, Y., Makris, C., Li, Z., Karin, M., Ware, C.F., Green, D.R., Diego, S., 2002. The Lymphotoxin-b Receptor Induces Different Patterns of Gene Expression via Two NF-kB Pathways University of

California San Diego 17, 525–535. https://doi.org/http://dx.doi.org/10.1016/j.jterra.2014.05.006

del Rio-Hortega, P.I., 1919. La microglia en estado normal, Bol la soc. ed.

Di Pardo, A., Amico, E., Scalabrì, F., Pepe, G., Castaldo, S., Elifani, F., Capocci, L., De Sanctis, C., Comerci, L., Pompeo, F., D'esposito, M., Filosa, S., Crispi, S., Maglione, V., 2017. Impairment of blood-brain barrier is an early event in R6/2 mouse model of Huntington Disease. Sci. Rep. 7, 1–8. https://doi.org/10.1038/srep41316

Didangelos, A., Puglia, M., Iberl, M., Sanchez-Bellot, C., Roschitzki, B., Bradbury, E.J., 2016. High-throughput proteomics reveal alarmins as amplifiers of tissue pathology and inflammation after spinal cord injury. Sci. Rep. 6, 1–15. https://doi.org/10.1038/srep21607

Dinarello, C.A., 2015. The history of fever, leukocytic pyrogen and interleukin-1. Temperature 2, 8–16. https://doi.org/10.1080/23328940.2015.1017086

Dinarello, C.A., 2014. Interleukin-1α neutralisation in patients with cancer. Lancet. Oncol. 15, 552–3. https://doi.org/10.1016/S1470-2045(14)70164-0

Dinarello, C.A., 2013. Overview of the interleukin-1 family of ligands and receptors. Semin. Immunol. 25, 389–393. https://doi.org/10.1016/j.smim.2013.10.001

Dinarello, C.A., 2009. Immunological and Inflammatory Functions of the Interleukin-1 Family. Annu. Rev. Immunol. https://doi.org/10.1146/annurev.immunol.021908.132612

Dinarello, C.A., 1994. The interleukin-1 family: 10 years of discovery. FASEB J. 8, 1314–1325. https://doi.org/10.1096/fasebj.8.15.8001745

Dinarello, C.A., 1991. Interleukin-1 and interleukin-1 antagonism. Blood 77, 1627–52. https://doi.org/10.3109/08830189809043005

Dinarello, C.A., Goldin, N.P., Wolff, S.M., 1974. Demonstration and characterization of

two distinct human leukocytic pyrogens. J. Exp. Med. 139, 1369–1381. https://doi.org/10.1084/jem.139.6.1369

Ding, A.H., Nathan, C.F., Stuehr, D.J., 1988. Release of Reactive Nitrogen Intermediates and Reactive Oxygen Intermediates From Mouse Peritoneal Macrophages. J. Immunol. 141, 2407–2412.

Domercq, M., Perez-Samartin, A., Aparicio, D., Alberdi, E., Pampliega, O., Matute, C., 2010. P2X7 receptors mediate ischemic damage to oligodendrocytes. Glia 58, 730–740. https://doi.org/10.1002/glia.20958

Donnelly, D.J., Longbrake, E.E., Shawler, T.M., Kigerl, K.A., Lai, W., Amy Tovar, C., Ransohoff, R.M., Popovich, P.G., 2011. Deficient CX3CR1 signaling promotes recovery after mouse spinal cord injury by limiting the recruitment andactivation of Ly6Clo/iNOS+ macrophages. J. Neurosci. 31, 9910–9922. https://doi.org/10.1523/JNEUROSCI.2114-11.2011

Dowling, D., Hamilton, C.M., O'Neill, S.M., 2008. A comparative analysis of cytokine responses, cell surface marker expression and MAPKs in DCs matured with LPS compared with a panel of TLR ligands. Cytokine 41, 254–262. https://doi.org/10.1016/j.cyto.2007.11.020

Dröge, W., 2002. Free radicals in the physiological control of cell function. Physiol. Rev. 82, 47–95. https://doi.org/10.1152/physrev.00018.2001

Duncan, G.J., Manesh, S.B., Hilton, B.J., Assinck, P., Liu, J., Moulson, A., Plemel, J.R., Tetzlaff, W., 2018. Locomotor recovery following contusive spinal cord injury does not require oligodendrocyte remyelination. Nat. Commun. 9. https://doi.org/10.1038/s41467-018-05473-1

Eddleston, M., Mucke, L., 1993. Molecular profile of reactive astrocytes-Implications for their role in neurologic disease. Neuroscience 54, 15–36. https://doi.org/10.1016/0306-4522(93)90380-X

Eigenbrod, T., Park, J.-H., Harder, J., Iwakura, Y., Núñez, G., 2008. Cutting edge: critical

role for mesothelial cells in necrosis-induced inflammation through the recognition of IL-1 alpha released from dying cells. J. Immunol. 181, 8194–8. https://doi.org/10.4049/jimmunol.181.12.8194

Elliott Donaghue, I., Tator, C.H., Shoichet, M.S., 2015. Sustained delivery of bioactive neurotrophin-3 to the injured spinal cord. Biomater. Sci. 3, 65–72. https://doi.org/10.1039/c4bm00311j

Elmore, M.R.P., Najafi, A.R., Koike, M.A., Dagher, N.N., Spangenberg, E.E., Rice, R.A., Kitazawa, M., Matusow, B., Nguyen, H., West, B.L., Green, K.N., 2014. Colony-stimulating factor 1 receptor signaling is necessary for microglia viability, unmasking a microglia progenitor cell in the adult brain. Neuron 82, 380–97. https://doi.org/10.1016/j.neuron.2014.02.040

Emery, B., 2010. Regulation of oligodendrocyte differentiation and myelination. Science (80-.). 330, 779–782. https://doi.org/10.1126/science.1190927

Emery, E., Aldana, P., Bunge, M.B., Puckett, W., Srinivasan, A., Keane, R.W., Bethea, J., Levi, A.D.O., 1998. Apoptosis after traumatic human spinal cord injury. J. Neurosurg. 89, 911–920. https://doi.org/10.3171/jns.1998.89.6.0911

Enokido, Y., Yoshitake, A., Ito, H., Okazawa, H., 2008. Age-dependent change of HMGB1 and DNA double-strand break accumulation in mouse brain. Biochem. Biophys. Res. Commun. 376, 128–133. https://doi.org/10.1016/j.bbrc.2008.08.108

Erblich, B., Zhu, L., Etgen, A.M., Dobrenis, K., Pollard, J.W., 2011. Absence of colony stimulation factor-1 receptor results in loss of microglia, disrupted brain development and olfactory deficits. PLoS One 6. https://doi.org/10.1371/journal.pone.0026317

Faber-Elman, A., Solomon, A., Abraham, J.A., Marikovsky, M., Schwartz, M., 1996. Involvement of wound-associated factors in rat brain astrocyte migratory response to axonal injury: In vitro simulation. J. Clin. Invest. 97, 162–171. https://doi.org/10.1172/JCI118385

Faraco, G., Fossati, S., Bianchi, M.E., Patrone, M., Pedrazzi, M., Sparatore, B., Moroni, F.,

Chiarugi, A., 2007. High mobility group box 1 protein is released by neural cells upon different stresses and worsens ischemic neurodegeneration in vitro and in vivo. J. Neurochem. 103, 590–603. https://doi.org/10.1111/j.1471-4159.2007.04788.x

Faulkner, J.R., 2004. Reactive Astrocytes Protect Tissue and Preserve Function after Spinal Cord Injury. J. Neurosci. 24, 2143–2155. https://doi.org/10.1523/JNEUROSCI.3547-03.2004

Fehlings, M.G., Tetreault, L.A., Aarabi, B., Anderson, P., Arnold, P.M., Brodke, D.S., Burns, A.S., Chiba, K., Dettori, J.R., Furlan, J.C., Hawryluk, G., Holly, L.T., Howley, S., Jeji, T., Kalsi-Ryan, S., Kotter, M., Kurpad, S., Kwon, B.K., Marino, R.J., Martin, A.R., Massicotte, E., Merli, G., Middleton, J.W., Nakashima, H., Nagoshi, N., Palmieri, K., Singh, A., Skelly, A.C., Tsai, E.C., Vaccaro, A., Wilson, J.R., Yee, A., Harrop, J.S., 2017. A Clinical Practice Guideline for the Management of Patients With Acute Spinal Cord Injury: Recommendations on the Type and Timing of Anticoagulant Thromboprophylaxis. Glob. Spine J. 7, 212S-220S. https://doi.org/10.1177/2192568217702107

Feil, R., Wagner, J., Metzger, D., Chambon, P., 1997. Regulation of Cre recombinase activity by mutated estrogen receptor ligand-binding domains. Biochem. Biophys. Res. Commun. 237, 752–7. https://doi.org/10.1006/bbrc.1997.7124

Feil, S., Valtcheva, N., Feil, R., 2009. Inducible Cre mice. Methods Mol. Biol. 530, 343–63. https://doi.org/10.1007/978-1-59745-471-1_18

Feuvre, R.A. Le, Brough, D., Touzani, O., Rothwell, N.J., 2003. Role of P2X 7 Receptors in Ischemic and Excitotoxic Brain Injury In Vivo. Blood 23, 381–384. https://doi.org/10.1097/01.WCB.0000048519.34839.97

Fiske, C.H., Subbarow, Y., 1929. Phosphorus compounds of muscle and liver. Science (80-.). https://doi.org/10.1126/science.70.1816.381-a

Fleming, J.C., Norenberg, M.D., Ramsay, D.A., Dekaban, G.A., Marcillo, A.E., Saenz, A.D., Pasquale-Styles, M., Dietrich, W.D., Weaver, L.C., 2006. The cellular

inflammatory response in human spinal cords after injury. Brain 129, 3249–3269. https://doi.org/10.1093/brain/awl296

Floriddia, E.M., Lourenço, T., Zhang, S., van Bruggen, D., Hilscher, M.M., Kukanja, P., Gonçalves dos Santos, J.P., Altınkök, M., Yokota, C., Llorens-Bobadilla, E., Mulinyawe, S.B., Grãos, M., Sun, L.O., Frisén, J., Nilsson, M., Castelo-Branco, G., Wai, M., 2020. Distinct oligodendrocyte populations have spatial preference and different responses to spinal cord injury 1–15. https://doi.org/10.1038/s41467-020-19453-x

Fogarty, M., Richardson, W.D., Kessaris, N., 2005. A subset of oligodendrocytes generated from radial glia in the dorsal spinal cord. Development 132, 1951–1959. https://doi.org/10.1242/dev.01777

Freigang, S., Ampenberger, F., Weiss, A., Kanneganti, T.D., Iwakura, Y., Hersberger, M., Kopf, M., 2013. Fatty acid-induced mitochondrial uncoupling elicits inflammasome-independent IL-1α and sterile vascular inflammation in atherosclerosis. Nat. Immunol. 14, 1045–1053. https://doi.org/10.1038/ni.2704

Freinbichler, W., Colivicchi, M.A., Stefanini, C., Bianchi, L., Ballini, C., Misini, B., Weinberger, P., Linert, W., Varešlija, D., Tipton, K.F., Della Corte, L., 2011. Highly reactive oxygen species: Detection, formation, and possible functions. Cell. Mol. Life Sci. 68, 2067–2079. https://doi.org/10.1007/s00018-011-0682-x

Fu, H., Hu, D., Zhang, L., Shen, X., Tang, P., 2018. Efficacy of Oligodendrocyte Progenitor Cell Transplantation in Rat Models with Traumatic Thoracic Spinal Cord Injury: A Systematic Review and Meta-Analysis. J. Neurotrauma 35, 2507–2518. https://doi.org/10.1089/neu.2017.5606

Fünfschilling, U., Supplie, L.M., Mahad, D., Boretius, S., Saab, A.S., Edgar, J., Brinkmann, B.G., Kassmann, C.M., Tzvetanova, I.D., Möbius, W., Diaz, F., Meijer, D., Suter, U., Hamprecht, B., Sereda, M.W., Moraes, C.T., Frahm, J., Goebbels, S., Nave, K.A., 2012. Glycolytic oligodendrocytes maintain myelin and long-term axonal integrity. Nature 485, 517–521. https://doi.org/10.1038/nature11007

Furusho, M., Roulois, A.J., Franklin, R.J.M., Bansal, R., 2015. Fibroblast growth factor signaling in oligodendrocyte-lineage cells facilitates recovery of chronically demyelinated lesions but is redundant in acute lesions. Glia 63, 1714–28. https://doi.org/10.1002/glia.22838

Gadani, S.P., Walsh, J.T., Smirnov, I., Zheng, J., Kipnis, J., 2015. The Glia-Derived Alarmin IL-33 Orchestrates the Immune Response and Promotes Recovery following CNS Injury. Neuron 85, 703–709. https://doi.org/10.1016/j.neuron.2015.01.013

Galea, J., Ogungbenro, K., Hulme, S., Patel, H., Scarth, S., Hoadley, M., Illingworth, K., McMahon, C.J., Tzerakis, N., King, A.T., Vail, A., Hopkins, S.J., Rothwell, N., Tyrrell, P., 2018. Reduction of inflammation after administration of interleukin-1 receptor antagonist following aneurysmal subarachnoid hemorrhage: Results of the Subcutaneous Interleukin-1Ra in SAH (SCIL-SAH) study. J. Neurosurg. 128, 515–523. https://doi.org/10.3171/2016.9.JNS16615

Galvan, M.D., Luchetti, S., Burgos, A.M., Nguyen, H.X., Hooshmand, M.J., Hamers, F.P.T., Anderson, A.J., 2008. Deficiency in complement C1q improves histological and functional locomotor outcome after spinal cord injury. J. Neurosci. 28, 13876–13888. https://doi.org/10.1523/JNEUROSCI.2823-08.2008

Garlanda, C., Dinarello, C.A., Mantovani, A., 2013. The interleukin-1 family: back to the future. Immunity 39, 1003–18. https://doi.org/10.1016/j.immuni.2013.11.010

Gasque, P., Singhrao, S.K., Neal, J.W., Wang, P., Sayah, S., Fontaine, M., Morgan, B.P., 1998. The receptor for complement anaphylatoxin C3a is expressed by myeloid cells and nonmyeloid cells in inflamed human central nervous system: analysis in multiple sclerosis and bacterial meningitis. J. Immunol. 160, 3543–54.

Geissmann, F., Manz, M.G., Jung, S., Sieweke, M.H., Merad, M., Ley, K., 2010. Development of monocytes, macrophages, and dendritic cells. Science 327, 656–61. https://doi.org/10.1126/science.1178331

Genoud, S., Lappe-Siefke, C., Goebbels, S., Radtke, F., Aguet, M., Scherer, S.S., Suter, U.,

Nave, K.A., Mantei, N., 2002. Notch1 control of oligodendrocyte differentiation in the spinal cord. J. Cell Biol. 158, 709–718. https://doi.org/10.1083/jcb.200202002

Gery, I., Waksman, B.H., 1972. Potentiation of the T-lymphocyte response to mitogens: II. The cellular source of potentiating mediator(s). J. Exp. Med. 136, 143–155. https://doi.org/10.1084/jem.136.1.143

Ginhoux, F., Greter, M., Leboeuf, M., Nandi, S., See, P., Gokhan, S., Mehler, M.F., Conway, S.J., Ng, L.G., Stanley, E.R., Samokhvalov, I.M., Merad, M., 2010. Fate mapping analysis reveals that adult microglia derive from primitive macrophages. Science 330, 841–5. https://doi.org/10.1126/science.1194637

Givogri, M.I., Costa, R.M., Schonmann, V., Silva, A.J., Campagnoni, A.T., Bongarzone, E.R., 2002. Central nervous system myelination in mice with deficient expression of Notch1 receptor. J. Neurosci. Res. 67, 309–320. https://doi.org/10.1002/jnr.10128

Goldmann, T., Wieghofer, P., Müller, P.F., Wolf, Y., Varol, D., Yona, S., Brendecke, S.M., Kierdorf, K., Staszewski, O., Datta, M., Luedde, T., Heikenwalder, M., Jung, S., Prinz, M., 2013. A new type of microglia gene targeting shows TAK1 to be pivotal in CNS autoimmune inflammation. Nat. Neurosci. 16, 1618–1626. https://doi.org/10.1038/nn.3531

Goldstein, R.S., Gallowitsch-Puerta, M., Yang, L., Rosas-Ballina, M., Huston, J.M., Czura, C.J., Lee, D.C., Ward, M.F., Bruchfeld, A.N., Wang, H., Lesser, M.L., Church, A.L., Litroff, A.H., Sama, A.E., Tracey, K.J., 2006. Elevated high-mobility group box 1 levels in patients with cerebral and myocardial ischemia. Shock. https://doi.org/10.1097/01.shk.0000209540.99176.72

Gong, G., Xiang, L., Yuan, L., Hu, L., Wu, W., Cai, L., Yin, L., Dong, H., 2014. Protective effect of glycyrrhizin, a direct HMGB1 inhibitor, on focal cerebral ischemia/reperfusion-induced inflammation, oxidative stress, and apoptosis in rats. PLoS One 9. https://doi.org/10.1371/journal.pone.0089450

Göritz, C., Dias, D.O., Tomilin, N., Barbacid, M., Shupliakov, O., Frisén, J., 2011. A

pericyte origin of spinal cord scar tissue. Science 333, 238–42. https://doi.org/10.1126/science.1203165

Graesser, D., Solowiej, A., Bruckner, M., Osterweil, E., Juedes, A., Davis, S., Ruddle, N.H., Engelhardt, B., Madri, J.A., 2002. Altered vascular permeability and early onset of experimental autoimmune encephalomyelitis in PECAM-1-deficient mice. J. Clin. Invest. 109, 383–392. https://doi.org/10.1172/JCI0213595

Graves, B.J., Hatada, M.H., Hendrickson, W.A., Miller, J.K., Madison, V.S., Satow, Y., 1990a. Structure of Interleukin lα at 2.7-Å Resolution. Biochemistry 29, 2679–2684. https://doi.org/10.1021/bi00463a009

Graves, B.J., Hatada, M.H., Hendrickson, W.A., Miller, J.K., Madison, V.S., Satow, Y., 1990b. Structure of interleukin 1 alpha at 2.7-A resolution. Biochemistry. https://doi.org/10.1021/bi00463a009

Gregorian, C., Nakashima, J., Belle, J. Le, Ohab, J., Kim, R., Liu, A., Smith, K.B., Groszer, M., Garcia, A.D., Sofroniew, M. V., Carmichael, S.T., Kornblum, H.I., Liu, X., Wu, H., 2009. Pten deletion in adult neural stem/progenitor cells enhances constitutive neurogenesis. J. Neurosci. 29, 1874–1886. https://doi.org/10.1523/JNEUROSCI.3095-08.2009

Gris, D., Marsh, D.R., Oatway, M.A., Chen, Y., Hamilton, E.F., Dekaban, G.A., Weaver, L.C., 2004. Transient Blockade of the CD11d/CD18 Integrin Reduces Secondary Damage after Spinal Cord Injury, Improving Sensory, Autonomic, and Motor Function. J. Neurosci. 24, 4043–4051. https://doi.org/10.1523/JNEUROSCI.5343-03.2004

Groß, O., Yazdi, A.S., Thomas, C.J., Masin, M., Heinz, L.X., Guarda, G., Quadroni, M., Drexler, S.K., Tschopp, J., 2012. Inflammasome Activators Induce Interleukin-1α Secretion via Distinct Pathways with Differential Requirement for the Protease Function of Caspase-1. Immunity 36, 388–400. https://doi.org/10.1016/j.immuni.2012.01.018

Gu, N., Peng, J., Murugan, M., Wang, X., Eyo, U.B., Sun, D., Ren, Y., DiCicco-Bloom, E., Young, W., Dong, H., Wu, L.-J., 2016. Spinal Microgliosis Due to Resident Microglial Proliferation Is Required for Pain Hypersensitivity after Peripheral Nerve Injury. Cell Rep. 16, 605–14. https://doi.org/10.1016/j.celrep.2016.06.018

Guo, J., Li, Yiqiao, Chen, Z., He, Z., Zhang, B., Li, Yonghuan, Hu, J., Han, M., Xu, Y., Li, Yongfu, 2015. N-acetylcysteine treatment following spinal cord trauma reduces neural tissue damage and improves locomotor function in mice. Mol. Med. Rep. 12, 37–44. https://doi.org/10.3892/mmr.2015.3390

Ha, Y.M., Kim, M.Y., Park, M.K., Lee, Y.S., Kim, Y.M., Kim, H.J., Lee, J.H., Chang, K.C., 2012. Higenamine reduces HMGB1 during hypoxia-induced brain injury by induction of heme oxygenase-1 through PI3K/Akt/Nrf-2 signal pathways. Apoptosis 17, 463–474. https://doi.org/10.1007/s10495-011-0688-8

Halder, S.K., Ueda, H., 2018. Amlexanox inhibits cerebral ischemia-induced delayed astrocytic high-mobility group box 1 release and subsequent brain damages. J. Pharmacol. Exp. Ther. 365, 27–36. https://doi.org/10.1124/jpet.117.245340

Hammond, E., Lang, J., Maeda, Y., Pleasure, D., Angus-Hill, M., Xu, J., Horiuchi, M., Deng, W., Guo, F., 2015. The wnt effector transcription factor 7-like 2 positively regulates oligodendrocyte differentiation in a manner independent of wnt/^{2}-catenin signaling. J. Neurosci. 35, 5007–5022. https://doi.org/10.1523/JNEUROSCI.4787-14.2015

Hara, M., Kobayakawa, K., Ohkawa, Y., Kumamaru, H., Yokota, K., Saito, T., Kijima, K., Yoshizaki, S., Harimaya, K., Nakashima, Y., Okada, S., 2017. Interaction of reactive astrocytes with type i collagen induces astrocytic scar formation through the integrin-N-cadherin pathway after spinal cord injury. Nat. Med. 23, 818–828. https://doi.org/10.1038/nm.4354

Hashimoto, M., Nitta, A., Fukumitsu, H., Nomoto, H., Shen, L., Furukawa, S., 2005. Inflammation-induced GDNF improves locomotor function after spinal cord injury. Neuroreport 16, 99–102. https://doi.org/10.1097/00001756-200502080-00004

Hayakawa, K., Miyamoto, N., Seo, J.H., Pham, L.D.D., Kim, K.W., Lo, E.H., Arai, K., 2013. High-mobility group box 1 from reactive astrocytes enhances the accumulation of endothelial progenitor cells in damaged white matter. J. Neurochem. https://doi.org/10.1111/jnc.12120

Haynes, S.E., Hollopeter, G., Yang, G., Kurpius, D., Dailey, M.E., Gan, W.B., Julius, D., 2006. The P2Y12 receptor regulates microglial activation by extracellular nucleotides. Nat. Neurosci. 9, 1512–1519. https://doi.org/10.1038/nn1805

Hellal, F., Hurtado, A., Ruschel, J., Flynn, K.C., Laskowski, C.J., Umlauf, M., Kapitein, L.C., Strikis, D., Lemmon, V., Bixby, J., Hoogenraad, C.C., Bradke, F., 2011. Microtubule stabilization reduces scarring and causes axon regeneration after spinal cord injury. Science 331, 928–31. https://doi.org/10.1126/science.1201148

Herrmann, J.E., Imura, T., Song, B., Qi, J., Ao, Y., Nguyen, T.K., Korsak, R.A., Takeda, K., Akira, S., Sofroniew, M. V., 2008. STAT3 is a critical regulator of astrogliosis and scar formation after spinal cord injury. J. Neurosci. 28, 7231–7243. https://doi.org/10.1523/JNEUROSCI.1709-08.2008

Hesp, Z.C., Goldstein, E. a., Miranda, C.J., Kaspar, B.K., McTigue, D.M., 2015. Chronic Oligodendrogenesis and Remyelination after Spinal Cord Injury in Mice and Rats. J. Neurosci. 35, 1274–1290. https://doi.org/10.1523/JNEUROSCI.2568-14.2015

Heye, A.K., Culling, R.D., Valdés Hernández, M.D.C., Thrippleton, M.J., Wardlaw, J.M., 2014. Assessment of blood-brain barrier disruption using dynamic contrast-enhanced MRI. A systematic review. NeuroImage Clin. 6, 262–274. https://doi.org/10.1016/j.nicl.2014.09.002

Hoeffel, G., Chen, J., Lavin, Y., Low, D., Almeida, F.F., See, P., Beaudin, A.E., Lum, J., Low, I., Forsberg, E.C., Zolezzi, F., Larbi, A., Ng, L.G., Chan, J.K.Y., Becher, B., Samokhvalov, I.M., Merad, M., Ginhoux, F., 2016. HHS Public Access 42, 665–678. https://doi.org/10.1016/j.immuni.2015.03.011.C-Myb

Hoppe, G., Talcott, K.E., Bhattacharya, S.K., Crabb, J.W., Sears, J.E., 2006. Molecular

basis for the redox control of nuclear transport of the structural chromatin protein Hmgb1. Exp. Cell Res. 312, 3526–3538. https://doi.org/10.1016/j.yexcr.2006.07.020

http://www.who.int/mediacentre/factsheets/fs384/fr/ [WWW Document], n.d.

https://clinicaltrials.gov/ct2/home [WWW Document], n.d.

Huang, Y., Xu, Z., Xiong, S., Sun, F., Qin, G., Hu, G., Wang, J., Zhao, L., Liang, Y.X., Wu, T., Lu, Z., Humayun, M.S., So, K.F., Pan, Y., Li, N., Yuan, T.F., Rao, Y., Peng, B., 2018. Repopulated microglia are solely derived from the proliferation of residual microglia after acute depletion. Nat. Neurosci. 21, 530–540. https://doi.org/10.1038/s41593-018-0090-8

Hughes, E.G., Kang, S.H., Fukaya, M., Bergles, D.E., 2013. Oligodendrocyte progenitors balance growth with self-repulsion to achieve homeostasis in the adult brain. Nat. Neurosci. 16, 668–76. https://doi.org/10.1038/nn.3390

Hunter, K.E., Sporn, M.B., Davies, A.M., 1993. Transforming growth factor-βs inhibit mitogen-stimulated proliferation of astrocytes. Glia 7, 203–211. https://doi.org/10.1002/glia.440070303

Huttner, W.B., Brand, M., 1997. Asymmetric division and polarity of neuroepithelial cells. Curr. Opin. Neurobiol. 7, 29–39. https://doi.org/10.1016/S0959-4388(97)80117-1

Idan, C., Peleg, R., Elena, V., Martin, T., Cicerone, T., Mareike, W., Lydia, B., Marina, F., Gerhard, M., Elisa, F.M., Dinarello, C.A., Ron, A.N., Robert, S., 2015. IL-1α is a DNA damage sensor linking genotoxic stress signaling to sterile inflammation and innate immunity. Sci. Rep. https://doi.org/10.1038/srep14756

Inoue, K., Koizumi, S., Tsuda, M., Shigemoto-Mogami, Y., 2003. Signaling of ATP receptors in glia-neuron interaction and pain. Life Sci. 74, 189–197. https://doi.org/10.1016/j.lfs.2003.09.006

Itoh, Y., Hayashi, H., Miyazawa, K., Kojima, S., Akahoshi, T., Onozaki, K., 2007. 17β-Estradiol Induces IL-1 α Gene Expression in Rheumatoid Fibroblast-Like Synovial

Cells through Estrogen Receptor α (ERα) and Augmentation of Transcriptional Activity of Sp1 by Dissociating Histone Deacetylase 2 from ERα . J. Immunol. 178, 3059–3066. https://doi.org/10.4049/jimmunol.178.5.3059

Jack, C.S., Arbour, N., Manusow, J., Montgrain, V., Blain, M., McCrea, E., Shapiro, A., Antel, J.P., 2005. TLR Signaling Tailors Innate Immune Responses in Human Microglia and Astrocytes. J. Immunol. 175, 4320–4330. https://doi.org/10.4049/jimmunol.175.7.4320

Jan, Y.N., Jan, L.Y., 2001. Development: Asymmetric cell division in the Drosophila nrevous system. Nat. Rev. Neurosci. 2, 772–779. https://doi.org/10.1038/35097516

Jansen, J., Hanks, S., Thompson, J.M., Dugan, M.J., Akard, L.P., 2005. Transplantation of hematopoietic stem cells from the peripheral blood. J. Cell. Mol. Med. 9, 37–50. https://doi.org/10.1111/j.1582-4934.2005.tb00335.x

Jansson, D., Rustenhoven, J., Feng, S., Hurley, D., Oldfield, R.L., Bergin, P.S., Mee, E.W., Faull, R.L.M., Dragunow, M., 2014. A role for human brain pericytes in neuroinflammation. J. Neuroinflammation 11, 1–20. https://doi.org/10.1186/1742-2094-11-104

Jantzen, H.M., Admon, A., Bell, S.P., Tjian, R., 1990. Nucleolar transcription factor hUBF contains a DNA-binding motif with homology to HMG proteins. Nature. https://doi.org/10.1038/344830a0

John, G.R., Lee, S.C., Song, X., Rivieccio, M., Brosnan, C.F., 2005. IL-1-regulated responses in astrocytes: relevance to injury and recovery. Glia 49, 161–76. https://doi.org/10.1002/glia.20109

Juurlink, B.H.J., 1997. Response of glial cells to ischemia: Roles of reactive oxygen species and glutathione. Neurosci. Biobehav. Rev. 21, 151–166. https://doi.org/10.1016/S0149-7634(96)00005-X

Kadi, L., Selvaraju, R., de Lys, P., Proudfoot, A.E.I., Wells, T.N.C., Boschert, U., 2006. Differential effects of chemokines on oligodendrocyte precursor proliferation and

myelin formation in vitro. J. Neuroimmunol. 174, 133–146. https://doi.org/10.1016/j.jneuroim.2006.01.011

Kang, C.E., Poon, P.C., Tator, C.H., Shoichet, M.S., 2009. A new paradigm for local and sustained release of therapeutic molecules to the injured spinal cord for neuroprotection and tissue repair. Tissue Eng. - Part A 15, 595–604. https://doi.org/10.1089/ten.tea.2007.0349

Kang, N., Hai, Y., Yang, J., Liang, F., Gao, C.-J., 2015. Hyperbaric oxygen intervention reduces secondary spinal cord injury in rats via regulation of HMGB1/ TLR4/NF-κB signaling pathway. Int. J. Clin. Exp. Pathol. 8, 1141–1153.

Karalija, A., Novikova, L.N., Kingham, P.J., Wiberg, M., Novikov, L.N., 2012. Neuroprotective effects of N-acetyl-cysteine and acetyl-L-carnitine after spinal cord injury in adult rats. PLoS One 7. https://doi.org/10.1371/journal.pone.0041086

Karin, M., Ben-Neriah, Y., 2000. Phosphorylation meets ubiquitination: the control of NF-[kappa]B activity. Annu. Rev. Immunol. 18, 621–63. https://doi.org/10.1146/annurev.immunol.18.1.621

Kawase, T., Sato, K., Ueda, T., Yoshida, M., 2008. Distinct domains in HMGB1 Are involved in specific intramolecular and nucleosomal interactions. Biochemistry 47, 13991–13996. https://doi.org/10.1021/bi8013449

Kessaris, N., Fogarty, M., Iannarelli, P., Grist, M., Wegner, M., Richardson, W.D., 2006. Competing waves of oligodendrocytes in the forebrain and postnatal elimination of an embryonic lineage. Nat. Neurosci. 9, 173–179. https://doi.org/10.1038/nn1620

Khan, M., Im, Y. Bin, Shunmugavel, A., Gilg, A.G., Dhindsa, R.K., Singh, A.K., Singh, I., 2009. Administration of S-nitrosoglutathione after traumatic brain injury protects the neurovascular unit and reduces secondary injury in a rat model of controlled cortical impact. J. Neuroinflammation 6, 32. https://doi.org/10.1186/1742-2094-6-32

Kierdorf, K., Erny, D., Goldmann, T., Sander, V., Schulz, C., Perdiguero, E.G., Wieghofer, P., Heinrich, A., Riemke, P., Hölscher, C., Müller, D.N., Luckow, B., Brocker, T.,

Debowski, K., Fritz, G., Opdenakker, G., Diefenbach, A., Biber, K., Heikenwalder, M., Geissmann, F., Rosenbauer, F., Prinz, M., 2013. Microglia emerge from erythromyeloid precursors via Pu.1-and Irf8-dependent pathways. Nat. Neurosci. 16, 273–280. https://doi.org/10.1038/nn.3318

Kigerl, K., McGaughy, V., Popovich, P., 2009. A comparative analysis of lesion development and intraspinal inflammation in mice following SCI. J. Comp. Neurol. 494, 578–594. https://doi.org/10.1002/cne.20827.A

Kigerl, K.A., Gensel, J.C., Ankeny, D.P., Alexander, J.K., Donnelly, D.J., Popovich, P.G., 2009. Identification of two distinct macrophage subsets with divergent effects causing either neurotoxicity or regeneration in the injured mouse spinal cord. J. Neurosci. 29, 13435–13444. https://doi.org/10.1523/JNEUROSCI.3257-09.2009

Kigerl, K.A., Lai, W., Wallace, L.M., Yang, H., Popovich, P.G., 2017. High mobility group box-1 (HMGB1) is increased in injured mouse spinal cord and can elicit neurotoxic inflammation. Brain. Behav. Immun. 1, 1–12. https://doi.org/10.1016/j.bbi.2017.11.018

Kim, B., Lee, Y., Kim, E., Kwak, A., Ryoo, S., Bae, S.H., Azam, T., Kim, S., Dinarello, C.A., 2013. The interleukin-1α precursor is biologically active and is likely a key alarmin in the IL-1 family of cytokines. Front. Immunol. 4, 1–9. https://doi.org/10.3389/fimmu.2013.00391

Kim, J. Bin, Joon, S.C., Yu, Y.M., Nam, K., Piao, C.S., Kim, S.W., Lee, M.H., Han, P.L., Park, J.S., Lee, J.K., 2006. HMGB1, a novel cytokine-like mediator linking acute neuronal death and delayed neuroinflammation in the postischemic brain. J. Neurosci. 26, 6413–6421. https://doi.org/10.1523/JNEUROSCI.3815-05.2006

Kimura, H., Inukai, Y., Takii, T., Furutani, Y., Shibata, Y., Hayashi, H., Sakurada, S., Okamoto, T., Inoue, J.I., Oomoto, Y., Onozaki, K., 1998. Molecular analysis of constitutive IL-1α gene expression in human melanoma cells: Autocrine stimulation through NF-κB activation by endogenous IL-1α. Cytokine 10, 872–879. https://doi.org/10.1006/cyto.1998.0369

Kinnally, K.W., Peixoto, P.M., Ryu, S.Y., Dejean, L.M., 2011. Is mPTP the gatekeeper for necrosis, apoptosis, or both? Biochim. Biophys. Acta - Mol. Cell Res. 1813, 616–622. https://doi.org/10.1016/j.bbamcr.2010.09.013

Klämbt, C., 2009. Modes and regulation of glial migration in vertebrates and invertebrates. Nat. Rev. Neurosci. 10, 769–779. https://doi.org/10.1038/nrn2720

Kobayashi, Y., Yamamoto, K., Saido, T., Kawasaki, H., Oppenheim, J.J., Matsushima, K., 1990. Identification of calcium-activated neutral protease as a processing enzyme of human interleukin 1 alpha. Proc. Natl. Acad. Sci. U. S. A. https://doi.org/10.1073/pnas.87.14.5548

Kogata, N., Arai, Y., Pearson, J.T., Hashimoto, K., Hidaka, K., Koyama, T., Somekawa, S., Nakaoka, Y., Ogawa, M., Adams, R.H., Okada, M., Mochizuki, N., 2006. Cardiac ischemia activates vascular endothelial cadherin promoter in both preexisting vascular cells and bone marrow cells involved in neovascularization. Circ. Res. 98, 897–904. https://doi.org/10.1161/01.RES.0000218193.51136.ad

Kohta, M., Kohmura, E., Yamashita, T., 2009. Inhibition of TGF-β1 promotes functional recovery after spinal cord injury. Neurosci. Res. 65, 393–401. https://doi.org/10.1016/j.neures.2009.08.017

Konishi, H., Okamoto, T., Hara, Y., Komine, O., Tamada, H., Maeda, M., Osako, F., Kobayashi, M., Nishiyama, A., Kataoka, Y., Takai, T., Udagawa, N., Jung, S., Ozato, K., Tamura, T., Tsuda, M., Yamanaka, K., Ogi, T., Sato, K., Kiyama, H., 2020. Astrocytic phagocytosis is a compensatory mechanism for microglial dysfunction. EMBO J. 1–18. https://doi.org/10.15252/embj.2020104464

Korhonen, P., Kanninen, K.M., Lehtonen, Š., Lemarchant, S., Puttonen, K.A., Oksanen, M., Dhungana, H., Loppi, S., Pollari, E., Wojciechowski, S., Kidin, I., García-Berrocoso, T., Giralt, D., Montaner, J., Koistinaho, J., Malm, T., 2015. Immunomodulation by interleukin-33 is protective in stroke through modulation of inflammation. Brain. Behav. Immun. 49, 322–336. https://doi.org/10.1016/j.bbi.2015.06.013

Kotter, M.R., Setzu, A., Sim, F.J., Van Rooijen, N., Franklin, R.J.M., 2001. Macrophage depletion impairs oligodendrocyte remyelination following lysolecithin-induced demyelination. Glia 35, 204–212. https://doi.org/10.1002/glia.1085

Kovac, A., Erickson, M.A., Banks, W.A., 2011. Brain microvascular pericytes are immunoactive in culture: Cytokine, chemokine, nitric oxide, and LRP-1 expression in response to lipopolysaccharide. J. Neuroinflammation 8, 139. https://doi.org/10.1186/1742-2094-8-139

Krasnow, S.M., Knoll, J.G., Verghese, S.C., Levasseur, P.R., Marks, D.L., 2017. Amplification and propagation of interleukin-1β signaling by murine brain endothelial and glial cells. J. Neuroinflammation 14, 1–18. https://doi.org/10.1186/s12974-017-0908-4

Kremer, D., Aktas, O., Hartung, H.P., Küry, P., 2011. The complex world of oligodendroglial differentiation inhibitors. Ann. Neurol. 69, 602–618. https://doi.org/10.1002/ana.22415

Kroner, A., Greenhalgh, A.D., Zarruk, J.G., PassosdosSantos, R., Gaestel, M., David, S., 2014. TNF and Increased Intracellular Iron Alter Macrophage Polarization to a Detrimental M1 Phenotype in the Injured Spinal Cord. Neuron 83, 1098–1116. https://doi.org/10.1016/j.neuron.2014.07.027

Krueger, H., Noonan, V.K., Trenaman, L.M., Joshi, P., Rivers, C.S., 2013. The economic burden of traumatic spinal cord injury in Canada. Chronic Dis. Inj. Can. 33, 113–22.

Kubes, P., Deniset, J.F., 2016. Recent advances in understanding neutrophils. F1000Research 5, 1–10. https://doi.org/10.12688/f1000research.9691.1

Kwon, B.K., Okon, E.B., Tsai, E., Beattie, M.S., Bresnahan, J.C., Magnuson, D.K., Reier, P.J., McTigue, D.M., Popovich, P.G., Blight, A.R., Oudega, M., Guest, J.D., Weaver, L.C., Fehlings, M.G., Tetzlaff, W., 2011. A grading system to evaluate objectively the strength of pre-clinical data of acute neuroprotective therapies for clinical translation in spinal cord injury. J. Neurotrauma 28, 1525–1543.

https://doi.org/10.1089/neu.2010.1296

Lacroix, S., Hamilton, L.K., Vaugeois, A., Beaudoin, S., Breault-Dugas, C., Pineau, I., Lévesque, S.A., Grégoire, C.A., Fernandes, K.J.L., 2014. Central canal ependymal cells proliferate extensively in response to traumatic spinal cord injury but not demyelinating lesions. PLoS One 9. https://doi.org/10.1371/journal.pone.0085916

Lagord, C., Berry, M., Logan, A., 2002. Expression of TGFβ2 but not TGFβ1 correlates with the deposition of scar tissue in the lesioned spinal cord. Mol. Cell. Neurosci. 20, 69–92. https://doi.org/10.1006/mcne.2002.1121

Lalancette-Hébert, M., Gowing, G., Simard, A., Yuan, C.W., Kriz, J., 2007. Selective ablation of proliferating microglial cells exacerbates ischemic injury in the brain. J. Neurosci. 27, 2596–2605. https://doi.org/10.1523/JNEUROSCI.5360-06.2007

Lawrence, T., 2009. The nuclear factor NF-kappaB pathway in inflammation. Cold Spring Harb. Perspect. Biol. 1, a001651. https://doi.org/10.1101/cshperspect.a001651

Lawson, L.J., Perry, V.H., Dri, P., Gordon, S., 1990. Heterogeneity in the distribution and morphology of microglia in the normal adult mouse brain. Neuroscience 39, 151–170. https://doi.org/10.1016/0306-4522(90)90229-W

Lawson, L.J., Perry, V.H., Gordon, S., 1992. Turnover of resident microglia in the normal adult mouse brain. Neuroscience 48, 405–415. https://doi.org/10.1016/0306-4522(92)90500-2

Lee, S.C., Liu, W., Dickson, D.W., Brosnan, C.F., Berman, J.W., 1993. Cytokine production by human fetal microglia and astrocytes. Differential induction by lipopolysaccharide and IL-1 beta. J. Immunol. 150, 2659–67.

Lee, S.M., Rosen, S., Weinstein, P., van Rooijen, N., Noble-Haeusslein, L.J., 2011. Prevention of both neutrophil and monocyte recruitment promotes recovery after spinal cord injury. J. Neurotrauma 28, 1893–1907. https://doi.org/10.1089/neu.2011.1860

Lefrançais, E., Cayrol, C., 2012. Mechanisms of IL-33 processing and secretion: Differences and similarities between IL-1 family members. Eur. Cytokine Netw. 23, 120–127. https://doi.org/10.1684/ecn.2012.0320

Lévesque, S.A., Paré, A., Mailhot, B., Bellver-Landete, V., Kébir, H., Lécuyer, M.-A., Alvarez, J.I., Prat, A., de Rivero Vaccari, J.P., Keane, R.W., Lacroix, S., 2016. Myeloid cell transmigration across the CNS vasculature triggers IL-1β-driven neuroinflammation during autoimmune encephalomyelitis in mice. J. Exp. Med. 213, 929–49. https://doi.org/10.1084/jem.20151437

Lewén, A., Matz, P., Chan, P.H., 2000. Free radical pathways in CNS injury. J. Neurotrauma 17, 871–890. https://doi.org/10.1089/neu.2000.17.871

Lewis, A.M., Varghese, S., Xu, H., Alexander, H.R., 2006. Interleukin-1 and cancer progression: The emerging role of interleukin-1 receptor antagonist as a novel therapeutic agent in cancer treatment. J. Transl. Med. 4, 1–12. https://doi.org/10.1186/1479-5876-4-48

Lewis, J., Raff, M., Roberts, K., 2002. Molecular Biology of the Cell (4th Ed). J. Biol. Educ. 37, 45–47. https://doi.org/10.1080/00219266.2002.9655847

Ley, K., Laudanna, C., Cybulsky, M.I., Nourshargh, S., 2007. Getting to the site of inflammation: The leukocyte adhesion cascade updated. Nat. Rev. Immunol. 7, 678–689. https://doi.org/10.1038/nri2156

Li, G.L., Farooque, M., Holtz, A., Olsson, Y., 1999. Apoptosis of oligodendrocytes occurs for long distances away from the primary injury after compression trauma to rat spinal cord. Acta Neuropathol. 98, 473–480. https://doi.org/10.1007/s004010051112

Li, M., Sun, L., Luo, Y., Xie, C., Pang, Y., Li, Y., 2014. High-mobility group box 1 released from astrocytes promotes the proliferation of cultured neural stem/progenitor cells. Int. J. Mol. Med. 34, 705–714. https://doi.org/10.3892/ijmm.2014.1820

Li, M.O., Flavell, R.A., 2008. TGF beta: A master of all T cell trades. Cell 134, 392–404. https://doi.org/10.1016/j.pestbp.2011.02.012.Investigations

Li, N., Leung, G.K.K., Li, N., Leung, G.K.K., 2015. Oligodendrocyte Precursor Cells in Spinal Cord Injury: A Review and Update. Biomed Res. Int. 2015, 1–20. https://doi.org/10.1155/2015/235195

Li, Q., Lin, Y., Huang, W., Zhou, Y., Chen, X., Wang, B., Cai, Z., Xue, J., Zhang, W., Yu, T., Wang, H., He, J., 2016. Serum IL-33 Is a Novel Diagnostic and Prognostic Biomarker in Acute Ischemic Stroke 7, 614–622.

Li, Q., Powell, N., Zhang, H., Belevych, N., Ching, S., Chen, Q., Sheridan, J., Whitacre, aroline, Quan, N., 2011. Endothelial IL-1R1 is a critical mediator of EAE pathogenesis. Brain. Behav. Immun. 25, 160–167. https://doi.org/10.1016/j.bbi.2010.09.009

Li, S., Stys, P.K., 2000. Mechanisms of ionotropic glutamate receptor-mediated excitotoxicity in isolated spinal cord white matter. J. Neurosci. 20, 1190–1198. https://doi.org/10.1523/jneurosci.20-03-01190.2000

Li, Y., Li, X., Qu, Y., Huang, J., Zhu, T., Zhao, F., Li, S., Mu, D., 2017. Role of HMGB1 translocation to neuronal nucleus in rat model with septic brain injury. Neurosci. Lett. 645, 90–96. https://doi.org/10.1016/j.neulet.2016.11.047

Liddelow, S., Barres, B., 2015. SnapShot: Astrocytes in Health and Disease. Cell 162, 1170-1170.e1. https://doi.org/10.1016/j.cell.2015.08.029

Liddelow, S.A., Guttenplan, K.A., Clarke, L.E., Bennett, F.C., Bohlen, C.J., Schirmer, L., Bennett, M.L., Münch, A.E., Chung, W.-S., Peterson, T.C., Wilton, D.K., Frouin, A., Napier, B.A., Panicker, N., Kumar, M., Buckwalter, M.S., Rowitch, D.H., Dawson, V.L., Dawson, T.M., Stevens, B., Barres, B.A., 2017a. Neurotoxic reactive astrocytes are induced by activated microglia. Nature. https://doi.org/10.1038/nature21029

Liddelow, S.A., Guttenplan, K.A., Clarke, L.E., Bennett, F.C., Bohlen, C.J., Schirmer, L., Bennett, M.L., Münch, A.E., Chung, W.S., Peterson, T.C., Wilton, D.K., Frouin, A., Napier, B.A., Panicker, N., Kumar, M., Buckwalter, M.S., Rowitch, D.H., Dawson, V.L., Dawson, T.M., Stevens, B., Barres, B.A., 2017b. Neurotoxic reactive astrocytes

are induced by activated microglia. Nature 541, 481–487. https://doi.org/10.1038/nature21029

Lin, J.T., Martin, S.L., Xia, L., Gorham, J.D., 2005. TGF-β1 Uses Distinct Mechanisms to Inhibit IFN-γ Expression in CD4 + T Cells at Priming and at Recall: Differential Involvement of Stat4 and T-bet . J. Immunol. 174, 5950–5958. https://doi.org/10.4049/jimmunol.174.10.5950

Lindholm, D., Castren, E., Kiefer, R., Zafra, F., Thoenen, H., 1992. Transforming growth factor-β1 in the rat brain: Increase after injury and inhibition of astrocyte proliferation. J. Cell Biol. 117, 395–400. https://doi.org/10.1083/jcb.117.2.395

Liou, G.Y., Storz, P., 2010. Reactive oxygen species in cancer, Free Radical Research. https://doi.org/10.3109/10715761003667554

Liu, D., Ling, X., Wen, J., Liu, J., 2000. The role of reactive nitrogen species in secondary spinal cord injury: Formation of nitric oxide, peroxynitrite, and nitrated protein. J. Neurochem. 75, 2144–2154. https://doi.org/10.1046/j.1471-4159.2000.0752144.x

Liu, D., Liu, J., Sun, D., Alcock, N.W., Wen, J., 2003. Spinal cord injury increases iron levels: catalytic production of hydroxyl radicals. Free Radic. Biol. Med. 34, 64–71. https://doi.org/10.1016/s0891-5849(02)01184-x

Liu, D., Liu, J., Sun, D., Wen, J., 2004. The time course of hydroxyl radical formation following spinal cord injury: The possible role of the iron-catalyzed Haber-Weiss reaction. J. Neurotrauma 21, 805–816. https://doi.org/10.1089/0897715041269650

Liu, D., Sybert, T.E., Qian, H., Liu, J., 1998. Superoxide production after spinal injury detected by microperfusion of cytochrome c. Free Radic. Biol. Med. 25, 298–304. https://doi.org/10.1016/S0891-5849(98)00055-0

Liu, X., Yamashita, T., Chen, Q., Belevych, N., McKim, D.B., Tarr, A.J., Coppola, V., Nath, N., Nemeth, D.P., Syed, Z.W., Sheridan, J.F., Godbout, J.P., Zuo, J., Quan, N., 2015. Interleukin 1 type 1 receptor restore: A genetic mouse model for studying interleukin 1 receptor-mediated effects in specific cell types. J. Neurosci. 35, 2860–

2870. https://doi.org/10.1523/JNEUROSCI.3199-14.2015

Llorens-Bobadilla, E., Chell, J.M., Le Merre, P., Wu, Y., Zamboni, M., Bergenstråhle, J., Stenudd, M., Sopova, E., Lundeberg, J., Shupliakov, O., Carlén, M., Frisén, J., 2020. A latent lineage potential in resident neural stem cells enables spinal cord repair. Science 370. https://doi.org/10.1126/science.abb8795

Logan, A., Berry, M., Gonzalez, A.M., Frautschy, S.A., Sporn, M.B., Baird, A., 1994. Effects of Transforming Growth Factor β1, on Scar Production in the Injured Central Nervous System of the Rat. Eur. J. Neurosci. 6, 355–363. https://doi.org/10.1111/j.1460-9568.1994.tb00278.x

Lomedico, P.T., Gubler, U., Hellmann, C.P., Dukovich, M., Giri, J.G., Pan, Y.C., Collier, K., Semionow, R., Chua, A.O., Mizel, S.B., n.d. Cloning and expression of murine interleukin-1 cDNA in Escherichia coli. Nature 312, 458–62. https://doi.org/10.1038/312458a0

Losey, P., Anthony, D.C., 2014. Impact of vasculature damage on the outcome of spinal cord injury: A novel collagenase-induced model may give new insights into the mechanisms involved. Neural Regen. Res. 9, 1783–1786. https://doi.org/10.4103/1673-5374.143422

Lotze, M.T., Tracey, K.J., 2005. High-mobility group box 1 protein (HMGB1): Nuclear weapon in the immune arsenal. Nat. Rev. Immunol. 5, 331–342. https://doi.org/10.1038/nri1594

Lu, Q.R., Yuk, D.I., Alberta, J.A., Zhu, Z., Pawlitzky, I., Chan, J., McMahon, A.P., Stiles, C.D., Rowitch, D.H., 2000. Sonic hedgehog-regulated oligodendrocyte lineage genes encoding bHLH proteins in the mammalian central nervous system. Neuron 25, 317–329. https://doi.org/10.1016/S0896-6273(00)80897-1

Luheshi, N.M., Kov??cs, K.J., Lopez-Castejon, G., Brough, D., Denes, A., 2011a. Interleukin-1?? expression precedes IL-1?? after ischemic brain injury and is localised to areas of focal neuronal loss and penumbral tissues. J. Neuroinflammation 8, 186.

https://doi.org/10.1186/1742-2094-8-186

Luheshi, N.M., Kovács, K.J., Lopez-Castejon, G., Brough, D., Denes, A., 2011b. Interleukin-1α expression precedes IL-1β after ischemic brain injury and is localised to areas of focal neuronal loss and penumbral tissues. J. Neuroinflammation 8, 4–8. https://doi.org/10.1186/1742-2094-8-186

Luheshi, N.M., Rothwell, N.J., Brough, D., 2009. The dynamics and mechanisms of interleukin-1α and β nuclear import. Traffic 10, 16–25. https://doi.org/10.1111/j.1600-0854.2008.00840.x

Luo, Q., Fan, Y., Lin, L., Wei, J., Li, Z., Li, Y., Nakae, S., 2018. N EUROSCIENCE Interleukin-33 Protects Ischemic Brain Injury by Regulating Specific Microglial Activities. Neuroscience 385, 75–89. https://doi.org/10.1016/j.neuroscience.2018.05.047

Lytle, J.M., Chittajallu, R., Wrathall, J.R., Gallo, V., 2009. NG2 cell response in the CNP-EGFP mouse after contusive spinal cord injury. Glia 57, 270–285. https://doi.org/10.1002/glia.20755

Lytle, J.M., Wrathall, J.R., 2007. Glial cell loss, proliferation and replacement in the contused murine spinal cord. Eur. J. Neurosci. 25, 1711–1724. https://doi.org/10.1111/j.1460-9568.2007.05390.x

Mabon, P.J., Weaver, L.C., Dekaban, G.A., 2000. Inhibition of monocyte/macrophage migration to a spinal cord injury site by an antibody to the integrin αD: A potential new anti-inflammatory treatment. Exp. Neurol. 166, 52–64. https://doi.org/10.1006/exnr.2000.7488

Mailhot, B., Christin, M., Tessandier, N., Sotoudeh, C., Bretheau, F., Turmel, R., Pellerin, È., Wang, F., Bories, C., Joly-Beauparlant, C., De Koninck, Y., Droit, A., Cicchetti, F., Scherrer, G., Boilard, E., Sharif-Naeini, R., Lacroix, S., 2020. Neuronal interleukin-1 receptors mediate pain in chronic inflammatory diseases. J. Exp. Med. 217, 1–19. https://doi.org/10.1084/jem.20191430

Man, S.M., Kanneganti, T.-D., 2015. Regulation of inflammasome activation. Immunol. Rev. 265, 6–21. https://doi.org/10.1111/imr.12296

Manuscript, A., Structures, T., 2009. HMGB1: The Jack-of-all-Trades Protein is a Master DNA Repair Mechanic 6, 247–253. https://doi.org/10.1111/j.1743-6109.2008.01122.x.Endothelial

March, C.J., Mosley, B., Larsen, A., Cerretti, D.P., Braedt, G., Price, V., Gillis, S., Henney, C.S., Kronheim, S.R., Grabstein, K., 1985. Cloning, sequence and expression of two distinct human interleukin-1 complementary DNAs. Nature. https://doi.org/10.1038/315641a0

Martinon, F., Burns, K., Tschopp, J., 2002. The inflammasome: a molecular platform triggering activation of inflammatory caspases and processing of proIL-beta. Mol. Cell 10, 417–26. https://doi.org/10.1016/s1097-2765(02)00599-3

Massagué, J., 2000. How cells read TGF-beta signals. Nat. Rev. Mol. Cell Biol. 1, 169–78. https://doi.org/10.1038/35043051

Matute, C., Domercq, M., Sánchez-Gómez, M.V., 2006. Glutamate-mediated glial injury: Mechanisms and clinical importance. Glia 53, 212–224. https://doi.org/10.1002/glia.20275

Matute, C., Sánchez-Gómez, M.V., Martínez-Millán, L., Miledi, R., 1997. Glutamate receptor-mediated toxicity in optic nerve oligodendrocytes. Proc. Natl. Acad. Sci. U. S. A. 94, 8830–8835. https://doi.org/10.1073/pnas.94.16.8830

Matute, C., Torre, I., Pérez-Cerdá, F., Pérez-Samartín, A., Alberdi, E., Etxebarria, E., Arranz, A.M., Ravid, R., Rodríguez-Antigüedad, A., Sánchez-Gómez, M.V., Domercq, M., 2007. P2X7 receptor blockade prevents ATP excitotoxicity in oligodendrocytes and ameliorates experimental autoimmune encephalomyelitis. J. Neurosci. 27, 9525–9533. https://doi.org/10.1523/JNEUROSCI.0579-07.2007

Mayadas, T.N., Cullere, X., Lowell, C.A., 2014. The multifaceted functions of neutrophils. Annu. Rev. Pathol. Mech. Dis. 9, 181–218. https://doi.org/10.1146/annurev-pathol-

020712-164023

McCandless, E.E., Budde, M., Lees, J.R., Dorsey, D., Lyng, E., Klein, R.S., 2009. IL-1R signaling within the central nervous system regulates CXCL12 expression at the blood-brain barrier and disease severity during experimental autoimmune encephalomyelitis. J. Immunol. 183, 613–20. https://doi.org/10.4049/jimmunol.0802258

McCarthy, D.A., Clark, R.R., Bartling, T.R., Trebak, M., Melendez, J.A., 2013a. Redox control of the senescence regulator interleukin-1α and the secretory phenotype. J. Biol. Chem. 288, 32149–32159. https://doi.org/10.1074/jbc.M113.493841

McCarthy, D.A., Ranganathan, A., Subbaram, S., Flaherty, N.L., Patel, N., Trebak, M., Hempel, N., Melendez, J.A., 2013b. Redox-control of the alarmin, Interleukin-1α. Redox Biol. 1, 218–225. https://doi.org/10.1016/j.redox.2013.03.001

Mcdonald, J.W., Althomsons, S.P., Hyrc, K.L., Choi, D.W., Goldberg, M.P., 1998. Oligodendrocytes from forebrain are highly vulnerable to AMPA/kainate receptor-mediated excitotoxicity. Nat. Med. 4, 291–297. https://doi.org/10.1038/nm0398-291

McDowell, T.L., Symons, J.A., Duff, G.W., 2005. Human interleukin-1α gene expression is regulated by Sp1 and a transcriptional repressor. Cytokine 30, 141–153. https://doi.org/10.1016/j.cyto.2004.12.010

McMahan, C.J., Slack, J.L., Mosley, B., Cosman, D., Lupton, S.D., Brunton, L.L., Grubin, C.E., Wignall, J.M., Jenkins, N.A., Brannan, C.I., 1991. A novel IL-1 receptor, cloned from B cells by mammalian expression, is expressed in many cell types. EMBO J. 10, 2821–32.

McTigue, D.M., Popovich, P.G., Morgan, T.E., Stokes, B.T., 2000. Localization of transforming growth factor-β1 and receptor mRNA after experimental spinal cord injury. Exp. Neurol. 163, 220–230. https://doi.org/10.1006/exnr.2000.7372

McTigue, D.M., Wei, P., Stokes, B.T., 2001. Proliferation of NG2-positive cells and altered oligodendrocyte numbers in the contused rat spinal cord. J. Neurosci. 21, 3392–400.

https://doi.org/0270-6474/01/213392-09$15.00/0

MEDAWAR, P.B., 1948. Immunity to homologous grafted skin; the fate of skin homografts transplanted to the brain, to subcutaneous tissue, and to the anterior chamber of the eye. Br. J. Exp. Pathol. 29, 58–69.

Medsker, B., Forno, E., Simhan, H., Juan, C., Sciences, R., 2016a. HHS Public Access 70, 773–779. https://doi.org/10.1097/OGX.0000000000000256.Prenatal

Medsker, B., Forno, E., Simhan, H., Juan, C., Sciences, R., 2016b. The redox state of the alarmin HMGB1 is a pivotal factor in neuroinflammatory and microglial priming: a role for the NLRP3 inflammasome 70, 773–779. https://doi.org/10.1097/OGX.0000000000000256.Prenatal

Melani, A., Amadio, S., Gianfriddo, M., Vannucchi, M.G., Volontè, C., Bernardi, G., Pedata, F., Sancesario, G., 2006. P2X7 receptor modulation on microglial cells and reduction of brain infarct caused by middle cerebral artery occlusion in rat. J. Cereb. Blood Flow Metab. 26, 974–982. https://doi.org/10.1038/sj.jcbfm.9600250

Melani, A., Turchi, D., Vannucchi, M.G., Cipriani, S., Gianfriddo, M., Pedata, F., 2005. ATP extracellular concentrations are increased in the rat striatum during in vivo ischemia. Neurochem. Int. 47, 442–448. https://doi.org/10.1016/j.neuint.2005.05.014

Meletis, K., Barnabé-Heider, F., Carlén, M., Evergren, E., Tomilin, N., Shupliakov, O., Frisén, J., 2008. Spinal cord injury reveals multilineage differentiation of ependymal cells. PLoS Biol. 6, 1494–1507. https://doi.org/10.1371/journal.pbio.0060182

Merkle, F.T., Tramontin, A.D., García-Verdugo, J.M., Alvarez-Buylla, A., 2004. Radial glia give rise to adult neural stem cells in the subventricular zone. Proc. Natl. Acad. Sci. U. S. A. 101, 17528–32. https://doi.org/10.1073/pnas.0407893101

Mhatre V. Ho and Kelsey C. Martin, J.-A.L., 2012. 基因的改变NIH Public Access. Bone 23, 1–7. https://doi.org/10.1002/stem.245.Human

Micheau, O., Tschopp, J., 2003. Induction of TNF receptor I-mediated apoptosis via two

sequential signaling complexes. Cell 114, 181–190. https://doi.org/10.1016/S0092-8674(03)00521-X

Mildner, A., Schmidt, H., Nitsche, M., Merkler, D., Hanisch, U.K., Mack, M., Heikenwalder, M., Brück, W., Priller, J., Prinz, M., 2007. Microglia in the adult brain arise from Ly-6ChiCCR2+ monocytes only under defined host conditions. Nat. Neurosci. 10, 1544–1553. https://doi.org/10.1038/nn2015

Miron, V.E., Boyd, A., Zhao, J.-W., Yuen, T.J., Ruckh, J.M., Shadrach, J.L., Wijngaarden, P. Van, Wagers, A.J., Williams, A., van Wijngaarden, P., Wagers, A.J., Williams, A., Franklin, R.J.M., Ffrench-Constant, C., 2013. Europe PMC Funders Group M2 microglia / macrophages drive oligodendrocyte differentiation during CNS remyelination. Nat. Neurosci. 16, 1211–1218. https://doi.org/10.1038/nn.3469.M2

Miyazono, K., ten Dijke, P., Heldin, C.H., 2000. TGF-beta signaling by Smad proteins. Adv. Immunol. 75, 115–57. https://doi.org/10.1016/s0065-2776(00)75003-6

Molofsky, A.B., Savage, A., Locksley, R.M., 2016. Interleukin-33 in tissue homeostasis, injury and inflammation Ari. Immunity 42, 1005–1019. https://doi.org/10.1016/j.immuni.2015.06.006.Interleukin-33

Monvoisin, A., Alva, J.A., Hofmann, J.J., Zovein, A.C., Lane, T.F., Iruela-Arispe, M.L., 2006. VE-cadherin-CreERT2 transgenic mouse: A model for inducible recombination in the endothelium. Dev. Dyn. 235, 3413–3422. https://doi.org/10.1002/dvdy.20982

Moreau-Fauvarque, C., Kumanogoh, A., Camand, E., Jaillard, C., Barbin, G., Boquet, I., Love, C., Jones, E.Y., Kikutani, H., Lubetzki, C., Dusart, I., Chédotal, A., 2003. The transmembrane semaphorin Sema4D/CD100, an inhibitor of axonal growth, is expressed on oligodendrocytes and upregulated after CNS lesion. J. Neurosci. 23, 9229–9239. https://doi.org/10.1523/jneurosci.23-27-09229.2003

Mosley, B., Urdal, D.L., Prickett, K.S., Larsen, A., Cosman, D., Conlon, P.J., Gillis, S., Dower, S.K., 1987. The interleukin-1 receptor binds the human interleukin-1 alpha precursor but not the interleukin-1 beta precursor. J. Biol. Chem.

Mosley, K., Cuzner, M.L., 1996. Receptor-mediated phagocytosis of myelin by macrophages and microglia: Effect of opsonization and receptor blocking agents. Neurochem. Res. 21, 481–487. https://doi.org/10.1007/BF02527713

Mrdjen, D., Pavlovic, A., Hartmann, F.J., Schreiner, B., Utz, S.G., Leung, B.P., Lelios, I., Heppner, F.L., Kipnis, J., Merkler, D., Greter, M., Becher, B., 2018. Erratum: High-Dimensional Single-Cell Mapping of Central Nervous System Immune Cells Reveals Distinct Myeloid Subsets in Health, Aging, and Disease (Immunity (2018) 48(2) (380–395.e6) (S1074761318300323) (10.1016/j.immuni.2018.01.011)). Immunity 48, 599. https://doi.org/10.1016/j.immuni.2018.02.014

Muhammad, S., Barakat, W., Stoyanov, S., Murikinati, S., Yang, H., Tracey, K.J., Bendszus, M., Rossetti, G., Nawroth, P.P., Bierhaus, A., Schwaninger, M., 2008. The HMGB1 Receptor RAGE Mediates Ischemic Brain Damage. J. Neurosci. https://doi.org/10.1523/JNEUROSCI.2435-08.2008

Nadeau, S., Rivest, S., 1999. Effects of circulating tumor necrosis factor on the neuronal activity and expression of the genes encoding the tumor necrosis factor receptors (p55 and p75) in the rat brain: A view from the blood-brain barrier. Neuroscience 93, 1449–1464. https://doi.org/10.1016/S0306-4522(99)00225-0

Nakajo, M., Uezono, N., Nakashima, H., Wake, H., Komiya, S., Nishibori, M., Nakashima, K., 2018. Therapeutic time window of anti-high mobility group box-1 antibody administration in mouse model of spinal cord injury. Neurosci. Res. 4–11. https://doi.org/10.1016/j.neures.2018.03.004

Nery, S., Wichterle, H., Fishell, G., 2001. Sonic hedgehog contributes to oligodendrocyte specification in the mammalian forebrain. Development 128, 527–540.

Nesic, O., Perez-Polo, R., Xu, G.Y., McAdoo, D., High, K.W., Hulsebosch, C., High, K.W., Hulsebosch, C., 2001. IL-1 receptor antagonist prevents apoptosis and caspase-3 activation after spinal cord injury. J. Neurotrauma 18, 947–956. https://doi.org/10.1089/089771501750451857

Netea, M.G., Quintin, J., Van Der Meer, J.W.M., 2011. Trained immunity: A memory for innate host defense. Cell Host Microbe 9, 355–361. https://doi.org/10.1016/j.chom.2011.04.006

Nguyen, G.T., Green, E.R., Mecsas, J., 2017. Neutrophils to the ROScue: Mechanisms of NADPH oxidase activation and bacterial resistance. Front. Cell. Infect. Microbiol. 7. https://doi.org/10.3389/fcimb.2017.00373

Nguyen, L., Rothwell, N.J., Pinteaux, E., Boutin, H., 2011. Contribution of interleukin-1 receptor accessory protein b to interleukin-1 actions in neuronal cells. NeuroSignals 19, 222–230. https://doi.org/10.1159/000330803

Nikić, I., Merkler, D., Sorbara, C., Brinkoetter, M., Kreutzfeldt, M., Bareyre, F.M., Brück, W., Bishop, D., Misgeld, T., Kerschensteiner, M., 2011. A reversible form of axon damage in experimental autoimmune encephalomyelitis and multiple sclerosis. Nat. Med. 17, 495–499. https://doi.org/10.1038/nm.2324

Nilsson, P., Hillered, L., Olsson, Y., Sheardown, M.J., Hansen, A.J., 1993. Regional Changes in Interstitial K^+ and Ca^{2+} Levels following Cortical Compression Contusion Trauma in Rats. J. Cereb. Blood Flow Metab. 13, 183–192. https://doi.org/10.1038/jcbfm.1993.22

Nimmerjahn, A., Kirchhoff, F., Helmchen, F., 2005. Resting microglial cells are highly dynamic surveillants of brain parenchyma in vivo. Neuroforum 11, 95–96. https://doi.org/10.1515/nf-2005-0304

Nishiyama, A., Komitova, M., Suzuki, R., Zhu, X., 2009. Polydendrocytes (NG2 cells): multifunctional cells with lineage plasticity. Nat. Rev. Neurosci. 10, 9–22. https://doi.org/10.1038/nrn2495

Noonan, V.K., Fingas, M., Farry, A., Baxter, D., Singh, A., Fehlings, M.G., Dvorak, M.F., 2012. Incidence and prevalence of spinal cord injury in Canada: A national perspective. Neuroepidemiology 38, 219–226. https://doi.org/10.1159/000336014

O'Neill, L.A.J., Dinarello, C.A., 2000. The IL-1 receptor/toll-like receptor superfamily:

Crucial receptors for inflammation and host defense. Immunol. Today 21, 206–209. https://doi.org/10.1016/S0167-5699(00)01611-X

Okada, S., Nakamura, M., Katoh, H., Miyao, T., Shimazaki, T., Ishii, K., Yamane, J., Yoshimura, A., Iwamoto, Y., Toyama, Y., Okano, H., 2006. Conditional ablation of Stat3 or Socs3 discloses a dual role for reactive astrocytes after spinal cord injury. Nat. Med. 12, 829–834. https://doi.org/10.1038/nm1425

Orentas, D.M., Hayes, J.E., Dyer, K.L., Miller, R.H., 1999. Sonic hedgehog signaling is required during the appearance of spinal cord oligodendrocyte precursors. Development 126, 2419–2429.

Osmanov, T., Ugrinova, I., Pasheva, E., 2013. The chaperone like function of the nonhistone protein HMGB1. Biochem. Biophys. Res. Commun. https://doi.org/10.1016/j.bbrc.2013.02.008

Oyinbo, C.A., 2011. Secondary injury mechanisms in traumatic spinal cord injury a nugget. Acta Neurobiol. Exp. (Wars). 71, 281–299.

P A Tranque, R Calle, F Naftolin, R.R., 1992. Involvement of protein kinase-C in the mitogenic effect of insulin-like growth factor-I on rat astrocytes. Endocrinology Volume 131.

Papatheodorou, A., Stein, A., Bank, M., Sison, C.P., Gibbs, K., Davies, P., Bloom, O., 2017. High-Mobility Group Box 1 (HMGB1) Is Elevated Systemically in Persons with Acute or Chronic Traumatic Spinal Cord Injury. J. Neurotrauma 34, 746–754. https://doi.org/10.1089/neu.2016.4596

Paré, A., Mailhot, B., Lévesque, S.A., Juzwik, C., Doss, P.M.I.A., Lécuyer, M.A., Prat, A., Rangachari, M., Fournier, A., Lacroix, S., 2018. IL-1β enables CNS access to CCR2hi monocytes and the generation of pathogenic cells through GM-CSF released by CNS endothelial cells. Proc. Natl. Acad. Sci. U. S. A. 115, E1194–E1203. https://doi.org/10.1073/pnas.1714948115

Parkhurst, C.N., Yang, G., Ninan, I., Savas, J.N., Yates, J.R., Lafaille, J.J., Hempstead,

B.L., Littman, D.R., Gan, W., 2013. Microglia promote learning-dependent synapse formation through brain-derived neurotrophic factor. Cell 155, 1596–609. https://doi.org/10.1016/j.cell.2013.11.030

Paul M Carvey, Bill Hendey, A.J.M., 2009. The Blood Brain Barrier in Neurodegenerative Disease: A. Journal. Neurochem. 111, 291–314. https://doi.org/10.1111/j.1471-4159.2009.06319.x.The

Pedata, F., Dettori, I., Coppi, E., Melani, A., Fusco, I., Corradetti, R., Pugliese, A.M., 2016. Purinergic signalling in brain ischemia. Neuropharmacology 104, 105–130. https://doi.org/10.1016/j.neuropharm.2015.11.007

Perdiguero, E.G., Klapproth, K., Schulz, C., Busch, K., Azzoni, E., Crozet, L., Garner, H., Trouillet, C., De Bruijn, M., Geissmann, F., Rodewald, H.-R., 2015. Tissue-resident macrophages originate from yolk sac-derived erythro-myeloid progenitors. Exp. Hematol. 43, S64. https://doi.org/10.1016/j.exphem.2015.06.130

Pérez-Cerdá, F., Sánchez-Gómez, M.V., Matute, C., 2015. Pío del Río hortega and the discovery of the oligodendrocytes. Front. Neuroanat. 9, 7–12. https://doi.org/10.3389/fnana.2015.00092

Pérez-Flores, G., Lévesque, S.A., Pacheco, J., Vaca, L., Lacroix, S., Pérez-Cornejo, P., Arreola, J., 2015. The P2X7/P2X4 interaction shapes the purinergic response in murine macrophages. Biochem. Biophys. Res. Commun. 467, 484–490. https://doi.org/10.1016/j.bbrc.2015.10.025

Perkins, N.D., Gilmore, T.D., 2006. Good cop, bad cop: The different faces of NF-κB. Cell Death Differ. 13, 759–772. https://doi.org/10.1038/sj.cdd.4401838

Peters, V.A., Joesting, J.J., Freund, G.G., 2013. IL-1 receptor 2 (IL-1R2) and its role in immune regulation. Brain. Behav. Immun. 32, 1–8. https://doi.org/10.1016/j.bbi.2012.11.006

Pichery, M., Mirey, E., Mercier, P., Lefrancais, E., Dujardin, A., Ortega, N., Girard, J.-P., 2012. Endogenous IL-33 Is Highly Expressed in Mouse Epithelial Barrier Tissues,

Lymphoid Organs, Brain, Embryos, and Inflamed Tissues: In Situ Analysis Using a Novel Il-33-LacZ Gene Trap Reporter Strain. J. Immunol. 188, 3488–3495. https://doi.org/10.4049/jimmunol.1101977

Pineau, I., Lacroix, S., 2007. Proinflammatory Cytokine Synthesis in the Injured Mouse Spinal Cord : Multiphasic Expression Pattern and Identification of the Cell Types Involved. J. Comp. Neurol. 285, 267–285. https://doi.org/10.1002/cne

Pineau, I., Sun, L., Bastien, D., Lacroix, S., 2010. Astrocytes initiate inflammation in the injured mouse spinal cord by promoting the entry of neutrophils and inflammatory monocytes in an IL-1 receptor/MyD88-dependent fashion. Brain. Behav. Immun. 24, 540–553. https://doi.org/10.1016/j.bbi.2009.11.007

Plemel, J.R., Manesh, S.B., Sparling, J.S., Tetzlaff, W., 2013. Myelin inhibits oligodendroglial maturation and regulates oligodendrocytic transcription factor expression. Glia 61, 1471–1487. https://doi.org/10.1002/glia.22535

Pomeshchik, Y., Kidin, I., Korhonen, P., Savchenko, E., Jaronen, M., Lehtonen, S., Wojciechowski, S., Kanninen, K., Koistinaho, J., Malm, T., 2015a. Interleukin-33 treatment reduces secondary injury and improves functional recovery after contusion spinal cord injury. Brain. Behav. Immun. 44, 68–81. https://doi.org/10.1016/j.bbi.2014.08.002

Pomeshchik, Y., Kidin, I., Korhonen, P., Savchenko, E., Jaronen, M., Lehtonen, S., Wojciechowski, S., Kanninen, K., Koistinaho, J., Malm, T., 2015b. Interleukin-33 treatment reduces secondary injury and improves functional recovery after contusion spinal cord injury. Brain. Behav. Immun. 44, 68–81. https://doi.org/10.1016/j.bbi.2014.08.002

Popovich, P.G., Guan, Z., McGaughy, V., Fisher, L., Hickey, W.F., Basso, D.M., 2002. The neuropathological and behavioral consequences of intraspinal microglial/macrophage activation. J. Neuropathol. Exp. Neurol. 61, 623–633. https://doi.org/10.1093/jnen/61.7.623

Popovich, P.G., Guan, Z., Wei, P., Huitinga, I., Van Rooijen, N., Stokes, B.T., 1999. Depletion of hematogenous macrophages promotes partial hindlimb recovery and neuroanatomical repair after experimental spinal cord injury. Exp. Neurol. 158, 351–365. https://doi.org/10.1006/exnr.1999.7118

Popovich, P.G., Hickey, W.F., 2001. Bone marrow chimeric rats reveal the unique distribution of resident and recruited macrophages in the contused rat spinal cord. J. Neuropathol. Exp. Neurol. 60, 676–685. https://doi.org/10.1093/jnen/60.7.676

Popovich, P.G., Wei, P., Stokes, B.T., 1997. Cellular inflammatory response after spinal cord injury in Sprague-Dawley and Lewis rats. J. Comp. Neurol. 377, 443–64. https://doi.org/10.1002/(sici)1096-9861(19970120)377:3<443::aid-cne10>3.0.co;2-s

Pradillo, J.M., Denes, A., Greenhalgh, A.D., Boutin, H., Drake, C., McColl, B.W., Barton, E., Proctor, S.D., Russell, J.C., Rothwell, N.J., Allan, S.M., 2012. Delayed administration of interleukin-1 receptor antagonist reduces ischemic brain damage and inflammation in comorbid rats. J. Cereb. Blood Flow Metab. 32, 1810–1819. https://doi.org/10.1038/jcbfm.2012.101

Pringle, N.P., Richardson, W.D., 1993. A singularity of PDGF alpha-receptor expression in the dorsoventral axis of the neural tube may define the origin of the oligodendrocyte lineage. Development 117, 525–533.

Prinz, M., Mildner, A., 2011. Microglia in the CNS: Immigrants from another world. Glia 59, 177–187. https://doi.org/10.1002/glia.21104

Proebstl, D., Voisin, M.B., Woodfin, A., Whiteford, J., D'Acquisto, F., Jones, G.E., Rowe, D., Nourshargh, S., 2012. Pericytes support neutrophil subendothelial cell crawling and breaching of venular walls in vivo. J. Exp. Med. 209, 1219–1234. https://doi.org/10.1084/jem.20111622

Profyris, C., Cheema, S.S., Zang, D., Azari, M.F., Boyle, K., Petratos, S., 2004. Degenerative and regenerative mechanisms governing spinal cord injury. Neurobiol. Dis. 15, 415–436. https://doi.org/10.1016/j.nbd.2003.11.015

Qian, J., Zhu, L., Li, Q., Belevych, N., Chen, Q., Zhao, F., Herness, S., Quan, N., 2012. Interleukin-1R3 mediates interleukin-1-induced potassium current increase through fast activation of Akt kinase. Proc. Natl. Acad. Sci. U. S. A. 109, 12189–12194. https://doi.org/10.1073/pnas.1205207109

Qiu, Y., Yang, J., Wang, W., Zhao, W., Peng, F., Xiang, Y., Chen, G., Chen, T., Chai, C., Zheng, S., Watkins, D.J., Feng, J., 2014. HMGB1-Promoted and TLR2/4-Dependent NK Cell Maturation and Activation Take Part in Rotavirus-Induced Murine Biliary Atresia. PLoS Pathog. 10. https://doi.org/10.1371/journal.ppat.1004011

Quail, D.F., Bowman, R.L., Akkari, L., Quick, M.L., Alberto, J., Huse, J.T., Holland, E.C., Sutton, J.C., Johanna, A., 2017. CSF1R inhibition in gliomas 352, 1–38. https://doi.org/10.1126/science.aad3018.The

Quarles, P.M. and R.H., 1998. Characteristic Composition of Myelin. Basic Neurochemistry: Molecular, Cellular and Medical Aspects. 6th edition.

Ransohoff, R.M., Cardona, A.E., 2010. The myeloid cells of the central nervous system parenchyma. Nature 468, 253–262. https://doi.org/10.1038/nature09615

Rapalino, O., Lazarov-Spiegler, O., Agranov, E., Velan, G.J., Yoles, E., Fraidakis, M., Solomon, A., Gepstein, R., Katz, A., Belkin, M., Hadani, M., Schwartz, M., 1998. Implantation of stimulated homologous macrophages results in partial recovery of paraplegic rats. Nat. Med. 4, 814–821. https://doi.org/10.1038/nm0798-814

Ravanelli, A.M., Appel, B., 2015. Motor neurons and oligodendrocytes arise from distinct cell lineages by progenitor recruitment. Genes Dev. 29, 2504–2515. https://doi.org/10.1101/gad.271312.115

Revised nomenclature for antigen-nonspecific T cell proliferation and helper factors., 1979. . J. Immunol. 123, 2928–9.

Rice, R.A., Spangenberg, E.E., Yamate-Morgan, H., Lee, R.J., Arora, R.P.S., Hernandez, M.X., Tenner, A.J., West, B.L., Green, K.N., 2015. Elimination of microglia improves functional outcomes following extensive neuronal loss in the hippocampus. J.

Neurosci. 35, 9977–9989. https://doi.org/10.1523/JNEUROSCI.0336-15.2015

Richardson, P.M., Lu, X., 1994. Inflammation and axonal regeneration. J. Neurol. 242, 3–5. https://doi.org/10.1007/BF00939244

Richardson, W.D., Smith, H.K., Sun, T., Pringle, N.P., Hall, A., Woodruff, R., 2000. Oligodendrocyte lineage and the motor neuron connection. Glia 29, 136–142. https://doi.org/10.1002/(SICI)1098-1136(20000115)29:2<136::AID-GLIA6>3.0.CO;2-G

Rider, P., Carmi, Y., Guttman, O., Braiman, A., Cohen, I., Voronov, E., White, M.R., Dinarello, C.A., Apte, R.N., 2011. IL-1 and IL-1 Recruit Different Myeloid Cells and Promote Different Stages of Sterile Inflammation. J. Immunol. 187, 4835–4843. https://doi.org/10.4049/jimmunol.1102048

Rider, P., Carmi, Y., Voronov, E., Apte, R.N., 2013a. Interleukin-1α. Semin. Immunol. 25, 430–438. https://doi.org/10.1016/j.smim.2013.10.005

Rider, P., Carmi, Y., Voronov, E., Apte, R.N., 2013b. Interleukin-1α. Semin. Immunol. 25, 430–438. https://doi.org/10.1016/j.smim.2013.10.005

Rider, P., Kaplanov, I., Romzova, M., Braiman, L., Braiman, A., Voronov, E., Apte, R.N., 2012. The transcription of the alarmin cytokine interleukin-1 alpha is controlled by hypoxia inducible factors 1 and 2 alpha in hypoxic cells. Front. Immunol. 3, 1–7. https://doi.org/10.3389/fimmu.2012.00290

Rivers, L.E., Young, K.M., Rizzi, M., Jamen, F., Psachoulia, K., Wade, A., Kessaris, N., Richardson, W.D., 2008. PDGFRA/NG2 glia generate myelinating oligodendrocytes and piriform projection neurons in adult mice. Nat. Neurosci. 11, 1392–401. https://doi.org/10.1038/nn.2220

Robinson, J.M., 2008. Reactive oxygen species in phagocytic leukocytes. Histochem. Cell Biol. 130, 281–297. https://doi.org/10.1007/s00418-008-0461-4

Rothwell, N.J., Luheshi, G.N., 2000. Interleukin 1 in the brain: Biology, pathology and

therapeutic target. Trends Neurosci. 23, 618–625. https://doi.org/10.1016/S0166-2236(00)01661-1

Rowitch, D.H., Kriegstein, A.R., 2010. Developmental genetics of vertebrate glial-cell specification. Nature 468, 214–222. https://doi.org/10.1038/nature09611

Rustenhoven, J., Jansson, D., Smyth, L.C., Dragunow, M., 2017. Brain Pericytes As Mediators of Neuroinflammation. Trends Pharmacol. Sci. 38, 291–304. https://doi.org/10.1016/j.tips.2016.12.001

Saab, A.S., Tzvetavona, I.D., Trevisiol, A., Baltan, S., Dibaj, P., Kusch, K., Möbius, W., Goetze, B., Jahn, H.M., Huang, W., Steffens, H., Schomburg, E.D., Pérez-Samartín, A., Pérez-Cerdá, F., Bakhtiari, D., Matute, C., Löwel, S., Griesinger, C., Hirrlinger, J., Kirchhoff, F., Nave, K.A., 2016. Oligodendroglial NMDA Receptors Regulate Glucose Import and Axonal Energy Metabolism. Neuron 91, 119–132. https://doi.org/10.1016/j.neuron.2016.05.016

Sapojnikova, N., Maman, J., Myers, F.A., Thorne, A.W., Vorobyev, V.I., Crane-Robinson, C., 2005. Biochemical observation of the rapid mobility of nuclear HMGB1. Biochim. Biophys. Acta - Gene Struct. Expr. 1729, 57–63. https://doi.org/10.1016/j.bbaexp.2005.03.002

Saraste, M., Sibbald, P.R., Wittinghofer, A., 1990. The P-loop - a common motif in ATP- and GTP-binding proteins. Trends Biochem. Sci. 15, 430–434. https://doi.org/10.1016/0968-0004(90)90281-F

Sas, A.R., Carbajal, K.S., Jerome, A.D., Menon, R., Yoon, C., Kalinski, A.L., Giger, R.J., Segal, B.M., 2020. A new neutrophil subset promotes CNS neuron survival and axon regeneration. Nat. Immunol. https://doi.org/10.1038/s41590-020-00813-0

Sauer, B., 1987. Functional expression of the cre-lox site-specific recombination system in the yeast Saccharomyces cerevisiae. Mol. Cell. Biol. 7, 2087–2096. https://doi.org/10.1128/mcb.7.6.2087

Sauer, B., Henderson, N., 1988. Site-specific DNA recombination in mammalian cells by

the Cre recombinase of bacteriophage P1. Proc. Natl. Acad. Sci. U. S. A. 85, 5166–5170. https://doi.org/10.1073/pnas.85.14.5166

Scaffidi, P., Misteli, T., Bianchi, M.E., 2002. Release of chromatin protein HMGB1 by necrotic cells triggers inflammation. Nature 418, 191–195. https://doi.org/10.1038/nature00858

Schmid, J.A., Birbach, A., 2008. IκB kinase β (IKKβ/IKK2/IKBKB)-A key molecule in signaling to the transcription factor NF-κB. Cytokine Growth Factor Rev. 19, 157–165. https://doi.org/10.1016/j.cytogfr.2008.01.006

Schmierer, B., Hill, C.S., 2007. TGFβ-SMAD signal transduction: Molecular specificity and functional flexibility. Nat. Rev. Mol. Cell Biol. 8, 970–982. https://doi.org/10.1038/nrm2297

Schnell, L., 1999. Acute inflammatory responses to mechanical lesions in the CNS: Differences between brain and spinal cord. Eur. J. Neurosci. 11, 3648–3658. https://doi.org/10.1046/j.1460-9568.1999.00792.x

Schoenwolf, G.C., Alvarez, I.S., 1989. Roles of neuroepithelial cell rearrangement and division in shaping of the avian neural plate. Development 106, 427–439.

Schroder, K., Tschopp, J., 2010. The Inflammasomes. Cell 140, 821–832. https://doi.org/10.1016/j.cell.2010.01.040

Schulz, C., Perdiguero, E.G., Chorro, L., Szabo-rogers, H., Pollard, J.W., Frampton, J., Liu, K.J., Geissmann, F., 2012. A Lineage of Myeloid Cells Independent of Myb and Hematopoietic Stem Cells 86–91.

Schulze, J., Zierath, D., Tanzi, P., Cain, K., Shibata, D., Dressel, A., Becker, K., 2013. Severe stroke induces long-lasting alterations of high-mobility group Box 1. Stroke 44, 246–248. https://doi.org/10.1161/STROKEAHA.112.676072

Schütze, S., Wiegmann, K., Machleidt, T., Krönke, M., 1995. TNF-Induced Activation of NF-κB. Immunobiology 193, 193–203. https://doi.org/10.1016/S0171-2985(11)80543-

7

Schwab, J.M., Guo, L., Schluesener, H.J., 2005. Spinal cord injury induces early and persistent lesional P2X4receptor expression. J. Neuroimmunol. 163, 185–189. https://doi.org/10.1016/j.jneuroim.2005.02.016

Senftleben, U., Cao, Y., Xiao, G., Greten, F.R., Krähn, G., Bonizzi, G., Chen, Y., Hu, Y., Fong, A., Sun, S.C., Karin, M., 2001. Activation by IKKα of a second, evolutionary conserved, NF-κB signaling pathway. Science (80-.). 293, 1495–1499. https://doi.org/10.1126/science.1062677

Shechter, R., London, A., Varol, C., Raposo, C., Cusimano, M., Yovel, G., Rolls, A., Mack, M., Pluchino, S., Martino, G., Jung, S., Schwartz, M., 2009. Infiltrating blood-derived macrophages are vital cells playing an anti-inflammatory role in recovery from spinal cord injury in mice. PLoS Med. 6. https://doi.org/10.1371/journal.pmed.1000113

Sheng, J., Ruedl, C., Karjalainen, K., 2015. Most Tissue-Resident Macrophages Except Microglia Are Derived from Fetal Hematopoietic Stem Cells. Immunity 43, 382–393. https://doi.org/10.1016/j.immuni.2015.07.016

Sheng, W.S., Hu, S., Feng, A., Rock, R.B., 2013. Reactive oxygen species from human astrocytes induced functional impairment and oxidative damage. Neurochem. Res. 38, 2148–59. https://doi.org/10.1007/s11064-013-1123-z

Shi, Y., Zhang, L., Teng, J., Miao, W., 2018. HMGB1 mediates microglia activation via the TLR4/NF-κB pathway in coriaria lactone induced epilepsy. Mol. Med. Rep. 17, 5125–5131. https://doi.org/10.3892/mmr.2018.8485

Siegenthaler, M.M., Tu, M.K., Keirstead, H.S., 2007. The extent of myelin pathology differs following contusion and transection spinal cord injury. J. Neurotrauma 24, 1631–1646. https://doi.org/10.1089/neu.2007.0302

Sierra, A., Encinas, J.M., Deudero, J.J.P., Chancey, J.H., Enikolopov, G., Overstreet-Wadiche, L.S., Tsirka, S.E., Maletic-Savatic, M., 2010. Microglia shape adult

hippocampal neurogenesis through apoptosis-coupled phagocytosis. Cell Stem Cell 7, 483–95. https://doi.org/10.1016/j.stem.2010.08.014

Silver, J, Miller, J.H., 2004. Regeneration beyond the glial scar. Nat. Rev. Neurosci. 5, 146–156. https://doi.org/10.1038/nrn1326

Silver, Jerry, Miller, J.H., 2004. Regeneration beyond the glial scar. Nat. Rev. Neurosci. 5, 146–156. https://doi.org/10.1038/nrn1326

Silverman, W.R., de Rivero Vaccari, J.P., Locovei, S., Qiu, F., Carlsson, S.K., Scemes, E., Keane, R.W., Dahl, G., 2009. The pannexin 1 channel activates the inflammasome in neurons and astrocytes. J. Biol. Chem. 284, 18143–18151. https://doi.org/10.1074/jbc.M109.004804

Simard, A.R., Soulet, D., Gowing, G., Julien, J.P., Rivest, S., 2006. Bone marrow-derived microglia play a critical role in restricting senile plaque formation in Alzheimer's disease. Neuron 49, 489–502. https://doi.org/10.1016/j.neuron.2006.01.022

Simi, A., Tsakiri, N., Wang, P., Rothwell, N.J., 2007. Interleukin-1 and inflammatory neurodegeneration. Biochem. Soc. Trans. https://doi.org/10.1042/BST0351122

Simon, H.U., Haj-Yehia, A., Levi-Schaffer, F., 2000. Role of reactive oxygen species (ROS) in apoptosis induction. Apoptosis 5, 415–418. https://doi.org/10.1023/A:1009616228304

Singh, N., Hopkins, S.J., Hulme, S., Galea, J.P., Hoadley, M., Vail, A., Hutchinson, P.J., Grainger, S., Rothwell, N.J., King, A.T., Tyrrell, P.J., 2014. The effect of intravenous interleukin-1 receptor antagonist on inflammatory mediators in cerebrospinal fluid after subarachnoid haemorrhage: A phase II randomised controlled trial. J. Neuroinflammation 11, 2–9. https://doi.org/10.1186/1742-2094-11-1

Smith, D.E., Lipsky, B.P., Russell, C., Ketchem, R.R., Kirchner, J., Hensley, K., Huang, Y., Friedman, W.J., Boissonneault, V., Plante, M.-M., Rivest, S., Sims, J.E., 2009. A novel CNS-restricted isoform of the IL-1R accessory protein modulates neuronal responses to IL-1. Immunity 30, 817–31.

https://doi.org/10.1016/j.immuni.2009.03.020

Sofroniew, M. V., 2009. Molecular dissection of reactive astrogliosis and glial scar formation. Trends Neurosci. 32, 638–47. https://doi.org/10.1016/j.tins.2009.08.002

Sofroniew, M. V., Vinters, H. V., 2010. Astrocytes: Biology and pathology. Acta Neuropathol. 119, 7–35. https://doi.org/10.1007/s00401-009-0619-8

Sofroniew, M. V, 2015. Astrocyte barriers to neurotoxic inflammation. Nat. Rev. Neurosci. 16, 249–63. https://doi.org/10.1038/nrn3898

Somjen, G.G., 1988. Nervenkitt: Notes on the history of the concept of neuroglia. Glia 1, 2–9. https://doi.org/10.1002/glia.440010103

Squarzoni, P., Oller, G., Hoeffel, G., Pont-Lezica, L., Rostaing, P., Low, D., Bessis, A., Ginhoux, F., Garel, S., 2014. Microglia Modulate Wiring of the Embryonic Forebrain. Cell Rep. 8, 1271–1279. https://doi.org/10.1016/j.celrep.2014.07.042

Sriram, K., O'Callaghan, J.P., 2007. Divergent roles for tumor necrosis factor-α in the brain. J. Neuroimmune Pharmacol. 2, 140–153. https://doi.org/10.1007/s11481-007-9070-6

Sternberg, N., Hamilton, D., 1981. Bacteriophage P1 site-specific recombination. I. Recombination between loxP sites. J. Mol. Biol. 150, 467–486. https://doi.org/10.1016/0022-2836(81)90375-2

Stirling, D.P., Khodarahmi, K., Liu, J., McPhail, L.T., McBride, C.B., Steeves, J.D., Ramer, M.S., Tetzlaff, W., 2004. Minocycline Treatment Reduces Delayed Oligodendrocyte Death, Attenuates Axonal Dieback, and Improves Functional Outcome after Spinal Cord Injury. J. Neurosci. 24, 2182–2190. https://doi.org/10.1523/JNEUROSCI.5275-03.2004

Stirling, D.P., Liu, S., Kubes, P., Yong, V.W., 2009. Depletion of Ly6G/Gr-1 leukocytes after spinal cord injury in mice alters wound healing and worsens neurological outcome. J. Neurosci. 29, 753–764. https://doi.org/10.1523/JNEUROSCI.4918-

08.2009

Stirling, D.P., Yong, V.W., 2008a. Dynamics of the inflammatory response after murine spinal cord injury revealed by flow cytometry. J. Neurosci. Res. 86, 1944–1958. https://doi.org/10.1002/jnr.21659

Stirling, D.P., Yong, V.W., 2008b. Dynamics of the inflammatory response after murine spinal cord injury revealed by flow cytometry. J. Neurosci. Res. 86, 1944–1958. https://doi.org/10.1002/jnr.21659

Stokes, B.T., Fox, P., Hollinden, G., 1983. Calcium Activity in the Injured Spinal Cord. Exp. Neurol. 572, 561–572.

Stott, K., Watson, M., Howe, F.S., Grossmann, J.G., Thomas, J.O., 2010. Tail-mediated collapse of HMGB1 is dynamic and occurs via differential binding of the acidic tail to the A and B domains. J. Mol. Biol. 403, 706–722. https://doi.org/10.1016/j.jmb.2010.07.045

Stout, C., Charles, A., 2003. Modulation of intercellular calcium signaling in astrocytes by extracellular calcium and magnesium. Glia 43, 265–273. https://doi.org/10.1002/glia.10257

Štros, M., 2010. HMGB proteins: Interactions with DNA and chromatin. Biochim. Biophys. Acta - Gene Regul. Mech. 1799, 101–113. https://doi.org/10.1016/j.bbagrm.2009.09.008

Stylianou, E., O'Neill, L.A.J., Rawlinson, L., Edbrooke, M.R., Woo, P., Saklatvala, J., 1992. Interleukin 1 induces NF-κB through its type I but not its type II receptor in lymphocytes. J. Biol. Chem. 267, 15836–15841.

Sugimori, M., Nagao, M., Parras, C.M., Nakatani, H., Lebel, M., Guillemot, F., Nakafuku, M., 2008. Ascl1 is required for oligodendrocyte development in the spinal cord. Development 135, 1271–1281. https://doi.org/10.1242/dev.015370

Sun, L., Li, M., Ma, X., Feng, H., Song, J., Lv, C., He, Y., 2017. Inhibition of HMGB1

reduces rat spinal cord astrocytic swelling and AQP4 expression after oxygen-glucose deprivation and reoxygenation via TLR4 and NF-KB signaling in an IL-6-dependent manner. J. Neuroinflammation 14, 1–18. https://doi.org/10.1186/s12974-017-1008-1

Sun, L., Li, M., Ma, X., Zhang, L., Song, J., Lv, C., He, Y., 2019. Inhibiting high mobility group box-1 reduces early spinal cord edema and attenuates astrocyte activation and aquaporin-4 expression after spinal cord injury in rats. J. Neurotrauma 36, 421–435. https://doi.org/10.1089/neu.2018.5642

Sun, W., Cornwell, A., Li, J., Peng, S., Joana Osorio, M., Aalling, N., Wang, S., Benraiss, A., Lou, N., Goldman, S.A., Nedergaard, M., 2017. SOX9 is an astrocyte-specific nuclear marker in the adult brain outside the neurogenic regions. J. Neurosci. 37, 4493–4507. https://doi.org/10.1523/JNEUROSCI.3199-16.2017

Sweeney, M.D., Sagare, A.P., Zlokovic, B. V., 2018. Blood–brain barrier breakdown in Alzheimer's disease and other.pdf. Nat. Rev. Neurol. 14, 133–150. https://doi.org/10.1038/nrneurol.2017.188.Blood

Szalay, G., Martinecz, B., Lénárt, N., Környei, Z., Orsolits, B., Judák, L., Császár, E., Fekete, R., West, B.L., Katona, G., Rózsa, B., Dénes, Á., 2016. Microglia protect against brain injury and their selective elimination dysregulates neuronal network activity after stroke. Nat. Commun. 7. https://doi.org/10.1038/ncomms11499

Takeuchi, O., Akira, S., 2010. Pattern Recognition Receptors and Inflammation. Cell 140, 805–820. https://doi.org/10.1016/j.cell.2010.01.022

Tang, X., Davies, J.E., Davies, S.J.A., 2003. Changes in distribution, cell associations, and protein expression levels of NG2, neurocan, phosphacan, brevican, versican v2, and tenascin-C during acute to chronic maturation of spinal cord scar tissue. J. Neurosci. Res. 71, 427–444. https://doi.org/10.1002/jnr.10523

Tao, X., Sun, X., Yin, L., Han, X., Xu, L., Qi, Y., Xu, Y., Li, H., Lin, Y., Liu, K., Peng, J., 2015. Dioscin ameliorates cerebral ischemia/reperfusion injury through the downregulation of TLR4 signaling via HMGB-1 inhibition. Free Radic. Biol. Med. 84,

103–115. https://doi.org/10.1016/j.freeradbiomed.2015.03.003

Tator, C.H., 1995. Update on the Pathophysiology and Pathology of Acute Spinal Cord Injury. Brain Pathol. 5, 407–413. https://doi.org/10.1111/j.1750-3639.1995.tb00619.x

Tator, C.H., Fehlings, M.G., 1991. Review of the secondary injury theory of acute spinal cord trauma with emphasis on vascular mechanisms. J. Neurosurg. 75, 15–26. https://doi.org/10.3171/jns.1991.75.1.0015

Tator, C.H., Koyanagi, I., 1997. Vascular mechanisms in the pathophysiology of human spinal cord injury. J. Neurosurg. 86, 483–492. https://doi.org/10.3171/jns.1997.86.3.0483

Tay, T.L., Mai, D., Dautzenberg, J., Fernández-Klett, F., Lin, G., Sagar, S., Datta, M., Drougard, A., Stempfl, T., Ardura-Fabregat, A., Staszewski, O., Margineanu, A., Sporbert, A., Steinmetz, L.M., Pospisilik, J.A., Jung, S., Priller, J., Grün, D., Ronneberger, O., Prinz, M., 2017. A new fate mapping system reveals context-dependent random or clonal expansion of microglia. Nat. Neurosci. 20, 793–803. https://doi.org/10.1038/nn.4547

Thawer, S.G., Mawhinney, L., Chadwick, K., De Chickera, S.N., Weaver, L.C., Brown, A., Dekaban, G.A., 2013. Temporal changes in monocyte and macrophage subsets and microglial macrophages following spinal cord injury in the lys-egfp-ki mouse model. J. Neuroimmunol. 261, 7–20. https://doi.org/10.1016/j.jneuroim.2013.04.008

Thornton, P., McColl, B.W., Greenhalgh, A., Denes, A., Allan, S.M., Rothwell, N.J., 2010a. Platelet interleukin-1alpha drives cerebrovascular inflammation. Blood 115, 3632–9. https://doi.org/10.1182/blood-2009-11-252643

Thornton, P., McColl, B.W., Greenhalgh, A., Denes, A., Allan, S.M., Rothwell, N.J., 2010b. Platelet interleukin-1?? drives cerebrovascular inflammation. Blood 115, 3632–3639. https://doi.org/10.1182/blood-2009-11-252643

Thundyil, J., Lim, K.L., 2015. DAMPs and neurodegeneration. Ageing Res. Rev. 24, 17–28. https://doi.org/10.1016/j.arr.2014.11.003

Tjoa, T., Strausbaugh, H.J., Maida, N., Dazin, P.F., Rosen, S.D., Noble-Haeusslein, L.J., 2003. The use of flow cytometry to assess neutrophil infiltration in the injured murine spinal cord. J. Neurosci. Methods 129, 49–59. https://doi.org/10.1016/S0165-0270(03)00205-X

Tremblay, M.Ě., Lowery, R.L., Majewska, A.K., 2010. Microglial interactions with synapses are modulated by visual experience. PLoS Biol. 8. https://doi.org/10.1371/journal.pbio.1000527

Tripathi, R., McTigue, D.M., 2007. Prominent oligodendrocyte genesis along the border of spinal contusion lesions. Glia 55, 698–711. https://doi.org/10.1002/glia.20491

Tripathi, R.B., McTigue, D.M., 2008. Chronically increased ciliary neurotrophic factor and fibroblast growth factor-2 expression after spinal contusion in rats. J. Comp. Neurol. 510, 129–144. https://doi.org/10.1002/cne.21787

Trotter, J., Karram, K., Nishiyama, A., 2010. NG2 cells: Properties, progeny and origin. Brain Res. Rev. 63, 72–82. https://doi.org/10.1016/j.brainresrev.2009.12.006

Turrens, J.F., 2003. Mitochondrial formation of reactive oxygen species. J. Physiol. https://doi.org/10.1111/j.1469-7793.2003.00335.x

Tynan, G.A., Hearnden, C.H., Oleszycka, E., Lyons, C.L., Coutts, G., O'Connell, J., Corrigan, M.A., Lynch, L., Campbell, M., Callanan, J.J., Mok, K.H., Geoghegan, J., O'Farrelly, C., Allan, S.M., Roche, H.M., O'Shea, D.B., Lavelle, E.C., 2014. Endogenous oils derived from human adipocytes are potent adjuvants that promote IL-1α-dependent inflammation. Diabetes 63, 2037–2050. https://doi.org/10.2337/db13-1476

Uezono, N., Zhu, Y., Fujimoto, Y., Yasui, T., Matsuda, T., Nakajo, M., Abematsu, M., Setoguchi, T., Mori, S., Takahashi, H.K., Komiya, S., Nishibori, M., Nakashima, K., 2018. Prior Treatment with Anti-High Mobility Group Box-1 Antibody Boosts Human Neural Stem Cell Transplantation-Mediated Functional Recovery After Spinal Cord Injury. Stem Cells 737–750. https://doi.org/10.1002/stem.2802

Vallstedt, A., Klos, J.M., Ericson, J., 2005. Multiple dorsoventral origins of oligodendrocyte generation in the spinal cord and hindbrain. Neuron 45, 55–67. https://doi.org/10.1016/j.neuron.2004.12.026

van Tilborg, E., de Theije, C.G.M., van Hal, M., Wagenaar, N., de Vries, L.S., Benders, M.J., Rowitch, D.H., Nijboer, C.H., 2018. Origin and dynamics of oligodendrocytes in the developing brain: Implications for perinatal white matter injury. Glia 66, 221–238. https://doi.org/10.1002/glia.23256

Vanlandewijck, M., He, L., Mäe, M.A., Andrae, J., Ando, K., Del Gaudio, F., Nahar, K., Lebouvier, T., Laviña, B., Gouveia, L., Sun, Y., Raschperger, E., Räsänen, M., Zarb, Y., Mochizuki, N., Keller, A., Lendahl, U., Betsholtz, C., 2018. A molecular atlas of cell types and zonation in the brain vasculature. Nature 554, 475–480. https://doi.org/10.1038/nature25739

Venereau, E., Casalgrandi, M., Schiraldi, M., Antoine, D.J., Cattaneo, A., De Marchis, F., Liu, J., Antonelli, A., Preti, A., Raeli, L., Shams, S.S., Yang, H., Varani, L., Andersson, U., Tracey, K.J., Bachi, A., Uguccioni, M., Bianchi, M.E., 2012. Mutually exclusive redox forms of HMGB1 promote cell recruitment or proinflammatory cytokine release. J. Exp. Med. 209, 1519–1528. https://doi.org/10.1084/jem.20120189

Vogelgesang, A., May, V.E.L., Grunwald, U., Bakkeboe, M., Langner, S., Wallaschofski, H., Kessler, C., Bröker, B.M., Dressel, A., 2010. Functional Status of Peripheral Blood T-Cells in Ischemic Stroke Patients. PLoS One 5, e8718. https://doi.org/10.1371/journal.pone.0008718

Voisin, M.B., Pröbstl, D., Nourshargh, S., 2010. Venular basement membranes ubiquitously express matrix protein low-expression regions: Characterization in multiple tissues and remodeling during inflammation. Am. J. Pathol. 176, 482–495. https://doi.org/10.2353/ajpath.2010.090510

Von Leden, R.E., Yauger, Y.J., Khayrullina, G., Byrnes, K.R., 2017. Central Nervous System Injury and Nicotinamide Adenine Dinucleotide Phosphate Oxidase: Oxidative Stress and Therapeutic Targets. J. Neurotrauma 34, 755–764.

https://doi.org/10.1089/neu.2016.4486

Wang, C., Jiang, J., Zhang, X., Song, L., Sun, K., Xu, R., 2016. Inhibiting HMGB1 Reduces Cerebral Ischemia Reperfusion Injury in Diabetic Mice. Inflammation 39, 1862–1870. https://doi.org/10.1007/s10753-016-0418-z

Wang, D., Liu, K., Wake, H., Teshigawara, K., Mori, S., Nishibori, M., 2017. Anti-high mobility group box-1 (HMGB1) antibody inhibits hemorrhage-induced brain injury and improved neurological deficits in rats. Sci. Rep. 7, 1–16. https://doi.org/10.1038/srep46243

Wang, H., Bloom, O., Zhang, M., Vishnubhakat, J.M., Ombrellino, M., Che, J., Frazier, A., Yang, H., Ivanova, S., Borovikova, L., Manogue, K.R., Faist, E., Abraham, E., Andersson, J., Andersson, U., Molina, P.E., Abumrad, N.N., Sama, A., Tracey, K.J., 1999. HMG-1 as a late mediator of endotoxin lethality in mice. Science (80-.). 285, 248–251. https://doi.org/10.1126/science.285.5425.248

Wang, H., Li, W., Zhu, S., Li, J., D'Amore, J., Ward, M.F., Yang, H., Wu, R., Jahnen-Dechent, W., Tracey, K.J., Wang, P., Sama, A.E., 2010. Peripheral administration of fetuin-A attenuates early cerebral ischemic injury in rats. J. Cereb. Blood Flow Metab. 30, 493–504. https://doi.org/10.1038/jcbfm.2009.247

Wang, H., Mei, X., Cao, Y., Liu, C., Zhao, Z., Guo, Z., Bi, Y., Shen, Z., Yuan, Y., Guo, Y., Song, C., Bai, L., Wang, Y., Yu, D., 2017. HMGB1/Advanced Glycation End Products (RAGE) does not aggravate inflammation but promote endogenous neural stem cells differentiation in spinal cord injury. Sci. Rep. 7, 1–12. https://doi.org/10.1038/s41598-017-10611-8

Wang, S., Sdrulla, A.D., DiSibio, G., Bush, G., Nofziger, D., Hicks, C., Weinmaster, G., Barres, B.A., 1998. Notch receptor activation inhibits oligodendrocyte differentiation. Neuron 21, 63–75. https://doi.org/10.1016/S0896-6273(00)80515-2

Wang, X., Arcuino, G., Takano, T., Lin, J., Peng, W.G., Wan, P., Li, P., Xu, Q., Liu, Q.S., Goldman, S.A., Nedergaard, M., 2004. P2X7 receptor inhibition improves recovery

after spinal cord injury. Nat. Med. 10, 821–827. https://doi.org/10.1038/nm1082

Wang, Y., Nakayama, M., Pitulescu, M.E., Schmidt, T.S., Bochenek, M.L., Sakakibara, A., Adams, S., Davy, A., Deutsch, U., Lüthi, U., Barberis, A., Benjamin, L.E., Mäkinen, T., Nobes, C.D., Adams, R.H., 2010. Ephrin-B2 controls VEGF-induced angiogenesis and lymphangiogenesis. Nature 465, 483–486. https://doi.org/10.1038/nature09002

Wanner, I.B., Anderson, M.A., Song, B., Levine, J., Fernandez, A., Gray-Thompson, Z., Ao, Y., Sofroniew, M. V., 2013. Glial scar borders are formed by newly proliferated, elongated astrocytes that interact to corral inflammatory and fibrotic cells via STAT3-dependent mechanisms after spinal cord injury. J. Neurosci. 33, 12870–12886. https://doi.org/10.1523/JNEUROSCI.2121-13.2013

Warden, P., Bamber, N.I., Li, H., Esposito, A., Ahmad, K.A., Hsu, C.Y., Xu, X.M., 2001. Delayed glial cell death following wallerian degeneration in white matter tracts after spinal cord dorsal column cordotomy in adult rats.PG. Exp Neurol 168, 213–224. https://doi.org/10.1006/exnr.2000.7622

Watanabe, M., Toyama, Y., Nishiyama, A., 2002. Differentiation of proliferated NG2-positive glial progenitor cells in a remyelinating lesion. J. Neurosci. Res. 69, 826–836. https://doi.org/10.1002/jnr.10338

Weber, A., Wasiliew, P., Kracht, M., 2010. Interleukin-1 (IL-1) Pathway 3, 1–7.

Wedi, B., Straede, J., Wieland, B., Kapp, A., 1999. Eosinophil apoptosis is mediated by stimulators of cellular oxidative metabolisms and inhibited by antioxidants: Involvement of a thiol-sensitive redox regulation in eosinophil cell death. Blood 94, 2365–2373. https://doi.org/10.1182/blood.v94.7.2365.419k08_2365_2373

Werman, A., Werman-Venkert, R., White, R., Lee, J.K., Werman, B., Krelin, Y., Voronov, E., Dinarello, C.A., Apte, R.N., 2004. The precursor form of IL-1α is an intracrine proinflammatory activator of transcription. Proc. Natl. Acad. Sci. U. S. A. 101, 2434–2439. https://doi.org/10.1073/pnas.0308705101

Wessendorf, J.H.M., Garfinkel, S., Zhan, X., Brown, S., Maciag, T., 1993. Identification of

a nuclear localization sequence within the structure of the human interleukin-1α precursor. J. Biol. Chem. 268, 22100–22104.

Wierstra, I., 2008. Sp1: Emerging roles-Beyond constitutive activation of TATA-less housekeeping genes. Biochem. Biophys. Res. Commun. 372, 1–13. https://doi.org/10.1016/j.bbrc.2008.03.074

Winkler, E.A., Bell, R.D., Zlokovic, B. V, 2011. Central nervous system pericytes in health and disease. Nat. Neurosci. 14, 1398–1405. https://doi.org/10.1038/nn.2946

Wolswijk, G., Noble, M., 1989. Identification of an adult-specific glial progenitor cell. Development 105, 387–400. https://doi.org/10.1016/0922-3371(89)90618-7

Woodruff, R.H., Tekki-Kessaris, N., Stiles, C.D., Rowitch, D.H., Richardson, W.D., 2001. Oligodendrocyte development in the spinal cord and telencephalon: Common themes and new perspectives. Int. J. Dev. Neurosci. 19, 379–385. https://doi.org/10.1016/S0736-5748(00)00083-6

Wynn, T. a., Chawla, A., Pollard, J.W., 2013. Origins and Hallmarks of Macrophages: Development, Homeostasis, and Disease. Nature 496, 445–455. https://doi.org/10.1038/nature12034.Origins

Wyss-Coray, T., Mucke, L., 2002. Inflammation in neurodegenerative disease - A double-edged sword. Neuron 35, 419–432. https://doi.org/10.1016/S0896-6273(02)00794-8

Xie, Z.F., Xin, G., Xu, Y.X., Su, Y., Li, K.S., 2016. LPS-Primed Release of HMGB-1 from Cortical Astrocytes is Modulated Through PI3K/AKT Pathway. Cell. Mol. Neurobiol. 36, 93–102. https://doi.org/10.1007/s10571-015-0223-5

Xin, Q., Cheng, B., Pan, Y., Liu, H., Yang, C., Chen, J., Bai, B., 2015. Neuroprotective effects of apelin-13 on experimental ischemic stroke through suppression of inflammation. Peptides 63, 55–62. https://doi.org/10.1016/j.peptides.2014.09.016

Xiong, Y., Rabchevsky, A.G., Hall, E.D., 2007. Role of peroxynitrite in secondary oxidative damage after spinal cord injury. J. Neurochem. 100, 639–649.

https://doi.org/10.1111/j.1471-4159.2006.04312.x

Xiwei Zheng, Cong Bi, Marissa Brooks, and D.S.H., 2015. Targeting HMGB1 in inflammation. Anal Chem. 25, 368–379. https://doi.org/10.1016/j.cogdev.2010.08.003.Personal

Yanagisawa, D., Kitamura, Y., Takata, K., Hide, I., Nakata, Y., Taniguchi, T., 2008. Possible involvement of P2X7 receptor activation in microglial neuroprotection against focal cerebral ischemia in rats. Biol Pharm Bull 31, 1121–1130. https://doi.org/JST.JSTAGE/bpb/31.1121 [pii]

Yanai, H., Ban, T., Wang, Z., Choi, M.K., Kawamura, T., Negishi, H., Nakasato, M., Lu, Y., Hangai, S., Koshiba, R., Savitsky, D., Ronfani, L., Akira, S., Bianchi, M.E., Honda, K., Tamura, T., Kodama, T., Taniguchi, T., 2009. HMGB proteins function as universal sentinels for nucleic-acid-mediated innate immune responses. Nature 462, 99–103. https://doi.org/10.1038/nature08512

Yang, H., Lundbäck, P., Ottosson, L., Erlandsson-Harris, H., Venereau, E., Bianchi, M.E., Al-Abed, Y., Andersson, U., Tracey, K.J., Antoine, D.J., 2012. Redox modification of cysteine residues regulates the cytokine activity of high mobility group box-1 (HMGB1). Mol. Med. 18, 250–9. https://doi.org/10.2119/molmed.2011.00389

Yang, J., Xiong, L.L., Wang, Y.C., He, X., Jiang, L., Fu, S.J., Han, X.F., Liu, J., Wang, T.H., 2018. Oligodendrocyte precursor cell transplantation promotes functional recovery following contusive spinal cord injury in rats and is associated with altered MicroRNA expression. Mol. Med. Rep. 17, 771–782. https://doi.org/10.3892/mmr.2017.7957

Yang, Y., Bazhin, A. V., Werner, J., Karakhanova, S., 2013. Reactive oxygen species in the immune system. Int. Rev. Immunol. 32, 249–270. https://doi.org/10.3109/08830185.2012.755176

Yang, Y., Liu, H., Zhang, H., Ye, Q., Wang, J., Yang, X., Mao, L., Zhu, W., Leak, R.K., Xiao, B., Lu, B., Chen, X.J., Hu, X., 2017. ST2 / IL-33-Dependent Microglial

Response Limits Acute Ischemic Brain Injury 37, 4692–4704. https://doi.org/10.1523/JNEUROSCI.3233-16.2017

Yarmolinsky, M., Hoess, R., 2015. The Legacy of Nat Sternberg: The Genesis of Cre- lox Technology . Annu. Rev. Virol. 2, 25–40. https://doi.org/10.1146/annurev-virology-100114-054930

Yona, S., Viukov, S., Guilliams, M., Misharin, A., 2013. Tissue Macrophages Under Homeostasis. Immunity 38, 79–91. https://doi.org/10.1016/j.immuni.2012.12.001.Fate

Yu, J., Wei, M., Becknell, B., Trotta, R., Liu, S., Boyd, Z., Jaung, M.S., Blaser, B.W., Sun, J., Benson, D.M., Mao, H., Yokohama, A., Bhatt, D., Shen, L., Davuluri, R., Weinstein, M., Marcucci, G., Caligiuri, M.A., 2006. Pro- and Antiinflammatory Cytokine Signaling: Reciprocal Antagonism Regulates Interferon-gamma Production by Human Natural Killer Cells. Immunity 24, 575–590. https://doi.org/10.1016/j.immuni.2006.03.016

Yuan, F., Gu, L., Guo, S., Wang, C., Li, G.M., 2004. Evidence for involvement of HMGB1 protein in human DNA mismatch repair. J. Biol. Chem. 279, 20935–20940. https://doi.org/10.1074/jbc.M401931200

Zamanian, J.L., Xu, L., Foo, L.C., Nouri, N., Zhou, L., Giffard, R.G., Barres, B.A., 2012. Genomic analysis of reactive astrogliosis. J. Neurosci. 32, 6391–6410. https://doi.org/10.1523/JNEUROSCI.6221-11.2012

Zeisel, A., Muñoz-Manchado, A.B., Codeluppi, S., Lönnerberg, P., La Manno, G., Juréus, A., Marques, S., Munguba, H., He, L., Betsholtz, C., Rolny, C., Castelo-Branco, G., Hjerling-Leffler, J., Linnarsson, S., 2015. Brain structure. Cell types in the mouse cortex and hippocampus revealed by single-cell RNA-seq. Science 347, 1138–42. https://doi.org/10.1126/science.aaa1934

Zhang, J., Takahashi, H.K., Liu, K., Wake, H., Liu, R., Maruo, T., Date, I., Yoshino, T., Ohtsuka, A., Mori, S., Nishibori, M., 2011. Anti-high mobility group box-1 monoclonal antibody protects the blood-brain barrier from ischemia-induced

disruption in rats. Stroke 42, 1420–1428. https://doi.org/10.1161/STROKEAHA.110.598334

Zheng, Y., Humphry, M., Maguire, J.J., Bennett, M.R., Clarke, M.C.H., 2013. Intracellular Interleukin-1 Receptor 2 Binding Prevents Cleavage and Activity of Interleukin-1α, Controlling Necrosis-Induced Sterile Inflammation. Immunity. https://doi.org/10.1016/j.immuni.2013.01.008

Zhou, X., He, X.J., Ren, Y., 2014. Function of microglia and macrophages in secondary damage after spinal cord injury. Neural Regen. Res. 9, 1787–1795. https://doi.org/10.4103/1673-5374.143423

Zhu, L., Liu, X., Nemeth, D.P., DiSabato, D.J., Witcher, K.G., Mckim, D.B., Oliver, B., Le, X., Gorantla, G., Berdysz, O., Li, J., Ramani, A.D., Chen, Z., Wu, D., Godbout, J.P., Quan, N., 2019. Interleukin-1 causes CNS inflammatory cytokine expression via endothelia-microglia bi-cellular signaling. Brain. Behav. Immun. 81, 292–304. https://doi.org/10.1016/j.bbi.2019.06.026

Zhu, Z., Wang, D., Jiao, W., Chen, G., Cao, Y., Zhang, Q., Wang, J., 2017. Bioinformatics analyses of pathways and gene predictions in IL-1α and IL-1β knockout mice with spinal cord injury. Acta Histochem. 119, 663–670. https://doi.org/10.1016/j.acthis.2017.07.007

Zong, S., Zeng, G., Wei, B., Xiong, C., Zhao, Y., 2012. Beneficial effect of interleukin-1 receptor antagonist protein on spinal cord injury recovery in the rat. Inflammation 35, 520–526. https://doi.org/10.1007/s10753-011-9341-5